

**Predictive Modeling of Large-Scale Integrated Refinery Reaction
and Fractionation Systems from Plant Data: Fluid Catalytic
Cracking (FCC) and Continuous Catalyst Regeneration (CCR)
Catalytic Reforming Processes**

Kiran Pashikanti

Dissertation submitted to the faculty of the Virginia Polytechnic Institute and State University in
partial fulfillment of the requirements for the degree of

Doctor of Philosophy

In

Chemical Engineering

Y. A. Liu, Chair

Luke E. K. Achenie

Richey M. Davis

Preston L. Durrill

August 31, 2011

Blacksburg, VA

Keywords: modeling, refining, FCC, CCR, reforming, fractionation

Predictive Modeling of Large-Scale Integrated Refinery Reaction and Fractionation Systems from Plant Data: Fluid Catalytic Cracking (FCC) and Continuous Catalyst Regeneration (CCR) Catalytic Reforming Processes

Kiran Pashikanti

ABSTRACT

This dissertation includes two accounts of rigorous modeling of petroleum refinery modeling using rigorous reaction and fractionation units. The models consider various process phenomena and have been extensively used during a course of a six-month study to understand and predict behavior. This work also includes extensive guides to allow users to develop similar models using commercial software tools.

(1) Predictive Modeling of Large-Scale Integrated Refinery Reaction and Fractionation Systems from Plant Data: Fluid Catalytic Cracking (FCC) Process with Planning

Applications: This work presents the methodology to develop, validate and apply a predictive model for an integrated fluid catalytic cracking (FCC) process. We demonstrate the methodology by using data from a commercial FCC plant in the Asia Pacific with a feed capacity of 800,000 tons per year. Our model accounts for the complex cracking kinetics in the riser-regenerator and associated gas plant phenomena. We implement the methodology with Microsoft Excel spreadsheets and a commercial software tool, Aspen HYSYS/Petroleum Refining from Aspen Technology, Inc. The methodology is equally applicable to other commercial software tools. This model gives accurate predictions of key product yields and properties given feed qualities and operating conditions. This work differentiates itself from previous work in this area through

the following contributions: (1) detailed models of the entire FCC plant, including the overhead gas compressor, main fractionator, primary and sponge oil absorber, primary stripper and debutanizer columns; (2) process to infer molecular composition required for the kinetic model using routinely collected bulk properties of feedstock; (3) predictions of key liquid product properties not published alongside previous related work (density, D-86 distillation curve and flash point); (4) case studies showing industrially useful applications of the model; and (5) application of the model with an existing LP-based planning tool.

(2) Predictive Modeling of Large-Scale Integrated Refinery Reaction and Fractionation Systems from Plant Data: Continuous Catalyst Regeneration (CCR) Reforming Process:

This work presents a model for the rating and optimization of an integrated catalytic reforming process with UOP-style continuous catalyst regeneration (CCR). We validate this model using plant data from a commercial CCR reforming process handling a feed capacity of 1.4 million tons per year in the Asia Pacific. The model relies on routinely monitored data such as ASTM distillation curves, paraffin-naphthene-aromatic (PNA) analysis and operating conditions. We account for dehydrogenation, dehydrocyclization, isomerization and hydrocracking reactions that typically occur with petroleum feedstock. In addition, this work accounts for the coke deposited on the catalyst and product recontacting sections. This work differentiates itself from the reported studies in the literature through the following contributions: (1) detailed kinetic model that accounts for coke generation and catalyst deactivation; (2) complete implementation of a recontactor and primary product fractionation; (3) feed lumping from limited feed information; (4) detailed procedure for kinetic model calibration; (5) industrially relevant case studies that highlight the effects of changes in key process variables; and (6) application of the model to refinery-wide production planning.

ACKNOWLEDGEMENTS

First and foremost, I must acknowledge my advisor, Dr. Y. A. Liu. His tireless enthusiasm for the pursuit of knowledge and gracious spirit has made this long journey worthwhile. He has not only offered his own vast experience but provided me with many opportunities to learn from researchers and practitioners all over the world.

I would also like to thank Drs. Achenie, Davis and Durill for serving on my committee. They have selflessly given of their time and agreed to meet on short notice and tight deadlines. I am indebted to them for their support and hope that this work meets their high expectations.

Graduate school can often be a lonely place. It is rare to find colleagues that can be good friends. Ai-Fu Chang has been my interpreter, tour-guide, relentless critic, ardent supporter and most importantly, a good friend. Without his help, much of this work could not have been possible. He patiently listened to my wild ideas and always managed to salvage something usable. I will always remember our meandering discussions and conversations. I cannot thank him enough for being fellow traveler on this journey.

I express my deepest gratitude to my parents, Narender and Vanaja Pashikanti. I thank them for giving me the greatest gift of all: the love of learning. They have made great sacrifices, offered unyielding support and given me more than I could acknowledge in a few sentences. I hope to emulate their spirit of kindness, hard work and optimism in my own life. I also thank all my family (Soni, keep watching that B5) and friends for helping and supporting me throughout this endeavor.

Finally, I would also like to thank all of our research sponsors here at Virginia Tech, specifically SINOPEC and AspenTech. They have offered our research group many challenges and supported us throughout this long process. I have learned a great deal from our collaboration and hope that future students continue to benefit from this unique university-industry partnership.

FORMAT OF DISSERTATION

This dissertation is written in journal format. Chapter 1 offers a relevant introduction and identifies the scope of this work. Chapters 2 and 3 are self-contained works that describe the modeling of an industrial Fluid Catalytic Cracking (FCC) and Continuous Catalyst Regeneration (CCR) Catalytic Reforming unit, respectively. Chapters 4 and 5 present detailed guides for modeling these units using commercial software, Aspen HYSYS/Petroleum Refining. Chapter 6 summarizes the work presented in this dissertation and includes several concluding remarks.

TABLE OF CONTENTS

ABSTRACT.....	ii
ACKNOWLEDGEMENTS	iv
FORMAT OF DISSERTATION	vi
LIST OF FIGURES	xi
LIST OF TABLES.....	xviii
1. Introduction.....	1
1.1 Overview	1
1.2 Issues addressed in this work	2
1.3 Original contributions of this work	3
2. Predictive Modeling of the Fluid Catalytic Cracking (FCC) Process	4
2.1 Abstract	4
2.2 Introduction	5
2.3 Process Description	6
2.3.1 Riser-Regenerator Complex.....	6
2.3.2 Downstream Fractionation.....	8
2.4 Process Chemistry	12
2.5 Literature Review	16
2.5.1 Kinetic Models	16
2.5.2 Unit-level Models	24
2.6 Aspen HYSYS/Petroleum Refining FCC Model	27
2.6.1 Slip factor and average voidage.....	30
2.6.2 21-Lump Kinetic Model	31
2.6.3 Catalyst Deactivation	33
2.7 Calibrating the Aspen HYSYS/Petroleum Refining FCC Model	34
2.8 Fractionation.....	36
2.9 Mapping Feed Information to Kinetic Lumps.....	41
2.9.1 Fitting Distillation Curves.....	41
2.9.2 Inferring Molecular Composition	44
2.9.3 Convert Kinetic Lumps to Fractionation Lumps	49

2.10	Overall Modeling Strategy	51
2.11	Results	54
2.12	Applications	67
2.12.1	Improving Gasoline Yield.....	67
2.12.2	Increasing unit throughput	71
2.12.3	Sulfur content in gasoline	73
2.13	Refinery Planning.....	76
2.13	Conclusions	84
2.14	Acknowledgements	85
2.15	Nomenclature	85
2.16	References	88
3.	Predictive Modeling of the Continuous Catalyst Regeneration (CCR) Reforming Process .	93
3.1	Abstract	93
3.2	Introduction	94
3.3	Process Overview	95
3.4	Process Chemistry	104
3.5	Literature Review	108
3.5.1	Kinetic models and networks.....	109
3.5.2	Unit-level models.....	115
3.6	Aspen HYSYS/Petroleum Refining Catalytic Reformer Model.....	119
3.7	Thermophysical Properties.....	125
3.8	Fractionation System.....	126
3.9	Feed Characterization.....	129
3.10	Model Implementation	135
3.10.1	Data consistency	136
3.10.2	Feed characterization	137
3.10.3	Calibration.....	138
3.11	Overall modeling strategy	143
3.12	Results	146
3.13	Applications	154
3.13.1	Effect of reactor temperature on process yield	155

3.13.2	Effect of feed rate on process yield.....	158
3.13.3	Combined effects on process yield	161
3.13.4	Effect of feedstock quality on process yield	162
3.13.5	Chemical feedstock production.....	164
3.13.6	Energy utilization and process performance.....	167
3.14	Refinery Planning.....	170
3.15	Conclusions	176
3.16	Acknowledgements	177
3.17	Nomenclature	177
3.18	References	179
4.	Guide for modeling FCC units in Aspen HYSYS/Petroleum Refining	183
4.1	Introduction	183
4.2	Process Overview	183
4.3	Process Data	186
4.4	Aspen HYSYS and initial component and thermodynamics setup.....	190
4.5	Workshop I: Basic FCC model	197
4.6	FCC Feed configuration	202
4.7	FCC Catalyst configuration.....	208
4.8	FCC Operating variables configuration	212
4.9	Initial model solution	216
4.10	Viewing model results.....	219
4.11	Workshop II: Calibrating basic FCC model.....	224
4.12	Workshop III: Build main fractionator and gas plant system	235
4.13	Workshop IV: Perform case study to identify different gasoline production scenarios 239	
4.14	Workshop V: Generate DELTA-BASE vectors for linear programming (LP) based planning.....	250
4.15	References	258
5.	Guide for modeling CCR units in Aspen HYSYS/Petroleum Refining	259
5.1	Introduction	259
5.2	Process Overview and Relevant Data	259

5.3	Aspen HYSYS and initial component and thermodynamics setup.....	264
5.4	Workshop I: Basic reformer configuration	270
5.5	Input feedstock and process variables	274
5.6	Solver parameters and running initial model	281
5.7	Viewing model results.....	284
5.8	Updating results with molecular composition information.....	288
5.9	Workshop II: Model calibration.....	291
5.10	Workshop III: Build a downstream fractionation	310
5.11	Workshop IV: Case study to vary RON and product distribution profile.....	318
6.	Conclusions	328
6.1	Summary	328
6.2	Future Directions.....	329

LIST OF FIGURES

Figure 2.1: General schematic of typical FCC reactor-regenerator unit.....	8
Figure 2.2: Downstream fractionation (Main fractionator)	10
Figure 2.3: FCC gas plant section.....	12
Figure 2.4: Lumped model from Takatsuka et al. ⁹ : VR= Vacuum Residue, CSO = Coke Slurry Oil, HCO = Heavy cycle oil and LCO= Light cycle oil.....	17
Figure 2.5: Ten-lump model from Jacob et al. ¹³	17
Figure 2.6: Typical SOL Lumping (From Ref. 20)	19
Figure 2.7: Summary of kinetic models.....	20
Figure 2.8: Overview of the major submodels that make up the Aspen HYSYS/Petroleum Refining FCC model (Adapted from Ref. 6).....	27
Figure 2.9: “Back-blending” products to reconstitute FCC reactor effluent	39
Figure 2.10: Comparison between using the beta distribution and lognormal distribution to fit the same distillation data	44
Figure 2.11: Comparison of calculated and measured paraffin content in all fractions	47
Figure 2.12: Comparison of calculated and measured naphthene content in all fractions	47
Figure 2.13: Comparison of calculated and measured aromatic content in all fractions.....	48
Figure 2.14: Specific implementation of overall modeling strategy.....	53
Figure 2.15: Tracking aromatic content in the feed to ensure multiple operating scenarios	53
Figure 2.16: Overall Aspen HYSYS model of FCC unit and associated gas plant.....	56
Figure 2.17: ASTM D-86 distillation for the product diesel from the main fractionator (VALID- 1).....	59
Figure 2.18: ASTM D-86 distillation for the product gasoline from debutanizer column (VALID – 1).....	60
Figure 2.19: Gasoline density comparison.....	61
Figure 2.20: Diesel density comparison.....	61
Figure 2.21: Diesel flash point comparison	62
Figure 2.22: Main fractionator temperature profile	65
Figure 2.23: Primary Absorber Temperature profile	65
Figure 2.24: Debutanizer Temperature profile	66
Figure 2.25: Sponge oil Absorber Temperature Profile.....	66
Figure 2.26: Primary Stripper Temperature profile	67
Figure 2.27: Gasoline yield profile as a function of ROT	68
Figure 2.28: Yields of key products as functions of ROT	69
Figure 2.29: Coke yield as a function of ROT	70
Figure 2.30: Maximizing production of key products as a function of ROT	71
Figure 2.31: Mass yield and cat-oil ratio as function of feed rate	72
Figure 2.32: Gasoline yield as a function of feed rate	73
Figure 2.33: Scenario of feed sulfur change	74

Figure 2.34: Blending in varying amounts of Residue feed	75
Figure 2.35: Simplified view of FCC unit for a LP application	77
Figure 2.36: Process to generate DELTA-BASE vectors	81
Figure 3.1: Different types of reactors used in reforming processes [Adapted from Ref. 6]	96
Figure 3.2: Process flow diagram for CCR reforming process.....	98
Figure 3.3: Cutaway of gravity assisted reactor ⁹	102
Figure 3.4: Schematic of catalyst regeneration process ⁶	102
Figure 3.5: Relationship between catalyst features and reaction classes [Ref. 13, 14]	106
Figure 3.6: Basic lumping kinetic networks	112
Figure 3.7: Lumped kinetic network from Froment where $5 < x < 9$ [Ref. 12].....	113
Figure 3.8: Basic process flow for an integrated reformer model	116
Figure 3.9: Organization of Aspen HYSYS/Petroleum Refining CatReform model	120
Figure 3.10: Equilibrium composition of A8 isomers (assuming ideal gas conditions).....	124
Figure 3.11: Composition of A8 isomers over the study period.....	124
Figure 3.12: Correlation between prediction and measured composition	132
Figure 3.13: Comparison between measured and calculated TBP based on PNA lumping	134
Figure 3.14: Optimized distribution of paraffin, naphthene and aromatic for given feed type ..	135
Figure 3.15: Microsoft Excel-based spreadsheet tool for mass and hydrogen balance calculations	137
Figure 3.16: Variation in N5 and N6 content in feed	138
Figure 3.17: Overall modeling strategy	143
Figure 3.18: Variation in feed quality over the study period.....	146
Figure 3.19: Remixing section.....	146
Figure 3.20: Recontacting section.....	147
Figure 3.21: Combined reformer and primary fractionation	148
Figure 3.22: Temperature profile of column DA301	153
Figure 3.23: Temperature profile of column DA302.....	153
Figure 3.24: Change in C5+ yield (wt. %) as function of WAIT and H2HC ratio (WHSV = 1.37)	156
Figure 3.25: Change in C5+ RON as function of WAIT and H2HC ratio (WHSV = 1.37).....	156
Figure 3.26: Change in Total Aromatic Yield (wt. %) as function of WAIT and H2HC ratio (WHSV = 1.37).....	157
Figure 3.27: Change in light gas yield as function of WAIT and H2HC ratio (WHSV = 1.37)	157
Figure 3.28: Coke laydown rate (kg/hr) as function of WAIT and H2HC ratio (WHSV = 1.37)	158
Figure 3.29: Change in C5+ Yield (wt. %) as function of WHSV and WAIT	159
Figure 3.30: Change in C5+ RON as function of WHSV and WAIT	160
Figure 3.31: Change in Total Aromatics yield as functions of WHSV and WAIT	160
Figure 3.32: Corresponding WAIT and WHSV to obtain various C5+ RON in reactor products	161

Figure 3.33: Effect of C5+ Yield (wt. %) on C5+ RON.....	162
Figure 3.34: Effect of changing feed MCP composition on aromatic yields.....	164
Figure 3.35: Relative yields of aromatic components (where A6 refers to benzene, A7 refers to toluene and A8 refers to xylenes) as function of WHSV and WAIT = 495 °C	165
Figure 3.36: Relative yields of aromatic components (where A6 refers to benzene, A7 refers to toluene and A8 refers to xylenes) as function of WHSV and WAIT = 525 °C	166
Figure 3.37: Process to generate DELTA-BASE vectors from rigorous model.....	172
Figure 4.1: Reaction Section of FCC Unit.....	184
Figure 4.2: Main Fractionator associated with FCC.....	185
Figure 4.3: Gas plant associated with FCC unit	186
Figure 4.4: Initial Startup of Aspen HYSYS	190
Figure 4.5: Adding a component List	191
Figure 4.6: Adding petroleum component list	192
Figure 4.7: Initial Component list for petroleum component list process	193
Figure 4.8: Adding additional components to petroleum component list.....	193
Figure 4.9: Select Thermodynamics for Fluid Package.....	194
Figure 4.10: Thermodynamic options for Fluid Package	195
Figure 4.11: Binary interaction parameters for Fluid package	196
Figure 4.12: Initial Aspen HYSYS Flowsheet.....	197
Figure 4.13: Aspen HYSYS/Petroleum Refining unit operation palette	198
Figure 4.14: Adding initial FCC unit.....	198
Figure 4.15: Selecting FCC configuration.....	199
Figure 4.16: Sizing the dimensions of the FCC unit.....	200
Figure 4.17: Specifying heat loss from different locations of the FCC Unit.....	201
Figure 4.18: Select default calibration parameters	202
Figure 4.19: Assign feed types to feed data.....	203
Figure 4.20: FCC feed type library	204
Figure 4.21: Feed type template.....	205
Figure 4.22: Feed bulk property information window.....	206
Figure 4.23: Completed feed bulk property information window	207
Figure 4.24: Initial catalyst library window.....	209
Figure 4.25: Catalyst library	210
Figure 4.26: Catalyst parameters	210
Figure 4.27: Catalyst parameters	211
Figure 4.28: Catalyst activity factor and equilibrium metals content.....	212
Figure 4.29: Main application menu bar (hold solver)	213
Figure 4.30: Specify feed conditions	213
Figure 4.31: Riser conditions and steam input.....	214
Figure 4.32: Regenerator operating parameters.....	215
Figure 4.33: Pressure control (Reactor Pressure should be greater than regenerator pressure) .	216

Figure 4.34: Solver convergence options.....	217
Figure 4.35: Main application menu bar (activate solver).....	217
Figure 4.36: Add effluent stream to PFD.....	219
Figure 4.37: Navigate FCC results.....	220
Figure 4.38: Adjusted Kinetic Lumps.....	220
Figure 4.39: Square cut product yields	221
Figure 4.40: Properties of square cut products	222
Figure 4.41: Overall heat balance between riser and regenerator.....	223
Figure 4.42: Entering FCC calibration environment	224
Figure 4.43: FCC calibration window	225
Figure 4.44: Pull current simulation data into calibration environment	226
Figure 4.45: Specify cuts for plant measurement data.....	227
Figure 4.46: Measured light gas yield and composition	228
Figure 4.47: Measure liquid product yield and properties.....	229
Figure 4.48: Mass balance validation wizard	230
Figure 4.49: Calibrated activity factors	232
Figure 4.50: Calibrated heat balance between riser and regenerator	233
Figure 4.51: Save calibration factors for current calibration	234
Figure 4.52: Return calibration factors to main FCC environment	234
Figure 4.53: Aspen HYSYS configuration for the main fractionator	236
Figure 4.54: Pressure profile and temperature estimates	238
Figure 4.55: Converged FCC main fractionator	239
Figure 4.56: Convergence parameters for the inside-out method in Aspen HYSYS	239
Figure 4.57: Initialize Databook from Aspen HYSYS menu	240
Figure 4.58: Aspen HYSYS Variable Navigator.....	241
Figure 4.59: Variable navigator for FCC unit parameters and conditions.....	242
Figure 4.60: Add variables to databook.....	243
Figure 4.61: Select dependent and independent variables for case studies	244
Figure 4.62: Case study setup for feed rate change	245
Figure 4.63: Graphical results from case study	245
Figure 4.64: Tabular results from case study.....	245
Figure 4.65: Effect of feed rate change on product yield change	246
Figure 4.66: Increase feed flow rate for riser outlet temperature case study.....	247
Figure 4.67: Case study setup for riser outlet temperature	248
Figure 4.68: Graphical results from case study	249
Figure 4.69: Tabular results from case study.....	249
Figure 4.70: Product yield as a function of riser outlet temperature	249
Figure 4.71: Creating the DELTA-BASE utility from main application menu bar.....	250
Figure 4.72: Common Model Utility	251
Figure 4.73: Delta Base Utility	251

Figure 4.74: Delta-Base Utility Configuration window	252
Figure 4.75: Scope of Delta-Base utility.....	252
Figure 4.76: Adding specific gravity as an independent variable.....	253
Figure 4.77: All independent variables added to Delta Base Utility	254
Figure 4.78: Adding H2S yield as a dependent variable	254
Figure 4.79: All dependent variables added to Delta-Base Utility	255
Figure 4.80: Perturb independent variables	256
Figure 4.81: Results from Delta Base utility	256
Figure 4.82: PIMS style output for DELTA-BASE vectors	257
Figure 4.83: Renaming variables in Delta Base Utility	258
Figure 4.84: Renamed variables and tags in PIMS interface.....	258
Figure 5.1: Typical CCR Reforming Unit	260
Figure 5.2: Initial Startup of Aspen HYSYS	264
Figure 5.3: Adding a component List	265
Figure 5.4: Importing Reformer Component List.....	266
Figure 5.5: Initial Component list for reforming process	266
Figure 5.6: Select Thermodynamics for Fluid Package.....	267
Figure 5.7: Thermodynamic options for Fluid Package	268
Figure 5.8: Binary interaction parameters for Fluid package	269
Figure 5.9: Refining Reactor Palette.....	270
Figure 5.10: Reformer Icon in Refining Reactors Palette.....	271
Figure 5.11: Initial Reformer Window	271
Figure 5.12: Basic Reformer Configuration	272
Figure 5.13: Reactor dimensions and Catalyst loadings	273
Figure 5.14: Choose Calibration Factors	274
Figure 5.15: Primary Control Window for Reformer	275
Figure 5.16: Reformer Sub-Model Flowsheet	275
Figure 5.17: Feed Data Tab	276
Figure 5.18: Bulk Property Information	277
Figure 5.19: Hold Aspen HYSYS Solver	277
Figure 5.20: Feed Flow Rate Specifications	278
Figure 5.21: Reactor Temperature Specifications	279
Figure 5.22: Catalyst Specifications	280
Figure 5.23: Product Heater Specifications	280
Figure 5.24: Solver Parameters.....	281
Figure 5.25: Main Application Toolbar	282
Figure 5.26: Aspen HYSYS Flowsheet interface	282
Figure 5.27: Reformer results summary	285
Figure 5.28: Reformer yield results	285
Figure 5.29: Reactor performance results.....	286

Figure 5.30: Returning to the main flowsheet	286
Figure 5.31: Composition of Net H2 and Net Liquid streams	287
Figure 5.32: Connect External Streams to Reformer flowsheet	287
Figure 5.33: Feed blending results.....	288
Figure 5.34: Feed re-scaling spreadsheet.....	289
Figure 5.35: Changing from the bulk property data to kinetic lumps.....	290
Figure 5.36: Kinetic Lump composition entry window	291
Figure 5.37: Enter Lump Composition	291
Figure 5.38: Enter Lump Composition (After Normalization).....	291
Figure 5.39: Starting the Reformer Calibration Environment	292
Figure 5.40: Reformer Calibration Environment.....	293
Figure 5.41: Pull Data from model results.....	294
Figure 5.42: Importing initial model solution.....	295
Figure 5.43: Feed composition on weight basis.....	295
Figure 5.44: Reactor Performance Tab	296
Figure 5.45: Completed Reactor Performance Tab	297
Figure 5.46: Product measurement tab	298
Figure 5.47: Initial objective function	299
Figure 5.48: Pre-Calibration in the Reformer Calibration	301
Figure 5.49: Assign Bias.....	302
Figure 5.50: Assign Bias – Select Reformate	303
Figure 5.51: Calibration-Parameters	304
Figure 5.52: Set upper and lower bounds for global activity tuning factors.....	304
Figure 5.53: Calibration Factors-Analysis.....	307
Figure 5.54: Save Calibration Factor Set.....	307
Figure 5.55: Prompt to hold Aspen HYSYS solver	308
Figure 5.56: Verify feed basis for Feed Data.....	309
Figure 5.57: Flowsheet unit operation in Aspen HYSYS palette	310
Figure 5.58: Remixer subflowsheet configuration.....	310
Figure 5.59: Inlet-Outlet connections for Remixer subflowsheet.....	311
Figure 5.60: Subflowsheet for Remixer.....	311
Figure 5.61: Subflowsheet for Recontactor	312
Figure 5.62: Subflowsheet for Recontactor	312
Figure 5.63: Flowsheet for recontacting section.....	313
Figure 5.64: DA301 Preheater	314
Figure 5.65: DA301 Flowsheet.....	315
Figure 5.66: DA301 Configuration.....	315
Figure 5.67: DA301 Specifications.....	316
Figure 5.68: DA302 Flowsheet.....	317
Figure 5.69: DA302 Column configuration.....	317

Figure 5.70: DA302 specifications for aromatic splitter	318
Figure 5.71: Change reactor temperature to WAIT basis	320
Figure 5.72: Menu to create case study through Databook interface	320
Figure 5.73: Variable Navigator for Reformer object	321
Figure 5.74: Databook after adding variables	322
Figure 5.75: Selecting variable types for case study.....	323
Figure 5.76: Case study setup	323
Figure 5.77: Graphical results of case study.....	324
Figure 5.78: Numerical results for case study	325
Figure 5.79: RON as a function of WAIT and H2HC ratio.....	326
Figure 5.80: Aromatic Yield as a function of WAIT and H2HC ratio	326
Figure 5.81: Hydrogen Yield as a function of WAIT and H2HC ratio	327
Figure 5.82: Light Gas Yield as a function of WAIT and H2HC ratio	327

LIST OF TABLES

Table 2.1: Key classes of reactions with general formulas for products and reactants	13
Table 2.2: Survey of related published literature for integrated FCC modeling	21
Table 2.3: Required submodels for a basic simulation of a complete FCC unit	25
Table 2.4: Summary of Aspen HYSYS/Petroleum Refining FCC submodels (Adapted from Ref. 6).....	28
Table 2.5: Summary of 21-lump kinetics (Adapted from Ref. 6).....	32
Table 2.6: Key calibration parameters for FCC model.....	34
Table 2.7: Theoretical stages and efficiency factors for FCC fractionation	37
Table 2.8: Initialization and final specifications.....	40
Table 2.9: Typical distillation curve collected from D-1160.....	41
Table 2.10: Coefficients for paraffin content in petroleum fractions	46
Table 2.11: Coefficients for aromatic content in petroleum fractions	46
Table 2.12: Routinely monitored properties used for model development and calibration.....	53
Table 2.13: Product yield results, AAD = 0.96%	57
Table 2.14: Comparison of LPG composition, AAD = 1.2%	62
Table 2.15: Comparison of Dry gas composition, AAD = 1.8%	63
Table 2.16: Sample base vector with typical yields for a gasoline-maximizing FCC unit.....	78
Table 2.17: BASE and DELTA vectors with typical yields for a gasoline-maximizing FCC unit	79
Table 2.18: Existing DELTA-BASE vectors for FCC unit (normalized to a feed rate of 1.0)....	82
Table 2.19: DELTA-BASE vectors generated using rigorous model.....	83
Table 3.1: Typical reforming feedstock.....	103
Table 3.2: Examples of reactions from key reaction classes	105
Table 3.3: Behavior summary key reaction classes [Adapted from Ref. 6, 7, 8]	107
Table 3.4: Key rate equations from Taskar et al. ^{4,5}	113
Table 3.5: Summary of unit level models reported in literature	118
Table 3.6: Key reactions classes in Aspen HYSYS/Petroleum Refining Catalytic Reformer model	121
Table 3.7: Summary of overall efficiencies for product fractionation in CCR	127
Table 3.8: Key specifications in fractionation section.....	128
Table 3.9: Predicted PNA composition from parameter estimation process	133
Table 3.10: Optimized parameters for PNA beta distribution functions	133
Table 3.11: Major terms and their recommended weighting factors in the reformer model objective function for calibration	141
Table 3.12: Typical adjustment factors to calibrate reformer model.....	142
Table 3.13: Comparison of overall reactor model and plant yields, AAD = 0.85%.....	148
Table 3.14: Comparison of key reactor temperature drop in model and plant values, AAD (Total) = 1.7 °C.....	149

Table 3.15: Comparison of key model and plant yields in the reformate, AAD (Total) = 1.05; AAD (Aromatics) = 0.85	150
Table 3.16: Comparison of LPG composition from model and plant, AAD = 2.0 mol. %	151
Table 3.17: Base yields of aromatic components at various WAIT and H2HC ratio of 3.4	166
Table 3.18: Utility consumption data ^{6, 14}	168
Table 3.19: Reactor inlet temperature deviations	168
Table 3.20: Key model yields for fired duty case study	169
Table 3.21: Reformer yields at various N+2A and C5+ reformate RON from rigorous model	173
Table 3.22: Calculating the DELTA-BASE vectors for the C5+ RON = 102 case.....	174
Table 3.23: Comparison of yield predictions from rigorous model and LP yield model	175
Table 3.24: DELTA-BASE vectors for different RON cases	175
Table 4.1: Summary of liquid feeds and products	186
Table 4.2: Summary of gas flowrates and composition.....	188
Table 4.3: Riser and regenerator operating conditions	189
Table 4.4: Equilibrium catalyst properties.....	189
Table 4.5: Typical range of properties for FCC feed.....	207
Table 4.6: Initial solver output.....	218
Table 4.7: Solver output during calibration run.....	231
Table 4.8: Valid specifications for main fractionator	237
Table 5.1: Feed Properties	260
Table 5.2: Product Composition Profile	261
Table 5.3: DA301 Liquid Product Composition.....	262
Table 5.4: Overall Product Flowrate and yield.....	262
Table 5.5: Reactor Configuration	263
Table 5.6: Initial Solver output	283
Table 5.7: Weighting factors for less strict objective function.....	300
Table 5.8: Suggested activity factors for calibration	305
Table 5.9: Solver output during calibration	305
Table 5.10: Stream specifications for recontactor	313
Table 5.11: Variables for RON case study	321

1. Introduction

1.1 Overview

Petroleum refining continues to be a major contributor in the production of transportation fuels and chemicals. Current economic, regulatory and environmental concerns place significant pressure on refiners to optimize the refining process. New product demands have encouraged refiners to explore many new processing units and feedstocks. Consequently, refiners have invested in many new technologies to control and optimize the refining process.

Despite these changes, refiners still face the same issues as before: selection of crude feedstock on the basis of feasibility and profitability, optimal process conditions for the given feedstock (while meeting refinery constraints) and understanding how changes in a given unit cascade upstream and downstream to other units in the refinery. In the past, refiners have traditionally relied on experienced process operators and guesswork to tackle these issues. This approach is not only unreliable, but the growing tide of retiring industry professionals and prohibitive costs of test runs at the refinery makes it quite unfeasible. Hence, detailed modeling of refinery processes becomes increasingly critical and beneficial.

The primary goal of this work of this work is to present a rational methodology for the modeling of two key catalytic processes in the modern refinery: Fluid Catalytic Cracking (FCC) and Continuous Catalyst Regeneration (CCR) Catalytic Reforming. A rational methodology for modeling balances the demands of detailed kinetic models with the availability of plant data. It is unproductive to develop and use kinetic models that we cannot support using available plant data

for the purposes of refinery modeling and optimization. In this work, we discuss detailed approaches that combine reaction and fractionation units that meet this basis.

A secondary goal of this work is to serve as a guide for developing models for units whose details vary from those presented in this work. Using commercial software, in lieu of customized software, is very beneficial to engineers attempting to replicate the same work. Although we have used Aspen HYSYS from AspenTech, Inc. extensively in this work; much of the workflow described is applicable to other process simulation software or custom software. This guide is very important to ensure that models are used continually throughout the refining lifecycle and can be integrated into the overall workflow of the refinery.

1.2 Issues addressed in this work

We address several key overall issues in refinery modeling in this work:

1. Using existing plant data to build a model without special testing runs
2. Converting plant measurements into data that can be used by rigorous kinetic and fractionation models
3. Calibrating models without losing model rationality, fidelity and predictability while matching plant performance
4. Identify poor operating scenarios and improving process performance
5. Extending the use of rigorous models into refinery production planning

1.3 Original contributions of this work

This work presents several contributions, many of which have not appeared in the literature in conjunction with validated industrial plant data:

1. Detailed models of the entire FCC plant, including the overhead gas compressor, main fractionator, primary and sponge oil absorber, primary stripper and debutanizer columns
2. Process to infer molecular composition required for the FCC kinetic model using routinely collected bulk properties of feedstock
3. Predictions of key FCC liquid product properties not published alongside previous related work (density, D-86 distillation curve and flash point)
4. Case studies showing industrially useful applications of the FCC model
5. Application of the FCC model with an existing linear-programming (LP) based planning tool
6. Use of detailed kinetic model that accounts for coke generation and catalyst deactivation in the catalytic reforming process
7. Complete implementation of a reforming recontactor and reforming primary product fractionation
8. Feed lumping for reforming kinetic models from limited feed information
9. Detailed procedure for reformer kinetic model calibration
10. Industrially relevant case studies that highlight the effects of changes in key process variables in the reforming process
11. Application of the reforming model to refinery-wide production planning through linear programming (LP) models

2. Predictive Modeling of the Fluid Catalytic Cracking (FCC) Process

2.1 Abstract

This work presents the methodology to develop, validate and apply a predictive model for an integrated fluid catalytic cracking (FCC) process. We demonstrate the methodology by using data from a commercial FCC plant in the Asia Pacific with a feed capacity of 800,000 tons per year. Our model accounts for the complex cracking kinetics in the riser-regenerator with a 21-lump kinetic model. We implement the methodology with Microsoft Excel spreadsheets and a commercial software tool, Aspen HYSYS/Petroleum Refining from Aspen Technology, Inc. The methodology is equally applicable to other commercial software tools. This model gives accurate predictions of key product yields and properties given feed qualities and operating conditions. In addition, this work presents the first lumped FCC kinetic model integrated with a gas plant model in the literature. We validate this work using six months of plant data. We also perform several case studies to show how refiners may apply this work to improve gasoline yield and increase unit throughput.

A key application of the integrated FCC model is to generate DELTA-BASE vectors for linear-programming (LP)-based refinery planning to help refiners choose an optimum slate of crude feeds. DELTA-BASE vectors quantify changes in FCC product yields and properties as functions of changes in feed and operating conditions. Traditionally, refiners generated DELTA-BASE vectors using a combination of historical data and correlations. Our integrated model can eliminate guesswork by providing more robust predictions of product yields and qualities.

This work differentiates itself from previous work in this area through the following contributions:

(1) detailed models of the entire FCC plant, including the overhead gas compressor, main fractionator, primary and sponge oil absorber, primary stripper and debutanizer columns; (2) process to infer molecular composition required for the kinetic model using routinely collected bulk properties of feedstock; (3) predictions of key liquid product properties not published alongside previous related work (density, D-86 distillation curve and flash point); (4) case studies showing industrially useful applications of the model; and (5) application of the model with an existing LP-based planning tool.

2.2 Introduction

The current economic, political and regulatory climates place significant pressures on petroleum refiners to optimize and integrate the refining process. The FCC unit is the largest producer of gasoline and light ends in the refinery¹. It plays a critical role in the profitable operation of any refinery. Plant operators can make minor adjustments based on experience to improve the yield and efficiency of the FCC Unit. However, major improvements must come from a concerted effort that involves understanding the reaction chemistry, feed characteristics and equipment performance. In such an endeavor, the use of rigorous simulation models is critical. In particular, rigorous simulation models validated with plant data can identify key areas for process improvements.

There is significant previous work that addresses the issues of process dynamics and control for the integrated FCC unit. We particularly note the efforts by Arbel et al.² and McFarlane et al.³ in this regard. Subsequent authors^{4,5} use similar techniques and models to identify control schemes and yield behavior. However, most of the earlier work uses very a simplified reaction chemistry (yield

model) to represent the process kinetics. In addition, prior work in the literature (to our knowledge) does not connect the integrated FCC model with the complex FCC fractionation system. This work fills the gap between the development of a rigorous kinetic model and industrial application in a large-scale refinery.

2.3 Process Description

The FCC unit is the primary producer of gasoline and olefins in the refinery. Current FCC designs are based on continual improvements and advances in unit and catalyst design since 1940. There are many popular FCC designs in use today and we choose to focus on a UOP FCC unit. The Universal Oil Products (UOP) design includes many features that highlight the unique characteristics of the FCC process. Figure 2.1 shows a general schematic of the FCC unit. We discuss the process flow and unit design in the following section.

2.3.1 Riser-Regenerator Complex

Hot fluidized catalyst (1000 °F+ or 538 °C+) enters the bottom riser through a standpipe where it comes in contact with preheated gas-oil feed. The gas oil feed typically consists of vacuum gas oil (VGO) from the vacuum tower, coker gas oil (CGO) from the delayed coker and recycled products from the FCC main fractionator (Figure 2.2). The heat from the hot catalyst (and any additional steam or fuel gas added in to the standpipe) is sufficient to vaporize the gas oil feed. The components of the vaporized gas oil undergo several reactions over the catalyst surface: hydrocracking, isomerization, hydrogenation/de-hydrogenation, alkylation/de-alkylation, cyclization/de-cyclization and condensation. These reactions result in components that make up the product slate. The products typically present are dry gas (hydrogen, methane, ethane), liquid petroleum gas (propanes, propylene, butanes, butenes), gasoline (up to 430 °F), light cycle oil

(LCO), heavy cycle oil (HCO), slurry or decant oil and coke. Properties of the feed oil and impurities present on the catalyst significantly affect the distribution of products and the operating profile in the riser.

The catalyst travels to the top of the riser carrying heavy components and coke deposits from preceding reactions. The catalyst enters a stripping zone where some steam is added to further crack and remove the heavy hydrocarbons from the catalyst surface. The catalyst then enters the reactor section where a cyclone separates the catalyst from the product vapor. The separated product vapor is sent to the main fractionation column (Figure 2.2) that separates the product into gaseous and liquid products. The separated catalyst is piped into the regenerator where the coke on the catalyst is burned off.

The separated catalyst typically contains about 0.4-2.5% of coke by weight¹. Air and possibly pure oxygen (depending on unit configuration) also enter into the regenerator through additional ports. Fresh makeup coke also enters the FCC plant through additional ports. The coke is mostly oxidized, producing CO₂ and CO as primary products and SO_x and NO_x as secondary products. These flue gas products are typically used in heat-integration loops to provide steam to the plant. The catalyst is typically oxidized to a level containing 0.05% of coke by weight¹. This oxidation also heats the catalyst as it re-enters the riser through the standpipe.

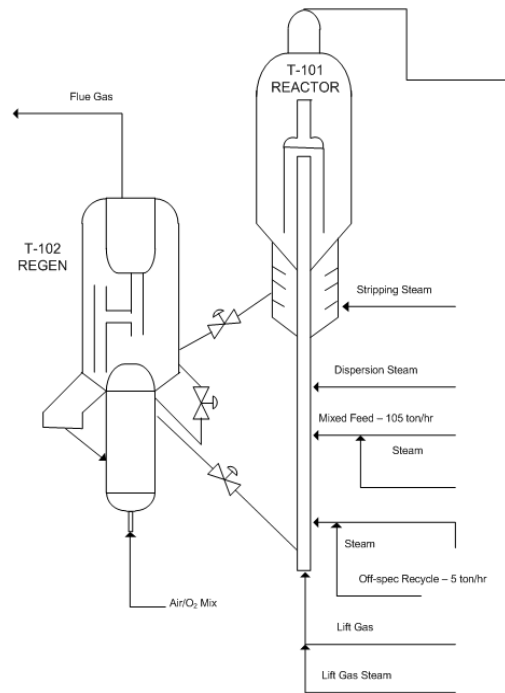


Figure 2.1: General schematic of typical FCC reactor-regenerator unit

2.3.2 Downstream Fractionation

The effluent from the FCC enters the main fractionator with a significant quantity of steam as shown in Figure 2.2. This fractionator separates the reactor effluent into four product groups: Light Gases (C1 – C4), Gasoline (C5+ to 430 °F or 221 °C), Light cycle oil (LCO) and Heavy cycle oil (HCO) (430 °F to 650 °F, or 221 °C to 343 °C) and Slurry/Decant oil (650+ °F or 343+ °C). The temperature range of these products varies in different refineries (or different operating scenarios in the same refinery) depending on product demand and current operating constraints. There are several pumpharounds associated with the main fractionator that help control the product distribution and temperature profiles. Most of the products from the main fractionator cannot be sent directly into the refinery’s product blending pool. Additional fractionation and product

isolation occurs in the gas plant associated with the FCC unit as shown in Figure 2.3. The overhead vapor contains some C5 components which must be recovered in the product gasoline. A portion of the LCO product is drawn off as sponge oil to recover gasoline in a sponge oil absorber. The liquid from the overhead condenser flows to the primary absorber where C3-C4 components are recovered.

There is significant value in separating and isolating the C3-C4 components. These components may be sold as LPG or serve as a valuable feedstock for other petrochemical processes. The FCC gas plant is responsible for the separation of C3-C4 components and stabilization of gasoline. The stabilization of gasoline refers to controlling the amount C4 components present in the product gasoline.

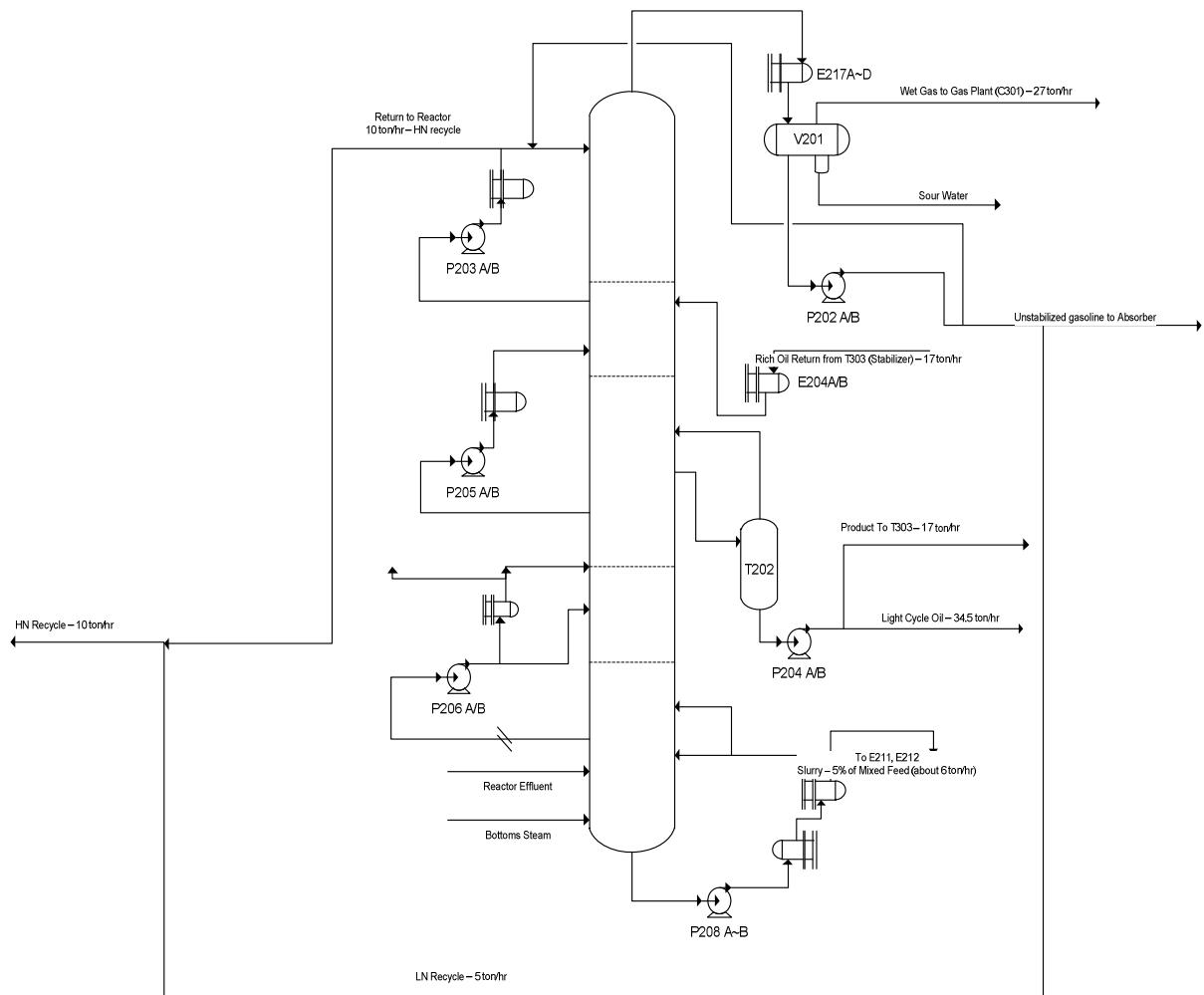


Figure 2.2: Downstream fractionation (Main fractionator)

The overhead vapor from the main fractionation column enters the wet gas compressor train. The vapor leaving the compressor train then enters a high-pressure flash system. The vapor from the high-pressure flash enters the primary absorber. The C5 components leave with the bottom product from the primary absorber. This bottom product reenters the high-pressure flash. The overhead vapor product enters a sponge oil absorber where it is contacted with LCO drawn off from the main fractionator. The overhead products of the sponge oil absorber are H₂, C₁ and C₂

components that can serve as feeds to meet the refinery's energy demands. The bottoms product from the sponge oil absorber is recycled back to the main fractionator.

The liquid product from the high-pressure flash enters the primary stripping column. The overhead product from the stripping column consists mainly of C2 components. This product is recycled back to the high-pressure flash. The bottom product from the column consists mainly of C3-C4 components and gasoline. This product enters the primary stabilizer (sometimes called a debutanizer), which separates most of the C3-C4 components into the overhead liquid. The stabilized gasoline (containing a regulated amount of C4) leaves as the bottom product.

Some FCC gas plants further separate the gasoline product leaving the stabilizer into heavy and light gasoline. We do not include additional gasoline splitting in this work. In addition, most plants contain a water wash or injection system to control the presence of acidic compounds that lead to corrosion. This water injection typically occurs between the stages of the overhead wet gas compressor. Most of this water leaves the process flow before entering the columns of the gas plant. This water wash has little effect on the overall simulation of the process, so we do not include it in this work.

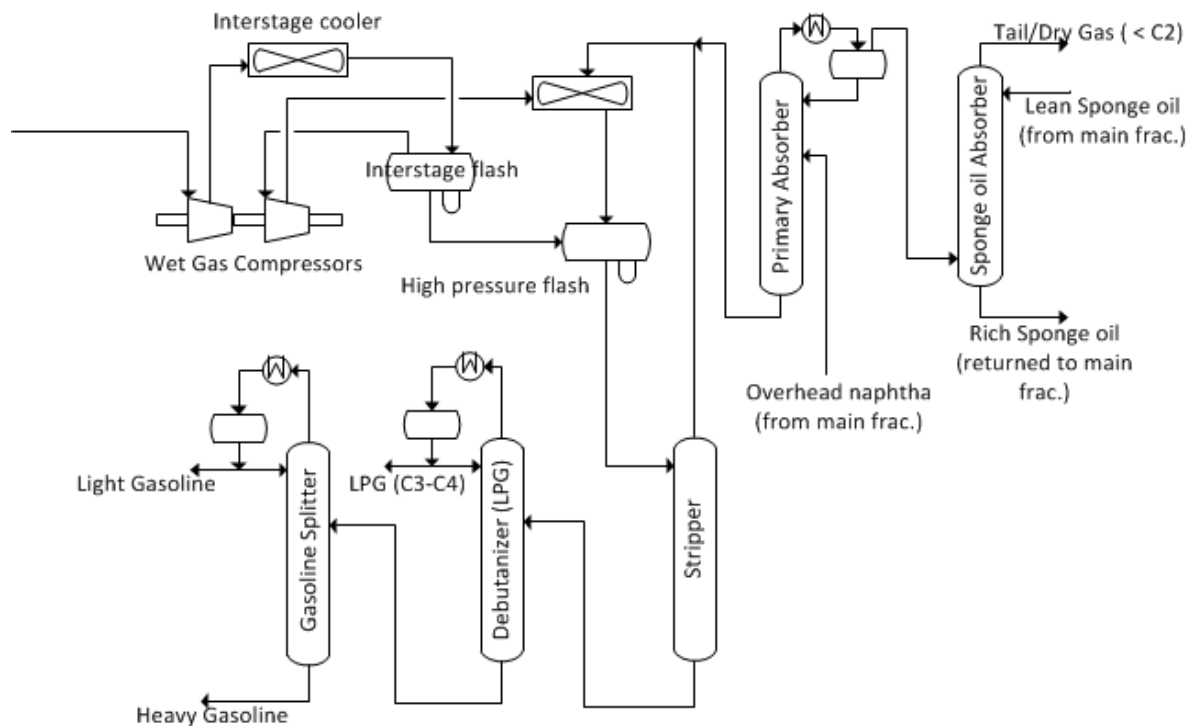


Figure 2.3: FCC gas plant section

2.4 Process Chemistry

The feed to the FCC unit is a complex mixture consisting of long chain paraffins, single and multiple ring cycloalkanes and large aromatic compounds. It is impossible to list every reaction that each individual molecule undergoes in the FCC riser. However, we can place each of the reactions into five different classes based on the type of reactants and products, effect on catalyst activity and contributions to product slate. In general, catalytic cracking occurs through formation of a carbocation (from feed hydrocarbon molecule) in conjunction with a catalyst acid site. This carbocation may then undergo cracking (to produce smaller molecules), isomerization (to rearrange molecules) and hydrogen transfer (to produce aromatic compounds). Table 2.1 gives a

simplified overview of key classes of reactions and the general formulas for reactants and products.

The most significant classes of reactions are cracking (reaction class 1), isomerization (reaction class 2) and hydrogen transfer (reaction class 3)^{1, 6, 7}. The remaining classes are undesirable and contribute to hydrogen or coke production. The acid-catalyzed cracking reactions from Reaction Class 1 form the primary pathway for light gas and LPG (C3-C4) components and the long-chain paraffin components of diesel. These reactions also provide some of the lighter aromatic components present in the products. When catalytic conditions are not present (e.g., contaminated /occluded catalyst or high temperatures), a thermal cracking process takes over, promoting lower-order cracking reactions. These lower-order cracking reactions tend to produce very large amounts of dry gas components (C1, C2) and result in higher coke production^{1, 6}. In addition, excessive thermal cracking is not an economically attractive operating scenario.

Isomerization reactions (reaction class 2) give an important pathway for high-octane components in the gasoline. This class of reactions is critical for producing high-octane components in the gasoline products. In addition, we find more valuable iso-butene components due to the isomerization of butanes. The iso-paraffins from the isomerization class of reactions also reduce the cloud point of the diesel product¹.

Table 2.1: Key classes of reactions with general formulas for products and reactants

<u>Reaction class 1: Cracking</u>	
<i>Description</i>	<i>General reaction formula for reactants and products</i>
Paraffin cracked to olefins	$C_{m+n}H_{2[(m+n)+2]} \rightarrow C_mH_{2m+2} + C_nH_{2n+2}$

and smaller paraffins	
Olefins cracked to smaller olefins	$C_{(m+n)}H_{2(m+n)} \rightarrow C_mH_{2m} + C_nH_{2n}$
Aromatic side-chain scission	$Ar-C_{(m+n)}H_{2(m+n)+1} \rightarrow Ar-C_mH_{2m-1} + C_nH_{2n+2}$
Naphthenes (cycloparaffins) cracked to olefins and smaller naphthenes	$C_{(m+n)}H_{2(m+n)}$ (Naphthene) $\rightarrow C_mH_{2m}$ (Naphthene) + C_nH_{2n} (Olefin)
<u>Reaction class 2: Isomerization</u>	
Olefin bond shift	$x-C_nH_{2n} \rightarrow y-C_nH_{2n}$ (x and y are different locations of the olefin)
Normal olefin to iso-olefin	$n-C_nH_{2n} \rightarrow i-C_nH_{2n}$
Normal paraffins to iso-paraffin	$n-C_nH_{2n+2} \rightarrow i-C_nH_{2n+2}$
Cyclo-hexane to Cyclo-pentane	C_6H_{12} (Naphthene) $\rightarrow C_5H_9-CH_3$ (Naphthene)
<u>Reaction class 3: Hydrogen transfer</u>	
Paraffins and olefins converted to aromatics and	C_nH_{2n} (Naphthene) + C_mH_{2m} (Olefin) $\rightarrow ArC_xH_{2x+1}$ (Aromatic) + C_pH_{2p+2} (Paraffin)

paraffins	(where $x = m + n - 6 - p$)
<u>Reaction class 4: Dehydrogenation and dealkylation (contaminated catalyst)</u>	
Metals catalyzed aromatic and light hydrocarbon production	$i-C_nH_{2n-1} + C_mH_{m-1} \rightarrow Ar + C_{(n+m-6)}H_{2(n+m-6)}$ $n-C_2H_{2n+2} \rightarrow C_nH_{2n} + H_2$
<u>Reaction class 5: Aromatic ring condensation</u>	
Condensation of single aromatic cores to produce multiple ring aromatic cores	$Ar-CHCH_2 + R_1CH-CHR_2 \rightarrow Ar - Ar + H_2$

Hydrogen-transfer reactions (reaction class 3) form a class of reactions that improves gasoline yield and stability (by lowering olefin content), but also lower the overall octane rating of the product. These reactions produce paraffins and aromatics that have low octane ratings. In addition, we cannot recover the olefins consumed by hydrogen transfer reactions in the LPG or the light ends of gasoline⁸.

Dehydrogenation (reaction class 4) is a result of the presence of metals such as nickel and vanadium on the catalyst. The metal sites on the catalyst promote dehydrogenation and dealkylation. These reactions tend to produce large amounts of H₂ and paraffin components with low octane ratings. The coking process follows a complicated series of reactions that include olefin polymerization and aromatic ring condensation (reaction class 5). The coking reactions dominate

when the unit is operating at a non-optimal temperature (typically less than 850 °F or 454 °C, or greater than 1050 °F or 566 °C) or when feed contains significant amounts of residue, recycled coke or olefins⁸.

2.5 Literature Review

We can divide the literature on FCC modeling into two categories: kinetic and unit-level models. Kinetic models focus on chemical reactions taking place within the riser or reactor section of the FCC unit, and attempt to quantify the feed as a mixture of chemical entities to describe the rate of reaction from one chemical entity to another. In contrast, unit-level models contain several submodels to take into account the integrated nature of modern FCC units. A basic unit-level model contains submodels for the riser/reactor, regenerator and catalyst transfer sections. The riser requires a kinetic model to describe the conversion of chemical entities. The regenerator contains another kinetic model to describe the process of coke removal from the catalyst. The unit-level model also captures the heat balance between the riser and the regenerator.

2.5.1 Kinetic Models

We classify kinetic models according to the chemical entities that makeup the model. Typically, the entities or “lumps” are boiling point lumps or yield lumps, grouped chemical lumps and full chemical lumps. Early kinetic models consist entirely of yield lumps, which represent the products that refiner collects from the main fractionator following the FCC unit. Figure 2.4 shows a typical kinetic model based on yield lumps by Takatsuka et al.⁹ Many similar models have appeared in the literature. The models differentiate themselves based on their number of lumps. Models may contain as few as two¹⁰ or three lumps¹¹ and as many as fifty lumps¹². We note that models with more lumps do not necessarily have more predictive capabilities than models with fewer lumps⁶.

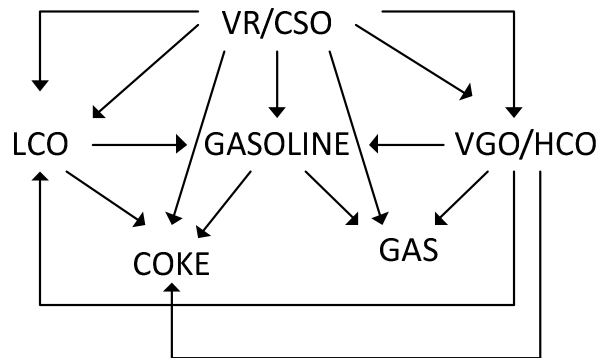


Figure 2.4: Lumped model from Takatsuka et al.⁹ : VR= Vacuum Residue, CSO = Coke Slurry Oil, HCO = Heavy cycle oil and LCO= Light cycle oil.

The next class of kinetic models considers both chemical type lumps and boiling point or yield lumps. For example, Jacob et al.¹³ present a popular 10-lump model (shown in Figure 2.5) that includes coke and light ends (C), gasoline (G, C5-221 °C), light paraffin P_l, heavy paraffin P_h, light naphthene N_l, heavy naphthene N_h, light aromatics A_l, heavy aromatics A_h, light aromatic with side chains CA_l, and heavy aromatic with side chains CA_h. The “l” subscript refers “light” lumps in the boiling point range between 221 °C and 343 °C, whereas the “h” subscript refers to “heavy” lumps that have boiling point above 343 °C.

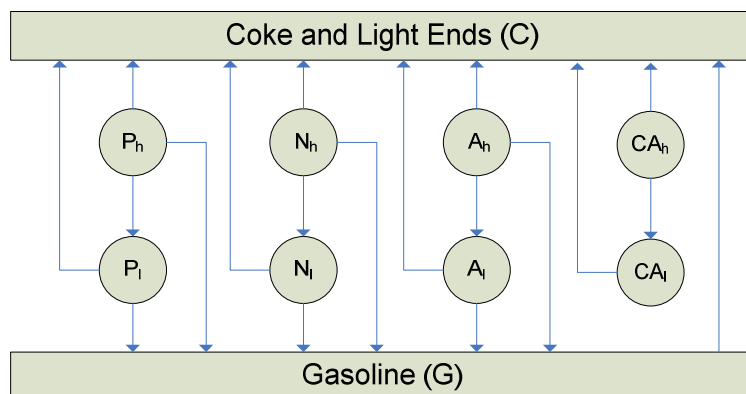


Figure 2.5: Ten-lump model from Jacob et al.¹³

The key advantage of this lumped kinetic model is that the composition of lumps can be measured with various experimental techniques. In addition, the rate constants that arise from the use of this model are less sensitive to changes in feed and process conditions¹⁴. This model has served as the basis for models that include more chemical types. Pitault et al.^{15,16} have developed a 19-lump model that includes several olefin lumps. AspenTech^{17,18} has developed a 21-lump model to address heavier and more aromatic feeds, which we will use to model the reaction section of the FCC unit. We discuss this 21-lump model in a subsequent section.

Hsu et al.⁶ state that “lumped kinetic models developed by the top-down route have limited extrapolative power.” To remedy this situation, many researchers have developed complex reaction schemes based on chemical first principles that involve thousands of chemical species. We can classify them into *mechanistic* models and *pathway* models. Mechanistic models track the chemical intermediates such as ions and free radicals that occur in the catalytic FCC process. Transition state theory helps in quantify the rate constants involved in adsorption, reaction and desorption of reactant and product species from the catalyst surface. Froment and co-workers¹⁹ have pioneered the use of such models in a refinery context and have developed a model for catalytic cracking of vacuum gas oil (VGO). Hsu et al.⁶ claim that using this method is challenging because of its large size and reaction complexity.

Structure-oriented lumping (SOL) is a leading example of the pathway-based models. Quann and Jaffe^{20, 21, 22} have developed a unique method for tracking molecules in the feed oil. The method tracks different compositional and structural attributes of a molecule (number of aromatic rings, number of nitrogen substituents, sulfur substituents, etc.) in a vector format. Figure 2.6 shows typical vectors for some sample molecules.



A6	A4	A2	N6	N5	N4	N3	N2	N1	R	br	me	IH	AA	NS	RS	AN	NN	RN	NO	RO	KO	
1	0	0	0	0	0	0	0	0	0	0	0	0	0	0	0	0	0	0	0	0	0	0



A6	A4	A2	N6	N5	N4	N3	N2	N1	R	br	me	IH	AA	NS	RS	AN	NN	RN	NO	RO	KO	
1	1	0	0	0	0	0	0	0	0	0	0	0	0	0	0	0	0	0	0	0	0	0

Figure 2.6: Typical SOL Lumping (From Ref. 20)

After developing these vectors for the feed oil, several rules are used to generate reactions paths that convert the feed vectors to product vectors. The rate constants and activation energies for these reactions are functions of the reaction type and the feed oil composition vector. Christensen et al.²³ discuss applying the SOL method to develop a FCC kinetic model, which contains over 30,000 chemical reactions and 3000 molecular species. The resulting model can accurately predict product yields, composition and quality over a wide range of operating conditions. Klein and co-workers²⁴ have also developed similar models for FCC and catalytic reforming.

Figure 2.7 compares these kinetic models on the basis of complexity and model fidelity. The yield lump models have the lowest complexity and require the least amount of data. Typically, the feed may be treated as a single lump and there are few reaction rates to calibrate. Chemical lumps require knowledge of chemical type of the lump, namely, the paraffin, naphthene and aromatic (PNA) content of each boiling point range. Pathway and mechanistic models require the detailed analysis of the feed data to develop molecular representation. Additionally, pathway and mechanistic models require more data to calibrate the numerous kinetic parameters⁶.

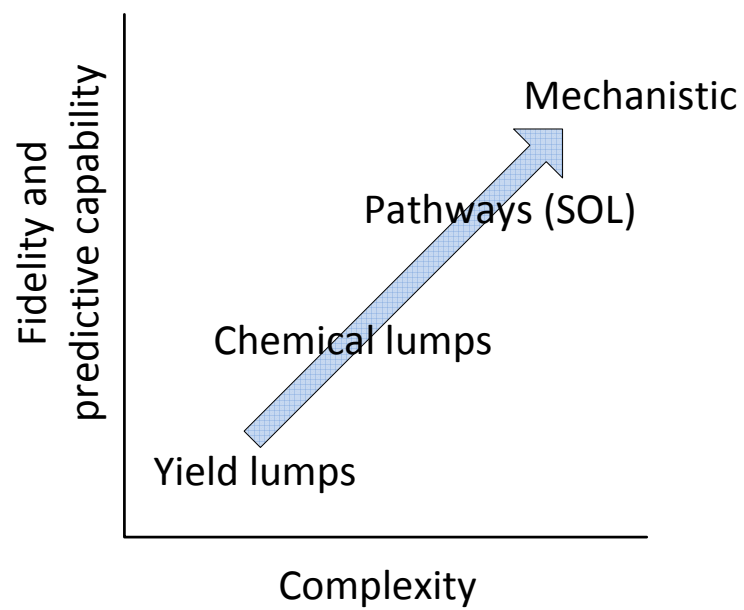


Figure 2.7: Summary of kinetic models

Table 2.2: Survey of related published literature for integrated FCC modeling

Reference	Application	Kinetics	Property predictions	Fractionation modeling	Validation data	Integration with production planning
Lee et al. ¹⁰ (1985)	Dynamic/Process Control	3 – Lump	None	None	None	None
McFarlane et al. ³ (1993)	Dynamic/Process Control	2 – Lump	None	None	None	None
Arbel et al. ² (1995)	Dynamic/Process Control	10 – Lump	None	None	Literature	None
Khandalekar et al. ⁵ (1995)	Dynamic/Process Control	3 – Lump	None	None	Literature	None
Kumar et al. ²⁵ (1995)	Steady state	10 – Lump	None	None	Literature	None
Chitnis et al. ⁴ (1998)	Dynamic/Online optimization	4 – Lump	None	None	Literature	None

Ellis et al. ²⁶ (1998)	Dynamic/Process Control	10 – Lump	Light gas composition (C1 – C4), RON/MON of gasoline products	None	Literature	None
Secchi et al. ²⁷ (2001)	Dynamic	10 – Lump	None	None	Industrial (Dynamic)	None
Mo et al. ²⁸ (2002)	Steady state/Online optimization	NA	Extensive properties of all key products	None	Industrial, pilot plant and experimental	
Elnashaie et al. ²⁹ (2004)	Steady state	3 – Lump	None	None	Industrial	None
Rao et al. ³⁰ (2004)	Steady state	11 – Lump	None	None	Industrial	None
Arajuo-Monroy et al. ³¹ (2006)	Steady state	6 – Lump	Light gas composition	None	Industrial	None
Bollas et al. ³² (2007)	Dynamic/Pilot plant process control	2 – Lump	None	None	Pilot plant	None

Fernandes et al. ³³ (2008)	Steady state/Dynamic	6 – Lump	None	None	Industrial	None
Shaikh et al. ³⁴ (2008)	Steady state	4 – Lump	None	None	Pilot plant	None
This work	Steady state	21 – Lump	Light gas composition, Flash point, density of key products and RON/MON	Main Fractionator, and associated gas plant	Industrial	Export model to LP-based planning tool

Note: RON/MON = Research Octane Number/Motor Octane Number.

2.5.2 Unit-level Models

Table 2.2 compares a selection of published work (after 1985) regarding modeling of an entire FCC unit. This table does not include work that only compares the performance of the riser with experimental or plant data. It includes work where the authors compare the predictions of the entire FCC unit model to published data, experimental data, or plant data. The work by Lee et al.¹⁰, McFarlane et al.³ and Arbel et al.² provide the basis for many dynamic and process control related models by later authors. These studies focus on optimal control strategies and the dynamic response of the FCC unit. There are few papers that compare the steady-state operation of the FCC unit with detailed predictions of yield and product properties with data. Notably, the work Fernandes et al.³³ follows an industrial FCC unit over course of three years and gives good predictions of the unit's performance. However, this work does not include any detailed predictions of product quality and composition. Additional work by Fernandes et al.³⁵ shows how feed and operating conditions such as coke composition, catalyst-to-oil ratio, concarbon residue (CCR) in feed, air-to-oil ratio and regenerator combustion modes can induce multiple steady-states with implications for a general unit control strategy.

A complete unit-level model for a FCC unit includes several submodels of varying degrees of rigor. A modern FCC unit involves complex kinetic, heat management and hydrodynamic issues. Necessarily, researchers develop models that focus on particular aspects of FCC operation. There is significant research³⁶ on the topic of complex hydrodynamics in the riser and regenerator sections using computational fluid dynamics (CFD). These models often require detailed information about the process that is proprietary. The focus of this paper is developing a model to predict key process output variables such as product yields, product properties and operating

profiles of the FCC unit and associated gas plant. We acknowledge that the hydrodynamics and complex kinetics have significant effects on these out variables¹. However, our goal is to develop a model that engineers can use and modify based on limited process data.

Arandes et al.³⁷ and Han et al.³⁸ summarize the key submodels required for a unit-level model that can provide necessary simulation fidelity for this work. We briefly summarize these submodels in Table 2.3, and refer readers to these two papers for detailed equations and additional references.

Table 2.3: Required submodels for a basic simulation of a complete FCC unit

Submodel	Purpose	Unit operation
Riser reactor	Crack feed species to product species	Plug-flow reactor (PFR) operating under pseudo-steady conditions Catalyst activity decay to due to coke formation as result of time on stream, coke on catalyst and catalyst type
Stripper	Remove of adsorbed hydrocarbons on the catalyst	Continuously stirred-tank reactor (CSTR) with well-mixed model
Regenerator	Combust coke present on the catalyst	Stoichiometric or partial combustion of coke

		Bubbling bed reactor with a dense phase and a dilute phase
Feed vaporizer	Vaporize the feed species for input into the riser model	Heater with associated two-phase flash
Valves	Control the flow and pressure drop from the riser/reactor section to regenerator section	Typical valve Eqs. based on pressure drop across the valve
Cyclones	Separate solids from the hydrocarbon and effluent vapors	Simple component splitter

Modern FCC units and catalyst have very high conversions in the riser section. The conversion of feed species to product species completes within the riser, so we require no additional sections for feed conversion. There are units where feed conversion may occur in locations other than the riser^{39,40}, but we have chosen to limit our discussion to the most common type of unit.

2.6 Aspen HYSYS/Petroleum Refining FCC Model

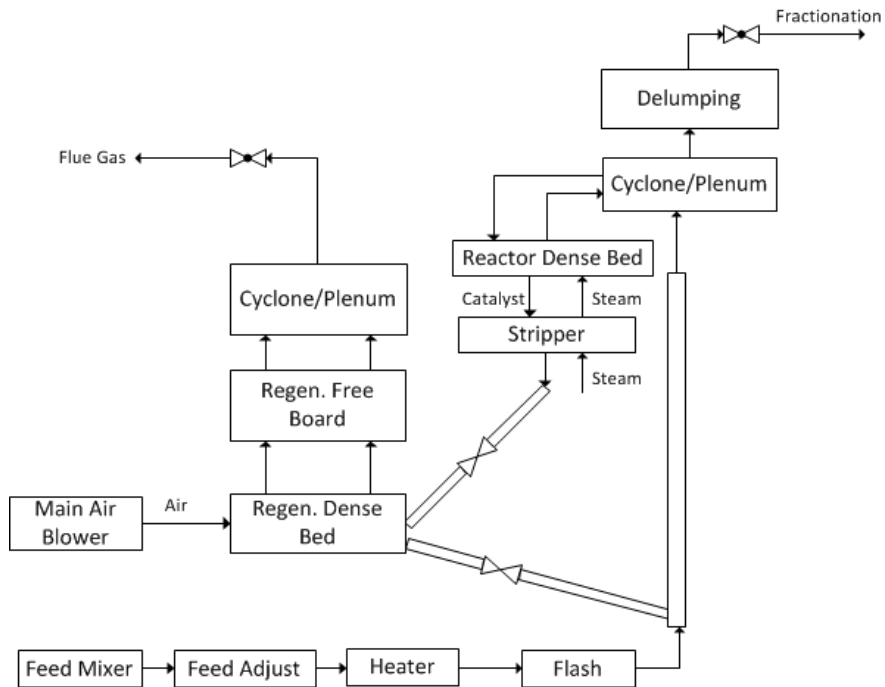


Figure 2.8: Overview of the major submodels that make up the Aspen HYSYS/Petroleum Refining FCC model (Adapted from Ref. 6)

The Aspen HYSYS/Petroleum Refining FCC model relies on a series of submodels that can simulate an entire operating unit while satisfying the riser and regenerator heat balance. Note that the configuration is similar to the minimum submodels listed in Table 2.3 of the previous section. We summarize Aspen HYSYS/Petroleum Refining submodels in Table 2.4 and highlight some key features in subsequent sections.

Table 2.4: Summary of Aspen HYSYS/Petroleum Refining FCC submodels (Adapted from Ref. 6)

Submodel	Purpose	Unit operation	Considerations
Riser (More than one can be present)	Convert feed to product species using 21-lump kinetics	Modified PFR	<p>Allows any angle of inclination</p> <p>Pressure drop is a combination of pressure drop due to solid and vapor phases</p> <p>Catalyst activity decay to due kinetic and metal coke on catalyst</p> <p>Slip factor correlations (difference between vapor and solid velocities) to estimate specie density</p>
Reactor/Stripper	Complete feed conversion and remove adsorbed hydrocarbons	Bubbling bed reactor with two phases	Switches to fluidized - bed reactor model for units with low catalyst

			holdup
Regenerator	Combust coke present on catalyst	Bubbling bed reactor with two phases	Kinetic models for coke combustion with air and enriching oxygen ⁴¹
Regenerator freeboard	Complete combustion of coke	Simple plug-flow reactor	Additional kinetics to match behavior of industrial units ⁴²
Cyclones	Separate solids from hydrocarbon and effluent vapors	Two-phase, pressure drop calculation	Pressure drop is a combination of pressure drop due to solid and vapor phases
Delumper	Converts lumped composition into set of true boiling point (TBP) pseudo-components suitable for fractionation	-	Carries chemical information about the kinetic lumps as an attribute of the pseudocomponent Additional delumping of light gas into C1-C4 components using known kinetics ⁴³

2.6.1 Slip factor and average voidage

An important concern in FCC riser submodels is how to calculate the slip factor, φ , and the average voidage, ϵ , of the riser. The slip factor is simply defined as the ratio between gas velocity and catalyst particle velocity. The slip factor plays an important part in determining the residence time of reactions, and thus, affects the overall conversion in the riser. Harriot describes a slip factor range of 1.2 to 4.0 for most FCC risers but also indicates that there is no reliable correlation available for prediction⁴⁴. Previous authors have used a variety of approaches including constant slip factor⁴⁵, multiple slip factors⁴⁶ and correlations⁴⁷. An alternative approach is to include additional momentum balance equations for the gas phase and catalyst phase⁴⁸. This approach allows users to calculate velocity profiles for each phase and the overall pressure drop in the riser directly.

Aspen HYSYS uses a custom correlation based on fully-developed flow (away from the catalyst particle acceleration zone) that accounts for various angles of riser inclination. We present a similar correlation from Bolkan-Kenny et al.⁴⁷ in Eq. (1) using dimensionless Froude numbers, Eqs. (2)-(3). This correlation is essentially a function of riser diameter, D ; gravitational constant, g ; superficial gas velocity, u_o and u_t , terminal settling velocity of the catalyst particle.

$$\varphi = 1 + \frac{5.6}{Fr} + 0.47Fr_t^{0.41} \quad (1)$$

$$Fr = \frac{u_o}{\sqrt{gD}} \quad (2)$$

$$Fr_t = \frac{u_t}{\sqrt{gD}} \quad (3)$$

2.6.2 21-Lump Kinetic Model

The 21-lump kinetic model in Aspen HYSYS/Petroleum Refining is similar to the popular 10-lump model from Jacob et al.¹³ (Figure 2.5). The 21-lump model follows the same basic structure and pathways as the 10-lump model by grouping lumps into boiling point ranges and chemical types within each boiling point range. In addition, the 21-lump model includes a boiling point range to deal with heavy feeds (boiling point greater than 510 °C) that the original 10-lump model cannot handle. To account for the differences in reactivity of various aromatic compounds, aromatic lumps are further split into lumps containing side chains and multiple rings separately. The 21-lump model also splits the original single lump for coke into two separate coke lumps. These separate lumps account for coke produced from cracking reactions (called kinetic coke) and coke produced from metal activity (called metal coke) individually. We note that the rate equations in the kinetic network in Aspen HYSYS/Petroleum Refining are largely similar to equations in the first-order network for 10-lump model. However, the rate equations

in the 21-lump model include additional terms to account for the adsorption of the heavy hydrocarbons (due to the extended boiling point range of the lumps) and the metal activity of the catalyst. Table 2.5 lists the kinetic lumps used in the 21-lump model.

Table 2.5: Summary of 21-lump kinetics (Adapted from Ref. 6)

Boiling point range	Lumps
< C5	Light gas lump
C5 – 221 °C	Gasoline
221 – 343 °C (VGO)	Light paraffin (PL) Light naphthene (NL) Light aromatics with side chains (ALs) One-ring light aromatics (ALr1) Two-ring heavy aromatics (ALr2)
343– 510 °C (Heavy VGO)	Heavy paraffin (PH) Heavy naphthene (NH) Heavy aromatics with side chains (AHs) One-ring heavy aromatics (AHr1) Two-ring heavy aromatics (AHr2) Three-ring heavy aromatics (AHr3)
510+ °C (Residue)	Residue paraffin (PR) Residue naphthene (NR) Residue aromatics with side chains (ARs) One- ring Residue aromatics (ARr1) Two-ring Residue aromatics (ARr2)

	Three-ring Residue aromatics (ARr3)
Coke	Kinetic coke (produced by reaction scheme) Metal coke (produced by metal activity on catalyst)

We can obtain the lump composition of the feedstock directly via GC/MS, ^1H NMR, ^{13}C NMR, HPLC and ASTM methods. However, this is infeasible on a regular basis for refineries given the changing nature of the feedstock. Aspen HYSYS/Petroleum Refining includes a method that uses existing feed analysis to infer feed composition using routinely collected data. . However, we have developed an alternative scheme to infer feed composition. We detail this method in Section 8.

2.6.3 Catalyst Deactivation

Another important consideration in the FCC unit model is the deactivation of catalyst as it circulates through the unit. Previous work has used two different approaches to model catalyst activity: time-on-stream and coke on catalyst⁴⁹. Since the 21-lump includes discrete lumps for the kinetic and metal coke, this work uses a coke on catalyst approach to model catalyst deactivation. In addition, this work includes a rate equation in the kinetic network for coke balance on the catalyst. The general deactivation function due to coke, ϕ_{COKE} , is given by Eq. (4).

$$\phi_{COKE} = \phi_{KCOKE} \phi_{MCOKE} = \exp(-a_{KCOKE} C_{KCOKE}) \exp(-a_{MCOKE} C_{MCOKE} f(C_{METALS})) \quad (4)$$

where a_{KCOKE} is the activity factor for kinetic coke, a_{MCOKE} is the activity factor for metal coke, C_{KCOKE} is the concentration of kinetic coke on the catalyst, a_{MCOKE} is the activity factor for metal coke, C_{MCOKE} is the concentration of metal coke on the catalyst and C_{METALS} represents the concentration of metals on the catalyst.

2.7 Calibrating the Aspen HYSYS/Petroleum Refining FCC Model

Given the variety of feedstock that the FCC unit processes, it is unlikely that a single set of kinetic parameters will provide accurate and industrially useful yield and property predictions. In addition, changes in catalyst may significantly alter the yield distribution. Therefore, it is necessary to calibrate the model to a base scenario. Table 2.6 lists the key calibration parameters for the FCC model. We group them by their effects on the model predictions.

Table 2.6: Key calibration parameters for FCC model

Parameter class	Calibration parameters
Overall reaction selectivity	Selectivity to C (Coke lump) Selectivity to G (Gasoline lump) Selectivity to L (VGO lump)
Distribution of light gas components (C1 – C4)	Selectivities to C1-C4 light gases
Deactivation	Factors accounting for the metals content and activity of the equilibrium catalyst (ECAT)
Equipment and process conditions	Activity for CO/CO ₂ generation from coke combustion in the regenerator

Aspen HYSYS/Petroleum Refining includes a base set of kinetic and calibration parameters regressed for a variety of feed oils and catalyst types. We use these as a starting point to calibrate the model to our specific operating scenario. Because of the chemical nature of the feed lumping, the calibration process results in only small changes in the values of calibration parameters. Significant changes from the base values may result in “overcalibration” and fix the model to a particular operating point. An “overcalibrated” model gives poor predictions even when we make small changes to input variables. It is critical to keep track of these changes in the calibration factors and make sure they are reasonable. The key steps in the calibration process are:

1. Obtain a base or reference set of operating data that fully defines the operation of the FCC unit and associated product yields. Table 2.12 lists the relevant data used for calibration in this work.
2. Use experimentally measured chemical composition of liquid products (or estimate using the methods given in Section 8) to calculate the expected effluent composition of kinetic lumps from FCC unit.
3. Vary the reaction selectivities for reaction paths (3 parameters) that lead to coke lumps (kinetic Coke and metal coke), Gasoline (G lump) and VGO (PH, NH, AHs, AHr1, AHr2 and AHr2 lumps); Deactivation activity factors (2 parameters) and coke burn activity (1 parameter) so that model predictions for kinetic lump compositions agree with measured (or estimated) kinetic lump compositions from step 2.
4. Vary the distribution selectivities (minimum 2 parameters – ratio between C1 and C2 and ratio between C3 and C4) for light gases to match total measured light gas composition from the dry gas and LPG stream of the refinery.

5. Once calibration is complete, verify that overall material and energy balances hold.

In Aspen HYSYS, we can modify the parameters in steps 3 and 4 concurrently to simplify the calibration process. We note that if the initial kinetic parameters have been regressed from a multiple variety of sources, small adjustments to calibration parameters are enough to match typical plant operation. In our work, the range of calibration parameters is roughly on the order of 0.5-1.5 times the initial calibration parameter values.

2.8 Fractionation

The fractionation sections use standard inside-out methods⁵⁰ implemented by many popular simulators including Aspen HYSYS. This method offers robust convergence and wide flexibility in specifications. The key issue in implementing fractionation models is whether to use stage efficiencies. Readers should be careful to avoid confusion with a related concept: overall efficiency. Overall efficiency refers to the ratio of theoretical stages used in simulations to physical stages in the actual column. For example, consider the case where we model a distillation column having 20 physical stages with simulator using only 10 theoretical stages. This column has overall efficiency of $10/20 = 0.50$. Note that each stage in the simulation operates under valid thermodynamic vapor-liquid equilibrium assumptions.

Alternatively, many simulators offer stage efficiency models under the name Murphree stage efficiency given by E in the following equation:

$$E = \frac{y_n - y_{n+1}}{y_n^* - y_{n+1}} \quad \text{or} \quad \frac{x_n - x_{n+1}}{x_n^* - x_{n+1}} \quad (5)$$

where x_n represents mole fraction of a given component in the liquid leaving stage n , x_{n+1} represents mole fraction of a given component in the liquid leaving stage $n+1$. The y_n and y_{n+1} refer to the vapor mole fraction of a given component leaving as vapor from stages n and $n+1$.

The E factor violates vapor-liquid equilibrium constraints and can predict unusual and unphysical solutions for stage-by-stage simulation models. Both Kister⁵⁰ and Kaes⁵¹ advise against the use of the stage efficiency models. They warn that simulations using these factors may lose predictive abilities and may not converge robustly. In our work, we use the rigorous stage-by-stage models for all fractionators with the overall efficiency concept. Kaes⁵¹ has documented the relevant overall efficiencies that are reasonable for modeling columns in the FCC gas plant. Table 2.7 shows the number of theoretical stages and efficiencies for FCC fractionation. We obtain the overall efficiency as the ratio of number of theoretical stages to actual physical stages in the column. For example, the main fractionator column typically has 30 to 40 physical stages and we find that 12 to 16 theoretical stages are sufficient for modeling purposes. Hence, the overall efficiency ranges from about 40% - 50%. We calculate overall efficiencies for other columns given in Table 2.7 using a typical range for the number of physical stages from various process design data.

Table 2.7: Theoretical stages and efficiency factors for FCC fractionation

Fractionator	Theoretical stages	Overall efficiency
Main Fractionator	12 – 16	40% - 50%
Primary absorber	6 – 10	20% - 30%
Primary stripper	12 – 15	40% - 50%
Secondary absorber	3 – 6	20% - 25%

Gasoline stabilizer	25 – 30	75% – 80%
LPG (C3/C4) splitter	25 – 30	75% - 80%

We can actually develop the initial model for the fractionation without connecting it to the FCC model. Here, we follow the process of “back-blending” as shown in Figure 2.9 to recover the reactor effluent (or fractionator feed) from a known set of product yield data⁵¹. This process requires that we know the yields and composition of all the key products from the FCC plant, the feed rate to the reactor and additional inputs (such as steam) to the reactor. We then use the composition data of the light products and the distillation curves of the liquid products to reconstruct a reactor effluent as the fractionator feed. We feed this effluent into the initial fractionation model and recover the products that are “back-blended”. There are two advantages to this process. First, we can verify that the fractionation model accurately reflects plant operation. We verify the fractionation model through accurate predictions of product yields, good overlap between plant and model distillation curves of liquid products, agreement of plant and model gas compositions (Dry Gas, LPG) and small deviations between the temperature profiles of plant and model columns. Second, this process can shorten the model development time since we can work on modeling FCC unit and the fractionation units at the same time.

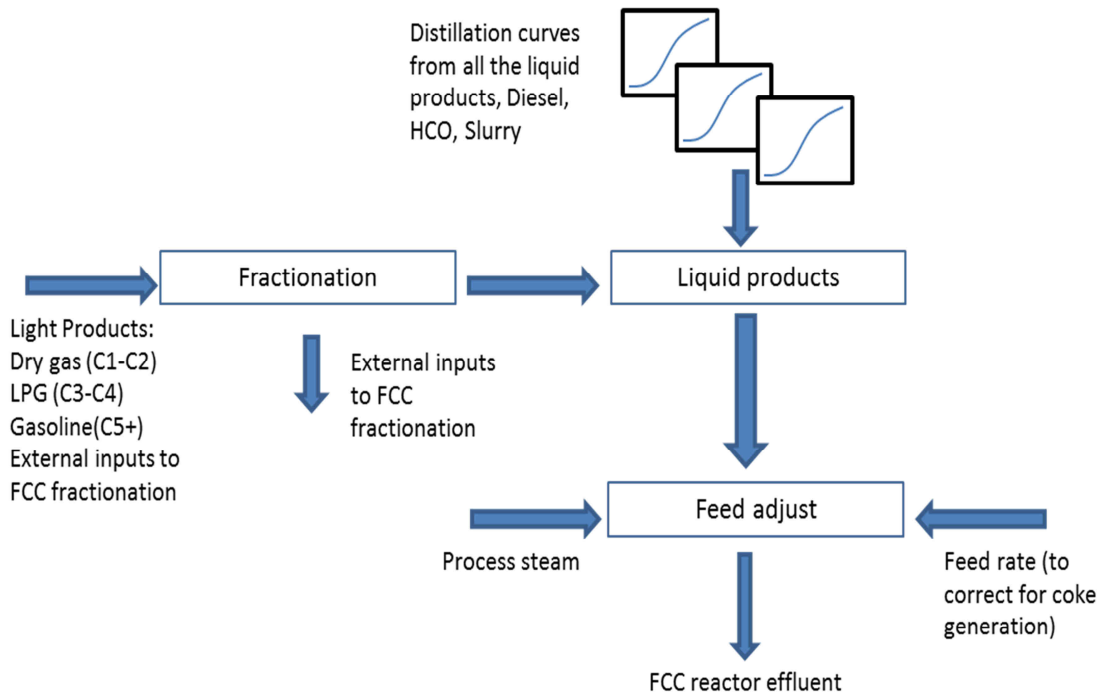


Figure 2.9: “Back-blending” products to reconstitute FCC reactor effluent

In this work, calibrating the fractionation section refers to the process of adjusting the number of theoretical stages in each zone (in the case of the main fractionator) or the number of theoretical stages between feed points. We use a set of a basic initialization specifications and efficiencies given in Table 2.7 to solve the column models. Typically, we only need to add or remove a few stages to calibrate the columns and achieve agreement with the plant operating profile. Once we converge the column models using the basic initialization specifications, we change (especially for the main fractionator) to specifications based on cut point and stage temperature. Kaes⁵¹ describes a similar process. We summarize the initial and final specifications in Table 2.8.

Table 2.8: Initialization and final specifications

Column	Initial specifications	Final specifications
Main fractionator	All pumparound rates and return temperatures (or temperature changes) Draw rates for all products Bottoms temperature Condenser temperature	Column overhead temperature Cut point for naphtha draws Pumparound duties Bottoms temperature Condenser temperature
Primary absorber	None	None
Primary stripper	None	None
Secondary absorber	None	None
Gasoline stabilizer	Reflux ratio (around 2.0) Overhead draw rate	Gasoline n-butane fraction or Reid Vapor Pressure (RVP) in bottoms Column overhead temperature or C5+ content in overhead
LPG stabilizer	Reflux ratio (around 3.0) Overhead draw rate	Reboiler temperature or bottoms temperature

		Fraction C4 in the column overhead
--	--	------------------------------------

2.9 Mapping Feed Information to Kinetic Lumps

Aspen HYSYS/Petroleum Refining includes a method to convert limited feed information (distillation curve, density, viscosity, refractive index, etc.) into kinetic lumps for use in the unit-level FCC model. In this section, we present an alternative method based on data and methods available in public literature. We extend the method based on work by Bollas et al.⁵² to infer the kinetic lump composition from limited process data. This method uses techniques to normalize the distillation curve, cut the distillation curve into boiling point lumps, and infer the composition of the each of these boiling point lumps. We have developed all of these techniques into spreadsheets using Microsoft Excel. These spreadsheets are available for the interested reader to download without charge on our group website (www.design.che.vt.edu).

2.9.1 Fitting Distillation Curves

Distillation curves for FCC feedstock can be limited. Because of the nature of the feedstock, complete true boiling point (TBP) analysis without D-2887/SimDist methods is frequently not possible. Many refiners still use a limited D-1160 distillation method to obtain some information about the distillation curve. Table 2.9 shows a typical D-1160 analysis for a heavy FCC feedstock.

Table 2.9: Typical distillation curve collected from D-1160

Recovery	Temperature (°C)
0 (Initial point)	253

10	355
50	453
73 (End point)	600

This curve does not contain enough information to convert into TBP curve using standard ASTM correlations. We must fit this data to a reasonable model to obtain estimates for the missing data points. Sanchez et al.⁵³ have evaluated several different types of cumulative probability distribution functions to fit distillation curves of crudes and petroleum products. They conclude that the cumulative beta function (with four parameters) can represent a wide range of petroleum products⁵³. We use this method to extend the measured partial distillation curve.

The beta cumulative density function is defined as:

$$f(x, \alpha, \beta, A, B) = \int_A^{x \leq B} \left(\frac{1}{B-A} \right) \frac{\Gamma(\alpha + \beta)}{\Gamma(\alpha)\Gamma(\beta)} \left(\frac{x-A}{B-A} \right)^{\alpha-1} \left(\frac{B-x}{B-A} \right)^{\beta-1} \quad (6)$$

where α and β refer to the positive valued parameters that control the shape of the distribution, Γ refers to the standard gamma function, A and B parameters set lower and upper bounds on the distribution and x represents normalized recovery.

We normalize all the temperatures between zero and one using the following equation:

$$\theta_i = \frac{T_i - T_0}{T_1 - T_0} \quad (7)$$

where T_0 and T_1 are reference temperatures. For this work, we choose, $T_0 = 250$ °C and $T_1 = 650$ °C. Then, we apply the cumulative beta function with each normalized recovery, x_i and initial

values for α , β , A and B parameters. If we choose good estimates for parameters, then the output of the beta function must be close to the corresponding recovery for each x_i . We define the following error terms:

$$RSS = \sum_{i=1}^n (x_{exp,i} - x_i)^2 \quad (8)$$

$$AAD = \frac{1}{n} \sum_{i=1}^n abs(x_{exp,i} - x_i) \quad (9)$$

where $x_{exp, i}$ represents the recovery measured in the distillation curve and x_i is the output of the beta function. RSS is the sum of least squares and AAD represents average absolute deviation. We now use the SOLVER method in Microsoft Excel to obtain optimized values of α , β , A and B.

Figure 2.10 shows how this fit compares to the result using a log-normal distribution⁵³ (with two fitting parameters) instead of the beta function. Using the beta function, we can generate the temperatures and recoveries needed for the conversion to TBP using standard ASTM methods.

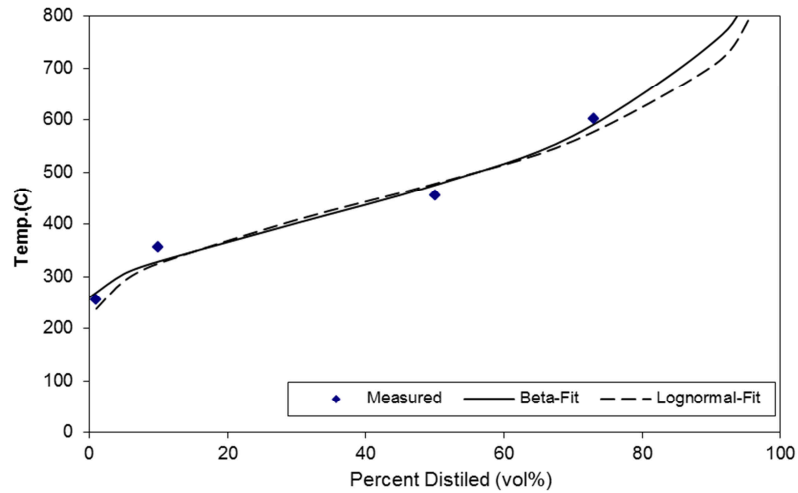


Figure 2.10: Comparison between using the beta distribution and lognormal distribution to fit the same distillation data

2.9.2 Inferring Molecular Composition

As mentioned earlier, we must also be able to infer the paraffin, naphthene and aromatic (PNA) composition of each boiling point range given certain measured bulk properties to completely map feed information to kinetic lumps. The API (Riazi-Daubert)^{54,55} is a popular chemical composition correlation that takes the form:

$$\%X_P \text{ or } \%X_N \text{ or } \%X_A = a + b \cdot R_i + c \cdot VGC' \quad (10)$$

where X_P and X_N represent the mole composition of paraffins (P), naphthenes (N); R_i is the refractive index and VGC' is either the viscosity gravity constant (VGC) or viscosity gravity factor (VGF). The parameters a , b and c take on different values for each molecule type (paraffin, naphthene or aromatic). Using the Riazi⁵⁵ correlation does not give sufficiently

accurate predictions for molecular compositions for this work. We note that this correlation encompasses a wide molecular weight range of 200-600⁵⁵.

We present an alternate correlation in Eqs. (11) and (12). Our correlation extends the original correlation from Riazi^{54, 55} by including specific gravity (SG) as an additional parameter and providing different sets of correlation coefficients (a, b, c and d) for different boiling point ranges.

$$\%X_P \text{ or } \%X_A = a + b \cdot SG + c \cdot R_i + d \cdot VGC' \quad (11)$$

$$\%X_N = 1 - (X_P + X_A) \quad (12)$$

where X_P , X_N and X_A represent the mole composition of paraffins (P), naphthenes (N) and aromatics (A) respectively; R_i is the refractive index and VGC' is either the viscosity gravity constant (VGC) or viscosity gravity factor (VGF). The parameters a, b, c and d can take on different values for different molecule type and boiling point ranges.

We used a total of 233 different data points containing laboratory measured chemical composition and bulk property information (distillation curve, density, refractive index and viscosity) for light naphtha, heavy naphtha, kerosene, diesel and VGO. These data points come from various plant measurements made over the six-month course of this study and a variety of light and heavy crude assay data (spanning several years) available to the refinery.

We used Microsoft Excel and the SOLVER method to fit values for the parameters a, b, c, and d that minimized the sum of squares residual between the measured %X_P and %X_A and calculated %X_P and %X_A. We calculated %X_N by difference as shown in Eq. (12). We show the results of our data regression with the associated average absolute deviation (AAD) in Table 2.10 and

Table 2.11. Figure 2.11 to Figure 2.13 compare measured and calculated molecular compositions.

Table 2.10: Coefficients for paraffin content in petroleum fractions

	Paraffin (vol. %)				
	A	B	C	D	AAD
Light Naphtha	311.146	-771.335	230.841	66.462	2.63
Heavy Naphtha	364.311	-829.319	278.982	15.137	4.96
Kerosene	543.314	-1560.493	486.345	257.665	3.68
Diesel	274.530	-712.356	367.453	-14.736	4.01
VGO	237.773	-550.796	206.779	80.058	3.41

Table 2.11: Coefficients for aromatic content in petroleum fractions

	Aromatic (vol. %)				
	A	B	C	D	AAD
Light Naphtha	-713.659	-32.391	693.799	1.822	0.51
Heavy Naphtha	118.612	-447.589	66.894	185.216	3.08
Kerosene	400.103	-1500.360	313.252	515.396	1.96
Diesel	228.590	-686.828	12.262	372.209	4.27

VGO	-159.751	380.894	-150.907	11.439	2.70
-----	----------	---------	----------	--------	------

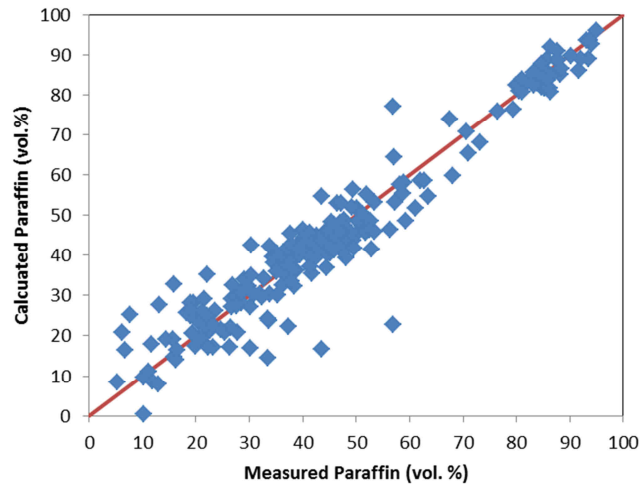


Figure 2.11: Comparison of calculated and measured paraffin content in all fractions

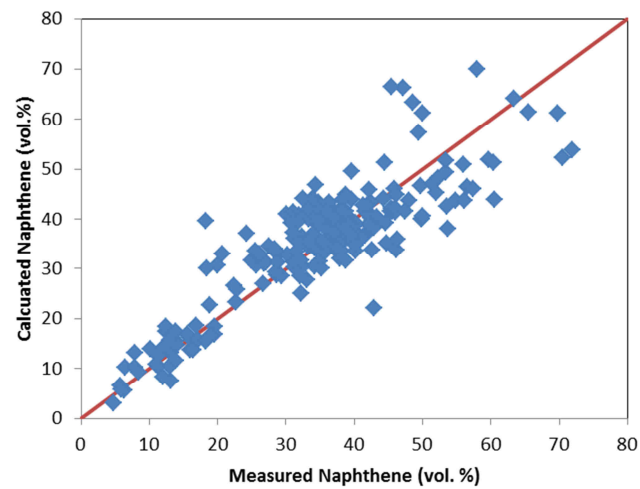


Figure 2.12: Comparison of calculated and measured naphthene content in all fractions

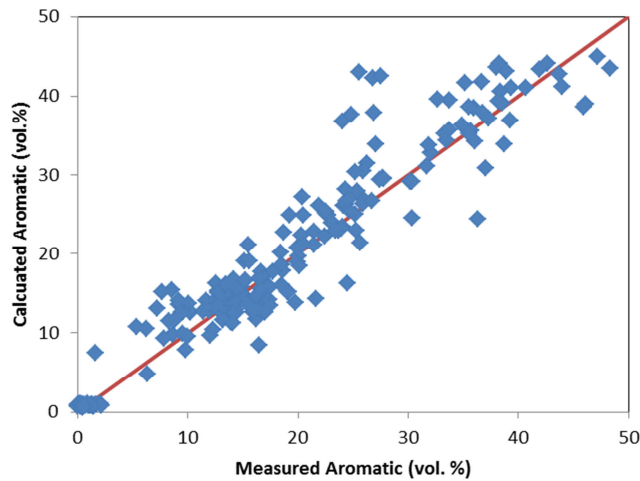


Figure 2.13: Comparison of calculated and measured aromatic content in all fractions

We can now use the two methods we have developed to propose a technique to use limited feed information to infer lumped composition. This technique is similar to the one given by Bollas et al.⁵². However, we make several changes to account for limited data sets. We outline the technique in the following steps (Changes from the procedure of Bollas et al.⁵² are indicated with a *):

1. Use the beta-distribution method to extend partial ASTM D-1160 distillation curves. (*)
2. Convert the ASTM D-1160 to a TBP curve using standard API correlations⁵⁴. (Note: We offer a spreadsheet to perform the standard correlations). (*)
3. Using the 50% point of the TBP, estimate the Watson factor (K_w). Set the 50% TBP temperature as an initial guess for the mean-average boiling point (MeABP).
4. Use the definition of K_w to create the specific gravity distribution of the fraction.
5. Calculate pseudo-component molecular weight using the correlation of Riazi⁵⁵.

6. Use densities and mole weights to calculate volume-, cubic-, molar- and mean-average boiling point of the total fraction⁵⁵.
7. If the MeABP from step 7 is close to the MeABP assumed in step 3, go to step 8. Otherwise, assume a new value for MeABP and go back to step 4.
8. Assign a lump to every boiling point range in the kinetic lumping. (*)
9. Calculate the boiling point, molecular weight, density, volume and weight and molar concentrations of each lump.
10. Use Goosen's correlation to estimate the refractive index of each lump⁵⁶.
11. Use correlations from Riazi⁵⁵ to estimate the viscosity of the lump. (*)
12. Calculate the relevant VGF or VGC⁵⁵ for the lump. (*)
13. Use correlations (with an appropriate choice for the set of correlation coefficients) proposed the preceding section to identify the PNA composition of the lump. (*)
14. If required, use correlations from Riazi⁵⁵ to estimate the number of aromatic rings in each aromatic fraction. (*)

We have found that this technique can provide reasonable estimates of kinetic lump composition. It is difficult to justify a more sophisticated scheme given the limited amount data available. Some refiners also make bulk chemical composition measurement of the feed which includes a measurement of the total aromatic content. The sum of the aromatic kinetic lumps generated from the above technique generally agrees with the measured aromatic content.

2.9.3 Convert Kinetic Lumps to Fractionation Lumps

A related problem is the conversion of kinetic lumps back to fractionation lumps required to build rigorous fractionation models. For our models, Aspen HYSYS gives a method to transition

the kinetic lumps to boiling-point-based pseudo-components typically used to model petroleum fractionation. We also propose an alternative technique that can provide similar results using methods developed in earlier in this section. Essentially, we must convert the kinetic lumps back into a TBP curve. The key steps in converting the kinetic lumps to boiling point pseudo-components are:

1. Using the “back-blending” concept from the previous section, develop a FCC effluent TBP curve from a reference set of product yields. These yields include all liquid products such as light and heavy naphtha, light and heavy cycle oil or diesel, slurry or decant oil.
2. Fit a cumulative beta distribution to this “back-blended” reference TBP curve and obtain the best values for the cumulative beta distribution fit. We calculate this initial set of parameters only once.
3. Run the model to obtain the product distribution in terms of kinetic lumps.
4. Apply steps 3 to 13 from the previously kinetic lumping procedure in reverse, i.e., we obtain the 50 % TBP point for each boiling point range from the known PNA distribution of the kinetic lumps involved.
5. Since we know initial and final boiling points for all the kinetic lumps (by definition), use these points in conjunction with calculated 50% TBP points to generate an updated FCC effluent TBP curve.
6. Fit a new cumulative beta distribution to the updated FCC effluent TBP curve using the initial set of cumulative distribution parameters as a starting guess.

7. Cut this new TBP curve into petroleum pseudo components using methods commonly available in process simulations. In addition, Riazi⁵⁵ discusses several strategies to cut a TBP curve into pseudo-components suitable for fractionation models.

2.10 Overall Modeling Strategy

This work relies primarily on data collected while the refinery is in regular operation. Related work in integrated FCC modeling often relies on pilot plant and experimental data. It is more difficult to produce a predictive model with plant operation data alone. The nature of plant operation means there may be abrupt changes in feed quality or operating parameters, poor measurements due to poorly calibrated or failing sensors and inconsistent data. Fernandes et al.³³ have encountered similar issues in the validation phase of their work. We outline the following strategy and our specific implementation in Figure 2.14:

- Obtain data on a continuous basis from the plant over a number of months
 - Reconcile data from multiple sources (DCS, Inventory, etc.) (Table 2.12)
 - Check the consistency of the data by ensuring mass balance and enthalpy balance
 - Accept a dataset when it is consistent
 - Track variation in the dataset to ensure there are multiple operating scenarios (Figure 2.15)
- Use the first accepted dataset to develop initial model for FCC unit and fractionation section
- Calibration

- The most basic calibration is to introduce a selectivity calibration factor for classes of the reactions in kinetic network.
- It is typically sufficient vary the calibration selectivity factors to match plant performance during the first accepted dataset.
- The user may introduce additional factors to account for significant changes in catalyst behavior of unit profile.
- The yield results from the initial model calibration should be within 1-2% of actual plant yield.
- Validation
 - Use the subsequently accepted datasets to verify and track the performance of the unit and fractionation sections with the model.
 - Make sure to examine to yield of the FCC unit independently of column accuracies in the fractionation section.
 - It is typically possible to predict yields of key products on a feed normalized mass basis with AAD of less than 2 to 3%.
- Case studies
 - The model is calibrated with a finite amount of plant data, so it may not be meaningful to study changing operating parameters of the FCC over a very wide range. However, case studies on the fractionation section can take on wide ranges.
 - Recalibrate the model when significant process changes occur.

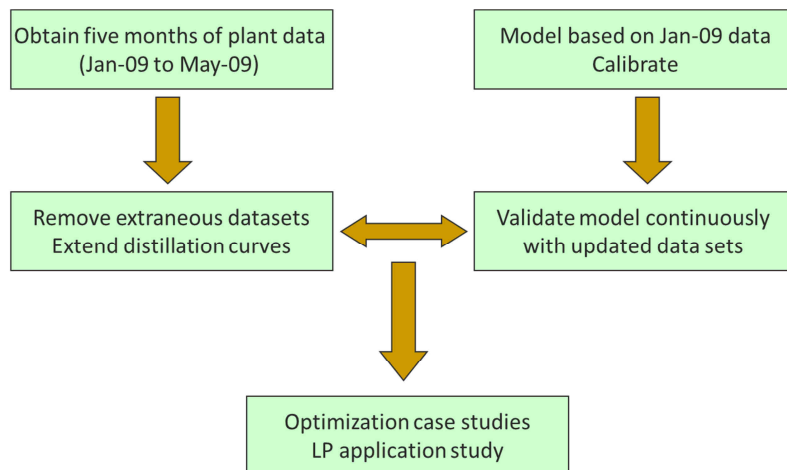


Figure 2.14: Specific implementation of overall modeling strategy

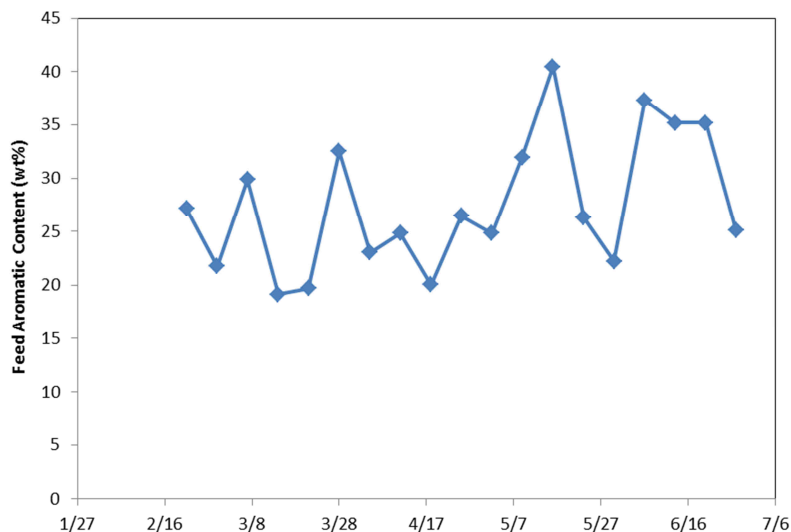


Figure 2.15: Tracking aromatic content in the feed to ensure multiple operating scenarios

Table 2.12: Routinely monitored properties used for model development and calibration

Feed	Products	FCC	Fractionation
Flow rate	Yield Composition	Temperatures (Feed, Riser outlet,	Temperature profile

Distillation curves	(for light products)	regenerator bed and flue gas)	Pressure profile
Specific Gravity	Density	Pressure differential between riser/reactor and regenerator	Draw rates
Conradson Carbon Residue (CCR)	RON/MON	Steam usage	Pump around flow rates and duties
Sulfur content (S)	Flash point	Main air blower flow rate	Set points (Usually temperatures)
Metals content (Fe, Na, Ni, V)	Sulfur content		
Saturates, Resins, Aromatics, Asphaltenes (SARA)			

2.11 Results

We evaluate the model using over six months of operating data from a commercial FCC unit in the Asia Pacific with a feed capacity of 800,000 ton per year operating under a maximum diesel and gasoline plan. Figure 2.16 shows a process flow diagram for the entire process. The evaluation of the model includes comparisons of overall reactor yield, light and heavy product composition, and operating profiles for key equipment in the gas plant. We note that in general, the model can accurately predict the product yield and composition over a variety of different feed conditions.

The most important prediction is the overall product yield from the reactor. A validated prediction of the overall product yields allow the refiner to use the model to study different kinds of the feedstock and operating conditions. Table 2.13 shows the results for product yields. The most important and valuable products are LPG, gasoline and diesel. We use operating data from the BASE run to calibrate the model. In terms of overall yield, the largest errors in the BASE case appear with prediction of LPG and slurry. The AAD for the product over all validation cases (VALID-1 to VALID-6) is 0.96%. The AAD is much lower than the previous AAD standard of 5% for yield predictions in the plant.

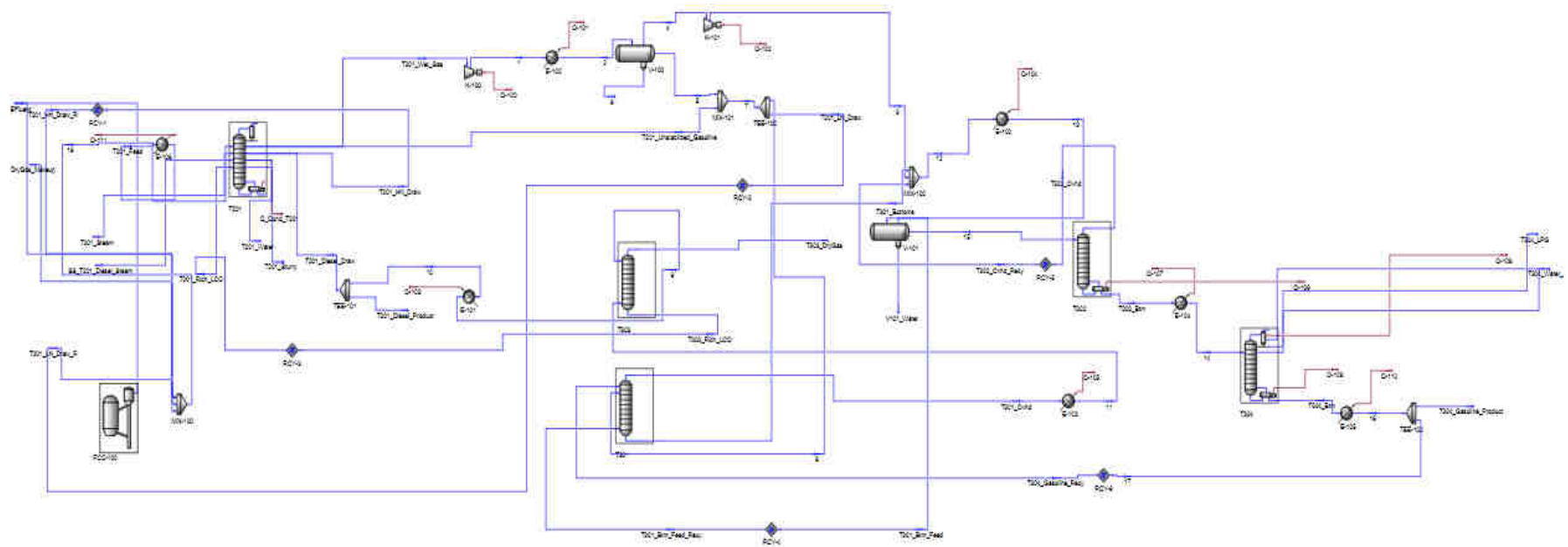


Figure 2.16: Overall Aspen HYSYS model of FCC unit and associated gas plant

Table 2.13: Product yield results, AAD = 0.96%

Yield Mass%	VALID-1		VALID-2		VALID-3	
	Model	Plant	Model	Plant	Model	Plant
Gasoline	43.3%	41.9%	43.3%	44.2%	40.1%	39.5%
Diesel	24.6%	23.7%	21.6%	22.0%	25.6%	25.2%
LPG	18.5%	20.1%	17.9%	19.9%	19.1%	21.1%
Dry Gas	4.9%	4.4%	5.0%	4.2%	4.7%	4.1%
Slurry	1.4%	4.0%	5.5%	3.8%	4.5%	3.9%
Coke	7.3%	5.9%	6.7%	6.0%	6.0%	6.3%
Yield Mass%	VALID-4		VALID-5		VALID-6	
	Model	Plant	Model	Plant	Model	Plant
Gasoline	41.5%	41.2%	44.1%	44.2%	40.8%	41.2%
Diesel	24.7%	24.6%	20.8%	20.9%	24.3%	24.5%
LPG	19.3%	21.6%	17.8%	20.6%	18.6%	20.2%
Dry Gas	4.8%	3.8%	4.7%	4.3%	5.3%	4.4%
Slurry	3.9%	3.9%	6.5%	3.9%	5.1%	4.0%
Coke	5.7%	4.8%	6.0%	6.2%	5.9%	5.6%

Another set of key indicators are the product properties of the liquid fuel from the FCC. The properties of interest to refiners are density, flash point (volatility), RON/MON (for gasoline), sulfur content and aromatic content. This is one of the areas where our model is different from other published work described earlier. We discussed a method to transition from kinetic lumping to fractionation lumping in Section 8. Not only does this method allow the user to observe the results

directly, we can also see the effect of the reactor conditions on fractionated properties. Using the results from the fractionator model, we can calculate the distillation curves of the liquid products. Figure 2.17 and Figure 2.18 show the distillation curves for one of the validation cases. In general, the model predicts key points from the D-86 curve (5%, 95%) within plant tolerance. Further refinement of this prediction requires accurate measures of the pumparound rates and the heat duty for each pumparound in the main fractionator. These data are not routinely measured.

We can use the predicted D-86 curves to calculate several other properties of interest. There are several methods to calculate the flash point and other volatility properties in using the distillation curve and density. In Figure 2.21, we compare our predictions using the API flash point correlations⁵⁴ to the measured data. We note good agreement for the flash point. In addition, Figure 2.19 and Figure 2.20 show the prediction of the densities for gasoline and diesel. We also see good agreement between the measured and predicted results for density.

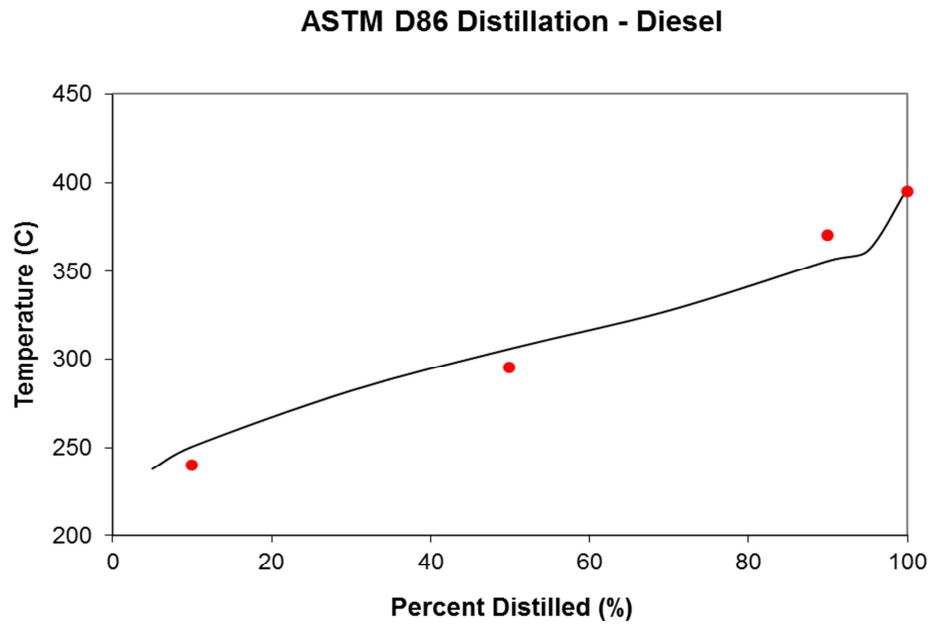


Figure 2.17: ASTM D-86 distillation for the product diesel from the main fractionator

(VALID-1)

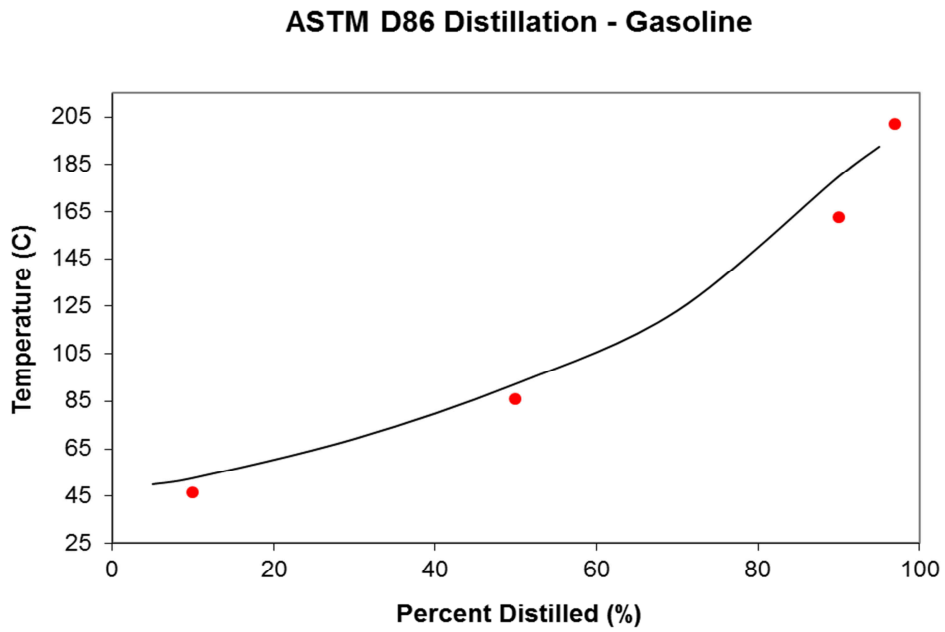


Figure 2.18: ASTM D-86 distillation for the product gasoline from debutanizer column

(VALID – 1)

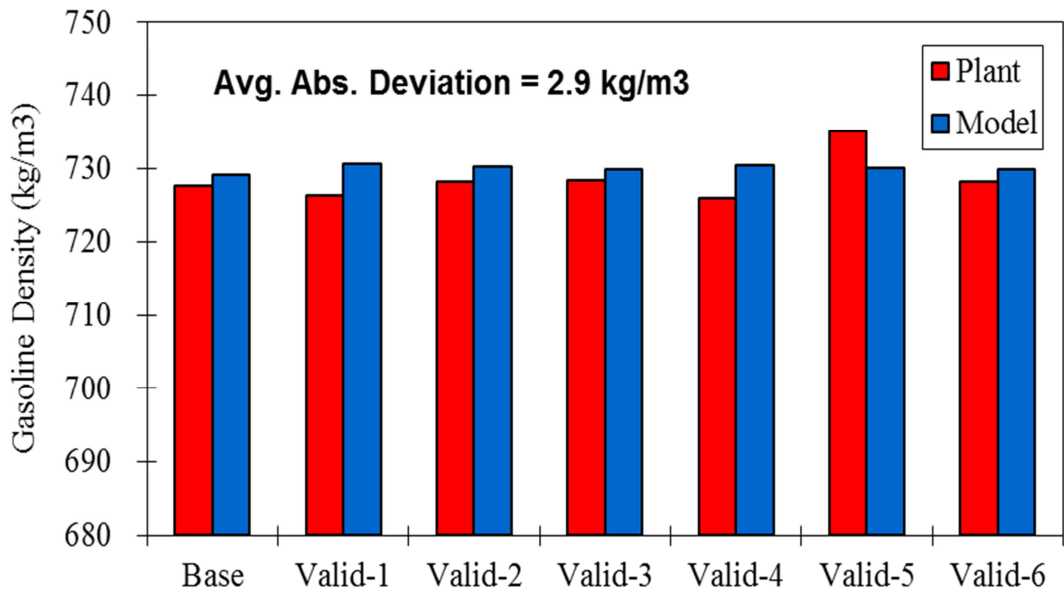


Figure 2.19: Gasoline density comparison

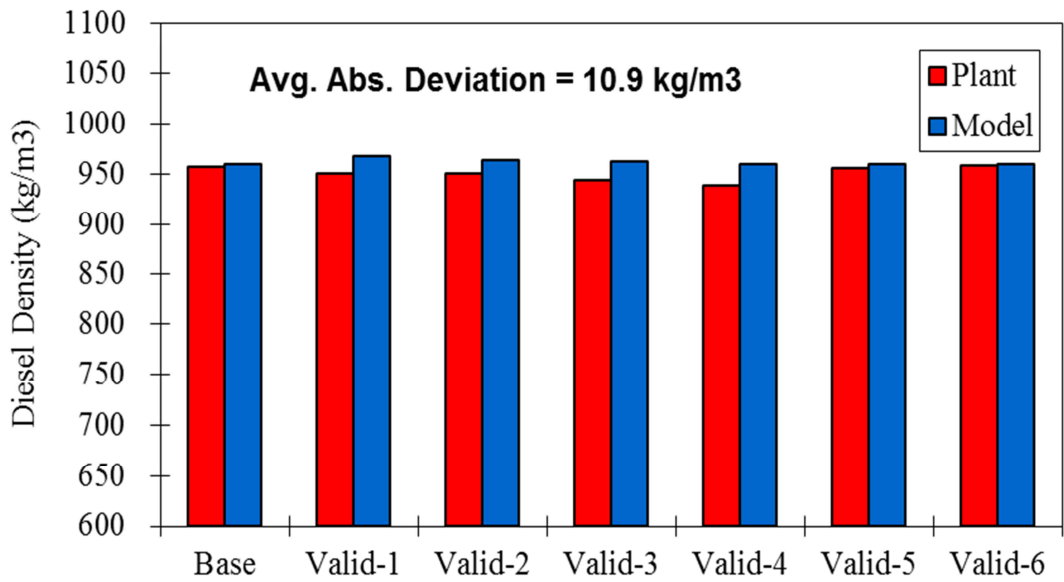


Figure 2.20: Diesel density comparison

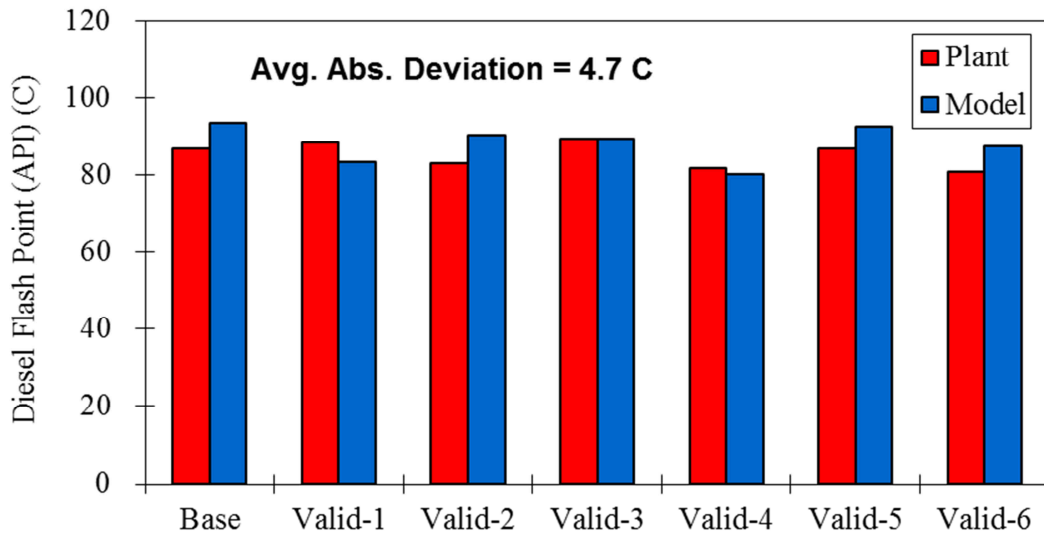


Figure 2.21: Diesel flash point comparison

Roughly 20-25% of the product in this FCC is LPG, which primarily consists of propane, propylene, butanes and butenes. The presence of significant amounts (greater than 0.5 %) C5+ products in LPG indicate that the fractionation process is not operating well. Therefore, the prediction of the composition of the all the gas and LPG products is essential to validate the model. Table 2.14 and Table 2.15 compare the operating data and model predictions for LPG and Dry Gas. The AAD for the predictions of mole compositions in LPG and Dry Gas are 1.2% and 1.8% respectively. We note that there is often more significant error in the prediction of hydrogen and nitrogen.

Table 2.14: Comparison of LPG composition, AAD = 1.2%

LPG	VALID-1		VALID-2		VALID-3	
MOLE%	Model	Plant	Model	Plant	Model	Plant

C3	13.9	15.5	13.9	14.9	14.7	13.3
C3=	36.6	38.3	35.1	35.9	38.3	38.4
NC4	4.5	5.3	4.1	5.6	4.0	5.6
IC4	17.5	17.1	16.9	18.8	16.1	18.0
IC4=	12.8	13.1	12.1	12.8	11.5	13.4
T-2-C4=	6.0	6.0	5.5	6.1	5.3	6.1
C-2-C4=	4.4	4.7	4.0	5.0	3.9	4.7
LPG	VALID-4		VALID-5		VALID-6	
MOLE%	Model	Plant	Model	Plant	Model	Plant
C3	14.2	13.2	15.6	12.2	15.5	13.0
C3=	34.5	39.0	35.9	41.7	37.0	39.4
NC4	4.3	4.9	4.5	3.4	4.5	4.5
IC4	16.6	18.4	18.2	18.0	17.5	18.6
IC4=	12.3	13.1	13.1	13.1	12.7	13.2
T-2-C4=	5.7	6.1	6.0	5.7	6.0	6.3
C-2-C4=	4.1	4.8	4.5	4.8	4.5	4.6

Table 2.15: Comparison of Dry gas composition, AAD = 1.8%

Dry Gas	VALID-1		VALID-2		VALID-3	
MOLE%	Model	Plant	Model	Plant	Model	Plant
H2	24.3	29.9	23.1	31.8	24.7	29.3
N2	21.0	20.1	19.5	16.7	19.7	19.1
CO	1.6	1.6	1.5	2.0	1.6	1.8

CO2	1.8	1.8	2.2	1.6	1.1	1.8
C1	24.8	23.0	24.5	24.8	25.6	23.1
C2	10.9	10.2	12.1	9.9	11.2	10.3
C2=	11.7	10.5	12.3	10.5	13.0	11.8
Dry Gas	VALID-4		VALID-5		VALID-6	
MOLE%	Model	Plant	Model	Plant	Model	Plant
H2	20.5	28.2	21.6	27.5	20.8	28.1
N2	19.7	22.5	19.7	20.3	18.9	19.8
CO	1.6	1.7	1.6	1.7	1.5	1.4
CO2	1.7	2.0	1.8	2.0	3.6	1.6
C1	27.7	21.4	26.6	23.1	24.5	23.6
C2	10.6	10.5	11.7	10.1	11.7	10.3
C2=	13.8	11.6	12.9	11.2	11.9	11.2

We also apply the model to predict all temperature profiles of columns for each validation case and compare the results with plant operation. We find good agreement between plant measurements for all columns with the exception of the debutanizer column (T302) (see Figure 2.24). This column is very sensitive to the LPG composition in the model. We recall that the BASE calibration case shows error in matching the LPG yield from the plant. It is possible to improve this prediction by including catalyst-specific parameters in the kinetic model to match the plant performance. However, we avoid this procedure at this time so we can provide a more broadly useful model. Figure 2.22 to Figure 2.26 compare model and plant values for temperature profiles for a single validation case (VALID-4).

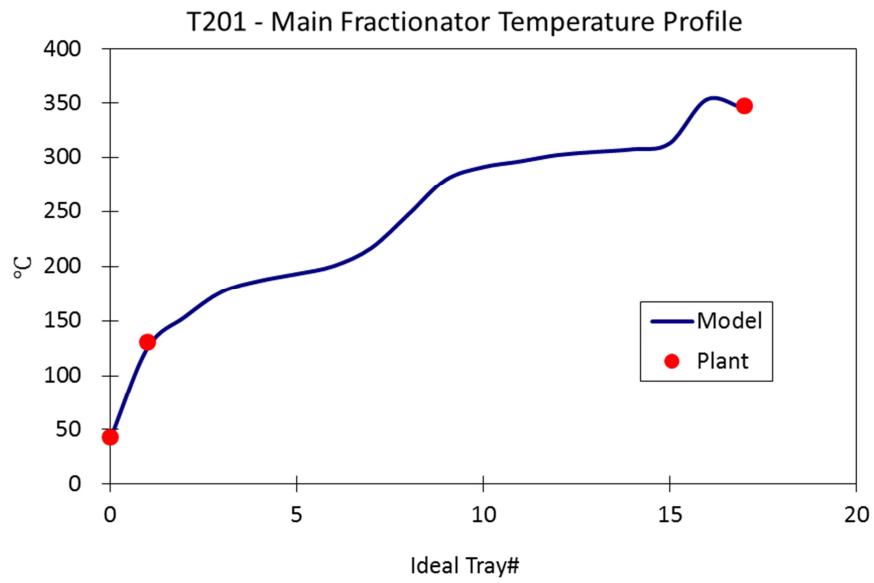


Figure 2.22: Main fractionator temperature profile

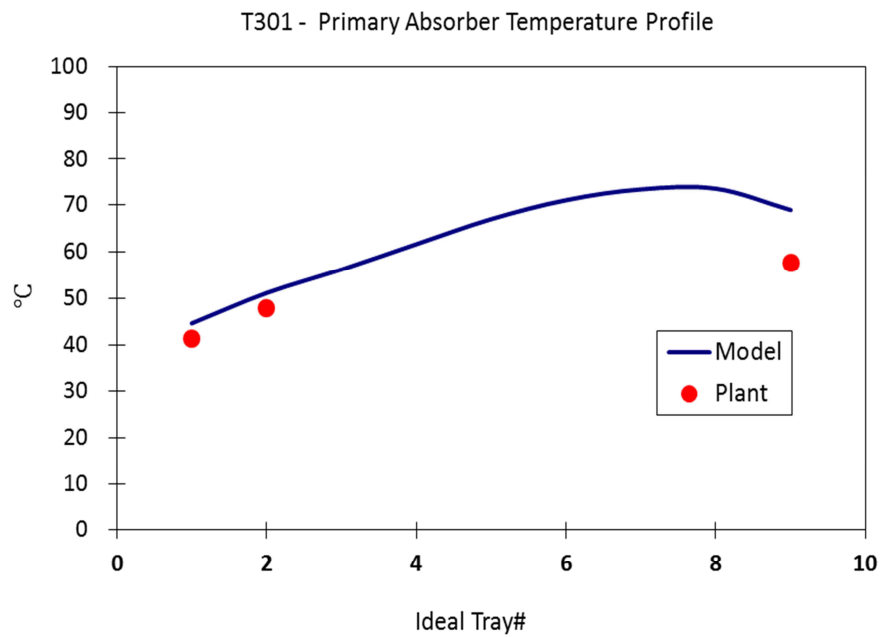


Figure 2.23: Primary Absorber Temperature profile

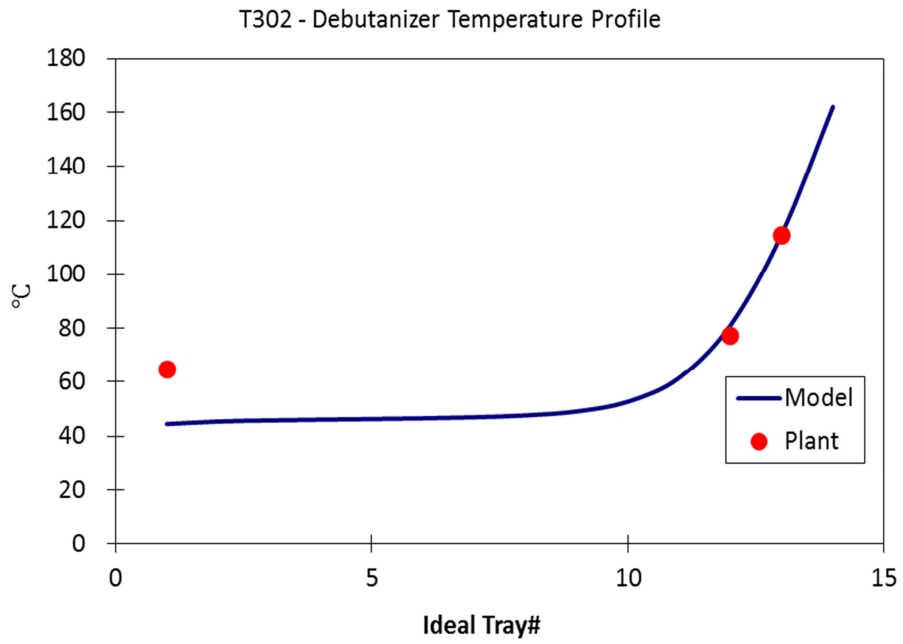


Figure 2.24: Debutanizer Temperature profile

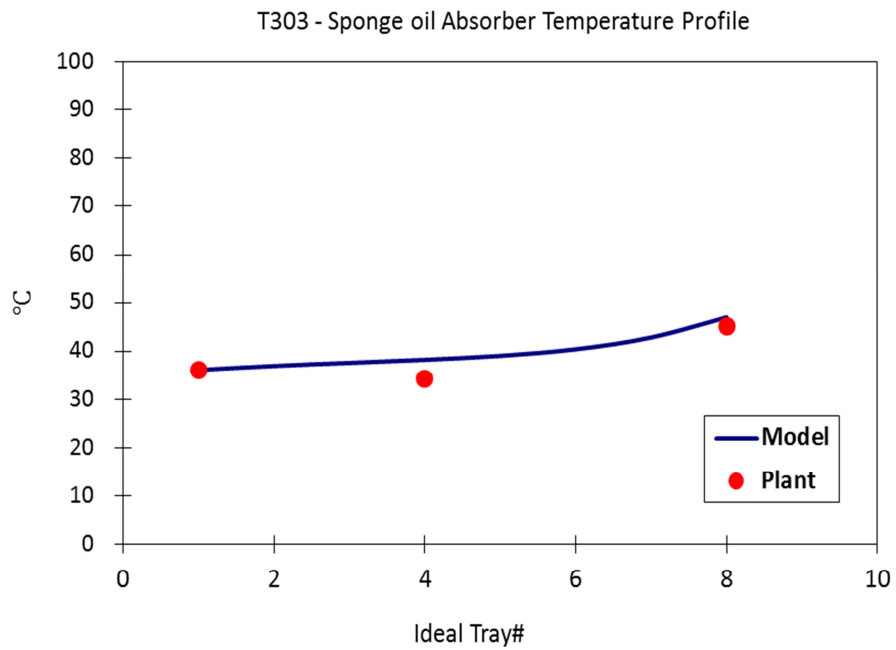


Figure 2.25: Sponge oil Absorber Temperature Profile

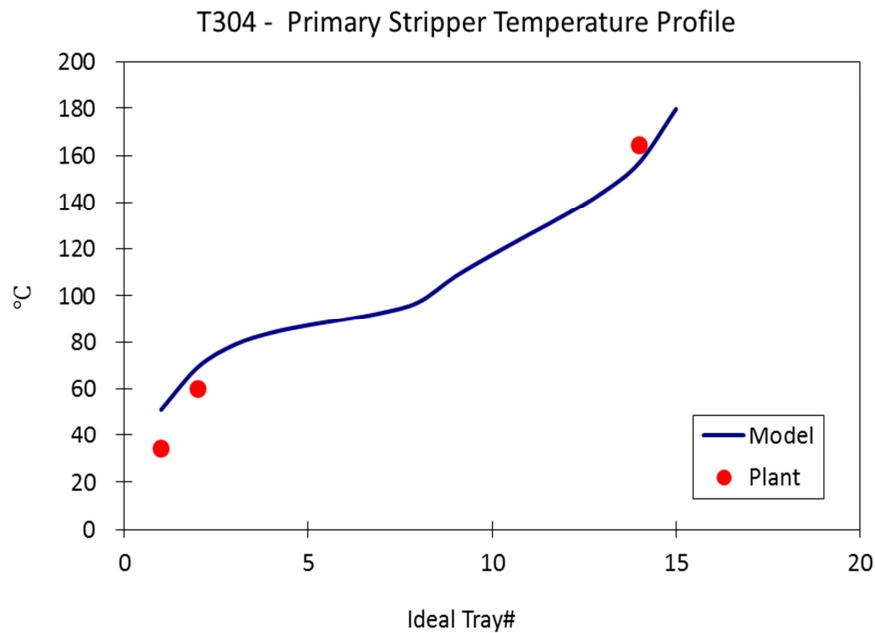


Figure 2.26: Primary Stripper Temperature profile

2.12 Applications

Refiners are very interested in obtaining optimal operating conditions that maximize the yield of a profitable product slate. However, unlike traditional chemical plants, the FCC unit generates several products that have different profit margins. Furthering complicating matters is that these profit margins may change depending on refinery constraints, market conditions and government regulations. Therefore, it is critical to understand how to manage the FCC unit under different operating scenarios. We consider two common scenarios in FCC operation: improving gasoline yield and increasing the throughput of the unit.

2.12.1 Improving Gasoline Yield

Gasoline yield is a typical a complex function of temperature, pressure, feed quality and catalyst-to-oil ratio⁸. We consider the case where the feed quality is fixed. An easily manipulated operating variable is the riser outlet temperature (ROT). Allowing the ROT to increase improves gasoline yield by promoting cracking and aromatic chain scission reactions that increase the yield of C5+ components. We compute the gasoline yield at various temperatures and show the results in Figure 27. The current ROT is 510 °C and is marked with a yellow square. The ROT that leads to the highest yield of gasoline is roughly 530 °C. Does this mean that we should allow the ROT to increase to 530 °C? To answer this question, we plot the yields of the other valuable products from the FCC in Figure 2.28.

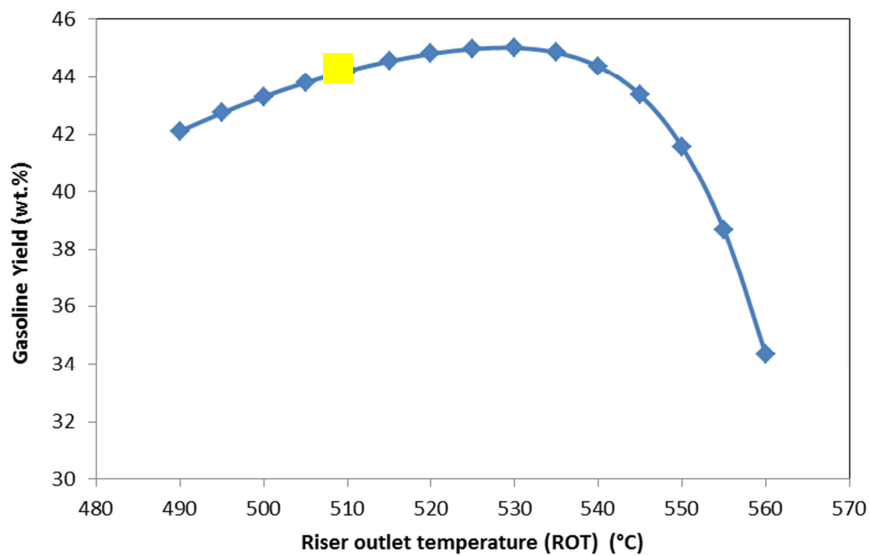


Figure 2.27: Gasoline yield profile as a function of ROT

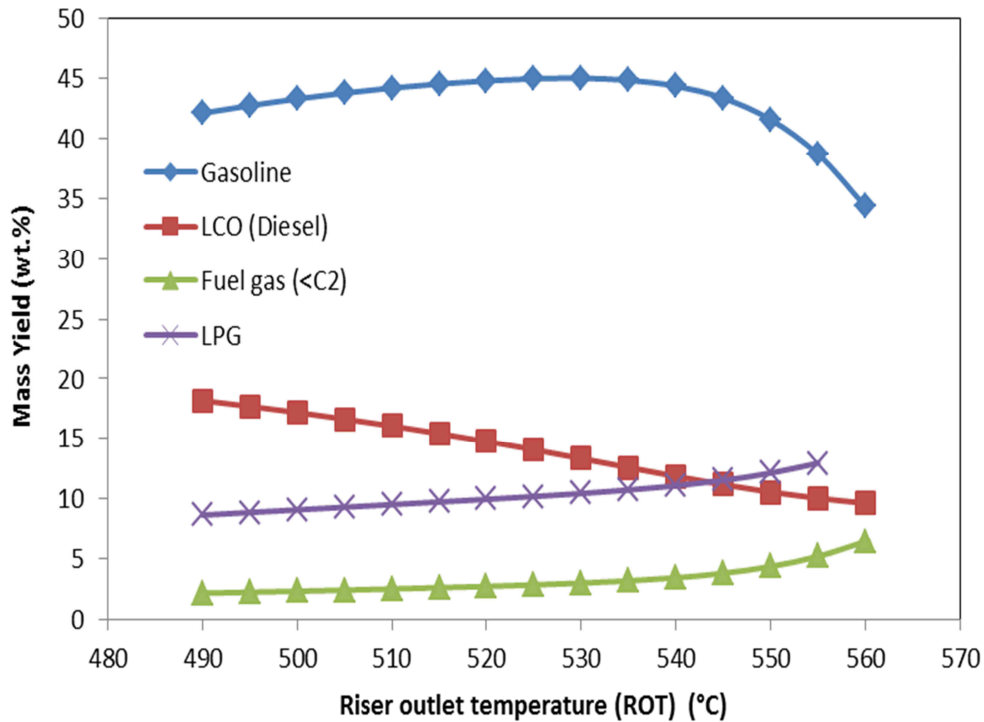


Figure 2.28: Yields of key products as functions of ROT

Figure 2.28 shows that while gasoline yield reaches the maximum at an ROT of 530 °C, the yields of other valuable products (i.e., diesel) drop significantly. In addition, the yield of fuel/dry gas (light gases) rises quickly. This indicates that we are “overcracking” the feed. The high temperature accelerates the production of C1 – C2 components (i.e., fuel/dry Gas) through the catalytic and thermal cracking pathway. This is clearly an undesired result. Dry gas is not of significant value and can easily overload the overhead wet gas compressor. In addition, Figure 2.29 shows the coke yield on the catalyst as a function of ROT. The amount of coke present on the catalyst leaving the riser is a strong function of ROT. Regenerating catalyst with higher coke deposits increases the utilities required to regenerate the coke to the same level. These side effects shrink the acceptable range of values for the ROT.

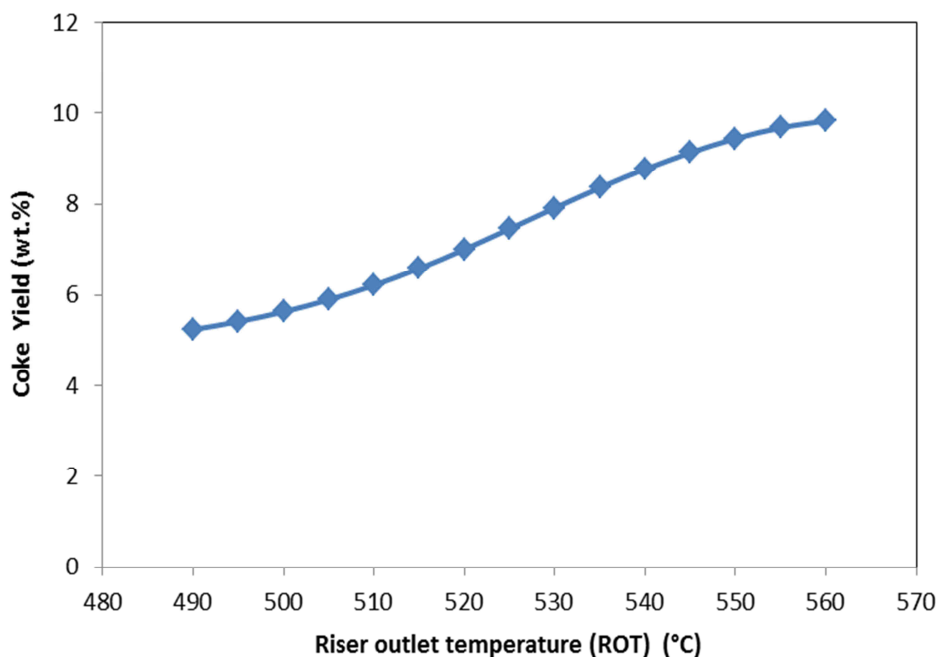


Figure 2.29: Coke yield as a function of ROT

We can combine the results from these graphs and consider scenarios where a refiner wants to maximize different products. For example, refiner may want to maximize the production of gasoline and diesel or maximize the production of gasoline and LPG depending on external constraints. We can easily use the model to generate a case study as shown in Figure 2.30. This figure shows that there are different optimum ROT values for different scenarios. The maximum gasoline and diesel production occurs in the range of 505-510C (confirming the refiner’s assertion where these data are obtained) whereas the maximum for gasoline and LPG production occurs in the range 530-540 C.

This example shows the importance of a model that accounts for all products, including light gases as a distinct lump. In addition, the integrated heat balance between the riser and regenerator allows us to provide useful estimates for the coke yield. We have not included the effect of these process

changes on the downstream fractionation unit in this study. However, we note that there are often significant equipment and process constraints (a prime example is the wet gas compressor) that restrict the acceptable range for the ROT.

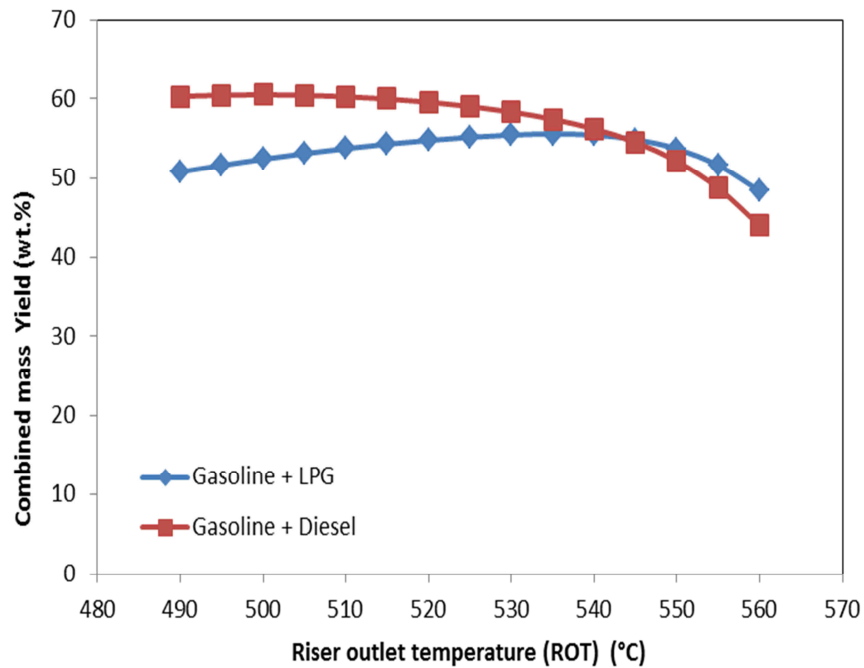


Figure 2.30: Maximizing production of key products as a function of ROT

2.12.2 Increasing unit throughput

Let us consider another scenario where we want to increase the throughput of the unit. The refiner typically wants to process the largest volume of feedstock possible. Ideally, we would like the FCC to maintain a similar mass yield of the most valuable product (i.e. gasoline). Figure 2.31 shows the mass yield of gasoline as a function of feed rate to the unit. The mass yield decreases almost linearly with increasing feed rate. How can we explain this phenomenon? Figure 2.31 also shows

the catalyst-to-oil ratio as a function of increasing feed rate. We note that the cat-oil ratio also decreases linearly.

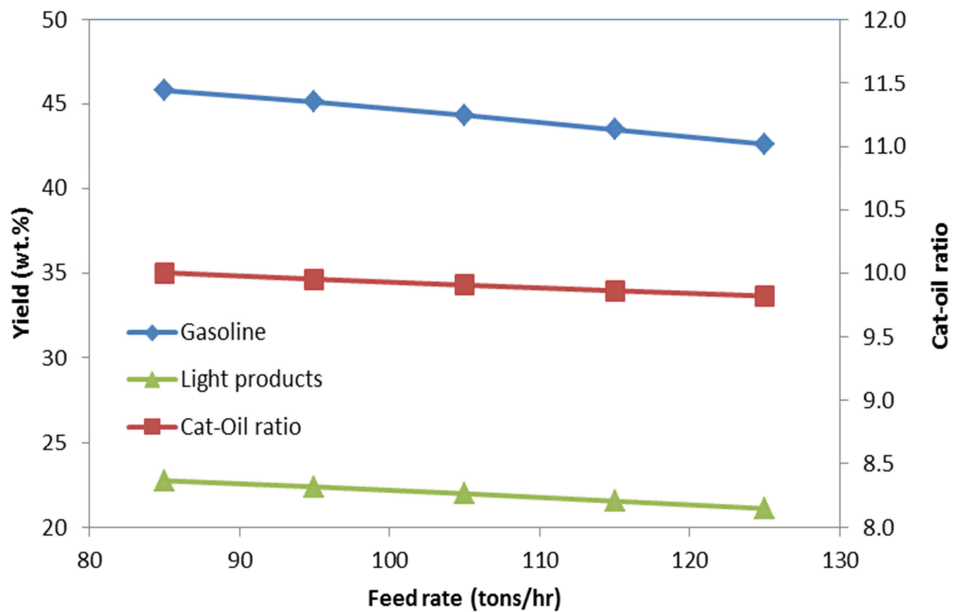


Figure 2.31: Mass yield and cat-oil ratio as function of feed rate

The decreased cat-oil ratio means that there is less contact time between the catalyst and the feed oil. Lower contact time will result in fewer species cracking and subsequently reduce the gasoline yield. However, we must not confuse this effect with “overcracking” described in the previous case study. Figure 2.31 also illustrates the difference between “overcracking” and a reduced cat-oil ratio. We note that yield of light products (dry gas and LPG) does not increase. This indicates that high temperature thermal or catalytic cracking is not taking place.

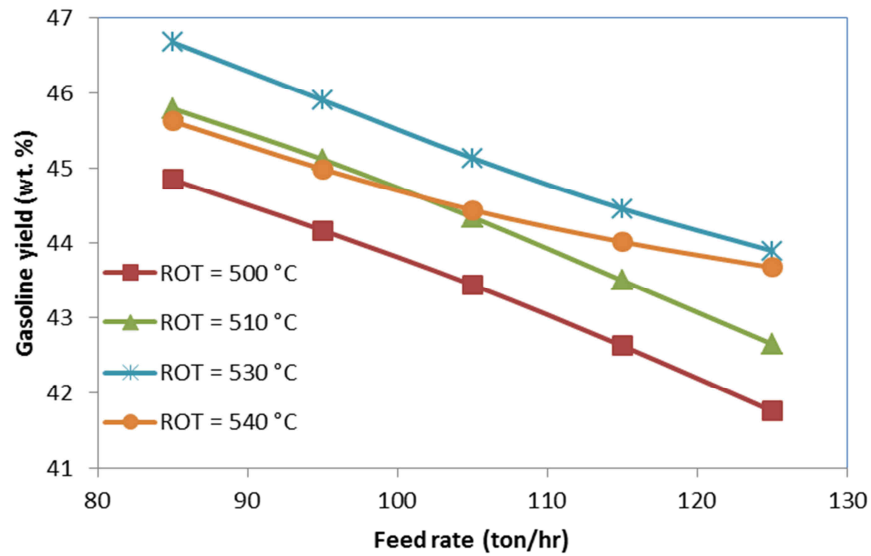


Figure 2.32: Gasoline yield as a function of feed rate

Let us now consider the scenario where we want to increase or maintain gasoline yield that corresponds to the base unit throughput. We will allow the ROT to increase, while also increasing the feed rate to the unit. Figure 2.32 shows the effect of the increasing feed rate and ROT. We note that the gasoline yield increases with rising ROT. However, once we reach the ROT of 540 °C, the gasoline yield drops quickly. This occurs because we have passed the “overcracking” peak for this particular feed.

2.12.3 Sulfur content in gasoline

Sulfur content in gasoline is an important regulatory constraint for refiners. Many schemes are in use to reduce the sulfur content in refinery products. In the case of the FCC unit, a significant portion of the sulfur in the feed leaves the process as a dry gas. However, the remaining sulfur leaves through the key liquid products.

Sadeghbeigi¹ and Gary et al.⁷ indicate that hydrotreating the feed significantly reduces the sulfur content in the non-slurry products. However, there may be an economic disadvantage in hydrotreating the feed to the FCC unit. In addition, low sulfur constraints may result in an excess of low value resid feeds in the refinery. Often, the refiner looks for ways to blend this high-sulfur resid feeds into processing units that can tolerate higher sulfur. In both cases, we need to understand how the changes in feed sulfur affect the sulfur distribution in the products.

Let us consider the situation where a cheaper feedstock, Vacuum Residue (VR) is available. The refiner may want to maximize the profitability of the unit by blending in VR with the existing vacuum gas oil (VGO) feed. Currently, 5.7 wt.% of the feed to the FCC unit is VR type feed. We would like to know how much VR we can blend into the VGO feed while meeting the constraint of stabilized gasoline.

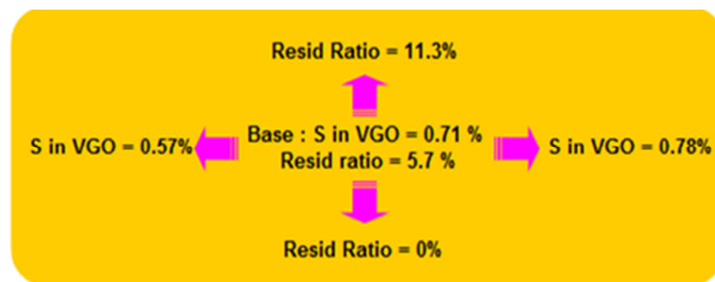


Figure 2.33: Scenario of feed sulfur change

To study this question, we must also consider that sulfur content in the feed VGO is changing as well. We vary both the sulfur content in the feed VGO and the amount of VR that is blended in.

Figure 2.33 shows the outline of the case study process.

We vary the feed ratio of VR from 0% to 11.3% and the associated sulfur content in the VGO. The corresponding sulfur limit for FCC gasoline in this refinery is 800 ppmwt. We use the model to predict the sulfur content in different cases of feed ratio and sulfur in VGO. We note that for the base case of 0.71 wt.% sulfur in feed VGO, we could blend in more than 10% VR while still meeting the sulfur constraint. However, if the sulfur in the VGO increases to 0.78 wt. %, we cannot blend in more than 4.5 wt. % of VR if we want to meet the sulfur constraint.

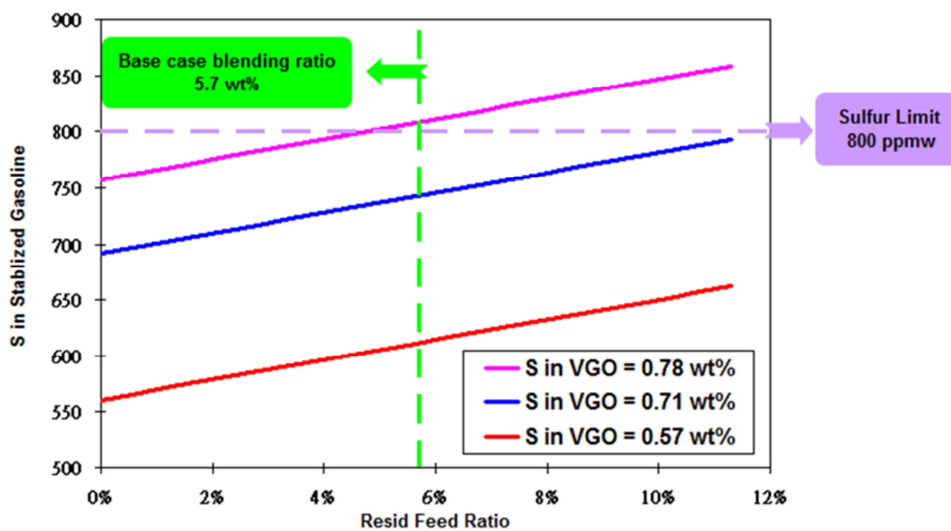


Figure 2.34: Blending in varying amounts of Residue feed

We note that all the above case studies and scenarios are limited to the FCC unit and the associated fractionation system. Modern refineries are highly integrated and changes that appear beneficial in one plant may not benefit another plant in the refinery. One way to apply these models in a larger context (in an existing refinery process) is through the linear program (LP) for refinery planning.

2.13 Refinery Planning

We briefly alluded to the complex nature of managing an FCC unit in the previous section. The typical refinery has many units in addition to the FCC (such as catalytic reforming and hydroprocessing) that have their own product distribution and associated profit margins. It is difficult to produce high profit margins dealing with each unit individually when the actual refinery process is highly integrated. The refiner needs methods to optimize feeds to each unit and related products on a refinery wide scale.

Refiners have typically solved this problem by using linear programming (LP) methods, which have been used extensively in refineries since 1950. Gary et al.⁷ state that “A site-wide model of the refinery is therefore, usually required to in order to properly determine refinery economics.”

Linear programming involves the maximization of a linear objective function of many variables subject to linear constraints on each variable⁵⁷. In the context of a refinery, the objective function can refer to overall profit generated from processing a particular set of crudes. The variables that affect this objective function are typically the amounts of different crudes purchased. The goal is to determine an optimal set of crudes that maximize the profit margin of the refinery. This scenario is an example of crude oil evaluation. Refiners typically use LP methods in other scenarios as well. Prominent examples are product blending (where two or more products from different units are mixed to form a single product) and production planning (determining the most profitable distribution of products while meeting site constraints).

A key issue in using LP methods is that the relationships between variables must be linear. In other words, all the equations used in the model must be linear with respect the variables involved. At

first, this requirement appears very confining. In fact, the FCC and gas plant models developed in previous sections of this work are highly non-linear. However, it is important to note that many units in the refinery have a small window of operating conditions during regular operation of the refinery. This allows us to linearize highly non-linear processes around the regular operating window of the refinery.

That being said, modern LP software such as Aspen PIMS includes many tools to deal with non-linear relationships. Aspen PIMS uses techniques such as “recursion” (a form of successive linear programming where the linear model runs many times with different coefficients to approximate non-linear behavior) and non-linear programming (NLP) techniques. These techniques can alleviate many problems that frequently arise, especially in product blending and property estimation, with linearized models. The focus of our application study is to improve an existing LP model for the FCC unit alone, therefore we do not consider more sophisticated techniques to deal with non-linear behavior.

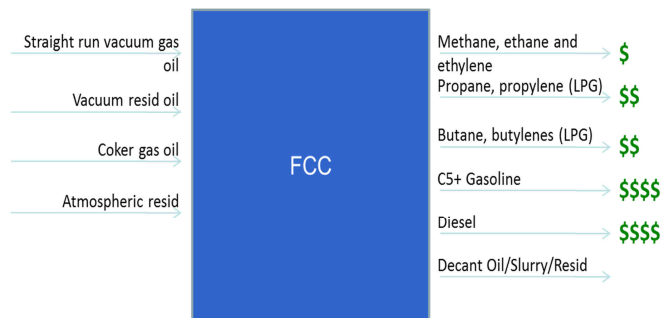


Figure 2.35: Simplified view of FCC unit for a LP application

Figure 35 represents a highly simplified view of a FCC unit. We can consider the FCC unit as a black-box that converts different types of feed into products with varying profit margins. The LP model expects that the profits or values of the products are readily available. If we consider that

only straight-run VGO enters the unit at fixed operating conditions (riser temperature, catalyst-to-oil ratio, etc.), we can represent the yield of the unit as:

$$1.0 \text{ (Normalized feed rate)} = \sum_{i=1}^N \text{Yield}_i \quad (13)$$

where we know all terms on the right-hand side to be fixed constants. The yield coefficients, Yield_i , correspond to each measured product of the FCC.

We consider the above equation to represent the base yield of the unit. In Aspen PIMS and other similar LP software, the base yield is called the base vector. We typically encode the base vector in a form shown in Table 2.16. The negative signs arise from moving all the terms from the right-hand side of the equation to the left-hand side.

Table 2.16: Sample base vector with typical yields for a gasoline-maximizing FCC unit

Row	Product	BASE
1	Feed	1.00
2	Dry Gas	-0.04
3	LPG	-0.18
4	Gasoline	-0.40
5	Diesel	-0.30
6	Loss and coke	-0.08

This base vector is sufficient to model a FCC unit that processes a single type of feed at fixed operating conditions. However, most FCC units do not operate this fashion. They accept multiple feed with varying composition and may operate at different conditions. To account for variations in

feed composition, the concept of the DELTA vector is useful. Every attribute (specific gravity, concarbon, sulfur content, etc.) of the feed that can affect the yield of the unit has its own DELTA vector. The DELTA vector can be thought of a slope that modifies the base yield of each product. If we consider the specific gravity (SPG) of the feed as an attribute that can change the product yields, we can now rewrite the yield equation as:

$$1.0 = \sum_{i=1}^N \text{Yield}_i + \sum_{i=1}^N (\text{Yield Modifier or DELTA})_i * \text{SPG} \quad (14)$$

where the SPG of the feed is a known quantity, Yield and DELTA coefficients are known for each product *i*. The products typically are Dry Gas, LPG, Gasoline, Diesel and Resid/Coke/Loss. Note the value of the DELTA coefficients correspond to the units of measurement of the particular feed attribute (in this case SPG). Table 2.17 gives sample BASE and DELTA vectors for a typical gasoline maximizing FCC unit.

Table 2.17: BASE and DELTA vectors with typical yields for a gasoline-maximizing FCC unit

Row	Product	BASE	SPG
1	Feed	1.00	-
2	Dry Gas	-0.04	-0.01
3	LPG	-0.18	0.02
4	Gasoline	-0.40	0.01
5	Diesel	-0.30	-0.01
6	Loss and coke	-0.08	-0.02

Refiners can typically obtain the base yield of the FCC unit by averaging the measured yields over some period of time. The DELTA vectors often come from estimations, refiner's internal correlations or published correlations^{7, 58, 59}. Previous work by Li et al.⁶⁰ uses correlations from Gary et al.⁷ to generate FCC DELTA-BASE vectors. These vectors are then combined with a blending and crude distillation unit model. This process results in two significant problems. The first problem is that the true yield of the FCC unit is not available to LP (only averaged yields). This leads to situations where the LP model can optimize the product distribution based on poor yield information. The second problem is that the DELTA vectors are fixed to particular correlations or estimates. These correlations may not correctly predict changes in yield accurately when the composition of the feed changes.

We overcome these problems by using the detailed FCC model developed in this work. We have shown that the FCC model can predict yields accurately for varying process conditions. To apply the FCC model into the refinery LP, we must first convert the large non-linear model into a linear yield model. We can then use coefficients from this generated linear yield model directly in the LP for the refinery. We show the process for generating the linear yield coefficients in Figure 2.36. We have found that 4% - 5% is a reasonable value for CHANGE% (variable perturbation) for most of the important feed attributes in the FCC process. For example, to generate the DELTA vector for sulfur content (SUL), we will first run the model at the base conditions and record these yields as the BASE vector. Next, we perturb the SUL variable by 5% and record the perturbed product yields. We divide the difference in base yields and perturbed yields by the change in the perturbed value to obtain the DELTA vector corresponding to the SUL variable.

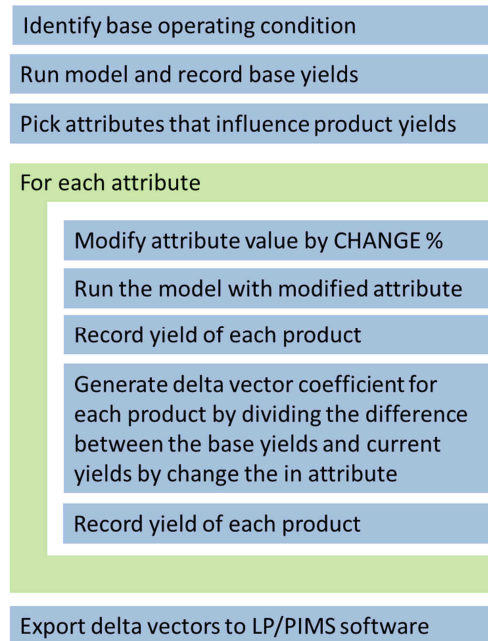


Figure 2.36: Process to generate DELTA-BASE vectors

It is important to note that the process in Figure 33 essentially generates an approximation to the Jacobian of the non-linear FCC unit model. If we consider the vector y represents the model outputs, then the \bar{y} vector represents the base case in our planning scenario and the Δx vector represents the change in model inputs from the base case. We then have a matrix of $\Delta y/\Delta x$ which represents the change from the base condition as a function of the selected feed attributes (or possibly process conditions). Eq. (15) illustrates the connection between the Jacobian and DELTA-BASE vectors

$$\begin{bmatrix} y_1 \\ y_2 \\ \vdots \\ y_m \end{bmatrix} (\text{PREDICTION}) = \begin{bmatrix} \bar{y}_1 \\ \bar{y}_2 \\ \vdots \\ \bar{y}_m \end{bmatrix} (\text{BASE}) + \begin{bmatrix} \frac{\Delta y_1}{\Delta x_1} & \dots & \frac{\Delta y_1}{\Delta x_n} \\ \vdots & \dots & \vdots \\ \frac{\Delta y_m}{\Delta x_1} & \dots & \frac{\Delta y_m}{\Delta x_n} \end{bmatrix} (\text{DELTA-BASE}) \cdot \begin{bmatrix} \Delta x_1 \\ \vdots \\ \Delta x_n \end{bmatrix} (\text{DELTA}) \quad (15)$$

Table 2.18: Existing DELTA-BASE vectors for FCC unit (normalized to a feed rate of 1.0)

Row	Product	BASE	SPG	CON	SUL
1	Feed	1.00	-	-	-
2	Sour Gas	-0.0065	-0.0003	-0.0004	-0.0082
3	Dry Gas	-0.0394	-0.0011	-0.0014	0.0000
3	LPG	-0.1740	0.0025	0.0041	0.0000
4	Gasoline	-0.3929	0.0098	0.0081	0.0000
5	Diesel	-0.2899	-0.0057	-0.0033	0.0000
6	Slurry	-0.0381	-0.0032	-0.0038	0.0082
7	Coke	-0.0544	-0.0020	-0.0034	0.0000
8	Loss	-0.0048	0.0000	0.0000	0.0000

Table 2.18 shows the existing base and DELTA vectors for the FCC unit. The base vectors come from averaged yields of the FCC unit during the previous quarter (ending December 08). The DELTA vectors come from refiner's internal correlations. The DELTA vectors refer the specific gravity of the feed (SPG), Conradson carbon (concarbon) in the feed (CON) and sulfur in the feed

(SUL). We note that this particular set of BASE and DELTA vectors do not accurately reflect the operation of the unit. As shown earlier in this work, the actual gasoline yield of the FCC unit ranges from 42-46%. The LP model underestimates the gasoline yield. In addition, since the FCC unit is the most significant producer of gasoline in the refinery, using the LP in crude selection context can lead to non-optimal crude selection.

Table 2.19: DELTA-BASE vectors generated using rigorous model

Row	Product	BASE	SPG	CON	SUL
1	Sour Gas	-0.00439	0.00068	0.0001	-0.0057
2	Dry Gas	-0.02527	0.00069	0.00033	0.00025
3	LPG	-0.19386	0.02213	0.00271	0.00164
4	Gasoline	-0.4421	0.09480	0.00621	0.00330
5	Coke	-0.06218	-0.05913	-0.00453	0.00038

Table 2.19 shows the DELTA-BASE vectors we generated using the procedure in Figure 2.36. The new BASE vector accurately reflects the current base gasoline and LPG yields of the FCC unit. In addition, as a consistency check, we note that SUL coefficient for the sour gas (row 1) has a negative coefficient. This indicates that sour gas increases as the sulfur in the feed increases. A similar consistency test with CON coefficient and coke (row 5) shows the same result. We can use the LP model optimally, knowing that LP model does not underestimate key product yields.

The advantage of this method is that LP now reflects the actual capabilities of the unit and not the perceived capabilities based historical data or correlations. In addition, if the rigorous simulation is updated alongside with plant retrofits, we can modify the LP model quickly to track these retrofits. The workflow we describe in Figure 2.36 is easy to integrate into existing process simulation and LP software. Aspen HYSYS/Petroleum Refining includes tools to automate the workflow and export the updated DELTA-BASE vectors to Aspen PIMS (LP software) directly. This automation allows quick updates of the LP model to accurately reflect unit performance.

2.13 Conclusions

In this work, we have developed a model for a FCC unit that includes a significant implementation of the associated gas plant using Aspen HYSYS. The key highlights of this work are:

1. Brief summary of existing literature for modeling a typical FCC unit
2. Description of the Aspen HYSYS FCC model and 21-Lump kinetics
3. Technique to fill out partial distillation curves using statistical functions
4. Regression of parameters for a new PNA correlation for petroleum fractions
5. Technique to infer molecular composition of FCC feedstock from routine analysis
6. Strategy to develop reasonable process models using industrial plant data
7. Application of the model to a large-scale refinery process showing less than 2.0% AAD for key product yields and satisfactory predictions of product composition and product quality (composition/distillation data, density and flash point)
8. Case studies that use the model to investigate industrially useful changes in operation
9. Strategy to transfer results from this model into LP-based refinery planning tool

Earlier work in this area has focused mostly on isolated parts (kinetic model, riser/regenerator, gas plant) of the FCC process. In this work, we show how to use routinely collected plant data with well-known commercial software tools to present an integrated process model that includes both reaction and fractionation systems. An integrated model allows users to identify opportunities to improve yield, to increase profitability and monitor the unit for predictable operation. This approach is critical for modern refineries that have increasingly complex process flows and require engineers to examine the performance of refinery units holistically.

2.14 Acknowledgements

We thank Mr. Stephen Dziuk of Aspen Technology for his valuable review comments. We thank Alliant Techsystems, Aspen Technology, China Petroleum and Chemical Corporation (SINOPEC), Milliken Chemical, Novozymes Biological, and Mid-Atlantic Technology, Research and Innovation Center (MATRIC) for supporting our educational programs in computer-aided design and process system engineering at Virginia Tech.

2.15 Nomenclature

VGO	Vacuum Gas Oil
CGO	Coker Gas Oil
LCO	Light Cycle Oil
HCO	Heavy Cycle Oil
TBP	True boiling point
C1	Methane
C2	Ethane

C3	Propane and Propylene
C4	Butanes and butenes
C5	Pentanes and pentenes
PNA	Paraffin, Naphthene and Aromatics
φ	Slip factor, unitless
ϵ	Voidage factor, unitless
D	Riser diameter, m
G	Acceleration due to gravity, $\text{m/s}^2 = 9.81 \text{ m/s}^2$
u_o	Superficial gas velocity, m/s
u_t	Terminal catalyst particle settling velocity, m/s
Fr	Froude number, unitless
Fr_t	Particle Froude number, unitless
ϕ_{COKE}	Total coke deactivation function, unitless
ϕ_{KCOKE}	Deactivation function due to kinetic coke, unitless
ϕ_{MCOKE}	Deactivation function due to metal coke, unitless
C_{KCOKE}	Kinetic coke on catalyst, kg kinetic coke/kg catalyst
C_{MCOKE}	Metal coke on catalyst, kg metal coke/kg catalyst
C_{METALS}	Metals composition on catalyst ppm metals/kg catalyst
a_{KCOKE}	Activity factor due to kinetic coke, unitless
a_{MCOKE}	Activity factor due to metal coke, unitless
E	Murphree stage efficiency factor
x_n	Mole fraction of liquid leaving stage n
y_n	Mole fraction of vapor leaving stage n

X	Normalized liquid recovery, unitless
x_{exp}	Normalized experimental liquid recovery, unitless
RSS	Sum of least squares
AAD	Average absolute deviation
A, B, α , β	Fitting parameters for cumulative beta distribution
θ	Normalized temperature
T_0	Lower reference temperature, °C
T_1	Upper reference temperature, °C
$\%X_p$	Mole composition of paraffins, unitless
$\%X_N$	Mole composition of naphthenes, unitless
$\%X_A$	Mole composition of aromatics, unitless
R_i	Refractive Index, unitless
VGC	Viscosity Gravity Constant, unitless
VGF	Viscosity Gravity Factor, unitless
a, b, c, d	Fitting parameters for PNA correlation
SG, SPG	Specific Gravity
K_w	Watson K-Factor, unitless
MeABP	Mean average boiling point temperature, R
RON	Research Octane Number
MON	Motor Octane Number
CCR, CON	Conradson carbon residue, wt. %
Yield _i	Yield coefficients for LP model, unitless
SUL	Sulfur content, wt. %

2.16 References

1. Sadeghbeigi, R. *Fluid Catalytic Cracking Handbook: Design, Operation and Troubleshooting of FCC Facilities*. **2000**. Gulf Publishing Company. Houston, TX.
2. Arbel, A.; Huang, Z.; Rinard, I. H.; Shinnar, R.; Sapre, A. V. *Ind. Eng. Chem. Res.* **1995**, 34, 1228-1243.
3. McFarlane, R. C.; Reineman, R. C.; Bartee, J. F.; Georgakis, C. *Computers Chem. Engng.* **1993**, 3, 275-300.
4. Chitnis, U. K; Corripio, A. B. *ISA Transactions*. **1998**, 37, 215-226.
5. Khandalekar, P. D.; Riggs, J. B. *Computers Chem. Engng.* **1995**, 19, 1153-1168.
6. Hsu, C. S; Robinson, P. R.; *Practical Advances in petroleum processing: Volume 1 &2*. **2006**. Springer. New York.
7. Gary, J. H.; Handwerk, G. E. *Petroleum Refining Technology and Economics* (4th ed.). Marcel-Dekker **2001**. New York.
8. Raseev, S. D.; *Thermal and catalytic processing in petroleum refining*. **2003**. CRC Press. Boca Raton, FL
9. Takatsuka, T.; Sato, S.; Morimoto, Y.; Hashimoto, H. *International Chemical Engineering*. **1987**, 27, 107-116.
10. Lee, E.; Groves, F. R. Jr., *Transactions of the Society for Computer Simulation*. **1985**, 2, 219-236.
11. Blanding, F. H. *Ind. Eng. Chem.* **1953**, 45, 1193 -1197
12. Gupta, R. K.; Kumar, V.; Srivastava, V. K. *Chemical Engineering Science*. **2007**, 62, 4510-4528.
13. Jacob, S. M.; Gross, B.; Voltz, S. E.; Weekman, V. W. *AIChE Journal*. **1976**, 22, 701-713.

14. Oliviera, L. L.; Biscasia, E. C. Jr. *Ind. Eng. Chem. Res.* **1989**, 28, 264-271.
15. Pitault, I.; Nevicato, D.; Forissier, M.; Bernard, J. R. *Chemical Engineering Science.* **1994**, 49, 4249-4262.
16. Van Landeghem, F.; Nevicato, D.; Pitault, I.; Forissier, M.; Turlier, P.; Derouin, C.; Bernard, J. R. *Applied Catalysis: A.* **1996**, 138, 381 – 405.
17. Aspen RefSYS Option Guide, AspenTech, Cambridge, MA (2006).
18. Aspen Plus FCC User's Guide, AspenTech, Cambridge, MA (2006).
19. Froment, G. F. *Catal. Rev.Sci. Eng.* **2005**, 47, 83.
20. Quann, R. J.; Jaffe, S. B. *Ind. Eng. Chem. Res.* **1992**, 31, 2483.
21. Quann, R. J.; Jaffe, S. B. *Chem. Eng. Sci.* **1996**, 51, 1615.
22. Quann, R. *Environ. Health Perspect. Suppl.* **1998**, 106, 1501.
23. Christensen, G.; Apelian, M. R.; Hickey, K. J.; Jaffe, S. B. *Chem. Eng. Sci.* **1999**, 54, 2753 – 2764.
24. Klein, M. T. *Molecular modeling in heavy hydrocarbon conversions.* **2006**. CRC Press. Boca Raton, FL.
25. Kumar, S.; Chadha, A.; Gupta, R.; Sharma, R. *Ind. Eng. Chem. Res.* **1995**, 34, 3737-3748.
26. Ellis, R. C.; Li, X.; Riggs, J. B. *J. AIChE.* **1998**, 44, 2068-2079.
27. Secchi, A. R.; Santos, M. G.; Neumann, G. A.; Trierwiler, J. O. *Computers and Chemical Engineering.* **2001**, 25, 851-858.
28. Mo, W.; Hadjigeorge, G.; Khouw, F. H. H.; van der Werf, R. P; Muller, F. *Hydrocarbon Asia.* October **2002**. 30-42.
29. Elnashaie, S. S. E. H.; Mohamed, N. F.; Kamal, M. *Chem. Eng. Comm.* **2004**, 191, 813-831.

30. Rao, R. M.; Rengaswamy, R.; Suresh, A. K.; Balaraman, K. S. *Trans IChemE: Part A*. **2004**, 82, 527-552.
31. Araujo-Monroy, C.; Lopez-Isunza, F. *Ind. Eng. Chem. Res.* **2006**, 45, 120-128.
32. Bollas, G. M.; Vasalos, I. A.; Lappas, A. A.; Iatridis, D. K.; Voutetakis, S. S.; Papadopoulou, S. *A. Chemical Engineering Science*. **2007**, 62, 1887 – 1904.
33. Fernandes, J. L.; Pinheiro, C. I. C.; Oliveira, N. M. C.; Inverno, J.; Ribeiro, F. R. *Ind. Eng. Chem. Res.* **2008**, 47, 850-866.
34. Shaikh, A. A.; Al-Mutairi, E. M.; Ino, T. *Ind. Eng. Chem. Res.* **2008**, 47, 9018-9024.
35. Fernandes, J. L.; Pinheiro, C. I. C.; Oliveira, N. M. C.; Neto, A. I.; F. Ramôa, R. *Chem. Engng. Sci.* **2007**, 62, 6308-6322.
36. Chang, S. L.; Zhou, C. Q. *Computational Mechanics*. **2003**, 31, 519 – 532.
37. Arandes, J. M.; Azkoti, M. J.; Bilbao, J.; de Lasa, H. I. *The Canadian Journal of Chemical Engineering*. **2000**, 78, 111-123.
38. Han, I. S.; Riggs, J. B.; Chung, C. B. *Chemical Engineering and Processing*. **2004**, 43, 1063-1084.
39. Paraskos, J. A.; Shah, Y. T.; McKinney, J. D.; Carr, N. L. *Ind. Eng. Chem. Process. Des. Dev.* **1976**, 15, 165 – 169.
40. Shah Y. T.; Huling, G. P.; Paraskos, J. A.; McKinney, J. D. *Ind. Eng. Chem. Process. Des. Dev.* **1977**, 16, 89 – 94.
41. Arandes, J. M.; Abajo, I.; Fernandez, I.; Lopez, D.; Bilbao, J. *Ind. Eng. Chem. Res.* **1999**, 38, 3255-3260.
42. De Lasa, H. I.; Grace, J. R. *The Canadian Journal of Chemical Engineering*. **1979**, 25, 984-990.

43. Rice, N. M.; Wojciechowski, B. W. *The Canadian Journal of Chemical Engineering* **1991**, 69, 1100-1105.
44. Harriot, P. *Chemical Reactor Design*. Marcel Dekker. 2003. New York, NY.
45. Malay, P.; Milne, B. J.; Rohani, S. *The Canadian Journal of Chemical Engineering*. **1999**, 77, 169-179.
46. Corella, J.; Frances, E. *Fluid catalytic cracking-II: Concepts in catalyst design*. **1991**, ACS Symposium Series, 452, 165–182. American Chemical Society, Washington, DC.
47. Bolkan-Kenny, Y. G.; Pugsley, T. S.; Berutti, F. *Ind. Eng. Chem. Res.* **1994**, 33, 3043-3052.
48. Han, I. S.; Chung, C. B. *Chem. Engng. Sci.* **2001**, 56, 1951-1971.
49. Froment, G. F.; Bischoff, K. B.; Wilde, J. D. *Chemical Reaction Analysis and Design*. 3rd Edition. Wiley, 2010.
50. Kister, H. Z. *Distillation Design*. **1992**. McGraw-Hill, Inc. New York, NY.
51. Kaes, G. L. *Refinery Process Modeling A Practical Guide to Steady State Modeling of Petroleum Processes*. **2000**. The Athens Printing Company: Athens, GA
52. Bollas, G. M; Vasalos, I. A.; Lappas, A. A.; Iatridis, D. K.; Tsioni, G. K. *Ind. Eng. Chem. Res.* **2004**, 43, 370-3281.
53. Sanchez, S.; Ancheyta, J.; McCaffrey, W. C. *Energy & Fuels*. **2007**, 21, 2955 – 2963.
54. Daubert, T. E.; Danner, R. P. *API Technical Data Book – Petroleum Refining*, 6th ed., American Petroleum Institute: Washington D.C., **1997**.
55. Riazi, M. R. *Characterization and Properties of Petroleum Fractions*; 1st ed., American Society for Testing and Materials: West Conshohocken, PA, **2005**.
56. Goosens, A. G. *Ind. Eng. Chem. Res.* **1997**, 36, 2500.

57. Bazaraa, M. S.; Jarvis, J. J.; Sherali, H. D. *Linear Programming and Network Flows*. John Wiley and Sons, **2009**. Hoboken, NJ.
58. Xu, C.; Gao, J.; Zhao, S.; Lin, S. *Fuel*. **2005**, 84, 669-674.
59. Ancheyta-Juarez, J.; Murillo-Hernandez, J. A. *Energy & Fuels*. **2000**, 14, 373-379.
60. Li, W.; Chi-Wai, H.; An-Xue, L. *Computers and Chemical Engineering*. **2005**, 29, 2010-2028.

3. Predictive Modeling of the Continuous Catalyst Regeneration (CCR) Reforming Process

3.1 Abstract

This work presents a model for the rating and optimization of an integrated catalytic reforming process with UOP-style continuous catalyst regeneration (CCR) using Aspen HYSYS/Petroleum Refining. The model relies on routinely monitored data such as ASTM distillation curves, paraffin-naphthene- aromatic (PNA) analysis and operating conditions. We use a lumped kinetic network with 64 species over a broad C1-C14 range. This network can represent the key dehydrogenation, dehydrocyclization, isomerization and hydrocracking reactions that typically occur with petroleum feedstock. The lumped kinetic scheme also allows us to make accurate predictions of benzene, toluene, ethylbenzene and xylenes (BTEX). In addition, this work accounts for the coke deposited on the catalyst and the associated catalyst regeneration. We implement the hydrogen recycle and product recontacting sections as separate unit operations connected to the CCR reformer model. In addition, we include rigorous tray-by-tray simulation models for primary product recovery.

We validate this model using six months of plant data from a commercial CCR reforming process handling a feed capacity of 1.4 million tons per year in the Asia Pacific. The validated model predicts key process yields and aromatic yields to within an average absolute deviation (AAD) of 1%. In addition, the model predicts liquid petroleum gas (LPG) composition to within 2.0% AAD. We also present several industrially useful case studies that display common interactions among process variables such as feed composition, reaction temperature, space velocity and hydrogen-to-hydrocarbon ratio (H₂HC). These case studies accurately quantify the effect of key process variables on process performance, and demonstrate the model applications for improving energy efficiency and for optimizing the reformer performance for chemical feedstock production.

This work differentiates itself from the reported studies in the literature through the following contributions: (1) detailed kinetic model that accounts for coke generation and catalyst deactivation; (2) complete implementation of a recontactor and primary product fractionation; (3) feed lumping from limited feed information; (4) detailed procedure for kinetic model calibration; (5) industrially relevant case studies that highlight the effects of changes in key process variables; and (6) application of the model to refinery-wide production planning.

3.2 Introduction

Catalytic reforming has long been a significant source of high-octane gasoline and aromatic components for chemical processes. Recently, there has also been renewed interest in processing non-conventional feedstock: synthetic crude, bio-oil, etc. Even with those technologies, which generally produce mostly paraffin-like feedstocks, the refinery needs reforming to convert these paraffins into high-octane components. With all these factors in play, it becomes critical to understand the reforming process on an industrial scale. This understanding must not be limited to the catalyst behavior itself, but also include the associated reforming technology and fractionation equipment.

It is in this context that we present the current work regarding the integrated modeling of the CCR process. There is significant previous work in the area, particularly those by Anchyeta-Juarez et al.^{1, 2, 3} and Taskar et al.^{4, 5}. While previous authors have provided significant details on reaction kinetics, there is not much information concerning the associated fractionation system and industrially useful case studies using a rigorous kinetic model. This work fills the gap between the development of a rigorous kinetic model and industrial application in a large-scale refinery.

3.3 Process Overview

The catalytic reforming unit exists primarily to upgrade the octane for gasoline-producing refineries or a rich source of aromatics for petrochemical complexes. The modern catalytic reforming process was first introduced by UOP in 1940⁶. Since then, there have been many different types of reforming processes developed. In general, current processes are of three distinct types:

1. Semi-regenerative
2. Cyclic
3. Moving-bed or continuous catalyst regeneration

Semi-regenerative processes generally involve a single reactor that processes feed. As the reactor processes feed, the catalyst begins to lose activity. At some point, typically around middle of the catalyst life cycle, the reactor is taken offline and the catalyst is regenerated. The advantages of this process are low capital investment and simple process flow. However, depending on the type of feed that the refiner processes, the regeneration cycle may be too long to maintain desired levels of production.

Cyclic processes involve a series of beds that operate on a rotating basis. There is a set of 5-6 reactors, however, only 3-4 may be active at any given time. When the catalyst activity for a given reactor falls below a certain value, that reactor is taken offline and the feed flow is shunted to a reactor with recently regenerated catalyst⁶.

Moving-bed or continuous catalyst regeneration (CCR) involves the continuous regeneration of the catalyst. This is possible through the construction of a special reactor that allows the continuous withdrawal of catalyst while the reactor is on-stream. The withdrawn catalyst enters a regeneration section 6. Figure 3.1 shows representative reactors from each of these processes.

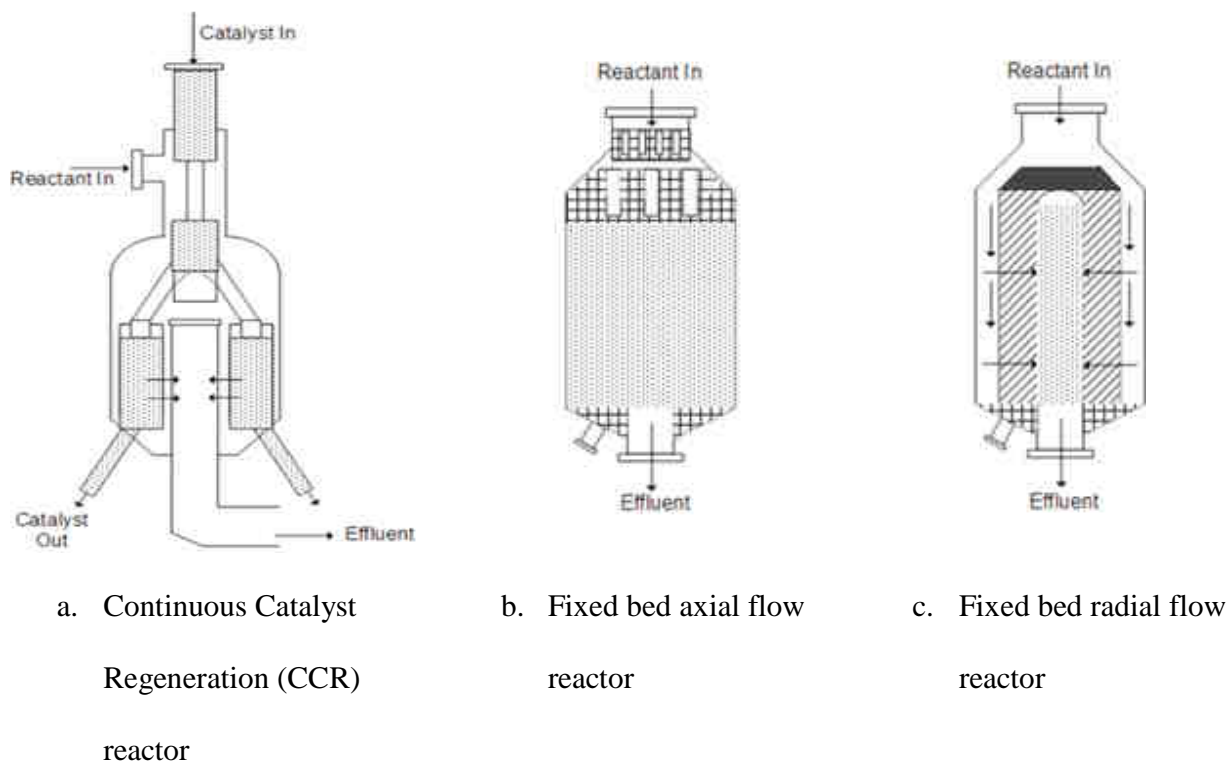


Figure 3.1: Different types of reactors used in reforming processes [Adapted from Ref. 6]

The UOP CCR process is by far the most popular reforming process. Over 50% of current reforming capacity originates from this process. This process relies on the continuous regeneration on the catalyst. This type of unit is the focus of this work and we document the process flow in the following section.

Figure 3.2 shows the process flow diagram of a commercial CCR reforming process in the Asia Pacific. This unit typically converts 1.4 million tons/yr (28,100 BPD) of straight-run naphtha into high-octane gasoline and aromatic components for use in subsequent chemical processes. The CCR unit is organized as a series of reaction sections each with differing loading (weight) of catalyst. Typically, the first unit has the least amount of catalyst and the last unit has the most. This distribution of catalyst loadings is common to all reformers and reflects the fact that during the initial stages of the reaction, highly endothermic reactions dominate the process. This effect slows

down the reaction rate; therefore the interstage heaters re-heat the reactor effluent from each section.

Reactor effluent heats the heavy naphtha (from Unit #200 in Figure 3.2) entering the process through a cross-exchanger. The hot feed enters the first interstage heater where the temperature rises to the reaction temperature. The feed contacts the moving bed of catalyst. The components in the feed undergo several reactions: dehydrogenation, dehydrocyclization, isomerization and hydrocracking. However, for a typical feed, the endothermic reactions (namely dehydrogenation) dominate and the temperature drops significantly as the reactants flow radially through the catalyst bed. The effluent leaves this reactor bed and enters the second interstage heater. A key process variable is the temperature of the feed entering each reaction section. Heaters typically operate to return the reactor effluent at a fixed temperature. The effluent from the first reactor enters the second interstage heater and leaves again at a set reaction temperature. This is due to the fact that most of the desirable reactions in reforming are endothermic. This process of heating and reaction continues until the effluent leaves the last reactor and heats up the feed into the reforming reactors. The effluent then enters the recontacting and hydrogen separation section of the process.

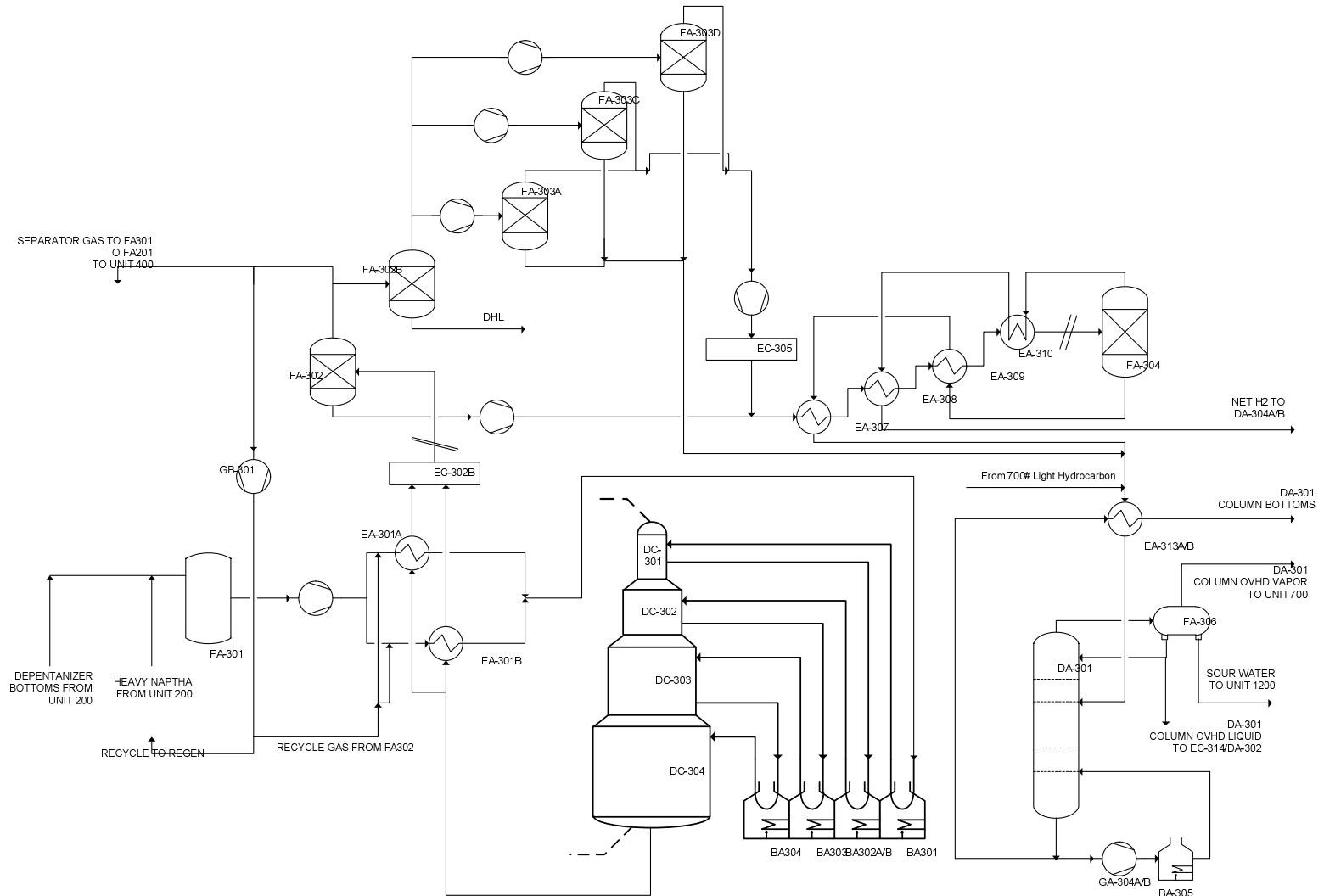


Figure 3.2: Process flow diagram for CCR reforming process

At the same time, small amounts of catalyst typically flow through the basket and enter the next reactive section. This is possible because through special gravity-assisted reactant flow shown in Figure 3.3. The CCR process is unique in that only relatively small amounts of catalyst leave the system for regeneration. Because the unit continuously regenerates the catalyst, the unit is designed to operate at much lower pressure than other reforming processes. Low-pressure operation encourages high severity but also increases the coke generation rate.

We show the process flow of a typical regeneration cycle in Figure 3.4. The spent catalyst leaves the last reactor and enters the regeneration unit. Several activities occur as the catalyst travels down the regeneration tower. Little⁶ indicates five operations that must take place during the catalyst regeneration process: Coke burn, oxidize the active metal promoters on the catalyst, adjust the chloride balance, dry the catalyst to remove unwanted moisture and finally reduce the metal promoters⁷. These processes occur in a step-wise, semi-regenerative fashion and can operate independently of the reforming process. In addition, the regeneration process operates at a much different time scale. It typically takes 5-7 days for the spent catalyst to return back to the reforming reactors^{7, 8}. This is in stark contrast with the fluid catalytic cracking (FCC) process, where reaction unit and regeneration unit are highly coupled. A key modeling implication of this regeneration time-scale and process flow is that we do not need a rigorous model of the regeneration cycle to effectively model the reforming process.

The cooled reactor effluent enters a series of separators (shown in Figure 3.2 as FA-302 through FA-304) that operate at increasing pressure. This process accounts for the fact that the CCR generally operates a much lower pressures than other reforming units. The objective is to improve the recovery of light LPG components (C3 – C4) and some C5 components. The liquid product from each of separators is subsequently cooled in several cross exchangers to recover

significant amounts of heat and condense additional light components in the liquid product. The combined liquid product enters a final separator where significant pressure change occurs and a H₂-rich (94-95 mol%) stream leaves as the vapor. This H₂-rich stream can typically supply hydrotreating and hydrocracking process in the refinery. The liquid product combined with other products (containing a significant quantity of aromatics) enters the fractionation section of the process.

Depending on the end-use of the reforming product (often called the reformate), there are two possible paths for production fractionation. If the purpose of the unit is gasoline production, the reformate enters a stabilization fractionator. This fractionator typically only separates the LPG-like portion of the reformate as the overhead product and the bottom product leaves as high-octane gasoline destined for the refinery blending pool. However, if the purpose of the unit is aromatics production to support a petrochemical complex, the stabilizer operates differently as a depentanizer (shown as DA301 in Figure 3.2). The depentanizer separates all the C₅ and lighter components as the overhead product. The bottom product largely contains all the aromatics and remaining paraffin and naphthenic content greater than C₆, and it then enters the BTX separation plant which may be located in a different area of the refinery all together.

The separation of product aromatics into discrete aromatic species depends on the refinery configuration. This process can be quite large and complex especially in the case of petrochemical refineries where aromatics can be recovered from many sources. Typically, a special solvent (e.g. sulfolane or polyglycols) separates out the benzene and toluene components from the feed to BTX separation plant. The separation of xylenes requires additional processing. Fractionation towers can separate ortho-xylene and ethylbenzene isomers. However, the meta-xylene and para-xylene isomers typically require a crystallization or adsorption on molecular

sieves (UOP Parex process)⁸. Because of the complexity of the BTX separation plant, we do not include BTX fractionation in this work. However, future work will address the special requirements and workflow for simulating a BTX separation plant.

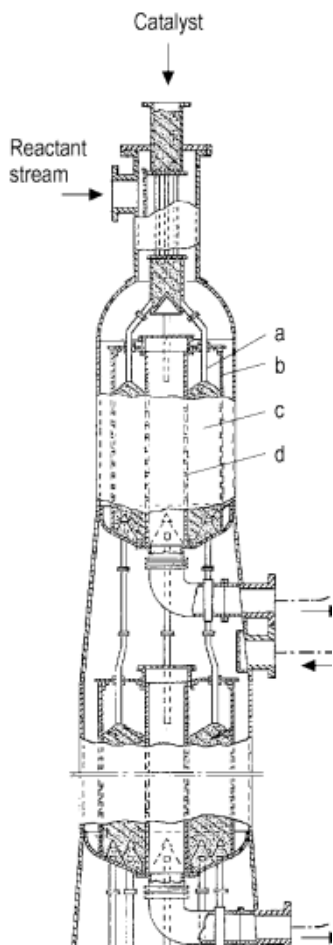


Figure 3.3: Cutaway of gravity assisted reactor⁹

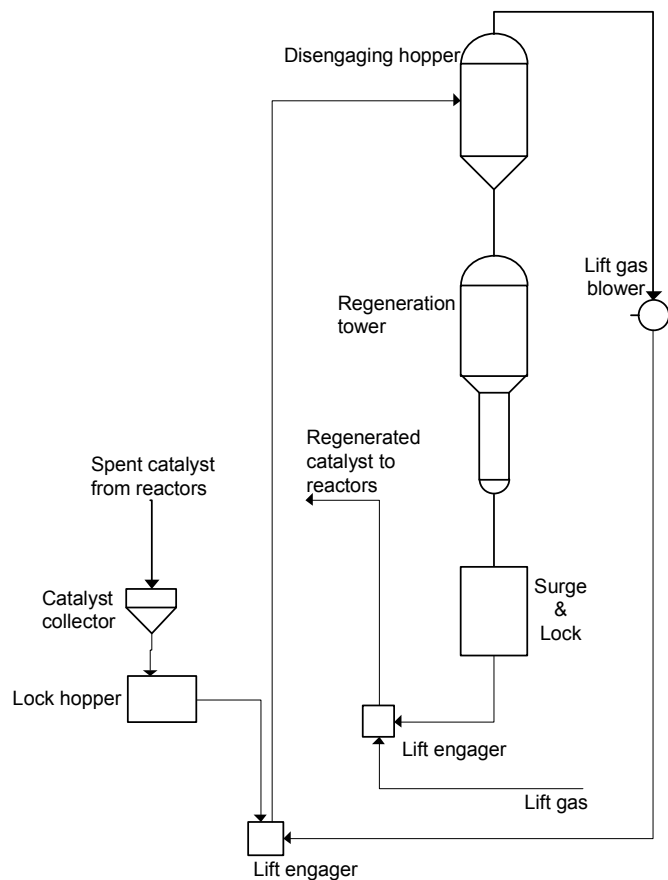


Figure 3.4: Schematic of catalyst regeneration process⁶

The feed to the reforming unit is an important process consideration. The feedstock to a reformer is typically a straight-run naphtha cut or hydrotreated gasoline cut from an FCC unit. In general, a feed that has an end boiling point (EBP) of 205-210 °C is not included. This feed encourages hydrocracking reactions and excessive coke generation. The feed usually hydrotreated because sulfur, nitrogen and other trace components can deactivate the catalyst significantly. In fact, many processes may also include several “guard reactors” to prevent sulfur

entering the reforming unit. Table 3.1 shows a typical distillation curve and basic compositional analysis of reformer feedstock.

Table 3.1: Typical reforming feedstock

ASTM-D86 (vol %)	(°C)	Group	Paraffin (wt%)	Naphthene (wt%)	Aromatic (wt%)
IBP	76	C5	1.00	0.47	-
5%	90	C6	6.85	6.66	0.88
10%	94	C7	11.25	13.17	2.31
30%	104	C8	9.42	14.02	3.02
50%	116	C9	7.35	10.79	3.04
70%	131	C10	4.45	5.31	0.00
90%	152	Total	40.32	50.42	9.25
95%	160	Specific Gravity (SG)			0.745
EBP	170	Sulfur/Nitrogen/Halide content (ppm)			0.5/0.5/NA

Refiners often consider the total naphthene (N) and aromatic (A) content of the feed as an indicator of how high an octane rating a feedstock can produce. This is referred to as N+A or N+2A indicator for the feed. Many correlations for reformer yield exist on the basis of these indicators. However, Little⁶ indicates that these correlations often have strong assumptions built in such as catalyst type and operating conditions. While it may serve for simple feedstock selection, it is not the only significant indicator of unit performance.

The catalyst in the unit is the most important consideration for optimal operation. Little⁶ identifies three key characteristics of reforming catalysts: activity, selectivity and stability. The

activity is a measure of how efficiently the catalyst can help convert the reactants into products.

In general, current reforming catalysts can operate at higher temperatures and maintain high reaction conversion when the reactant flow rate increases. The selectivity refers to the catalyst ability to produce more of the high-value products (aromatics) than low-value products. The stability refers the ability of the catalyst to maintain high activity and selectivity over long periods of time. The catalyst in modern reforming units is only changed once every 1-2 years⁷.

Modern reforming catalysts consist of an alumina base that supports platinum and rhenium particles to catalyze the desired reactions. Current consensus indicates that the platinum sites promote the dehydrogenation reactions and the alumina, acting as an acid site, promotes cyclization, isomerization and hydrocyclization^{7, 10, 11, 12}. These types of catalysts are known as bimetallic (and sometimes bifunctional catalysts). As the catalyst spends more time on stream, coke deposits and lack of acid sites prevent additional reaction. The rate of coke deposition is a function of olefin-like precursors that lead to the formation of a multi-aromatic ring¹³. At this point, the catalyst is taken off-stream and regenerated through several processes to restore its function. The reaction chemistry that occurs on these catalysts can be quite complex, and published experimental studies often do not reflect the conditions that a catalyst operates under in an industrial process. In the following section, we briefly survey some of the key process chemistry and operating parameters.

3.4 Process Chemistry

Table 3.2 lists the major reactions observed in the reforming process. This is by no means an exhaustive list. In general, the desired reactions take the following paths: (1) paraffins in the feed

convert isoparaffins or are cyclized into the naphthenes; (2) the naphthenes present convert to aromatic groups; and (3) olefins convert to paraffins through hydrogenation¹⁴.

A detailed study of many of the reactions is out of the scope of this work. We refer readers to Froment et al.^{10, 11, 12} for detailed experimental and mechanistic studies. These studies are very useful in the course of detailed catalyst design and kinetic network generation^{15, 16, 17, 18}.

However, neither of these topics is the subject of the current work. We present these reactions in the context of an integrated process model. As mentioned earlier in this work, the typical reactions in the reforming process are dehydrogenation, dehydrocyclization, isomerization and hydrocracking. Table 3.2 shows examples of these reaction classes.

Table 3.2: Examples of reactions from key reaction classes

Dehydrogenation of alkylcycloalkanes to aromatics	$MCH \rightarrow TOL + H_2$
Dehydroisomerization of alkylcyclopentanes	$MCP \rightarrow MCH$
Dehydrocyclization of paraffins to aromatics	$NP_7 \rightarrow TOL + H_2$
Isomerization of normal paraffins to isoparaffins	$NP \rightarrow IP$
Isomerization of alkylcyclopentanes to cyclohexanes	$MCP \rightarrow MCH$
Hydrocracking reactions	$P_X \rightarrow P_Y + P_Z$
Hydrogenolysis	$P_7 + 6H_2 \rightarrow 7P_1$

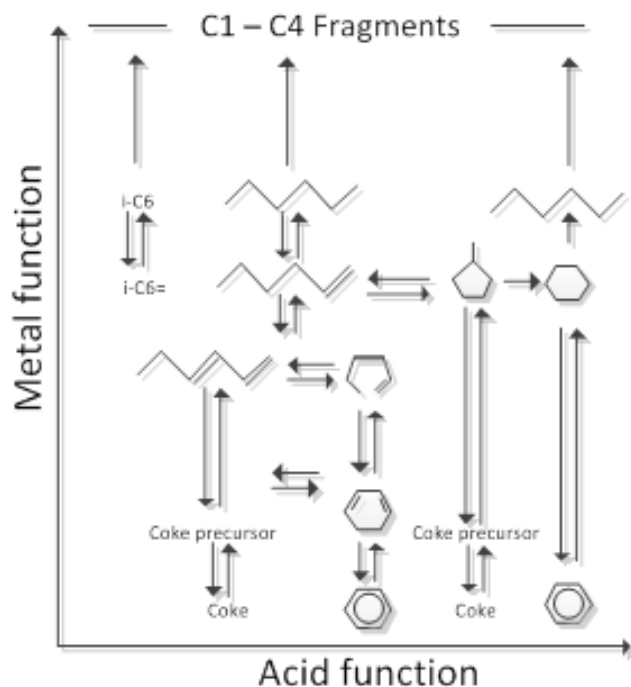


Figure 3.5: Relationship between catalyst features and reaction classes [Ref. 13, 14]

Figure 3.5 shows the relationship between the acid and metal functions of the catalyst and particular classes of reactions. The acidic function of the catalyst promotes the isomerization reactions, namely, reactions that convert paraffins into naphthenes and isoparaffins. Iso-paraffins are important contributors to high-octane number. The metal function promotes the dehydrogenation reactions, where the naphthenes are dehydrogenated into aromatics. The metal function is also a significant source of a coke (or polyaromatic compounds) that adsorb to the catalyst surface. In addition, the olefins are hydrogenated producing paraffins for further reaction.

The degree to which each reaction propagates is a function of temperature and pressure. High temperature and pressure tends to promote hydrocracking and the undesirable hydrogenolysis. The effect of pressure is quite significant on hydrogenolysis and modern reformers tend to operate at much lower pressures than their predecessors. Table 3.3 summarizes the effect of key operating variables on yields. In all cases, increase in reactor temperature increases the reaction rate.

Table 3.3: Behavior summary key reaction classes [Adapted from Ref. 6, 7, 8]

Reaction	Rate	Heat	Pressure	Hydrogen
Dehydrogenation (Naphthene)	Very fast	Endothermic	Negative	Produces
Isomerization (Naphthene)	Fast	Exothermic (Mild)	None	None
Isomerization (Paraffin)	Fast	Exothermic (Mild)	None	None
Cyclization	Slow	Exothermic (Mild)	Negative	Produces
Hydrocracking	Slowest	Exothermic	Positive	Consumes
Hydrogenolysis	Slowest	Exothermic (High)	Positive	Consumes

In addition to the operating variables of reactor, the feed composition also plays an important role in determining the distribution of products. Industrial experience and experimental studies of the chemistry of reforming reactions indicate several key trends^{7, 19}:

- The primary source of benzene in the reactor products is methylcyclopentane (MCP).

- Dimethylcyclopentane and cycloheptane form a key pathway to produce additional toluene.
- Dimethylcyclohexane and methylcyclohexane produces additional xylene in the product.

It is clear that in industrial operations, it is difficult to control many process variables to drive reactions to optimal product distributions. There are four primary control variables for reformers: reactor inlet temperatures, reactor pressures, hydrogen content, and feed rate. There are other variables such as feedstock properties and catalyst type. But these variables are generally fixed for a given period of time.

Refiners generally control the inlet temperature to each reactor bed or section. The inlet temperatures are typically averaged (weighted by the ratio of the catalyst in the given bed to the total catalyst) and presented as the weight-averaged inlet (WAIT) temperature. The pressure in sections of the reactor is typically fixed by design and does not vary significantly during operation. This is especially the case in CCR units where the pressure balance drives catalyst flow. Another important variable is the amount of hydrogen that is recycled back to unit along with fresh feed. Current reformers typically operate at high conversions and a significant quantity of hydrogen is required to prevent coke formation. During normal operation, the H₂/HC ratio (ratio of hydrogen to hydrocarbons) ranges from 3 to 4. The final control variable is typically the feed to the unit. High feed rates typically indicate the low contact time between the catalyst and feed.

3.5 Literature Review

There is a significant body of literature on the topic of modeling catalytic reformers. They consist of two types of models: kinetic models and unit-level models. Kinetic analysis refers to

detailed studies of the reaction mechanism and catalyst behavior. This work is necessarily experimental and based on lab studies of various feed compounds. Model development work uses the insights from the kinetic analysis to develop a kinetic network with associated rate constants and reaction orders. This work typically results in rate expressions that are verified using bench-scale reactors. The unit-level models focus on models that integrate the kinetic model in the context of pilot-scale or commercial reactors. This work often includes models for multiple reactor beds and associated process equipment (interstage heaters, etc.). We provide a brief survey of the current state of knowledge in each of these areas.

3.5.1 Kinetic models and networks

Mechanistic and experimental studies generally result in the creation of a kinetic network that quantitatively describes the path a particular reactant takes. Given the complexity of the reforming reactions and the number of species involved, many researchers have taken a “lumped” approach towards describing the kinetics. In a lumped approach, many different molecules are placed into a single group or lump. The reaction kinetics then assumes that all species in a lump behave identically. Recently, some researchers have presented models that involve hundreds of reaction species and thousands of reactions^{16, 18}. However, there is little published information about these complex kinetic models validated against industrial operation.

The earliest kinetic model for reforming is that of Smith²⁰, which assumes that the feed is a combination of three lumps: paraffins (P), naphthenes (N) and aromatic (A). We show a basic schematic of the network in Figure 3.6 (a). The kinetic network accounts for dehydrocyclization (P → N), dehydrogenation (N → A) and hydrocracking (A → P). The hydrocracking reactions in this model result in an equilibrium distribution of paraffins. This model does not include the

effect of reaction parameters such as pressure and excess hydrogen present. In addition, there is no deactivation factor due to the presence of coke or heavy adsorbed hydrocarbons. Krane et al.²¹ further refine this model by splitting up the each P, N and A lump into groups corresponding to the number of carbons. This model has 20 lumps and 53 reactions. Eq. (1) shows the basic form for each rate expression:

$$\frac{dN_i}{d\left(\frac{A_c}{W}\right)} = -k_i N_i \quad (1)$$

A significant oversight in Krane's model is the lack of the effect of catalyst activity and pressure. Henningsen et al.²² introduce a network that considers the different rates of reactivity between C5 and C6 naphthenes and an activity factor for catalyst deactivation. Jenkins et al.²³ include empirical correction factors for acid and pressure in the rate expression. Ancheyeta-Juarez^{2,3} also introduce a similar pressure correction term to account for pressures other than 300 psig specified in the Krane et al. model. Later work by Ancheyeta and co-workers includes additional pathways to deal with MCH as a primary precursor to benzene¹⁹ in the product pool and to deal with non-isothermal operation. Models derived from Krane et al. and Ancheyeta et al. have been used to model a variety of reforming processes, ranging from pilot plants to commercial operations. Hu et al.²⁴ use a similar approach to generate a kinetic network. Ancheyeta's modifications to Krane's original model still remains in use and work published recently shows good agreement with measure data and model predictions^{19,25,26}.

$$\frac{dN_i}{d\left(\frac{A_c}{W}\right)} = -k_i e^{(E_i/R)\left(\frac{1}{T_0} - \frac{1}{T}\right)} \left(\frac{P}{P_0}\right)^\alpha P_i \quad (2)$$

Krane's original model and modifications by Ancheyeta do not treat kinetic network as a catalytic process occurring heterogeneously and do not consider the difference in reactivities of

cyclopentanes and cyclohexanes. Figure 3.6 (c) shows the kinetic network from Henningsen et al. that includes separate pathways for cyclopentanes and cyclohexanes. Henningsen et al. apply this model with conjunction with a heat balance to account for the non-isothermal operation of the reactor. These works have generally shown excellent agreement with commercial and pilot-plant data.

$$\frac{dC_i}{dt} = \sum k_i e^{(E_i/RT)} P_i \quad (3)$$

A key limitation of the models derived from Krane et al. and Henningsen et al. is that the reaction network is not treated as a catalytic process. A catalytic reaction kinetics network must include terms to allow for inhibition and decrease in activity due to variety of factors. Raseev et al.¹⁴ present the earliest model treating the reaction network as a catalytic system. However, this study is limited due to the lack of experimental data. Figure 3.6 (d) shows the kinetic network from an extensive study by Ramage et al.²⁷ where independent pathways for cyclohexanes and cyclopentanes exist in addition to adsorption and pressure effects. However, this model is limited by the lumping into only C5- and C5+. Kmak presented a similar model that extends the lumping to include C7 components²⁸.

$$\frac{dw_i}{dv} = \frac{\left(\frac{PV}{FRT}\right) k_\phi}{1 + K_H P_H + (PF_c/F) \sum K_{w_i} w_i} \sum k_i w_i \quad (4)$$

Key work by Froment and co-workers^{7, 10, 11, 12} has produced a nearly complete lumping based reaction network for C5-C9 (and C1 – C5 for paraffins) components of reforming feed. This model includes several insights from experimental studies. They consider that the metal sites on

the catalyst promote only the dehydrogenation reactions, while the acid site promotes the cyclization, isomerization and hydrocracking reactions. We show the network in Figure 3.7.

<p>PNA-only model from Smith²⁰</p>	<p>PNA-only model from Ancheyta-Juarez et al.^{2, 3}</p>
<p>ACH and ACP model from Henningsen et al. 22</p>	<p>C5 – C8 lumping method from Ramage et al.²⁷</p>

Figure 3.6: Basic lumping kinetic networks

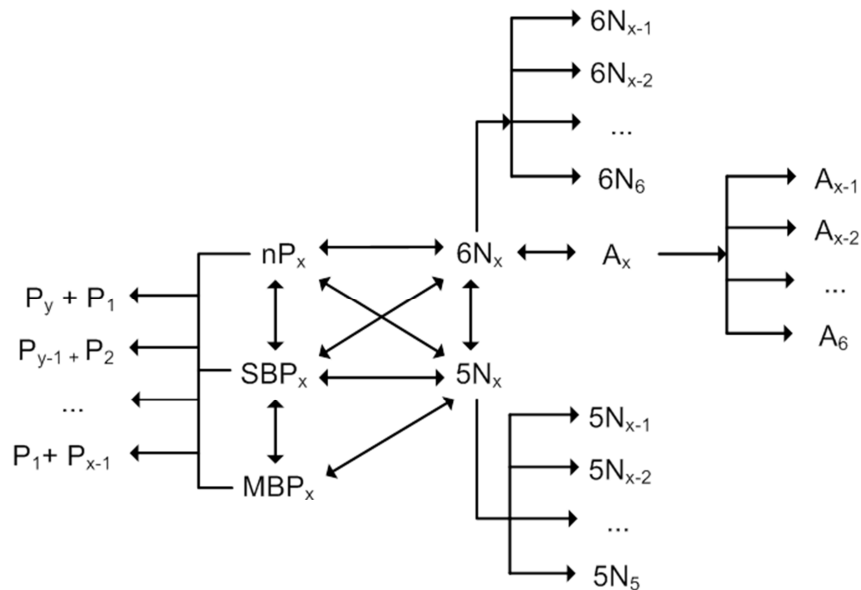


Figure 3.7: Lumped kinetic network from Froment where $5 < x < 9$ [Ref. 12]

The kinetic network in Figure 3.7 includes separate pathways for N5 and N6 components and accounts explicitly for light production (C1 – C5). This is critical to maintaining a good prediction of light gas components from industrial models. In addition, the adsorption factors include terms to account for hydrogen content, total pressure and adsorbed hydrocarbons. Additional work by Taskar et al.^{4,5} modifies this network to include the effects of catalyst deactivation. Table 3.4 shows the key rate equations for each class and the deactivation factor due to Taskar et al.

Table 3.4: Key rate equations from Taskar et al.^{4,5}

Isomerization of paraffins	$\phi \cdot A_0 e^{-E/RT} (P_A - P_B/K_{AB})/\Gamma$	(5)
Hydrocracking of paraffins	$\phi \cdot A_0 e^{-E/RT} (P_A P_B)/\Gamma$	(6)
Ring closure of paraffins	$\phi \cdot A_0 e^{-E/RT} (P_A - P_B P_H/K_{AB})/\Gamma$	(7)

Ring expansion (C5 to C6)	$\phi \cdot A_0 e^{-E/RT} (P_A - P_B) / \Gamma$ (8)
Dehydrogenation	$\phi \cdot A_0 e^{-E/RT} (P_A - P_B P_H^3 / K_{AB}) / (P_H \theta)^2$ (9)
Adsorption due to acid function	$\Gamma = (P_H + K_{C6-} P_{C6-} + K_{P7} P_{P7} + K_{N7} P_{N7} + K_{TOL} P_{TOL})$ (10)
Adsorption due to metal function	$\theta = 1 + K_{MCH1} P_{MCH} + K_{MCH2} (P_{MCH} / P_H^2)$ (11)
Deactivation term	$\phi = e^{-\alpha C_c}$ (12)

Recent advances in computational power and theoretical insight have led to the creation of mechanistic reaction pathways that can involve thousands of reactions and hundreds of species. The approach of Froment^{15, 16, 17} is called the single-event approach. In this approach, an algorithm generates a reaction network based on fundamental mechanisms such as hydride shifts and beta-scission. The use of structural relationships such as Evans-Polyanii reduces the number of parameters required for modeling significantly. Experimental data may be used to fit the remaining parameters (roughly 30-50). This approach has been successfully used for a variety of processes including methanol-to-olefins (MTO) and fluid catalytic cracking (FCC) that exhibit similar features as the catalytic reforming process. Due to limitations of feedstock analysis, this technique makes several assumptions to lump together components in the feedstock and presents rate equation that is the summation of many rate equations drawn from fundamental chemistry.

Another approach is the molecular modeling work by Klein and co-workers¹⁸. In their work, they propose technique of pathway modeling where a series of chemical reaction paths are applied to many hundreds (if not thousands) of feed species. They then construct a reaction path that only

contains the allowable reaction chemistry. Klein et al. also simplify the process of estimating kinetic parameters through the linear free energy relationships (LFER). The final network for naphtha reforming involves 116 species and 546 reactions. Several works report the success of this model through several pilot-plant studies. A key issue is the feedstock characterization. Klein et al.²⁹ use a stochastic approach where they pick combinations of thousands of species and attempt to match the calculated bulk properties (specific gravity, molecular weight, sulfur content, etc.) of a particular combination to measured bulk properties.

In the course of applying a model to a commercial plant, it is best to rely on kinetic models that only require the minimal amount of feedstock information and calibration. Feed to reformers may change quickly and without laboratory analysis, there is often no choice but to lump components together. In addition, it may not be possible to incorporate large complex models into existing highly integrated flowsheet models. These factors generally drive model developers to choose lumped kinetic networks.

3.5.2 Unit-level models

After choosing a representative kinetic model, we must decide how to represent the remaining units for a truly integrated model. Researchers have applied many of the kinetic networks described in the previous section in integrated process models. Figure 3.8 is an overview the key features of an integrated process model for a three-section reformer. This overview applies to both semi-regenerative fixed bed and CCR reformers.

First, the model must be able to take bulk property measurements and convert them into appropriate lumps for kinetic network. This step may be quite simple if the kinetic model chosen only includes total PNA content for the total fraction. However, if the kinetic lumping requires

detailed composition information, we must provide some way of estimating these lumps from limited composition information. Taskar et al.^{4,5} discuss a possible method based on measurements of certain bulk properties such gravity and distillation curve. We discuss the approach used in this work in a later section.

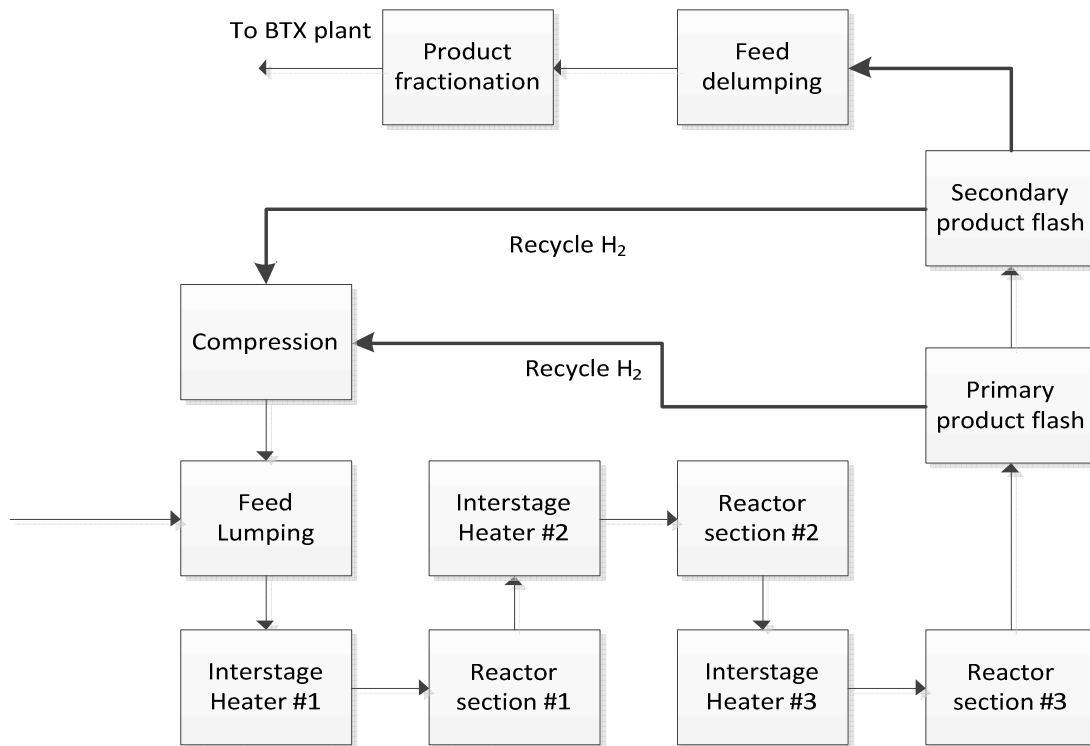


Figure 3.8: Basic process flow for an integrated reformer model

The second consideration is the model for the interstage heaters, product separators and compressors. In order to model these units meaningfully, we must have reasonable estimates for the key thermophysical properties of the lumps. In the case of the reformer, we must make reasonable prediction of reactant concentration (at system pressure), K-values (for the product separator) and heat capacity (to correctly model the reactor temperature drop and product temperatures). The reforming process generally operates at temperatures and pressures where the

ideal gas law applies for hydrocarbon species in the reactor section. Ancheyta-Juarez et al.^{1,2} use the ideal gas assumption to calculate the concentration of reactant species. In addition, they use the polynomial heat capacity correlations for pure components to approximate the heat capacity of the mixture. Work by Bommannan et al.³⁰ and Padmavathi et al.³¹ uses a fixed value for the heat capacity and K-value correlation to predict compositions in the primary product separator.

Most authors model the reactor section as a plug-flow reactor (PFR) of fixed length. This length is typically the size of the packing bed for a fixed bed semi-regenerative unit. This assumption works well with all the kinetic networks mentioned above. Modeling the flow through the CCR unit is slightly different in that reactants travel through a moving bed of catalyst particles. Hou et al.³² describe how to modify the standard PFR to account for a radial flow unit. Szczygiel³³ studied mass transfer and diffusional resistance in reforming reactors. However, these types of studies are difficult to apply in the context of commercial plants and many authors of integrated models have ignored these effects.

The final step in an integrated model is the delumping of kinetic lumps back to bulk properties and lumps suitable for fractionation models. Many authors do not consider this delumping process since they do not include a rigorous fractionation section. Typically, many studies report only properties such as RON and MON. If the kinetic lumping method used spans a significant range, then fractionation models can work directly with the kinetic lumps. Works by Hou et al.³² and Li et al.³⁴ use the kinetic lumps directly.

Table 3.5 summarizes the key features in reported unit- level models (using lumped kinetics) applied to reforming processes. We have only included studies where the authors compare their

results to pilot- plant or industrial data. In addition, we include those studies where the authors use the model for case studies and plant optimization.

Table 3.5: Summary of unit level models reported in literature

Reference	Application	Kinetics	Feed lumping	Calibration	Planning (LP)
Ramage et al. ²⁷ (1987)	Semiregenerative	C5-C8(P, N5, N6, A) lumps	None	Yes	Yes
Bommannan et al. ³⁰ (1989)	Semiregenerative	Simple lumps (P,N, A)	None	None	None
Anchyeta et al. ^{1,2} (1994)	Semiregenerative	C5-C10 (P, N, A)	None	None	None
Taskar ⁴⁵ (1996)	Semiregenerative	C5-C10 (P, N5, N6, A) lumps	Yes	Yes	None
Lee et al. ³⁵ (1997)	CCR	Simple lumps (P,N, A)	None	None	None
Padmavathi et al. ³¹ (1997)	Semiregenerative	C6-C9 (P, N5, N6, A) lumps	None	Yes	None

Ancheyta- Juarez et al. ¹⁹ (2002)	Pilot plant	C5-C11 (P, MCP, N6, A) lumps	None	Yes (Kinetic regression)	None
Hu et al. ³⁶ (2003)	CCR	C6-C9 (P, N, A) lumps	None	Yes	None
Li et al. ³⁴ (2005)	Semiregenerative	C1-C9 (P, N5, N5, A) lumps	None	Yes	None
Hou et al. ³² (2006)	CCR	C1-C9 (P, N, A) lumps	None	Yes	None
Stijepovic et al. ^{25,37} (2010)	Semiregenerative	C6-C9 (P, N, A) lumps	No	No	None
This work	CCR	C1-C14 (P, N5, N6, A) lumps	Yes	Yes	Yes

3.6 Aspen HYSYS/Petroleum Refining Catalytic Reformer Model

This section discusses the key features of the Aspen HYSYS/Petroleum Refining model we use throughout this work. While the features we discuss are specific to Aspen HYSYS/Petroleum Refining, there are other simulation programs (e.g., KBC Petro-Sim) that have similar

functionality. The goal of this section is to discuss the key features of the simulator that are relevant to developing an integrated reaction and fractionation model.

Figure 3.9 shows a basic outline of the key submodels in Aspen HYSYS/Petroleum Refining. This model contains all the key submodels identified in the previous section. The model presented in this work includes the additional fractionation units to model the separation of LPG (<C4) and the reformate into gasoline and high-octane compounds for blending and chemical purposes.

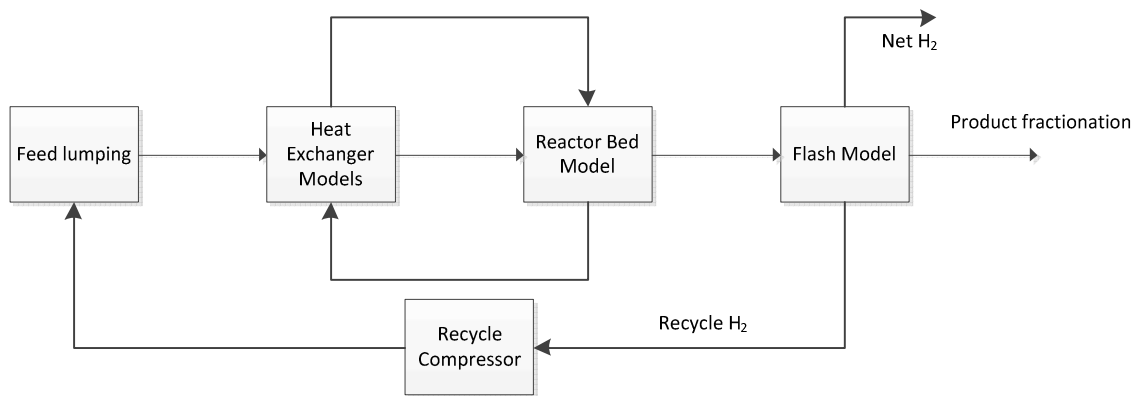


Figure 3.9: Organization of Aspen HYSYS/Petroleum Refining CatReform model

The feed lumping technique in the Aspen HYSYS/Petroleum Refining model relies on a base of compositions and a method to correct those measured compositions based on changes in measured bulk properties. The feed is broken into many (4-14) lumps for each chemical group. Typically, these measured properties are the distillation curve and total PNA content. In our work, we had access to detailed feed composition information, so we did not use this technique. However, we have developed an alternate technique of feed lumping based on minimal base

composition data and bulk property requirements. We discuss this technique in a subsequent section.

The reaction network in the reactor model is similar to the network presented by Froment et al.¹² and Taskar⁴. However, the reaction network supports higher aromatics up to C14. While these typically are not expected in reformer feeds, the kinetic model can handle them as well. In addition, the reactor model includes paths for the undesired hydrogenolysis reactions. These highly exothermic reactions do not occur in any significant degree in stable reforming units. However, older reactors may display this behavior so it is important to model them as well.

Table 3.6: Key reactions classes in Aspen HYSYS/Petroleum Refining Catalytic Reformer model

Isomerization of paraffins	$a_{class}a_{reaction}A_0e^{-E/RT}(P_A - P_B/K_{AB})/\Gamma$	(13)
Hydrocracking of paraffins	$a_{class}a_{reaction}A_0e^{-E/RT}(P_AP_B)/\Gamma$	(14)
Ring closure of paraffins	$a_{class}a_{reaction}A_0e^{-E/RT}(P_A - P_BP_H/K_{AB})/\Gamma$	(15)
Ring expansion (C5 to C6)	$a_{class}a_{reaction}A_0e^{-E/RT}(P_A - P_B)/\Gamma$	(16)
Dehydrogenation	$a_{class}a_{reaction}A_0e^{-E/RT}(P_A - P_BP_H^3/K_{AB})$ $/(P_H\theta)^2$	(17)

Equations 13-17 show the general form of the kinetic rate expression. The important thing to note is that there are two activity correction factors associated with each rate expression. The first correction factor, a_{class} , is fixed for a given class of reactions. For example, all the isomerization reactions may have a rate constant of 1.0. The second correction factor, $a_{reaction}$, refers to correction for an individual pathway. For example, the activity factor for the isomerization of C6 paraffins may have a correction factor of 0.5. The product of these two

factors presents the overall activity correction for that reaction. The individual rate constant and activation energy remain fixed. These factors been derived from experimental data over a variety of catalysts. In practice, however, even significant changes in unit operations do not require significant changes in values of these reaction activity factors.

Another significant feature is that the coke generation is rigorously modeled and included in the deactivation and adsorption factor, Γ , for each reaction. The deactivation factor is function of reactor pressure, adsorbed hydrocarbons, coke on catalyst and acid/metal function of the catalyst. This feature allows us to calibrate the model to a variety of operating conditions and catalyst behavior. In this work, we model a CCR with a hydrotreated feed; therefore, we do not include any significant changes in catalyst activity due to changes in acid of the catalyst.

The reactor model is based on a modified plug-flow reactor for a moving bed that accounts for catalyst flow in the CCR system. A key consideration in the reactor is the phenomenon of “pinning”^{38,39} in CCR reformers. “Pinning” refers the catalyst that is held immobile against the wall due to cross flow of reactants. It is important to model this effect, since pinning imposes a maximum flow rate on reactants. The reactor also correctly models the temperature drop due to heat of reaction in the exothermic and endothermic reactions. The other key variables are the weight-averaged inlet temperature (WAIT), weight-averaged bed temperature (WABT) and weighted hourly space velocity (WHSV).

As mentioned in a previous section, integrated model for CCR must also include rigorous models for interstage heaters to correctly predict energy consumption of the unit. The unit may be modeled as rigorous fired heaters or basic heat exchangers. We include a model to recompress the vapor from the primary product flash. Our work also includes the complete model for the

product recontacting section. We must model this section correctly in order to correctly predict the composition of the recycle stream entering the reformer. All of these units require thermophysical properties and methods to predict equilibrium. We use the Peng-Robinson (PR) equation state modified for hydrogen-containing systems. We describe how to obtain the relevant thermophysical properties for each lump in a subsequent section.

The final step in the integrated model before fractionation is the delumping of products and prediction of bulk properties. Since our lumping system is quite broad, we can just calculate key properties of the reformer effluent as combination of the individual properties of the lumps.

$$RON_{MIX} = \sum w_i RON_i \quad (18)$$

$$MON_{MIX} = \sum w_i MON_i \quad (19)$$

where RON_{MIX} and MON_{MIX} refer to the research and motor octane number of product measured in bulk, w_i refers to the weight fraction of each lump and RON_i and MON_i refer to the research and motor octane number of each lump.

Since we wish to use this model to model BTX production as well, we need to predict the composition of the all the relevant isomers of A8 (ethylbenzene, ortho-xylene, para-xylene, meta-xylene). In our model, we assume that these isomers take on fixed equilibrium ratios as a function of temperature. Figure 3.10 shows the equilibrium distribution of these isomers at various temperatures^{40, 41}. The distributions correspond to expected temperatures in the reforming process. Figure 3.11 shows the observed A8 isomer distribution measured at the plant. We note that it is remarkably stable over a lengthy operating period (six months) and a variety of feed conditions.

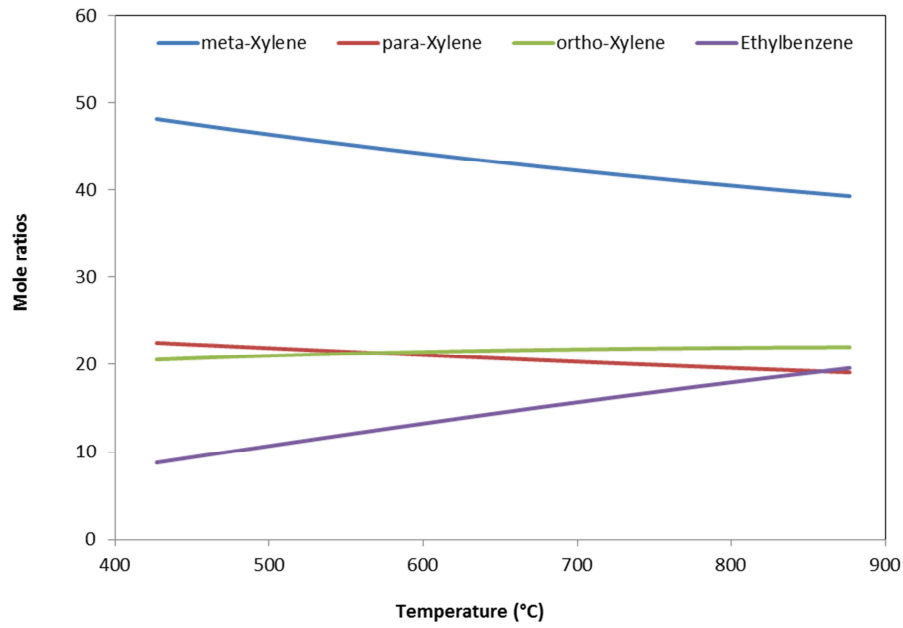


Figure 3.10: Equilibrium composition of A8 isomers (assuming ideal gas conditions)

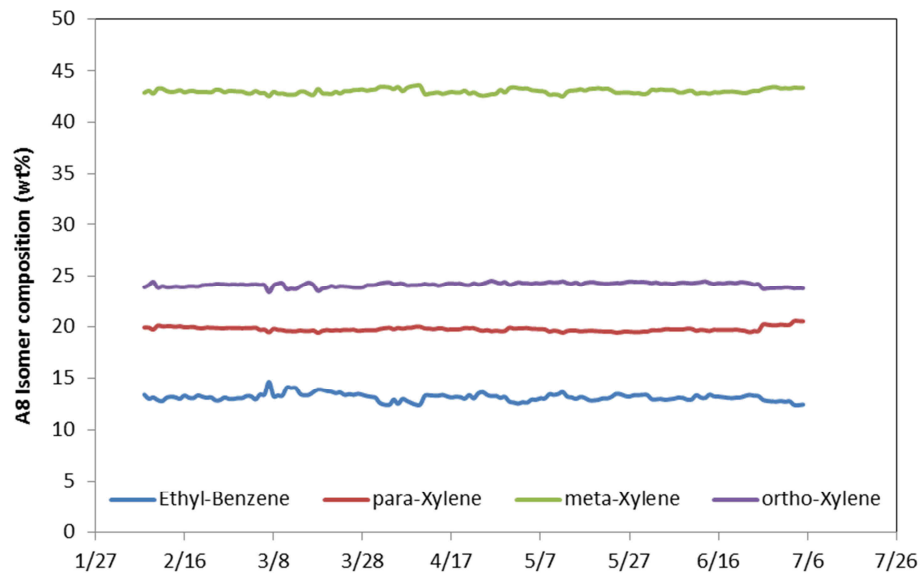


Figure 3.11: Composition of A8 isomers over the study period

This completes our description of the Aspen HYSYS/Petroleum Refining model. In subsequent sections, we discuss issues of thermophysical properties, fractionation and feed lumping. These issues are not specific to a simulation program and apply generally to any model of a reforming process.

3.7 Thermophysical Properties

The requirements for thermophysical properties depend on the kinetic lumping chosen for the process. Typically, the reactor model requires only the heat capacity and molecular weight. The fractionation section may require a correlation to predict K-values or critical parameters when an equation of state is used. One approach is to use one set of lumps for the reactor model and another set for the fractionation. However, this approach may cause problems when recycling material back into the reactor and makes producing an integrated model difficult. If possible, we suggest the use of uniform lumps across the reactor and fractionation models.

If the reactor lumps resemble real measured products (e.g., A8), then it is sufficient to use the known properties of one of the compounds comprising the lump as the properties of the lump. The kinetic lumps in this work resemble real lumps, so we use known compound properties. If this information is not available, we can use Riazi's correlations⁴² to estimate the relevant critical properties for different classes of compounds (paraffins, naphthenes and aromatics) given the molecular weight of a particular lump.

$$\theta = a(\text{MW})^b(\text{CH})^c \quad (20)$$

where θ represents critical temperature (T_c), critical pressure (P_c), critical volume (V_c), specific gravity (SG) or refractive index (I). Riazi⁴² provides values for a, b and c for different classes of compounds.

3.8 Fractionation System

We use the standard inside-out methods⁴³ implemented by many popular simulators including Aspen HYSYS/Petroleum Refining. This work only includes the primary product debutanizer and deheptanizer. These columns prepare the reactor effluent for further aromatic extraction in the BTX plant. We discuss the fractionation system in the BTX plant in a subsequent work.

The inside-out method provides quick convergence and wide flexibility in specifications. It is relatively easy to converge a column with a variety of specifications, but it remains difficult to produce a robust and predictive fractionation model. Many real-world fractionation systems do not operate with the ideal stage assumption used in standard distillation algorithms. A popular method to deal with the non-ideal tray behavior is the Murphree tray efficiency factor⁴³:

$$E = \frac{y_n - y_{n+1}}{y_n^* - y_{n+1}} \quad \text{or} \quad \frac{x_n - x_{n+1}}{x_n^* - x_{n+1}} \quad (21)$$

where x_n represents mole fraction of a given component in the liquid leaving tray n, x_{n+1} represents mole fraction of a given component in the liquid leaving tray n+1. The y_n and y_{n+1} refer to the vapor mole fraction of a given component leaving as vapor from trays n and n+1.

This efficiency factor is found many popular simulation programs. However, use of the efficiency factor essentially negates the assumption for the tray-by-tray ideal behavior by

modifying the vapor and liquid mole fractions. This results in unreliable predictions when the fractionation model moves to operating point. We agree with the recommendations of Kister⁴³ and Kaes⁴⁴ and advise against the use of efficiency factors.

We recommend the use of overall column efficiency factors. Overall column efficiency refers to the ratio of ideal (or theoretical) trays and actual physical trays. This is a single value that can range from 30% - 90%. If we consider the case of a distillation column having 20 physical trays and overall efficiency of 0.5, we would model it as a column with 10 ideal trays. With this approach, every tray remains in thermodynamic equilibrium and predictions away from the base operating scenario are reasonable. In the present work, we model the DA301, a reformate splitter and DA302, a deheptanizer. Table 3.7 shows the relevant overall efficiencies for these columns. We refer readers to Kaes⁴⁴ for information on how to model more complex fractionation systems in refineries.

Table 3.7: Summary of overall efficiencies for product fractionation in CCR

Fractionator	Theoretical trays	Overall efficiency
Reformate Splitter (Debutanizer)	26	70% - 80%
Deheptanizer	36	75% - 80%

An important consideration is the selection of specifications to converge columns. Modern simulation software makes it quite easy to choose a wide range of specifications. However, software generally does not provide a guide to choosing reasonable specifications. In our work, we use a two-stage process. We first choose specifications that we know converge easily for a

given a feed rate to the column. For a simple distillation column, these are typically the reflux ratio and overhead draw rate. In addition, we also provide temperature estimates. Once we obtain an initial solution, we introduce more difficult specifications such as temperature, mole recovery and control temperatures. Table 3.8 gives the specifications for relevant columns in the CCR fractionation process.

Table 3.8: Key specifications in fractionation section

Fractionator	Initial specifications	Final specifications
Reformate Splitter (Debutanizer)	<ol style="list-style-type: none"> 1. Reflux ratio 2. Overhead (or bottom) draw rate 3. Control stage temperature 	<ol style="list-style-type: none"> 1. Reflux ratio 2. Mole purity of C5 in the overhead 3. Control stage temperature
Deheptanizer	<ol style="list-style-type: none"> 1. Reflux ratio 2. Overhead draw rate 	<ol style="list-style-type: none"> 1. Reflux ratio 2. Control stage temperature

Another significant consideration is that model developers, especially when modeling an existing plant, be aware of what the key control variables in the column are. The final specifications in the column must reflect actual plant control variables. For example, we should not fix the temperature of a condenser in the model when the plant actually controls the column based on an overhead draw rate.

3.9 Feed Characterization

The most important consideration for a reactor model is an accurate measure of the feed composition. This is particularly troublesome when modeling refinery reaction processes. Feed to units may change quickly and unpredictably. While refinery techniques for online measurements of feed composition have improved, many still do not perform detailed molecular-based analysis required for complex kinetic models. Without an accurate and update-to-date feed composition, kinetic models fail to make reasonable predictions of product yield and process performance.

There are several methods to alleviate this issue. One method is to work from a standard set of pre-analyzed feeds and generate a set of base compositions. In addition, a large database of standard pre-analyzed feeds can provide a process to generate the composition-shift vectors. This is very similar to the process of generating delta-base vectors for refinery planning discussed in Part 1 of this series. We attempt to quantify the effects of changes in easily and routinely measured bulk properties such as TBP curves, specific gravity, molecular weight, viscosity, etc. on the changes in the feed composition. Aspen HYSYS/Petroleum Refining provides a method based on the presence of several feed types. The feed types refer to the origin of the feedstock entering the reforming unit. Depending on the size of the database used to generate these shift vectors, this method can be very accurate in practice.

Another method is to try and estimate the composition of the reactors based only on bulk property information. This bulk property information typically refers to routinely measured properties such density, distillation curves, etc. Klein and co-workers²⁹ have used a much more sophisticated version of this approach to probabilistically sample candidate molecules and

generate a very large list of molecules whose combined properties match the measured bulk properties. Hu et al.²⁴ use a probability distribution method to estimate to the PNA compositions for their approach towards refinery reactor modeling. The approach we describe is similar, but much simpler to use since it is targeted only for reformer feeds.

A key assumption in this method is that each class of molecules, i.e., paraffins, naphthenes and aromatics are statistically distributed around a certain mean value. For the case of reformer feed, we know that significant portion (80+ wt%) lies between the C6-C9 range. With this information, we assume that the each class centers around the C6-C9 range following a statistical distribution. Sanchez et al.⁴⁵ applied various statistical distributions to fit a variety of distillation data. They recommend the use of the beta statistical function to accurately represent distillation data.

A key criterion is that the normalized distributed be non-symmetrical since a certain class of compounds may exist in very narrow ranges. In addition, we would like a function that is easily accessible in popular software tools (e.g. Microsoft Excel) and has as few parameters as possible. Based on the observations by Sanchez et al.⁴⁵ and our criteria, we find that a two-parameter normalized beta statistical distribution for each class of molecules is sufficient for characterizing a reformer feed. The statistical beta function can be written as:

$$f(x, \alpha, \beta) = \frac{\Gamma(\alpha + \beta)}{\Gamma(\alpha)\Gamma(\beta)} x^{\alpha-1} (1 - x)^{\beta-1} \quad (22)$$

where α and β refer to the positive valued parameters that control the shape of the distribution, Γ refers to the standard gamma function and x identifies a given lump.

We apply the method in the following steps:

1. Choose the lumping range. In our work, we choose the PNA lumps in C5-C11 range.
2. Pre-compute the individual properties of each of the lumps (i.e. associate each lump with normal boiling point, standard liquid density, molecular weight, etc.). It is possible to compute each of properties using correlations from Riazi⁴².
3. Obtain as much bulk data about the feed as possible. The minimum requirements are specific gravity and true boiling point (TBP) curve.
4. If a TBP curve is not available, use API correlations to convert a D-86 distillation curve to a TBP curve.
5. This method requires the total PNA content expressed in either weight%, volume% or mole%. If this information is not available, the API correlation⁴² (requiring viscosity) can provide these values.
6. Guess values for the mean and standard deviation for each distribution to compute the fraction of each component in the C5-C11 (a total of six parameters). Since we know the total PNA (from step 5), we can normalize each distribution to make sure the sum of fractions of each class of lumps matches the total PNA.
7. Compute the bulk property information using the candidate lump compositions.
8. Arrange all the candidate lumps in order of increasing boiling point to generate candidate TBP curve.
9. Compute a residual between the measured or known bulk properties and calculated bulk properties in step 7.
10. Return to step 6 unless the residual is minimized to some small value.

In our experience, the last end points of a typical 5-point TBP curve (the end point or EBP, 90% vaporization point, 70% vaporization point), the molecular weight (measured or estimated from API correlation) and specific gravity are good candidate bulk properties to minimize against. This is a basic optimization problem. We have used the SOLVER add-in in Microsoft Excel with considerable success. We note that once an optimized solution has been reached for a base feed, it is often very simple (even manually) to adjust the parameters of the statistical distribution to fit a new feed type. We report the optimal values for the fitting parameters in Table 3.10.

We apply this method to the feed specified in Table 3.1 using the ASTM D-86 distillation, specific gravity and individual PNA composition. We convert the ASTM D-86 distillation curve to a TBP curve and estimate the molecular weight (using standard API correlations). We then optimize the parameters to match the EBP, 90% and 70% of the TBP curve, molecular weight and specific gravity. We compare the calculated and measured values in Figure 3.12 and Table 3.9.

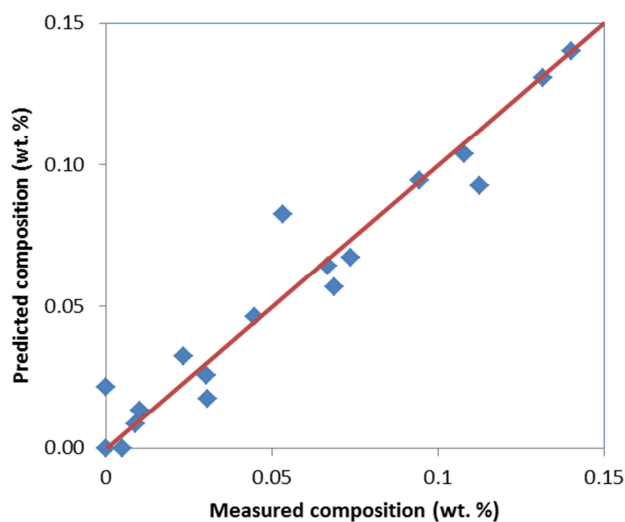


Figure 3.12: Correlation between prediction and measured composition

Table 3.9: Predicted PNA composition from parameter estimation process

	Predicted			Measured		
	P	N	A	P	N	A
C5	1.36%	0.00%	-	1.00%	0.47%	-
C6	5.70%	6.43%	0.85%	6.85%	6.66%	0.88%
C7	9.29%	13.09%	3.26%	11.25%	13.17%	2.31%
C8	9.46%	14.01%	2.57%	9.42%	14.02%	3.02%
C9	6.74%	10.38%	1.78%	7.35%	10.79%	3.04%
C10	4.64%	8.27%	2.17%	4.45%	5.31%	0.00%

Table 3.10: Optimized parameters for PNA beta distribution functions

Group	α	β
P	3.9145	6.6190
N	1.2454	4.5050
A	3.0402	6.9700

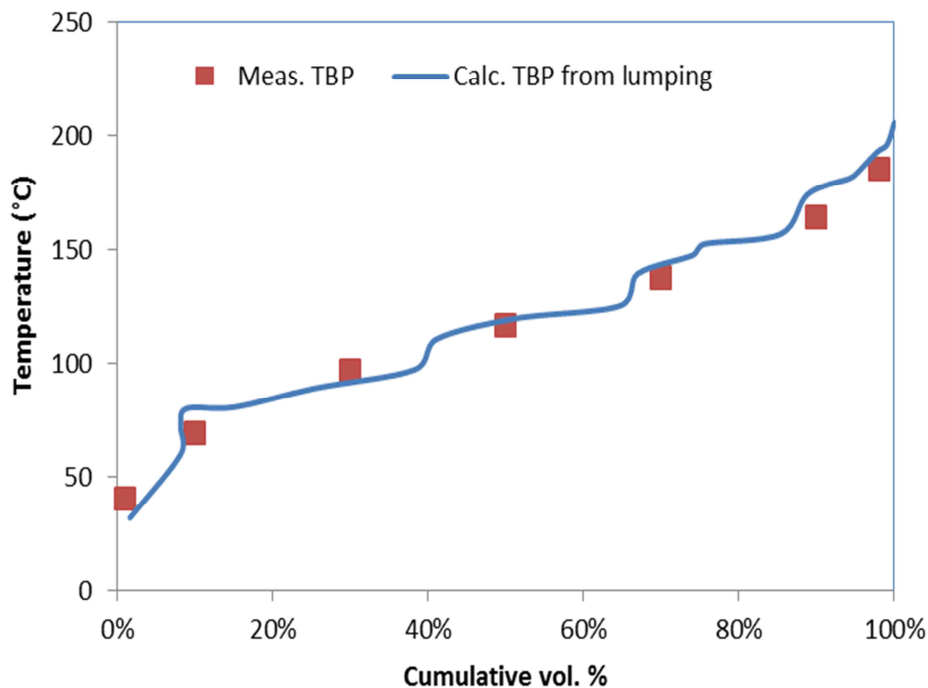


Figure 3.13: Comparison between measured and calculated TBP based on PNA lumping

There is good agreement between the measured TBP (converted from ASTM D-86 data) and calculated TBP curve. Note that we have not included all the TBP points in the optimization routine, but the optimized solution makes good predictions for the lower TBP points as well.

Figure 3.14 shows the optimized distribution of PNA for this feed. As the distribution function predicts an A5 lump (a physically impossible solution), we ignore this component when calculating the lump composition. We note that each of the distributions has a different shape that reflects the different nature of a specific component class. If we use a simple normal distribution function, it is unlikely that we would be able to represent many different types of feed.

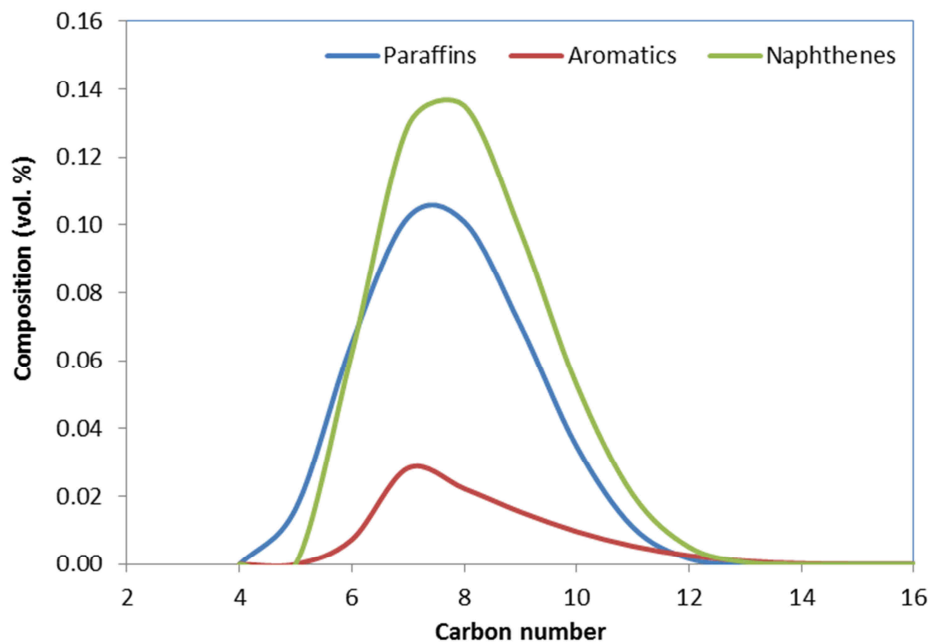


Figure 3.14: Optimized distribution of paraffin, naphthene and aromatic for given feed type

3.10 Model Implementation

There are three important considerations when building any reaction model based on plant data:

- Ensure the data consistency through accurate mass balance
- Characterize the feed based on limited information
- Calibrate the reactor model to a reasonable level of accuracy

In the following sections, we discuss several steps and tools to help with the implementation of the model. We provide access to the tools mentioned in section on our group website. Finally, we discuss an overall modeling strategy to model an existing reforming unit.

3.10.1 Data consistency

An important task during data collection and model calibration is the overall mass and hydrogen balance across the reformer unit. The overall mass balance is simply a difference between the sum of all the feeds entering the unit and sum of all products leaving the unit. While this concept is fundamentally simple, it can be difficult to realize in a real production plant. Many reformer units include feeds from other units that only enter plant through the fractionation section. This is typically the case when the refiner maximizes aromatics recovery produced by other units in the refinery.

We provide a spreadsheet (Figure 3.15) to account for feeds to the reforming plant that enter the reactor section and fractionation section. We can either subtract the feeds entering the unit or make sure they are accounted in the overall balance. We have successfully closed the mass balance to under 0.2-0.3% by making sure to account for all products. The advantages of a closed mass balance are not limited to the kinetic modeling process itself, since other refinery-wide modeling (such as production planning) often relies on accurate mass balances.

A secondary issue relates to the calibration and predictions from the rigorous reformer model. It is critical to ensure that the hydrogen balance is satisfactorily closed before beginning model development. We define the hydrogen balance as follows:

$$\text{Mass flow rate of hydrogen in the feed} = \text{Mass flow rate hydrogen leaving the unit} \quad (23)$$

Turpin⁴⁶ provides a simple formula for calculate the hydrogen content. We use a similar equation to verify the balance of the unit:

$$\text{HFACTOR}_{ij}(\text{for } C_iH_j) = \frac{j \cdot 1.01}{i \cdot 12.01 + j \cdot 1.01} \quad (24)$$

$$\text{Hydrogen flow of } C_iH_j = \text{HFACTOR}_{ij} \cdot \text{Mass flow of } C_iH_j \quad (25)$$

Turpin⁴⁶ recommends that hydrogen mass balances should be closed to less than 0.5% error. This can be difficult without detailed verification of measured flow rates. We recommend that calibration proceed even if the hydrogen balance cannot be closed. However, it may not be possible to perform a finely tuned calibration as a result.

	A	B	C	D	E	F	G	H	I	J	K	L	M	N
1	Enter Mass fractions in cells below title (Can convert from mole/vol. fraction to mass fraction using HYSYS if necessary)													
2														
3	Mass Balance													
4	In	Out												
5	1.834E+05	1.839E+05												
6	Error	-0.29%												
7														
8	Hydrogen Balance													
9	In	Out												
10	2.669E+04	2.836E+04												
11	Error	-6.25%												
12														
13		Grouped Compositions			H2 Flow (kg/h)	2.561E+04	2.918E+01	6.731E+02	3.851E+02		8.029E+03	8.370E+02	3.682E+03	1.582E+04
14	C Atoms		MW	Wt% H	Rate (kg/h)	1.759E+05	2.360E+02	4.410E+03	2.779E+03		1.295E+04	3.998E+03	2.090E+04	1.460E+05
15	0 H2		2.02	1.000	Feed	#500	#700	#7500			Net Gas	DA301 Ovhd V	DA301 Ovhd L	DA301 Btms
16	1 P1		16.04	0.251							52.34%	2.79%	0.07%	
17	2 P2		30.07	0.201			0.04%	0.09%			11.51%	4.34%	0.31%	
18	3 P3		44.10	0.183			2.23%	0.97%			14.69%	23.18%	5.24%	
							18.14%	6.20%			12.53%	36.88%	24.55%	

Figure 3.15: Microsoft Excel-based spreadsheet tool for mass and hydrogen balance calculations

3.10.2 Feed characterization

Section 8 discusses a method to obtain estimates for the composition when limited feed information (distillation curves and density) are available. While the method produces good estimates of the feed composition, it may fail to predict the correct amount of N5 and N6 in the

feed. Good estimates of the N5 and N6 are critical for a meaningful calibration since these components are the primary pathways to obtain benzene in the reformat.

We recommend that analysis be performed to determine the N5 and N6 composition before calibrating a detailed model of the reformer. Once feed analysis establishes a baseline N5 and N6 content, we can expect the calibration to reflect reactor operation more accurately. Figure 3.16 shows the variation in N5 and N6 content of the hydrotreated reformer feed over the course of our work. There is significant variation in the N6 content which justifies a detailed feed analysis before the model calibration.

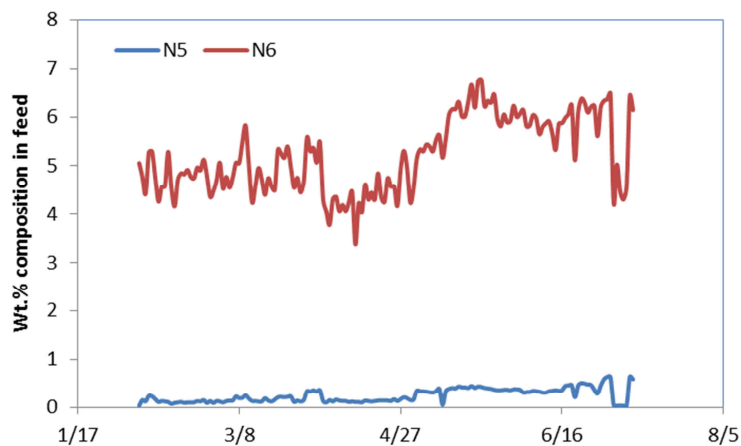


Figure 3.16: Variation in N5 and N6 content in feed

3.10.3 Calibration

Because of the number of unit-level and kinetic models available in the literature and commercially, it is impossible to prescribe a single a calibration method that will work for all models and methods. However, there are significant common features in all of the models to

allow for general recommendations. These recommendations form a simple workflow to manage the large number of parameters that many occur in a many models.

Modern calibration methods in current software allows users to change many (if not all parameters) in a particular model with ease. While this is a simple procedure, it is easy to “overcalibrate” the model and generates calibration values that basically ignore process chemistry and other phenomena. We believe it is better to follow a step-by-step process where we only change a few parameters (of the same class and with bounds) at a time.

We perform the calibration in two passes. The first pass is the coarse calibration of the model, while the second pass performs the fine calibration. The quality of the model calibration relies on consistent and reliable data. If we cannot find these data, it may be difficult to justify performing the fine calibration of the model. In fact, performing the fine calibration with poor quality data may result in an “overcalibrated” model. With that in mind, we propose a step-by-step process for calibration.

The key steps in calibration are:

1. Verify that the material and hydrogen balance is closed.
 - a. If the material balance has an error exceeding 1-2% percent, this data set should not be used for calibration.
 - b. If the total hydrogen balance has an error exceeding 2-3%, it is unlikely that fine tuning of the reactor model will be successful.

2. Obtain feed composition
 - a. Use detailed PNA information if possible.

- b. If detailed PNA information is not available, use total PNA information and feed characterization method described earlier.
 - c. If total PNA information is not available, it is possible to use bulk measurements such as viscosity, density and distillation data to estimate the PNA composition required for (b). These correlations are available from our previous work and Riazi⁴². In this case, fine tuning of the reactor model can become difficult.
3. Select objective function criteria:
 - a. Define the objective function to minimize as $\sum w_i (Measured_i - Predicted_i)^2$
 - b. Table 3.11 suggests terms and associated weightings for both coarse and fine calibrations.
 - c. If a detailed analysis of the reactor effluent is available, do not include every component in the objective function.
4. Coarse tuning
 - a. Select overall reactor selectivity only.
 - b. Use Table 3.11 to select terms for coarse tuning form of the objective function. A zero entry in the weighting factor indicates that the term should not be part of the objective function.
5. Second pass
 - a. Select overall reactor selectivity, overall reaction activity.
 - b. Use Table 3.12 to select terms for fine tuning form of the objective function

- c. Calibrate the model.
- d. Adjust selectivity for light ends (P1 – P3) as the last step in the calibration.

Table 3.11: Major terms and their recommended weighting factors in the reformer model objective function for calibration

Term	Coarse	Fine
Reactor delta temperature(s)	1.0	1.5 - 2.0
Total aromatics (wt%)	5.0	10.0
Benzene (wt%)	5.0	10.0
Toluene (wt%)	5.0	10.0
Xylenes (wt%)	1.0	10.0
A9+ (wt%)	0.0 (Ignore)	5.0
Paraffins (P1 – P3)	0.0 (Ignore)	0.5 (Last)
Paraffins (P4+)	0.0 (Ignore)	1.0
Paraffins (P8+)	0.0 (Ignore)	1.0
Naphthenes (N5, N6)	1.0	10.0
Ratio of isomer to normal paraffins	0.0 (Ignore)	0.5 (May not be predicted)
Net gas flow	1.0	1.0
Total heavy (wt%)	0.0 (Ignore)	1.0

It is important not include yields of every significant component. Including every possible measurement for optimization often results in a poor calibration. A poor calibration means that the model is essentially fixed to a single data point, and it will result in a model that responds

wildly even to small changes in the input variables. It is better to avoid poor calibration even at the expense of not agreeing plant measurements. When this situation happens, it means that there is likely mass imbalance or hydrogen imbalance in the feed and product measurements. It is best to recheck model inputs before attempting any further calibration.

Table 3.12: Typical adjustment factors to calibrate reformer model

Parameter	Range of deviation from the base
Overall reactor activities	0.1 – 10
Reaction class	
Dehydrogenation	0.1 – 1.1
Hydrocracking	0.1 – 1.1
Isomerization	0.1 – 1.1
Ring closure	0.1 – 1.1
Ring expansion	0.1 – 1.1
Light Ends tuning	
C1/C2/C3	0.1 – 5.0

We use the ranges for the adjustment factors and weightings for the error residual to generate constraints for an optimization procedure. Since the model is developed in an equation-oriented (EO) format, it is not difficult to apply an optimization procedure to generate optimal values for the adjustment factors. An objective value of less than 250 (using coarse weightings) is sufficient for coarse adjustment when significant feed information (such as composition) is missing or estimated. For fine adjustment, which is required in the case of accurate prediction for aromatic component composition, an objective value of less than 200 (using fine weightings) is required.

Obtaining a reasonable calibration using fine tuning requires accurate composition, feed rate, hydrogen yield and reactor operating parameters (temperature, pressure) measurements.

The adjustment factors in Table 3.12 are sufficient to represent a wide variety of operating behavior. Models may allow users to individual tune each reaction in the kinetic network.

Reaction specific tuning may result in very good agreement with plant data, but the model may lose predictive ability. The reaction specific tuning essentially fixes it to one operating point. In addition, models may include adjustment factors for the primary product separation. We do not adjust these values routinely as part of the calibration.

We note that it may not be possible to fine-tune the model to the prescribed limits earlier. Plant mass balance error, poor measurements and unexpected process variation may limit how well the model agrees with the plant data. However, by following the above calibration procedure, we can ensure that we do not “overcalibrate” the model and subsequently produce poor predictions.

3.11 Overall modeling strategy

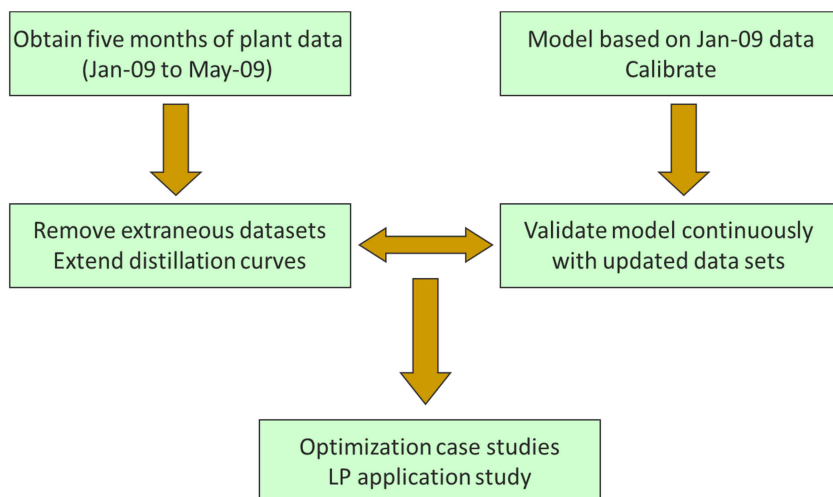


Figure 3.17: Overall modeling strategy

Figure 3.17 outlines the overall modeling strategy used in this work. We implement and calibrate the model while it is in regular operation in the refinery. Many factors such as abrupt changes in feed quality, operating parameters, poor measurements and inconsistent impede this process. Work by Fernandes et al.⁴⁷ documents the same difficulties while modeling a FCC unit. In our work, dataset refers to a collection measurements that reflect plant operation for a short period of time (less than one day). We propose the following steps to ensure that calibration results in a model that is predictive and not fixed to a single operating scenario:

- Record data on a continuous basis from the plant
 - Reconcile data from multiple sources (DCS, Inventory, etc.)
 - Check consistency of the dataset by performing material and hydrogen balance.
Use the criteria in previous section to accept or reject certain data.
 - Accept a dataset (or conditionally accept acknowledging that there may be significant error in calibration and prediction)
 - Track variation in the dataset to ensure that we verify the model against significant changes in feed and operating parameters. We show the significant changes in feed quality in our work in Figure 3.18.

- Develop fractionation models by backblending the measured reactor products and verify that the models agree with plant measurements
 - We provide guidelines for developing the fractionation system in the model development section of this work.

- Calibrate reactor model
 - Use calibration procedure to produce a coarsely and finely calibrated model
 - The product yields from the finely calibrated model should be within 1% of actual plant yield. If this is not the case, it is likely that the material balance and hydrogen was not closed sufficiently.
 - The outlet temperatures from the finely calibrated model should be within 3-5 C of measured plant values.

- Validation
 - Use accepted datasets track the performance of the reformer and fractionation sections with the model.
 - If possible, examine the yield of the reactor effluent directly with measure products. We can identify if errors arise from the reactor model or the fractionation section and isolate the section for further validation or calibration.
 - It is typically possible to predict yields of key products (BTX) on a feed normalized mass basis with AAD of less than 2-3%.

- Recalibration
 - We suggest recalibration when significant changes occur in the catalyst or regeneration section. The model can generally account for significant changes in feed stock and operating parameters.

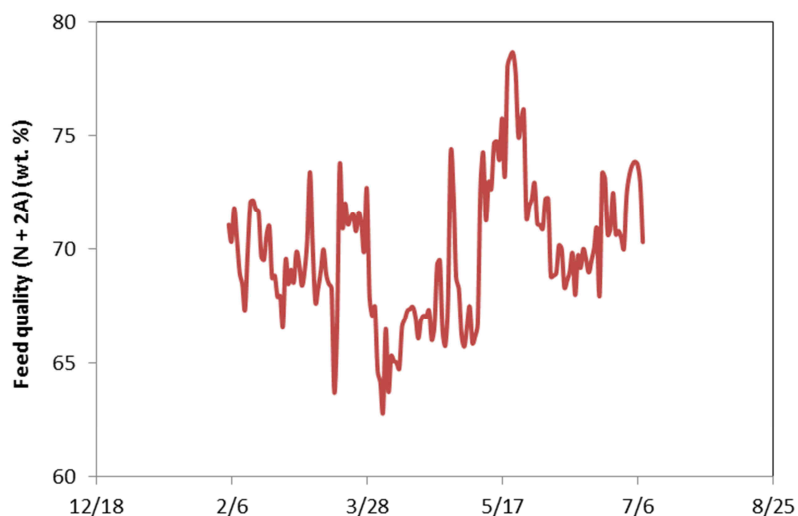


Figure 3.18: Variation in feed quality over the study period

3.12 Results

Figure 3.19 to Figure 3.21 show the completed HYSYS/Refining simulation models for UOP CCR reformer studied in this work. We evaluate the model using over 6 months of operating data from a refinery in the Asia Pacific processing hydrotreated naphtha. Key factors for the evaluation of the model are comparisons of overall reactor yield and operating profiles for key equipment in the gas plant. In general, the model accurately predicts the product yield, composition and operating profiles over wide range of feed conditions.

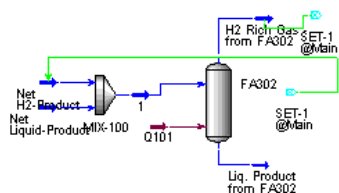


Figure 3.19: Remixing section

The fractionation section of model uses the Peng-Robinson equation of state and the kinetic lumps directly as the fractionation lumps. The remixing section is a simple way to reconstruct the plant effluent since the reactor model produces separate streams for the hydrogen product and liquid product. Remixing the streams allow us to model the recontacting sections to predict compositions reported in the actual hydrogen product and liquid product streams.

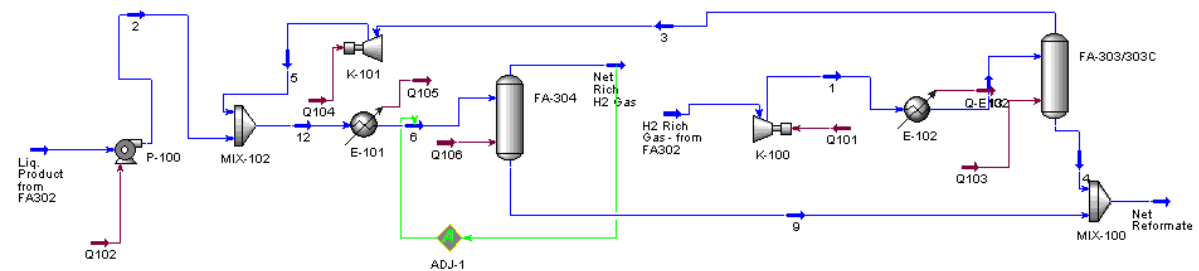


Figure 3.20: Recontacting section

The recontacting section in Figure 3.20 is different from the process flow shown in the plant PFD in Figure 3.2. We find that we do not require as many flash stages as the real process to obtain results similar to the plant. This is expected since each of the separators of in-plant PFD are likely not operating at equilibrium conditions. This is similar to the concept of using overall efficiency in our tray-by-tray fractionation models. We acknowledge that the simplified model of the recontacting section does not report the energy consumption (especially by the secondary compressors) correctly, but in practice, the total energy consumption reported by model and the plant is similar.

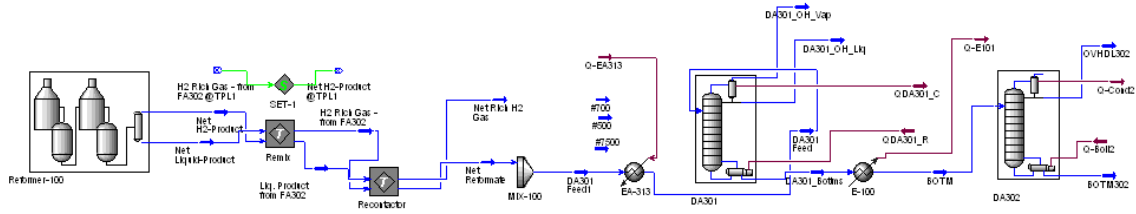


Figure 3.21: Combined reformer and primary fractionation

A well-calibrated model produces significant and repeatable predictions over a wide range of operating conditions. Table 3.13 to Table 3.16 summarize the predictions from model developed and calibrated according the previous sections. Each validation case represents roughly one month intervals of the reformer.

Table 3.13: Comparison of overall reactor model and plant yields, AAD = 0.85%

Yield Mass%	VALID-1		VALID-2		VALID-3	
	Model	Plant	Model	Plant	Model	Plant
Rich H2	6.1	6.9	6.4	7.2	6.5	7.0
DA301 Ovhd. Vapor	1.2	1.8	1.9	1.9	1.5	1.5
DA301 Ovhd. Liquid	13.0	12.0	14.2	12.4	12.6	12.4
DA301 Btm. Liquid	79.6	79.3	77.5	78.6	79.4	79.1
DA301 Ovhd. Liquid	43.4	45.1	43.4	44.1	42.6	44.6
DA301 Btm. Liquid	56.6	54.9	56.6	55.9	57.4	55.4
Yield Mass%	VALID-4		VALID-5		VALID-6	
	Model	Plant	Model	Plant	Model	Plant
Rich H2	6.3	7.0	6.5	6.7	6.6	6.8

DA301 Ovhd. Vapor	1.7	1.7	1.8	1.8	1.8	1.7
DA301 Ovhd. Liquid	13.6	12.2	11.2	12.0	11.1	12.3
DA301 Btm. Liquid	78.3	79.1	80.5	79.5	80.5	79.2
DA302 Ovhd. Liquid	45.9	45.3	45.4	46.2	45.4	43.2
DA302 Btm. Liquid	54.1	54.7	54.6	53.8	54.6	56.3

The most important prediction from the reactor model is the overall yield of all the key products from the unit. In case of the reformer, they are the net gas production, LPG (DA301 Ovhd. Liquid) and reformat (DA301 Btm. Liquid). The yields in the above table are from the rigorous tray-by-tray fractionation section. Therefore, the effect of downstream fractionation is also included in these predictions. We note good agreement with the plant values. The AAD (counting all products) is less than 1.0%.

Table 3.14: Comparison of key reactor temperature drop in model and plant values, AAD (Total) = 1.7 °C

Reactor Temp. Drop (°C)	VALID-1		VALID-2		VALID-3	
	Model	Plant	Model	Plant	Model	Plant
Reactor #1	108.2	109.9	107.3	106.0	114.1	111.5
Reactor #2	61.6	63.1	60.6	59.9	67.8	64.9
Reactor #3	33.7	35.2	32.1	33.9	38.0	37.0
Reactor #4	20.5	23.3	18.7	22.3	22.7	25.5
Reactor Temp. Drop (°C)	VALID-4		VALID-5		VALID-6	
	Model	Plant	Model	Plant	Model	Plant
Reactor #1	107.4	107.6	113.9	112.8	113.3	111.7

Reactor #2	60.7	61.9	66.7	67.0	66.1	66.2
Reactor #3	32.8	34.9	37.0	37.1	36.4	37.0
Reactor #4	19.6	23.3	22.1	24.2	21.7	24.6

The reactor performance is also a key indicator of model's calibration and prediction. We note that reactor model tracks reactors #1 - #3 with the roughly the same accuracy. We observe the larger error in reactor #4 because we do not allow significant changes in individual tuning of the reactions. In the final reactor, more exothermic reactions start to dominate and push the reactor into a region where paraffin cracking becomes significant. However, even this higher deviation of outlet temperature is within the expected deviation at the plant.

Table 3.15: Comparison of key model and plant yields in the reformat, AAD (Total) = 1.05; AAD (Aromatics) = 0.85

Reformat yields (wt%)	VALID-1		VALID-2		VALID-3	
	Model	Plant	Model	Plant	Model	Plant
Benzene (B)	7.5	7.9	7.7	7.1	7.0	6.4
Toluene (T)	21.3	20.7	22.0	21.1	20.9	19.9
Ethylbenzene (EB)	3.6	3.5	3.6	3.4	3.5	3.4
para-Xylene (PX)	5.5	5.1	5.6	5.3	5.5	5.1
meta-Xylene(MX)	11.9	11.1	12.1	11.7	11.8	11.2
ortho-Xylene(OX)	6.7	6.3	6.8	6.5	6.6	6.3
Higher aromatics (A9+)	40.5	38.1	39.2	41.6	41.5	43.3
Paraffins (P)	1.4	2.0	1.2	1.0	1.3	1.1
Napthenes (N)	12.5	14.5	11.9	14.0	12.7	14.5

Reformate yields (wt%)	VALID-4		VALID-5		VALID-6	
	Model	Plant	Model	Plant	Model	Plant
Benzene (B)	8.4	7.7	8.0	8.1	8.0	8.0
Toluene (T)	22.7	21.5	23.2	20.8	23.2	20.5
Ethylbenzene (EB)	3.6	3.3	3.6	3.4	3.6	3.4
Para-xylene (PX)	5.5	5.3	5.6	5.0	5.6	4.9
Ortho-xylene(OX)	11.9	11.4	12.1	11.0	12.1	10.7
Meta-xylene(MX)	6.7	6.4	6.8	6.3	6.8	6.1
Higher aromatics (A9+)	35.8	38.0	34.5	41.2	34.5	40.1
Paraffins (P)	1.4	1.2	1.5	1.4	1.5	1.4
Napthenes (N)	12.6	14.6	12.1	13.7	12.1	14.7

Since this reformer is part of a petrochemical complex, the predictions of individual molecules in the reformate are quite significant. An accurate prediction of the composition of benzene, toluene, ethylbenzene and xylenes (collectively referred to as BTEX) validates our model and provides feed values for the downstream model for the BTX separation plant. Table 3.15 compares the predicted values and plant data. The AAD for all the components is 1.05 wt%, whereas the aromatics show a deviation of only 0.85 wt%.

Table 3.16: Comparison of LPG composition from model and plant, AAD = 2.0 mol. %

DA301 Ovhd. Liquid (Mol. %)	VALID-1		VALID-2		VALID-3	
	Model	Plant	Model	Plant	Model	Plant
Ethane (C2)	8.7	8.3	8.3	8.1	7.5	9.5

Propane (C3)	25.4	28.3	24.9	26.8	23.6	28.0
iso-Butane (iC4)	23.4	20.3	23.9	19.3	23.6	19.2
n-Butane (nC4)	19.6	18.0	19.4	18.4	20.1	17.5
iso-Pentane (iC5)	14.1	16.0	14.6	17.7	16.0	15.9
n-Pentane(nC5)	6.2	7.6	6.2	8.5	6.7	7.8
DA301 Ovhd. Liquid	VALID-4		VALID-5		VALID-6	
(Mol. %)	Model	Plant	Model	Plant	Model	Plant
Ethane (C2)	8.4	9.4	7.1	7.4	7.0	8.0
Propane (C3)	26.0	29.5	25.1	28.5	25.0	26.9
iso-Butane (iC4)	23.5	20.6	23.6	20.7	23.6	19.6
n-Butane (nC4)	19.2	17.1	19.5	18.6	19.6	18.1
iso-Pentane (iC5)	13.9	15.3	15.1	16.4	15.1	17.3
n-Pentane(nC5)	5.9	6.4	6.4	7.1	6.5	8.5

A key part of this work in the development of fractionation sections for the reformat and A6 splitter. We compare the model predictions of the temperature profiles of the LPG column DA301 and reformat separator DA302. We note good agreement with plant measurements.

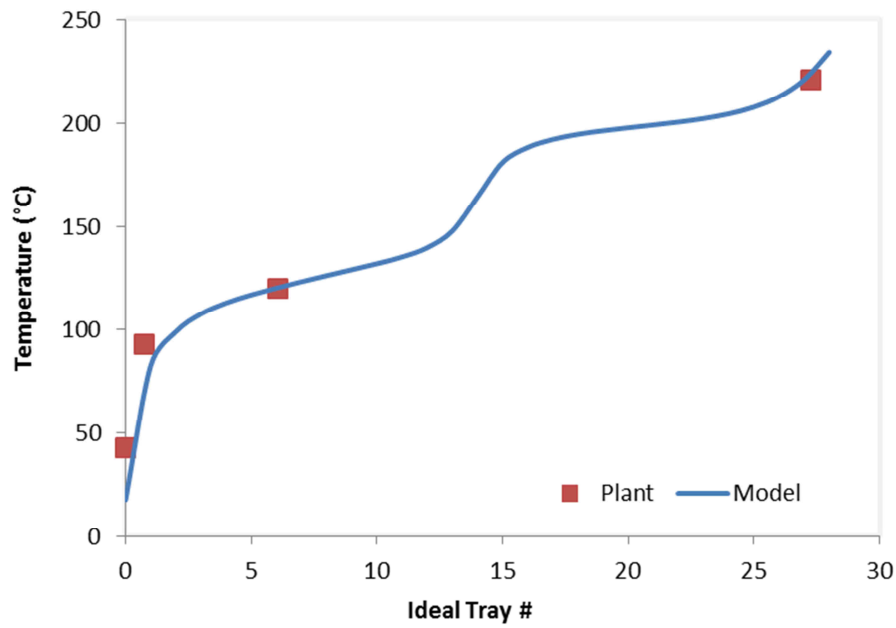


Figure 3.22: Temperature profile of column DA301

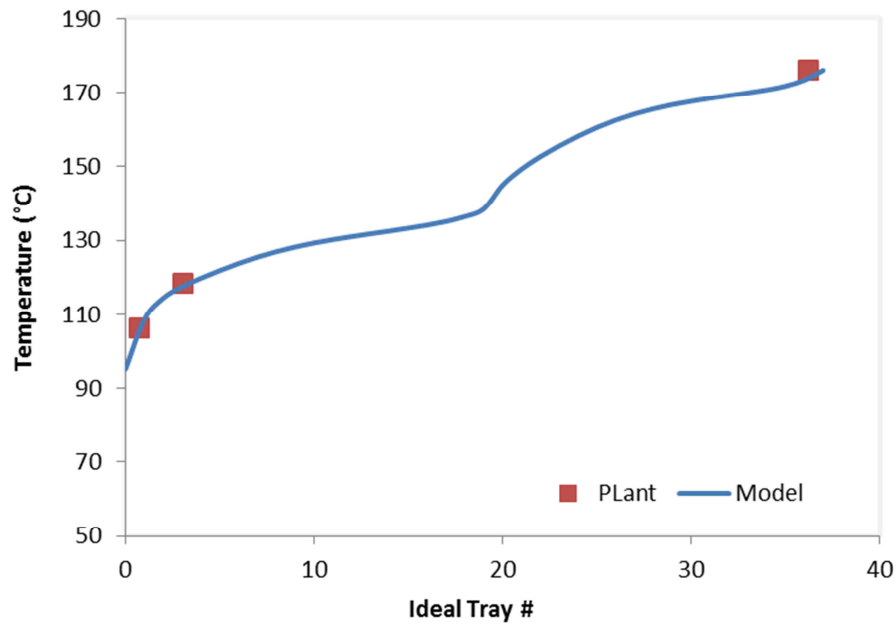


Figure 3.23: Temperature profile of column DA302

3.13 Applications

Refiners typically face two types of operating scenarios with reformers. The first type of scenario is *the “what-if” scenario*. In this scenario, we want to predict the process performance given a change in a key process variable. For CCR reformers, the typical operating variables for a given feedstock are reactor temperature, feed rate (or space velocity), reactor pressure, hydrogen to hydrocarbon ratio (H₂HC) and the activity of the catalyst. By making changes in the process variables, refiners can make significant shifts in the product distribution.

The second type of scenario is *the “how-to” scenario*. Modern reforming units may consume a variety of different feedstock while facing changing product demand. Because of the highly integrated nature of refineries, it is important to consider the effects of the upstream and downstream units on the reformer’s performance. There are several typical questions that form the “how” scenario: How can we reduce benzene in the reformer outlet? How can we use (or blend in) an additional feedstock? How can we account for changes in the reformer process on an economic basis?

Refiners often rely on performance charts, empirical correlations and historical data to study these types of scenarios. Gary et al.⁸ and Little⁶ provide examples of several types of these correlations. These methods can be unreliable because they assume a fixed feedstock and set of operating conditions. In addition, these methods often ignore the interaction between process variables and can mask optimal operating conditions. It is in this context that we consider the use of rigorous models to study various operating scenarios. Rigorous models can account for complex changes in process variables and provide detailed predictions of reactor performance.

3.13.1 Effect of reactor temperature on process yield

A typical operating scenario is the increase of reactor temperature to promote higher severity operation to produce high-octane reformate and aromatics. Figure 3.24 to Figure 3.31 indicate key changes in the reformer performance a function of WAIT in the process. In addition, we must also consider the effect of hydrogen partial pressure in the reactors. We study this effect by changing the WAIT and various values for the H₂HC ratio.

Increasing the reactor temperature through WAIT generally increases the yield of the aromatic components and the octane number. However, for a given H₂HC ratio, there is a maximum aromatic yield and octane number. This results from the increased relative of hydrocracking vs. dehydrogenation due to the temperature increase. Correspondingly, the C₅+ yield (sum of all components great than C₄) decreases with increasing octane number.

To consider operating at high WAIT conditions, it is possible to run the reactor at much higher H₂HC ratios. Figure 3.24 to Figure 3.26 show that we can reach a much higher octane number at high WAIT values. However, when the WAIT is low (compared to the octane peak), Figure 3.25 and Figure 3.26 show correspondingly lower aromatic yield. Therefore, there must be a balance between the H₂HC ratio and WAIT to produce optimal octane number and aromatic yield.

Another important consideration in increasing WAIT is production of undesirable side products and excessive coke generation. Figure 3.27 and Figure 3.28 show the effect of WAIT on the production of dry gas (methane and ethane) and the coke laydown rate.

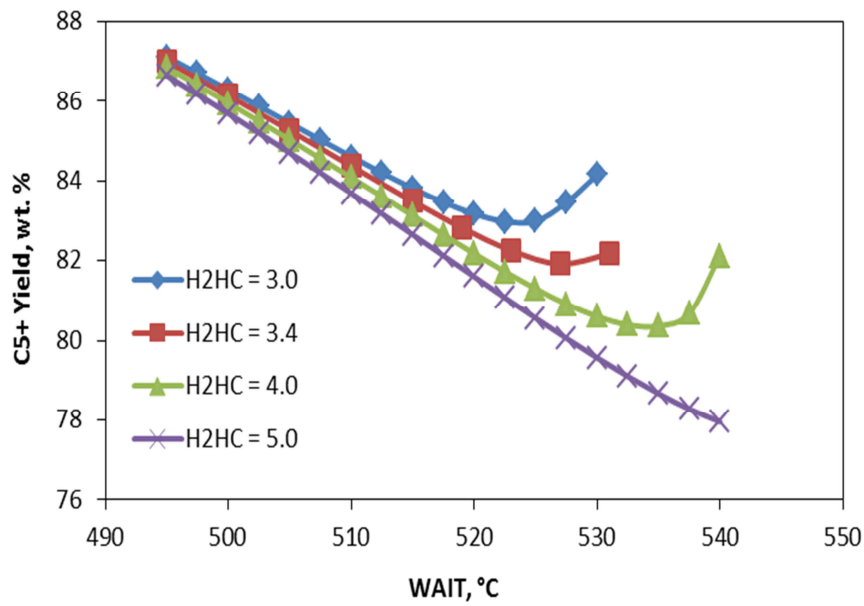


Figure 3.24: Change in C5+ yield (wt. %) as function of WAIT and H2HC ratio (WHSV = 1.37)

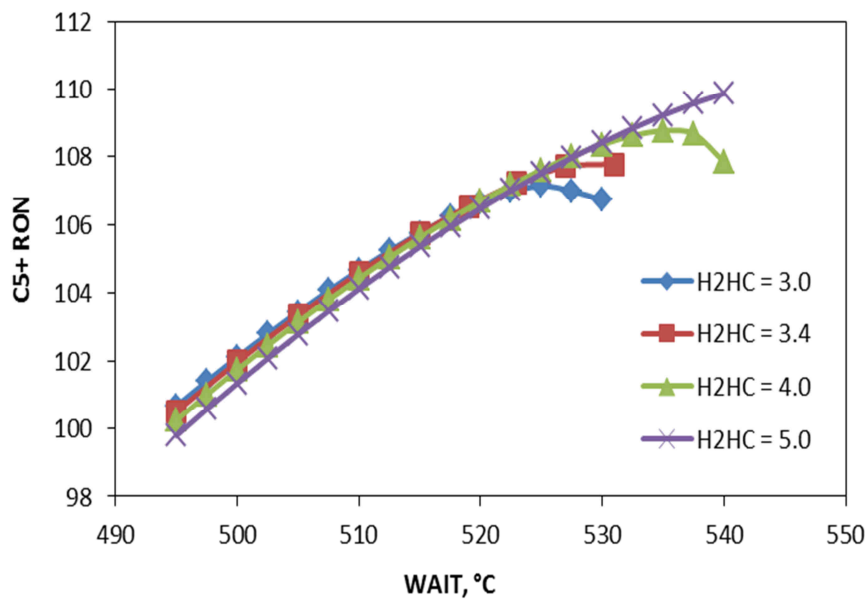


Figure 3.25: Change in C5+ RON as function of WAIT and H2HC ratio (WHSV = 1.37)

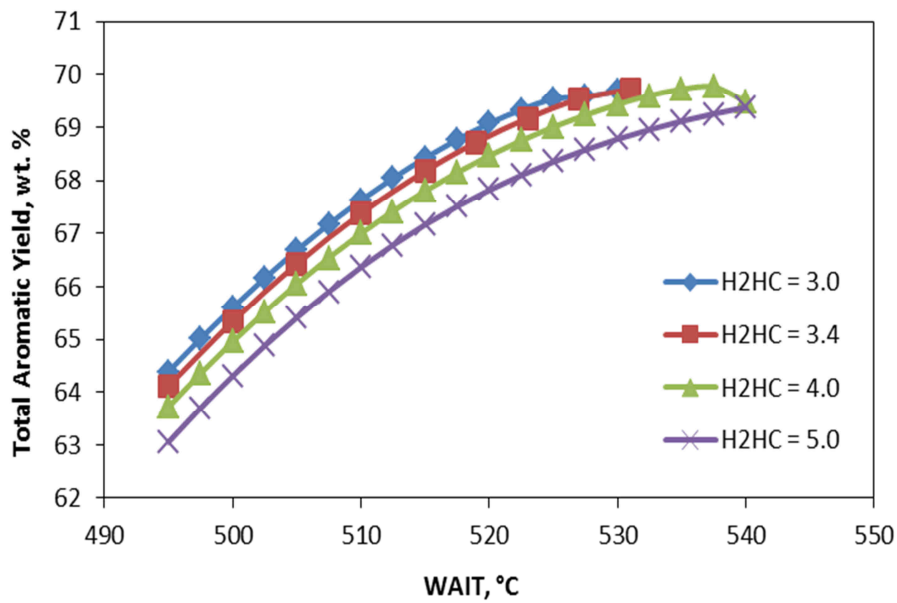


Figure 3.26: Change in Total Aromatic Yield (wt. %) as function of WAIT and H₂HC ratio (WHSV = 1.37)

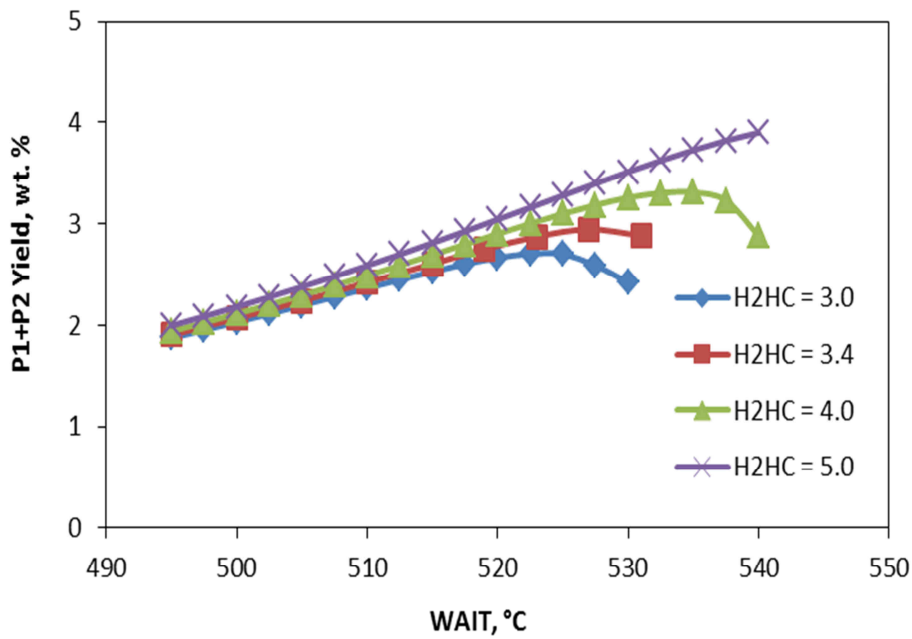


Figure 3.27: Change in light gas yield as function of WAIT and H₂HC ratio (WHSV = 1.37)

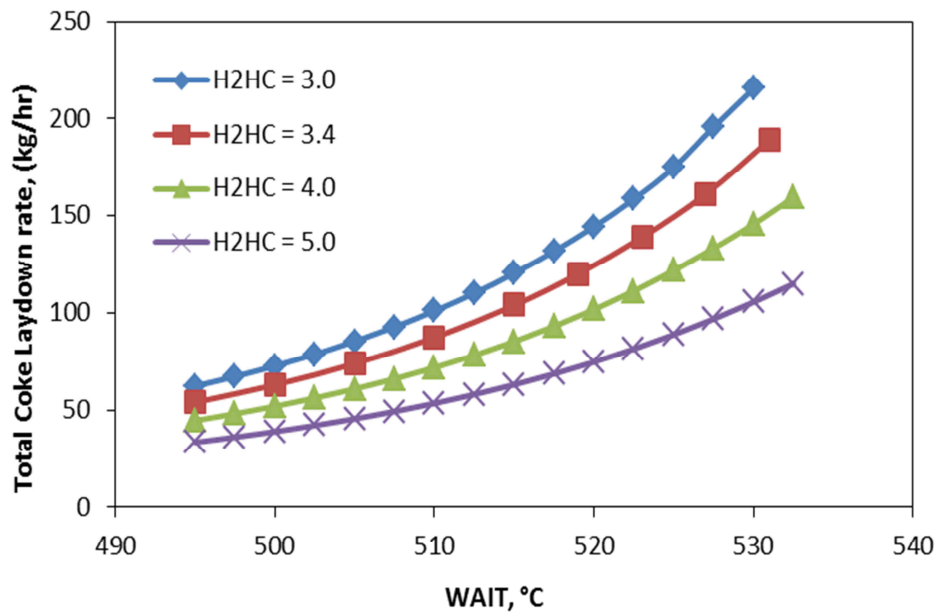


Figure 3.28: Coke laydown rate (kg/hr) as function of WAIT and H₂HC ratio (WHSV = 1.37)

Before we approach the octane maximizing peak, increasing the reactor temperature increases the yield of dry gas and the coke generation rate. The increase in dry gas yield can be problematic. The dry gas typically has little economic value and causes bottlenecks in the recycle compressors in the product separation section. Increasing the H₂HC ratio typically does not help reduce dry gas yield, since high partial pressure of hydrogen in the reactor promotes hydrocracking and subsequently increases the dry gas yield. In addition, the coke laydown rate increases exponentially with increased temperature and can put significant pressure on the regenerator section of the CCR. Operating at high temperatures may require a significant addition of fresh catalyst to maintain the same level of catalyst activity.

3.13.2 Effect of feed rate on process yield

The reactor temperature is a primary method of shifting the reactor yield to produce more valuable product distributions. Another process variable is the feed rate to the unit. The feed rate cannot take on drastically different values due to the demands of other units in the refinery. However, small changes in feed rate can influence the product distribution. This occurs because of the change in contact time with the catalyst. Higher contact times increase the conversion of feed to products.

Figure 3.29 to Figure 3.31 show the change in key reactor yields as functions of weight hourly space velocity (WHSV) and reactor temperature, WAIT. The figures show that as WHSV increases (feed rate increases), the conversion to aromatics decreases and the corresponding octane number decreases. This is consistent with our expectation of lower contact time. In general, the impact of changing feed rate is less than changing the reactor temperature. For significant changes in the RON and total aromatic yield, the reactor temperature is still the primary driver. In Figure 3.30 and Figure 3.31, the lines for high WAIT approach a minimum slope, since we are approaching the octane peak for the baseline H2HC ratio.

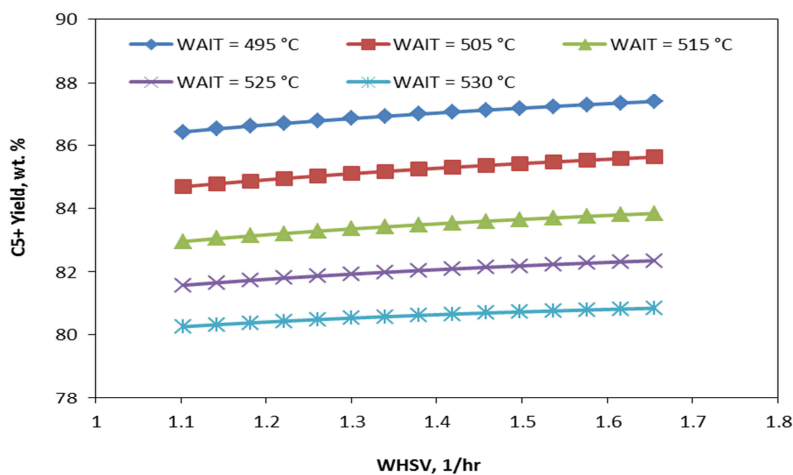


Figure 3.29: Change in C5+ Yield (wt. %) as function of WHSV and WAIT

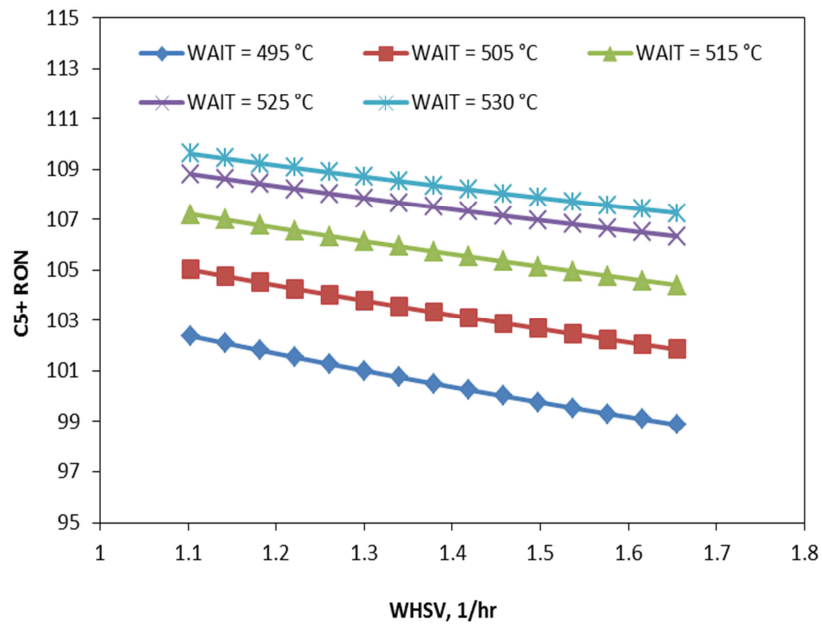


Figure 3.30: Change in C5+ RON as function of WHSV and WAIT

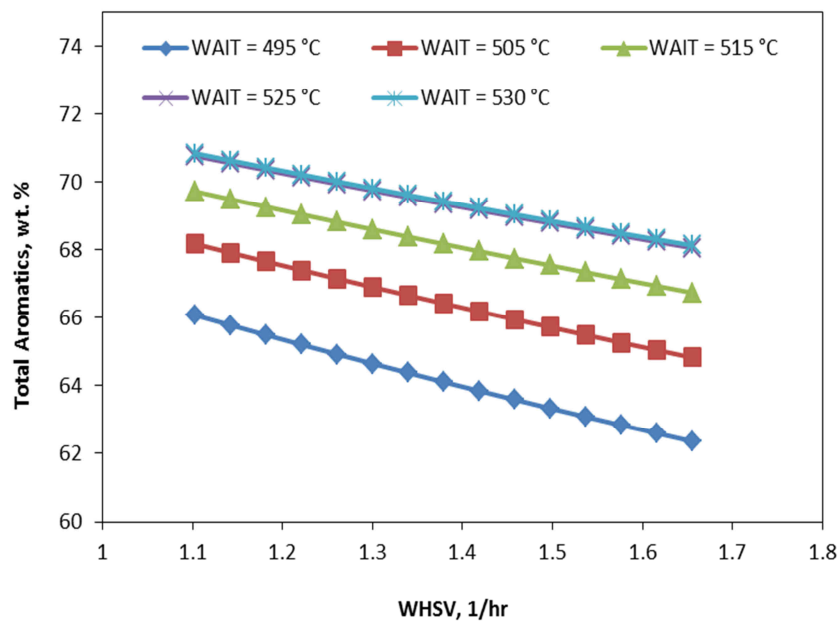


Figure 3.31: Change in Total Aromatics yield as functions of WHSV and WAIT

3.13.3 Combined effects on process yield

Therefore, changes in octane number and total aromatic yield reflect the coupled effects of feed rate and reactor temperature. We can use the model to provide reactor temperatures that correspond to a fixed RON and varying feed rate. Figure 3.32 shows the relevant WAIT and WSHV to obtain a given C5+ RON. We note that at high C5+ RON operation and high WSHV, the required reactor temperature increases significantly. As shown in Figure 3.27 and Figure 3.28, this increases the unwanted dry gas yield and produces excessive amounts of coke. By using Figure 3.32, we can determine how to change process variables to achieve desired C5+ RON.

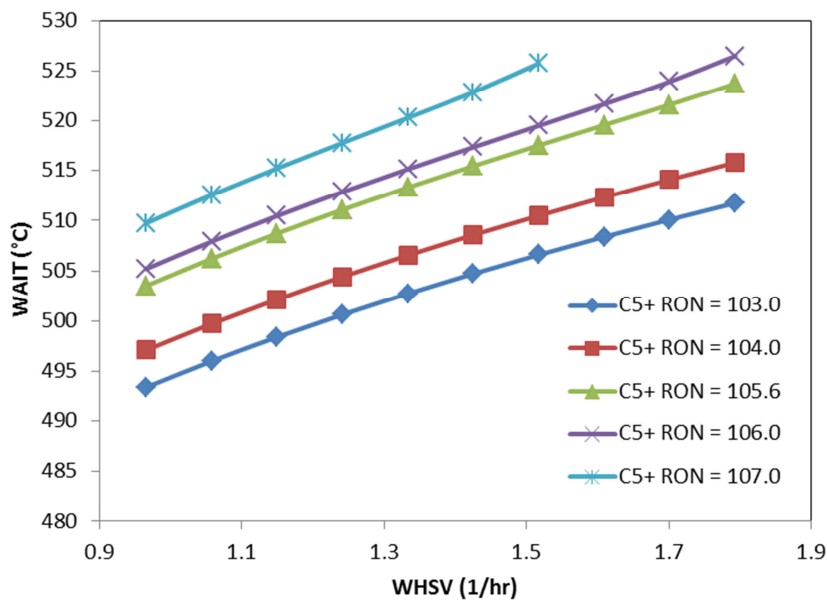


Figure 3.32: Corresponding WAIT and WSHV to obtain various C5+ RON in reactor products

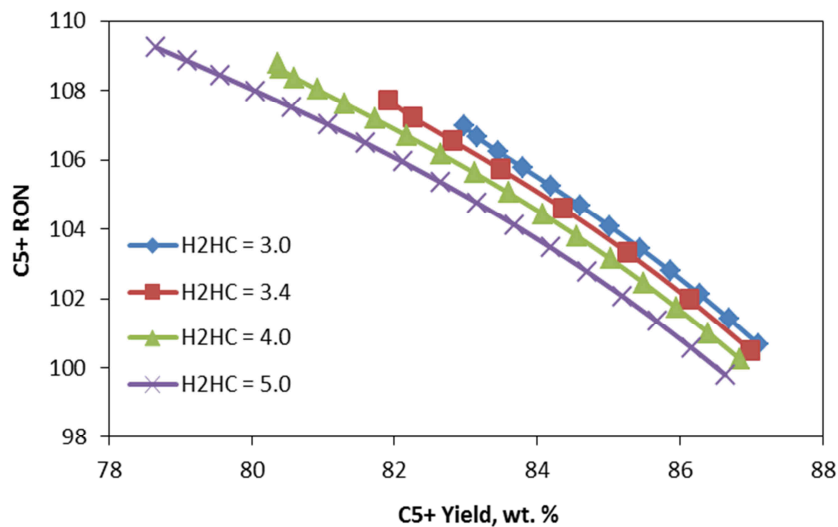


Figure 3.33: Effect of C5+ Yield (wt. %) on C5+ RON

We show a related study (Figure 3.33), indicating how C5+ yield changes with increasing values for C5+ RON. Figure 3.33 helps the refiner identify the range of values that H2HC ratio may take to obtain the same C5+ RON. Combined with Figure 3.32, we can identify possible operating windows for WAIT, H2HC and WHSV for a given feedstock composition.

3.13.4 Effect of feedstock quality on process yield

All the previous studies involve a uniform feedstock composition. In practice, however, feed composition can change significantly over the course of regular refinery operation (see Figure 3.18). So, it is important study changes in product distribution when the feed composition varies. The benzene content of reformate is of particular interest to refiners. Recent regulations have imposed strict limits on the amount of benzene present in the gasoline pool. Since the reformer is the primary source of benzene, we look for ways to reduce the benzene in reformate.

The primary contributors to benzene and toluene are methylcyclopentane (MCP) and methylcyclohexane (MCH). Various authors have commented on the significance of this pathway to produce aromatics^{48, 49}. We study the effect of the MCP in the yield of benzene, toluene and xylenes in Figure 3.34. We use the standard operating parameters as with other case studies in this work. Figure 3.34 shows that increasing MCP concentration has a strong effect on the benzene yield in the reformat. In addition, MCP composition has little effect on the composition of the higher aromatics.

In practice, a refiner does not directly control the feed composition of MCP to the unit. Typically, we blend in additional feed that has an IBP greater than 95 – 100 °C. Feeds with IBPs greater than 95 – 100 °C contain little amounts of MCP and this ratio can be used to control the benzene yield of the unit. By contrast, a refiner who wants to increase the production of benzene (to supply a chemical process) may want to increase the feed of MCP instead of operating the reformer at increasing severity and converting reactor products to benzene. Using a rigorous model can help us find and understand these types of trade-offs.

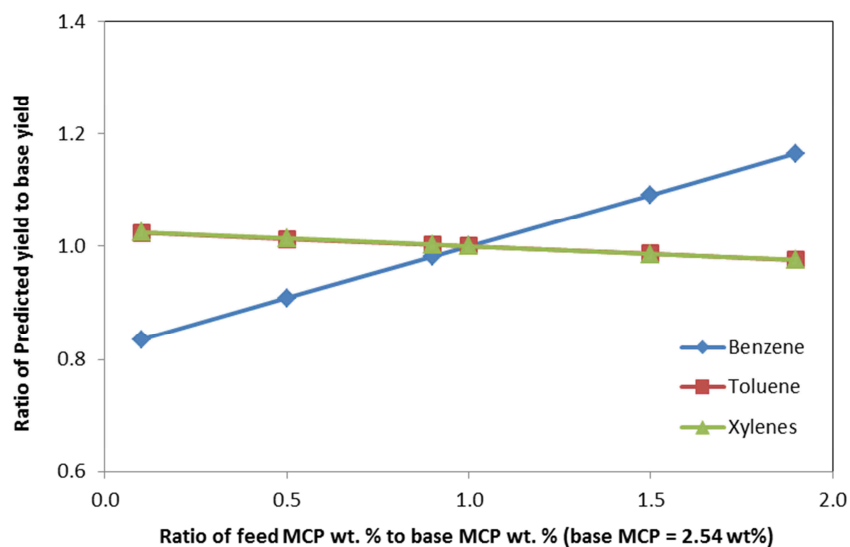


Figure 3.34: Effect of changing feed MCP composition on aromatic yields

3.13.5 Chemical feedstock production

Many reformers are now part of integrated petrochemical complexes and produce aromatics (benzene, toluene and xylenes or BTX) to feed into chemical processes for polystyrene, polyesters and other commodity chemicals. As such, it is important to consider how models can help in optimizing the BTX operation. Model developers and users must also be aware that complete BTX operation may not be the most profitable reformer operation scenario. Economic analyses are required to justify changes from a gasoline-producing to a BTX-producing scenario.

In general, many of the case studies show in earlier sections (relating to higher octane operation) apply to the BTX scenario as a well. Figure 3.25 and Figure 3.26 show the relationship between octane number and aromatic yield. We repeat some of the case studies shown in previous sections, showing the effect of process variables on BTX yields. In Figure 3.35 and Figure 3.36,

the yields of aromatic yields at WHSV of 1.34 and H2HC ratio of 3.41 were taken as base yields.

Table 3.17 shows the base yields at several temperatures.

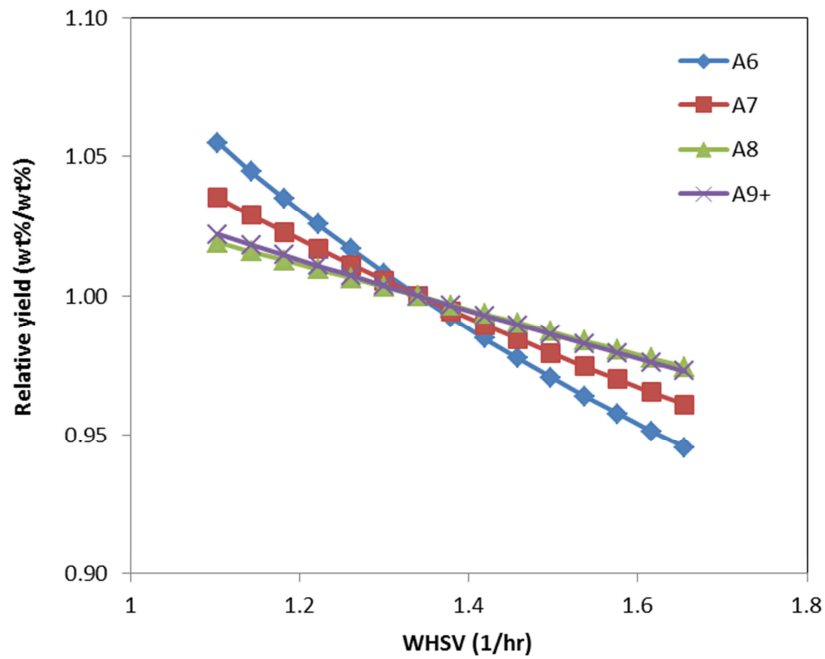


Figure 3.35: Relative yields of aromatic components (where A6 refers to benzene, A7 refers to toluene and A8 refers to xylenes) as function of WHSV and WAIT = 495 °C

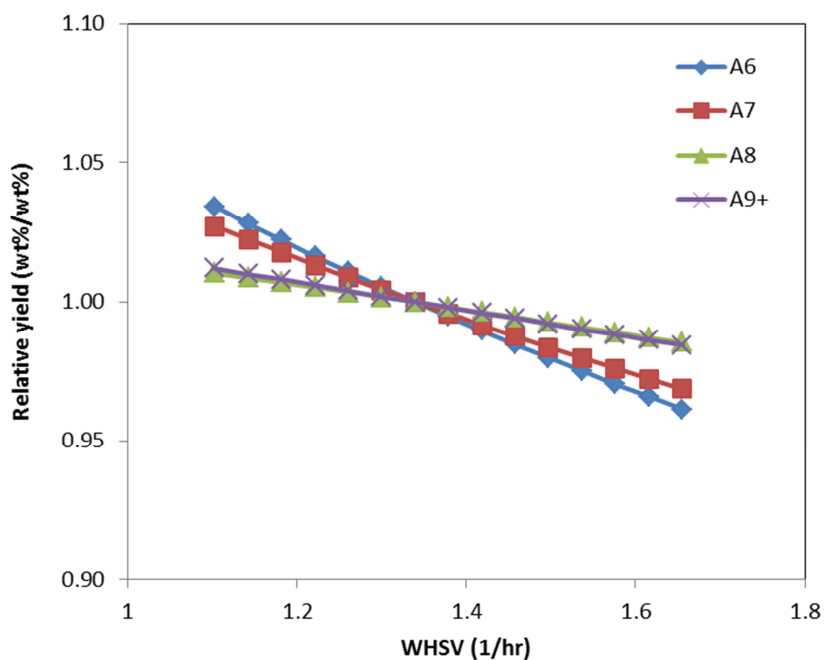


Figure 3.36: Relative yields of aromatic components (where A6 refers to benzene, A7 refers to toluene and A8 refers to xylenes) as function of WHSV and WAIT = 525 °C

Table 3.17: Base yields of aromatic components at various WAIT and H2HC ratio of 3.4

WAIT	A6 Yield (wt%)	A7 Yield (wt%)	A8 Yield (wt%)	A9+ Yield (wt%)
495 °C	4.15	15.90	21.70	22.63
515 °C	6.09	17.13	22.16	23.01
525 °C	6.88	17.56	22.17	22.94

As reaction temperature (WAIT) increases, the yield of aromatic components yields significantly. However, at higher temperatures (greater than 520 °C), the H2HC ratio is not sufficient to prevent undesired hydrocracking reactions. These reactions will decrease the yield

of higher aromatics and favor light gas production. Table 3.17 shows that the rate of increase in the production A7 and higher components decreases rapidly. In the case of A9+ yield, we actually show decrease in yield even though the reactor is operating at higher temperatures. In this case, the refiner may choose to increase H₂/HC ratio to continue producing high yields of aromatic components at expense of increased recycle compressor duties and increased severity during catalyst regeneration. If the recycle compressor is already operating close to the design limit then an extensive (and costly) revamp may be required to produce additional aromatics. In such a situation, the use of a model to predict alternative scenarios can be very cost-effective.

Another important issue is the effect of feed rate (WHSV) on the yield of key aromatics. We note that at lower reaction temperature (WAIT), the effect of WHSV is more pronounced. High feed rates and low reaction temperatures tend to make the process more selective toward toluene (see Figure 3.35). At higher temperatures and high feed rates, as Figure 3.36 shows, there is little difference between the yields of benzene and toluene. It is possible to take advantage of these differences in selectivity to help favor one aromatic component over another. In addition, changes in aromatic precursors (such as MCP) can also significantly shift the aromatic production profile. We studied the effect of feed composition in previous section in the context of reducing benzene content in gasoline (Figure 3.34).

3.13.6 Energy utilization and process performance

The modern refinery is not only concerned with meeting product specifications and demands but also the energy and utility (cooling water, power) consumption of various units. Table 3.18 lists some of the utility consumption data based on various catalytic reforming processes.

Table 3.18: Utility consumption data^{6, 14}

Fuel (BTU/barrel of feed)	200e3 – 350e3
Power (kW-hr/barrel of feed)	0.6 – 6
Cooling water (gal/barrel of feed)	40 – 200

In the reforming process, significant energy consuming steps are interstage heating and recycle compression. About 65-80% of the energy input into the reformer drives the fired heaters responsible for interstage heating. Modest changes in the operation of these fired heaters can provide significant energy savings. Improving the operation of the fired heaters directly can be a significant undertaking⁵⁰ and is outside the scope of this work. However, we can study in the effect of changing the reactor inlet temperatures (fired heater outlet temperatures) on the product yield and required heater duty.

We consider the scenario in Table 3.19, where reactor inlet temperature for each reactor bed is fixed to certain values. The values in parenthesis indicate change from the base case. We change the reactor inlet temperatures by values given in the table for four subsequent model runs. We choose these values to highlight the effect of reactor inlet temperatures on the initial, final and intermediate beds independently. The results of this case study appear in Table 3.20.

Table 3.19: Reactor inlet temperature deviations

Scenario	Bed #1(°C)	Bed #2(°C)	Bed #3(°C)	Bed #4(°C)	WAIT (°C)
BASE	515.9	513.6	513.6	515.0	514.5

CASE-1	510.9 (-5.0)	513.6 (0.0)	513.6 (0.0)	515.0 (0.0)	514.0
CASE-2	510.9 (-5.0)	513.6 (0.0)	513.6 (0.0)	510.0 (-5.0)	511.6
CASE-3	515.9 (0.0)	508.6 (-5.0)	508.6 (-5.0)	515.0 (0.0)	512.5
CASE-4	515.9 (0.0)	513.6 (0.0)	513.6 (0.0)	515.0 (-5.0)	512.2

Table 3.20: Key model yields for fired duty case study

Scenario	Total Fired Duty (kJ/kg)	Aromatic Yield (wt%)	C5+ RON	C5+ Yield (wt%)	Fired Duty Deviation
BASE	1001.4	66.26	101.1	91.52	0.00%
CASE-1	996.0	66.08	100.9	91.59	-0.54%
CASE-2	987.0	65.76	100.4	91.74	-1.92%
CASE-3	987.8	65.82	100.5	91.74	-1.35%
CASE-4	987.5	65.94	100.7	91.67	-1.39%

While initially the fired duty reductions appear quite small (0.5 – 1.4%), this may lead to significant energy savings in fuel costs for the fired heater. Vinayagam⁵¹ states that even a 1% reduction in fuel consumption can provide significant cost savings. We note that these energy savings appears as a result of small octane loss and aromatic yield loss. If the reformer is already operating at high severity, this type of energy analysis may allow for some flexibility in the

operating costs of the unit. In addition, this type of analysis serves as a starting point for a larger heat integration analysis to understand how to reduce energy consumption of the overall unit.

3.14 Refinery Planning

Production planning is an important activity in modern refineries. The modern refinery is a combination of many complex units such Catalytic Reforming, Fluid Catalytic Cracking (FCC), Hydroprocessing, etc. While it is possible to tune each unit to an optimal yield, the optimum yield of a particular unit may not reflect a true optimum because of the demands and prices for the wide range of product that the refiner produces. Therefore, it is important to consider each unit in the context of the whole refinery. The activity of choosing feedstock to refinery (and its constituent units) that produces optimal economic benefit while meeting equipment, business and regulatory constraints is called production planning.

The refinery production planning problem has been traditionally solved using linear programming (LP) techniques. LP is a mathematical technique that maximizes a linear objective function of many variables with respect to linear constraints on these variables. Bazaraa et al.⁵¹ have described the theory and applications of LP techniques extensively. It is well known that LP techniques have several deficiencies which include linearization of inherently non-linear process behavior. This often results in finding local optimum instead of a global optimum. Many authors have worked on several different techniques to use non-linear programming in refinery production planning. However, LP techniques are still popular because they easy to use and incorporate into existing refineries.

A refinery LP and linear unit model represents a set of linear correlations that predict yield given an average yield value and changes in the certain operating variables. In this section, we discuss

how to apply the rigorous reforming model in the context of a linear unit model. The key information for a linear model of a nonlinear process is the DELTA-BASE vector:

$$\begin{bmatrix} y_1 \\ y_2 \\ \vdots \\ y_m \end{bmatrix} (\text{PREDICTION}) = \begin{bmatrix} \bar{y}_1 \\ \bar{y}_2 \\ \vdots \\ \bar{y}_m \end{bmatrix} (\text{BASE}) + \begin{bmatrix} \frac{\Delta y_1}{\Delta x_1} & \dots & \frac{\Delta y_1}{\Delta x_n} \\ \vdots & \dots & \vdots \\ \frac{\Delta y_m}{\Delta x_1} & \dots & \frac{\Delta y_m}{\Delta x_n} \end{bmatrix} (\text{DELTA-BASE}) \cdot \begin{bmatrix} \Delta x_1 \\ \vdots \\ \Delta x_n \end{bmatrix} (\text{DELTA}) \quad (26)$$

The DELTA-BASE relates the prediction of a new reactor yield (PREDICTION, y_m) given an average starting prediction value (BASE, \bar{y}_m) and the change in operating variables (DELTA, Δx_n). We note that this DELTA-BASE matrix ($\Delta y_n / \Delta x_n$) is essentially the Jacobian matrix for our nonlinear process model centered on a given operating point.

Refiners often develop the linear yield correlations for the LP in a simple fashion. The average value of historical unit yields over a significant period of time (e.g. one operating quarter) form the BASE yield of the unit. The DELTA-BASE may be calculated from published or internal refiner correlations for the given unit. Alternatively, the DELTA-BASE vectors may be generated from the change in yields recorded while the operating conditions of the unit change. In either approach, the BASE yield and DELTA-BASE matrix represent average values (fixed to certain operating conditions) and may not correctly reflect the true operation of unit. In this work, we use the rigorous non-linear model to supply the BASE and DELTA-BASE values.

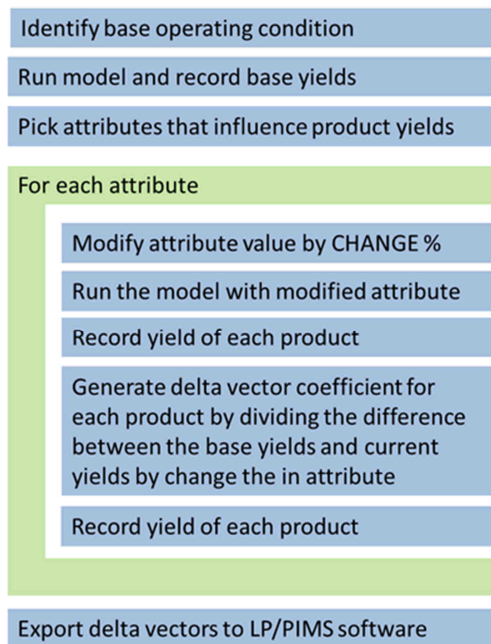


Figure 3.37: Process to generate DELTA-BASE vectors from rigorous model

Another important consideration is the choice of operating variables to manipulate in the DELTA vector. It is not useful to map the entire nonlinear model with all of its variables into the LP. We must choose key operating variables that we can track throughout the whole LP. Typically, each unit model only includes the feedstock characteristics. For catalytic reforming, the choice of operating variables depends on how the refiner deals with the reformer products. If the reformer is primarily a generator of high-octane gasoline for the gasoline pool, it is sufficient to include only a few feed quality parameters such as N+2A and feed IBP (Initial boiling point). However, if the reformer is a source of aromatics destined for a chemical complex, there may be cause to include additional feed quality descriptions such as feed content of cyclopentane (CP), methylcyclopentane (MCP), etc.

In this work, we restrict ourselves to the gasoline-producing reformer. Figure 3.37 outlines the general process to generate DELTA-BASE vectors. We choose the feed N+2A as the single input variable and the output variables are yields of hydrogen, dry gas yield and yield of the reformat. We also generate the BASE and DELTA-BASE vectors for several cases of varying C5+ reformat RON. Table 3.21 shows the relevant yields of the reactor model. The feed composition for the given N+2A corresponds to measured plant data. We fix the RON of the C5+ reformat and calculate the required WAIT during model execution.

Table 3.21: Reformer yields at various N+2A and C5+ reformat RON from rigorous model

WAIT (°C)	501.1	500.8	508.5	508.1	517.2	516.5
N + 2A	64	72	64	72	64	72
Product	Yield (wt. %)					
Hydrogen	2.96	3.13	3.03	3.23	3.10	3.31
Methane	0.59	0.47	0.66	0.53	0.75	0.61
Ethane	1.76	1.41	1.98	1.59	2.25	1.82
Propane	3.38	2.86	3.87	3.27	4.46	3.77
Isobutane	3.36	2.63	3.81	2.99	4.35	3.43
n-Butane	3.10	2.46	3.24	2.58	3.36	2.70
C5+ 102 RON Reformat	84.82	87.00	-	-	-	-
C5+ 104 RON Reformat	-	-	83.37	85.78	-	-
C5+ 106 RON	-	-	-	-	81.69	84.34

Reformate						
Other	0.03	0.02	0.03	0.03	0.04	0.03

We use the yield information from the rigorous model in Table 3.21 to construct the LP yield vectors. The BASE vector is the average of the yields in each RON case. We choose the average value of N+2A (64) to compute the Δx_n . We then use one of the N+2A data points to compute the DELTA-BASE vector. We show the steps and results of this calculation for RON 102 case in Table 3.22. We compare the results of the linear yield vector predictions and model predictions for an intermediate N+2A value of 66.6 in Table 3.23. Table 3.24 shows the DELTA-BASE calculated for all the RON cases.

Table 3.22: Calculating the DELTA-BASE vectors for the C5+ RON = 102 case

		Dev. to N+2A = 72	Dev. to N+2A = 64
Avg. N+2A	68	4	-4
	(wt. %)	DELTA-BASE	PREDICTION
Hydrogen	3.05	0.022	2.96
Methane	0.53	-0.014	0.59
Ethane	1.59	-0.043	1.76
Propane	3.12	-0.066	3.38
Isobutane	3.00	-0.091	3.36
n-Butane	2.78	-0.079	3.10
Reformate	85.91	0.273	84.82

Table 3.23: Comparison of yield predictions from rigorous model and LP yield model

	Rigorous model prediction	LP vector prediction	AAD
N+2A	66.6	66.6	
	(wt. %)	(wt. %)	
Hydrogen	3.18	3.17	0.01
Methane	0.73	0.71	0.02
Ethane	2.17	2.11	0.06
Propane	4.45	4.24	0.21
Isobutane	4.14	4.05	0.09
n-Butane	3.16	3.14	0.02
Reformate	82.13	82.55	0.41

Table 3.24: DELTA-BASE vectors for different RON cases

	RON = 102	N+2A = 68	RON = 104	N+2A = 68	RON = 106	N+2A = 68
	BASE	DELTA-BASE	BASE	DELTA-BASE	BASE	DELTA-BASE
Hydrogen	3.05	0.022	3.13	0.024	3.20	0.027
Methane	0.53	-0.014	0.60	-0.016	0.68	-0.018
Ethane	1.59	-0.043	1.79	-0.049	2.04	-0.055
Propane	3.12	-0.066	3.57	-0.075	4.12	-0.086

Isobutane	3.00	-0.091	3.40	-0.103	3.89	-0.116
n-Butane	2.78	-0.079	2.91	-0.081	3.03	-0.082
Reformate	85.91	0.273	84.57	0.301	83.01	0.331

We can repeat the process outlined in Figure 3.37 and Table 3.24 for any number of feed composition variables. In general, for typical process changes in feed quality (10% - 15%), the LP yield vectors can provide reasonable predictions for the process yield. A potential problem is that LP yield prediction can be poor when operating close to process minima or maxima (such as octane number at fixed H₂HC ratio). In addition, N+2A may not be detailed descriptor for feedstock changes. If these problems occur in practice, the LP may require more frequent updates to reflect true unit operation.

3.15 Conclusions

In this work, we have developed an integrated model for an UOP CCR unit in Aspen HYSYS/Petroleum Refining. We use detailed feed composition (PNA content) and the routinely collected data such as operating profiles of reactor, product yields and fractionator temperature profiles. The key highlights of this work are:

- Detailed process description and overview of process chemistry relevant to modeling the reactor
- Brief survey of existing kinetic and unit level models for reforming processes
- Discussion of kinetic and reactor model in Aspen HYSYS/Petroleum Refining
- Guidelines for dealing with the physical properties of the kinetic lumps in the context of the radial flow reactors and fractionator

- Detailed process to infer molecular composition of feed when little plant information is available
- Identified key issues relevant to calibration and how to prevent over-calibration of reactor model
- Used industrial plant data to obtain workflow that produces a reasonable model
- Applied model to industrial plant data and showed good agreement with plant measurements in yield and composition of key products
- Investigation of the effects of various process parameters on product yield and composition
- Transitioned the results from rigorous non-linear model to the LP model for the refinery

3.16 Acknowledgements

We thank Mr. Stephen Dziuk of Aspen Technology for his valuable review comments. We thank Alliant Techsystems, Aspen Technology, China Petroleum and Chemical Corporation (SINOPEC), Milliken Chemical, Novozymes Biological, and Mid-Atlantic Technology, Research and Innovation Center (MATRIC) for supporting our educational programs in computer-aided design and process system engineering at Virginia Tech.

3.17 Nomenclature

α	Beta distribution shape parameter
A_c	Catalyst activity factor
A_i	Aromatic lump containing i carbon atoms ($i \geq 6$)
α_j	Pressure effect exponent for reaction class j

A_o	Pre-exponential factor in rate constant (1/s)
a_x	Activity factor for reaction group x
β	Beta distribution shape parameter
BEN	Benzene
CH	Carbon to hydrogen weight ratio
C_i	Concentration of component i
CP	Cyclopentane
E	Tray efficiency factor
EBP	End boiling point ($^{\circ}\text{C}$)
E_i	Activation energy associated with reaction I (J/kmol)
ϕ	Catalyst deactivation due to coke on catalyst
F	Total molar flow rate (kmol/hr)
F_i	Molar flow rate of component i (kmol/hr)
Γ	Combined adsorption factor due to acid function
H2HC	Hydrogen to hydrocarbon mole ratio
HFACTOR _{ij}	Hydrogen to carbon weight ratio for component C_iH_j
IBP	Initial boiling point ($^{\circ}\text{C}$)
IP_x	Iso (or branched) paraffin containing x carbon atoms
k_i	Rate constant associated with reaction or component i (kmol/kg-cat-s)
K_i	Adsorption factor for component i (1/kPa)
MBP _x	Multiple branched paraffin containing x carbon atoms
MCH	Methylcyclohexane
MCP	Methylcyclopentane
MON	Motor Octane Number
MON _i	Motor Octane Number of component or lump i
MW	Molecular weight
N_i	Naphthene lump containing i carbon atoms ($i \geq 5$)
N_i	Weight or mole fraction of given lump i
5N _i	5-membered naphthene lump containing i carbon atoms ($i \geq 5$)
6N _i	6-membered naphthene lump containing i carbon atoms ($i \geq 6$)
NP _x	Normal paraffin containing x carbon atoms
P	Pressure (kPa)
P_i	Partial pressure of component i (kPa)
P_o	Reference Pressure (kPa)
P_x	General paraffin containing x carbon atoms ($x \geq 1$)
θ	Combined adsorption factor due to metal function
R	Universal gas constant (J/kmol-K)
RON	Research Octane Number

RON _i	Research Octane Number of component or lump i
SBP _x	Single branched paraffin containing x carbon atoms
T	Temperature (K)
TBP	True boiling point curve (°C)
T _o	Reference temperature (K)
TOL	Toluene
W	Space velocity (1/hr)
WAIT	Weight averaged inlet temperature (°C)
WHSV	Weight hourly space velocity (1/hr)
w _i	Weight fraction of component i
x _n	Molar composition of liquid leaving a given tray
y _n	Molar composition of vapor leaving a given tray

3.18 References

1. Ancheyta-Juarez, J.; Villafuerte-Macias, E. *Energy & Fuels* **2000**, 14, 1032-1037.
2. Aguilar-Rodriguez, E.; Ancheyta-Juarez, J. *Oil & Gas Journal* **1994**, 92, 80-83.
3. Ancheyta-Juarez, J.; Aguilar-Rodriguez, E. *Oil & Gas Journal* **1994**, 92, 93-95.
4. Taskar, U. M. Ph.D. Diss. **1996**. Texas Tech University, Lubbock, TX.
5. Taskar, U. M.; Riggs, J. B. *AIChE J.* **1997**, 43, 740-753.
6. Little, D.; *Catalytic Reforming*. Penwell Books, **1985**. Tulsa, OK.
7. Antos, G. J; Aitaini, A. M. *Catalytic Naphtha Reforming*; 2nd Edition; Marcel Dekker **2004**. New York, NY.
8. Gary, J. H.; Handwerk, G. E.; Kaiser, M. J. *Petroleum Refining: Technology and Economics*; 5th Edition; CRC Press **2007**. Boca Raton, FL.
9. UOP, US Patent 3706536, **1971** (A. R. Greenwood et al.)
10. Hosten, L. H; Froment, G. F. *Ind. Eng. Chem. Process Des. Develop* **1971**, 10, 280-287.
11. Selman, D. M; Voorhies, A. *Ind. Eng. Chem., Prod. Res. Dev.* **1975**, 14, 118-123.

12. Froment, G. F. *Chemical Engineering Science* **1987**, 42, 1073-1087.
13. Menon, P. G.; Paal, Z. *Ind. Eng. Chem. Res.* **1997**, 36, 3282-3291.
14. Raseev, S. *Thermal and Catalytic Processes in Petroleum Refining*; Marcel Dekker **2003**.
New York, NY.
15. Svoboda, G. D.; Vynckier, E.; Debrabandere, B.; Froment, G. F. *Ind. Eng. Chem. Res.* **1995**, 34, 3793-3800.
16. Froment, G. F. *Catalysis Reviews* **2005**, 47, 83 – 124.
17. Sotelo-Boyas, R.; Froment, G. F. *Ind. Eng. Chem. Res.* **2009**, 48, 1107-1119.
18. Wei, W.; Bennet, C. A.; Tanaka, R.; Hou, G.; Klein, M. T. *Fuel Process Technology* **2008**, 89, 344 – 349.
19. Ancheyta-Juarez, J.; Macias-Villafuerte, E.; Schachat, P.; Aguilar-Rodriguez, E.; Gonzales-Arredondo, E. *Chem. Eng. Technol.* **2002**, 25, 541-546.
20. Smith, R. B., *Chemical Engineering Progress.* **1959**, 55, 76-80.
21. Krane, H. G.; Groth, B. A.; Schulman, L. B.; Sinfeld, H. J. *Fifth World Petroleum Congress Section III*, New York, **1959**, 39.
22. Henningsen, J.; Bundgaard-Nielson, M. *British Chemical Engineering* **1970**, 15, 1433-1436.
23. Jenkins, H.; Stephens, T. W. *Hydrocarbon processing* November, **1980**. 163 – 167.
24. Hu, S.; Zhu, X. X. *Chem. Eng. Comm.*, **2004**, 191, 500-512.
25. Stijepovic, M. Z.; Vojvodic-Ostojic, A.; Milenkovic, I.; Linke, P. *Energy & Fuels* **2009**, 23, 979-983.
26. Tailleux, R. G.; Davila, Y. *Energy & Fuels* **2008**, 2892-2901.
27. Ramage, M. P.; Graziani, K. R.; Schipper, P. H.; Krambeck, F. J.; Choi, B. C. *Advances in Chemical Engineering* **1987**, 13, 193-266.

28. Kmak, W. S. *AIChE National Meeting*, Houston, TX, **1972**.
29. Klein, M. T. *Molecular modeling in heavy hydrocarbon conversions*. CRC Press **2006**. Boca Raton, FL.
30. Bommannan, D.; Srivastava, R. D.; Saraf, D. N. *The Canadian Journal of Chemical Engineering* **1989**, 67, 405-411.
31. Padmavathi, G.; Chaudhuri, K. K. *The Canadian Journal of Chemical Engineering* **1997**, 75, 930-937.
32. Hou, W.; Su, H.; Hu, Y.; Chu, J. *Chinese J. Chem. Eng.* **2006**, 14, 584-591.
33. Szczygiel, J. *Energy & Fuels* **2005**, 19, 7-21.
34. Li, J.; Tan, Y.; Liao, L. *2005 IEEE Conference on Control Applications* **2005**, 867-872.
35. Lee, J. W.; Ko, Y. C.; Lee, K. S.; Yoon, E. S. *Computers Chem. Engng.* **1997**, 21, S1105 – S1110.
36. Hu, Y.; Su, H.; Chu, J. *Proceedings of the 42nd IEEE December* **2003**, 6206-6211.
37. Stijepovic, M. Z.; Linke, P.; Kijevcannin, M. *Energy & Fuels* **2010**, 24, 1908-1916.
38. Ginestra, J. C.; Jackson, R. *Ind. Eng. Chem. Fundam.* **1985**, 24, 121 – 128.
39. Doyle, F. J. III, Jackson, R.; Ginestra, J. C. *Chem. Eng. Sci.* **1986**, 41, 1485 – 1495.
40. Bhatia, S.; Chandra, S.; Das, T. *Ind. Eng. Chem. Res.* **1989**, 28, 1185-1190.
41. Chirico, R. D.; Steele, W. V. J. *Chem. Eng. Data* **1997**, 42, 784-790.
42. Riazi, M. R. *Characterization and Properties of Petroleum Fractions*; 1st ed., American Society for Testing and Materials: West Conshohocken, PA, **2005**.
43. Kister, H. Z. *Distillation Design*; McGraw-Hill, Inc.: New York, NY, **1992**.
44. Kaes, G. L. *Refinery Process Modeling A Practical Guide to Steady State Modeling of Petroleum Processes*; The Athens Printing Company: Athens, GA, **2000**.

45. Sanchez, S.; Ancheyta, J.; McCaffrey, W. C. *Energy & Fuels* **2007**, 21, 2955 – 2963.
46. Aitani, G. M; Parera, J. M *Catalytic Naphtha Reforming (Science and Technology)* 1st Edition, Marcel Dekker, New York, **1995**.
47. Fernades, J. L.; Pinheiro, C. I. C.; Oliviera, N. M. C.; Inverno, J.; Ribiero, F. R. *Ind. Eng. Chem. Res.* **2008**. 47. 850-866.
48. Van Trimpont, P. A; Marin, G. B; Froment, G. F. *Ind. Eng. Chem. Fundam.* **1986**, 25, 544-553.
49. Van Trimpont, P. A.; Marin, G. B.; Froment, G. F. *Ind. Eng. Chem. Res.* **1988**, 27, 51-57.
50. Garg, A. *Hydrocarbon processing* June, **1997**. 97 – 105.
51. Vinayagam, K. *Hydrocarbon processing* October, **2007**. 95-104.
52. Bazaraa, M. S.; Jarvis, J. J.; Sherali, H. D. *Linear Programming and Network Flows*. John Wiley and Sons **2009**. Hoboken, NJ.

4. Guide for modeling FCC units in Aspen HYSYS/Petroleum Refining

4.1 Introduction

In this chapter, we go through an example of how to organize data, build and calibrate a model for a fluid catalytic cracking (FCC) unit using Aspen HYSYS/Petroleum Refining. We discuss some key issues in model development and how to estimate missing data required by Aspen HYSYS/Petroleum Refining. We divide this chapter into four workshops:

- a. Workshop I: Building a basic FCC Model
- b. Workshop II: Calibrating the basic FCC Model
- c. Workshop III: Build main fractionator and gas plant system
- d. Workshop IV: Perform case study to identify different gasoline production scenarios
- e. Workshop V: Generate DELTA-BASE vectors for linear programming (LP) based planning

4.2 Process Overview

Figure 4.1 and Figure 4.2 show process flow diagrams (PFD) for the FCC unit and downstream fractionation units that we will use to build the model in question. We extensively discussed the features and operating issues associated with this type unit in Chapter 2. In the context of this chapter, we also build models for the main fractionator and associated gas plant.

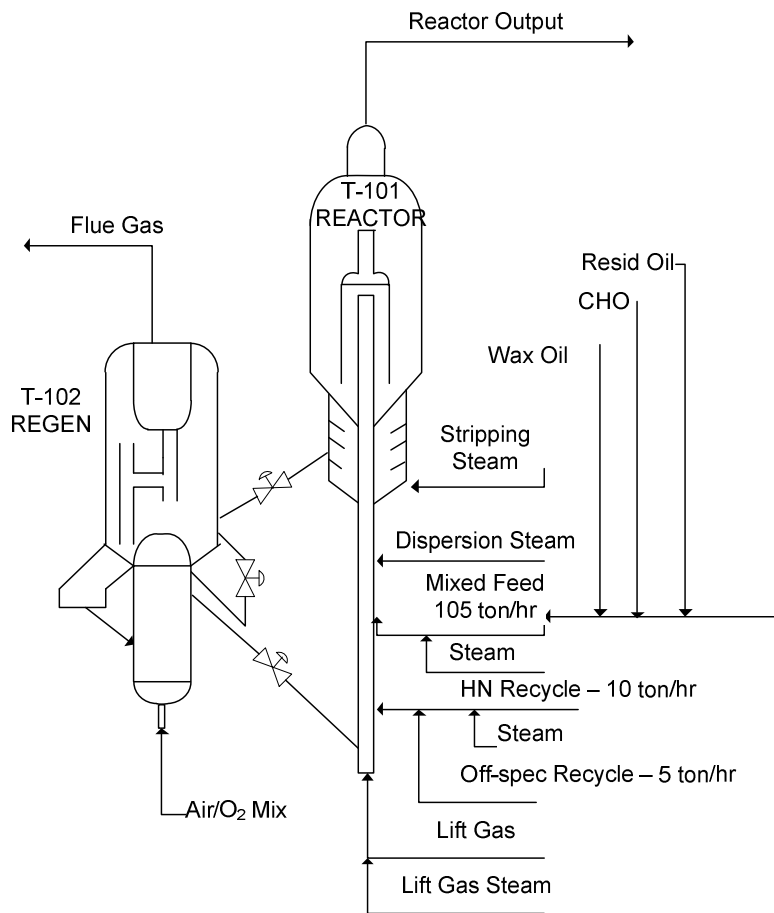


Figure 4.1: Reaction Section of FCC Unit

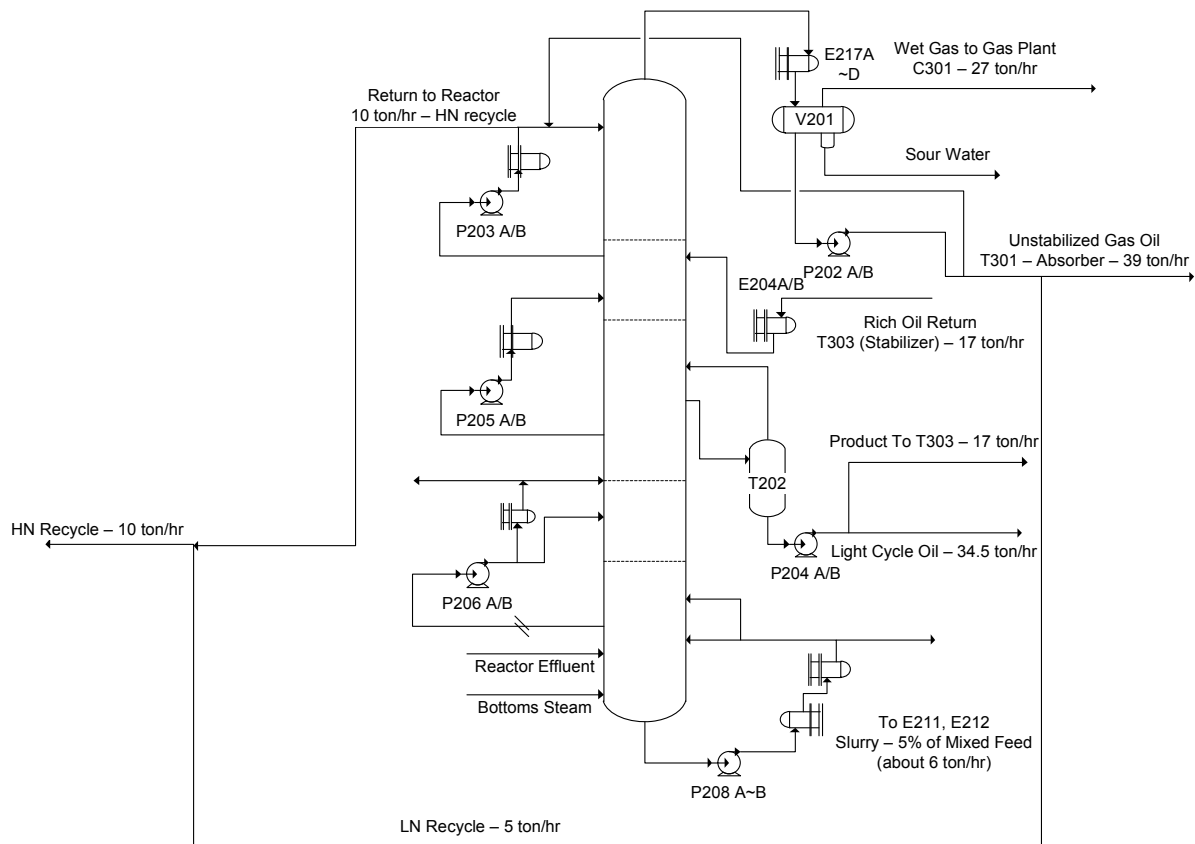


Figure 4.2: Main Fractionator associated with FCC

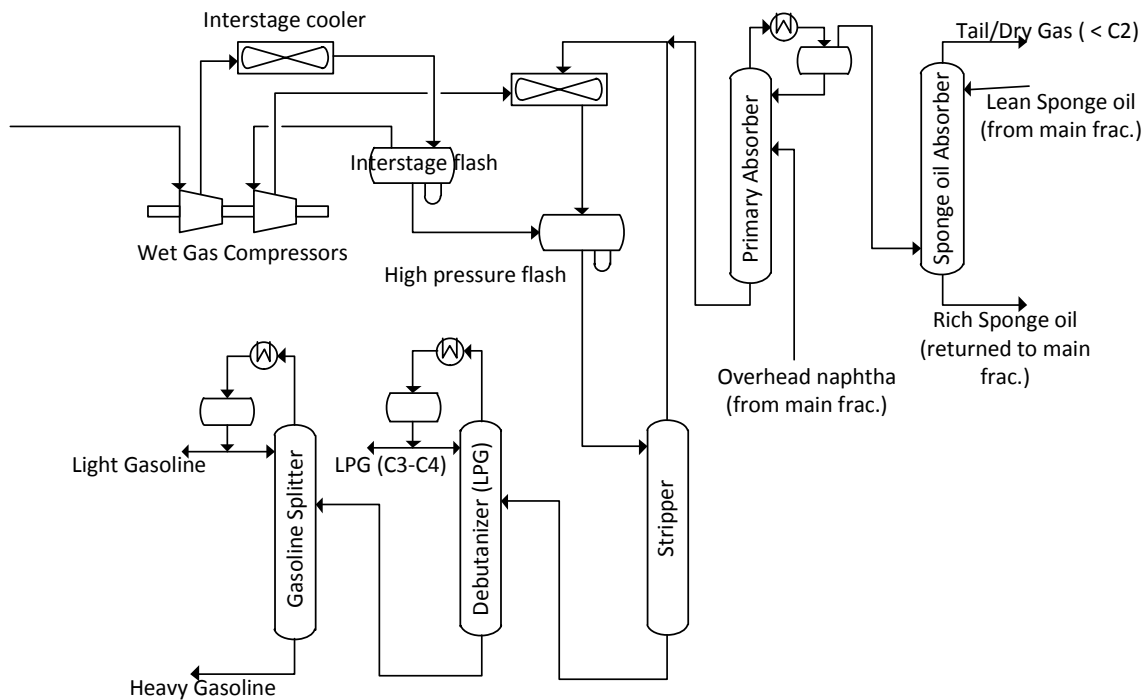


Figure 4.3: Gas plant associated with FCC unit

4.3 Process Data

Table 4.1 to Table 4.4 give detailed feeds, products and operation data for a typical UOP FCC process. Values that have been estimated are marked with a *. We extensively discussed methods to estimate required properties for FCC modeling in a preceding chapter. Operating conditions for the fractionation section largely depend on the FCC unit effluent and are relatively static, so they are not given here.

Table 4.1: Summary of liquid feeds and products

Feed/Products	Feed	Naphtha	Light Cycle Oil	Bottoms

Flow rate (kg/hr)	108208	46583	24333	4125
Specific gravity	0.9	0.7	1.0	1.0
Distillation Type	D-1160	D-86	D-86	TBP
Initial Point (°C)	269.0	35.7	217.9	221*
5%	358.6	40.8	235.9	314*
10%	376.4	45.6	246.6	343.3*
30%	419.0	64.7	275.7	382.2*
50%	452.3	86.4	300.3	426.7*
70%	488.0	115.0	326.9	468.3*
90%	541.8*	165.4	365.4	496.1*
95%	567.9*	191.4	382.5	545.1*
End Point	665.8*	255.4	418.9	649*
Nitrogen (ppmwt)	2409.0	9.0	127.8	324.3
Sulfur (wt. %)	0.56	0.06	0.91	1.96
CCR (wt. %)	1.86	0.01	0.11	0.38
Vanadium (ppmwt)	0.3	-	-	-
Nickel (ppmwt)	3	-	-	-
Sodium (ppmwt)	0.3	-	-	-
Iron (ppmwt)	2.1	-	-	-
Copper (ppmwt)	0.1	-	-	-
RON/MON	-	92/82	-	-
Olefins (Liq. vol%)	28.5	-	-	-
Naphthenes (Liq.	8.529	-	-	-

vol%)				
Aromatics (Liq. vol%)	23.6	-	-	-
Cloud Point (°C)	-	-	-10	-

Table 4.2: Summary of gas flowrates and composition

	Dry Gas	Sour Gas	LPG	Regen. Flue Gas
Flow rate (kg/hr)	4833	667	19542	-
			vol.	Mol. %
Composition	mol. %	mol. %	%	
N2	22.5	0.6	-	NA
CO	1.7	-	-	NA
CO2	1.8	30.5	-	NA
O2	-	-	-	2.8
H2S	0.0	68.5	-	NA
H2	25.5	-	-	NA
C1	23.3	0.2	-	NA
C2	11.2	0.2	-	NA
C2=	11.3	-	-	-
C3	0.3	-	13.5	-
C3=	1.0	-	41.5	-
nC4	0.2	-	4.7	-

iC4	0.4	-	18.0	-
iC4=	0.4	-	12.5	-
1-C4=	-	-	-	-
c2-C4=	-	-	4.0	-
t2-C4=	-	-	5.7	-
c2-C5=	0.2	-	-	-
t2-C5=	0.2	-	-	-

Table 4.3: Riser and regenerator operating conditions

	Flowrate (kg/hr)	Temperature (°C)	Pressure (kPa)
Riser Feed Pre-heat Temperature	-	175	-
Riser Inlet Steam	5000	200	1301
Riser Outlet Temperature	-	518	-
Stripping Steam	5000	200	1301
Regenerator Dense Bed Temperature	-	680	-
Regenerator Pressure	-	-	-

Table 4.4: Equilibrium catalyst properties

Metals content (V/ Ni/ Na/ Fe/ Cu) (ppmwt)	5000/4044/3103/5553/57
Equilibrium Activity (%)	66

Inventory (kg)	150000
----------------	--------

4.4 Aspen HYSYS and initial component and thermodynamics setup

We start by opening Aspen HYSYS. The typical path to Aspen HYSYS is to enter the Start > Programs > AspenTech > Aspen Engineering Suite > Aspen HYSYS. Early versions may include a menu entry titled Aspen RefSYS. We dismiss the “Tip” dialog and select File > New > Case. We wish to include fractionation, so we do not choose “FCC” alone.

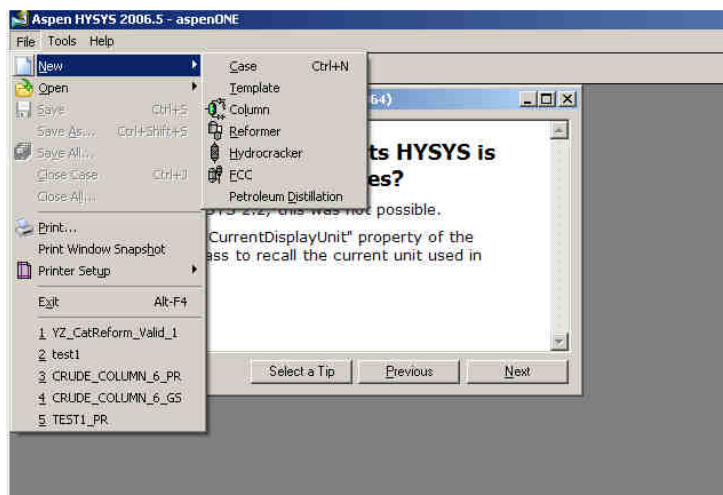


Figure 4.4: Initial Startup of Aspen HYSYS

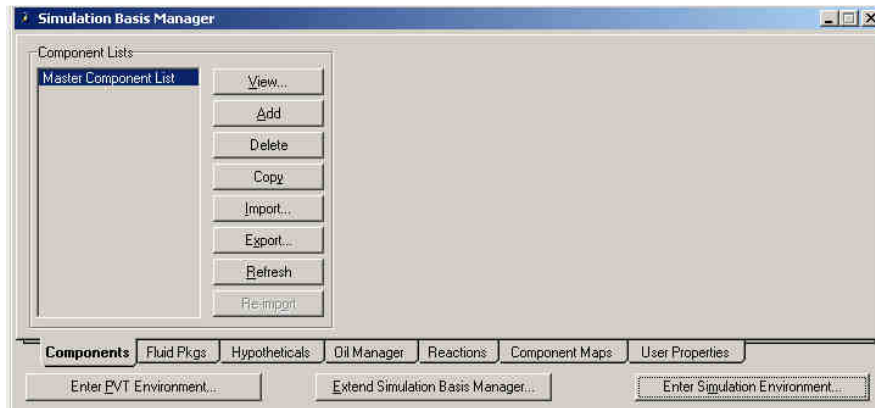


Figure 4.5: Adding a component List

The first in creating the model is the selection of a standard set of components and a thermodynamic basis to model the physical properties of these components. When we create a new simulation, we must choose the components and thermodynamics appropriate for the process using the Simulation Basis Manager. The Simulation Basis Manager allows us to define components and associated thermodynamics in Aspen HYSYS. Components may be added manually through the Add button shown in Figure 4.5. However, we have a predetermined set of the components for the FCC model.

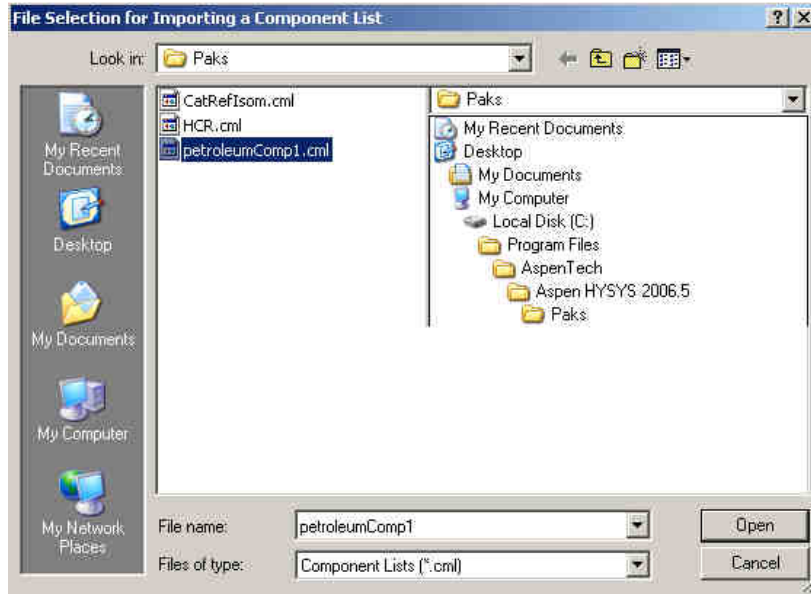


Figure 4.6: Adding petroleum component list

To import these components, we click ‘Import’ and navigate to the directory location, “C:\Program Files\AspenTech\Aspen HYSYS 2006.5” and select the “petroleumComp1.cml” as the component list (Figure 4.6). The path shown in this figure reflects a standard installation of Aspen HYSYS/Petroleum Refining software.

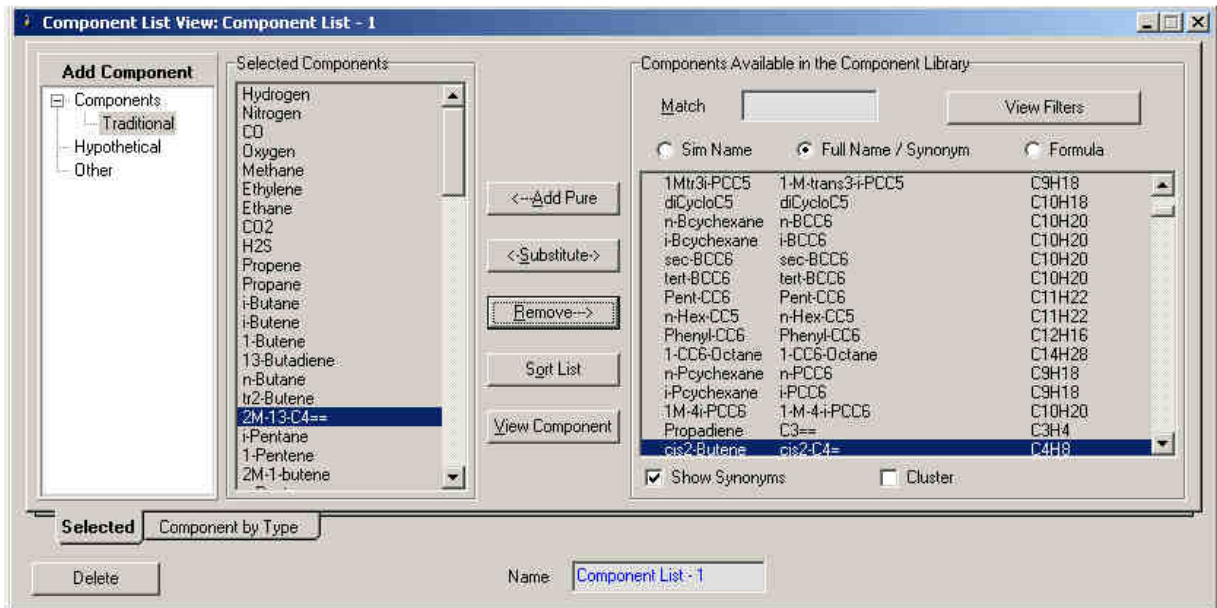


Figure 4.7: Initial Component list for petroleum component list process

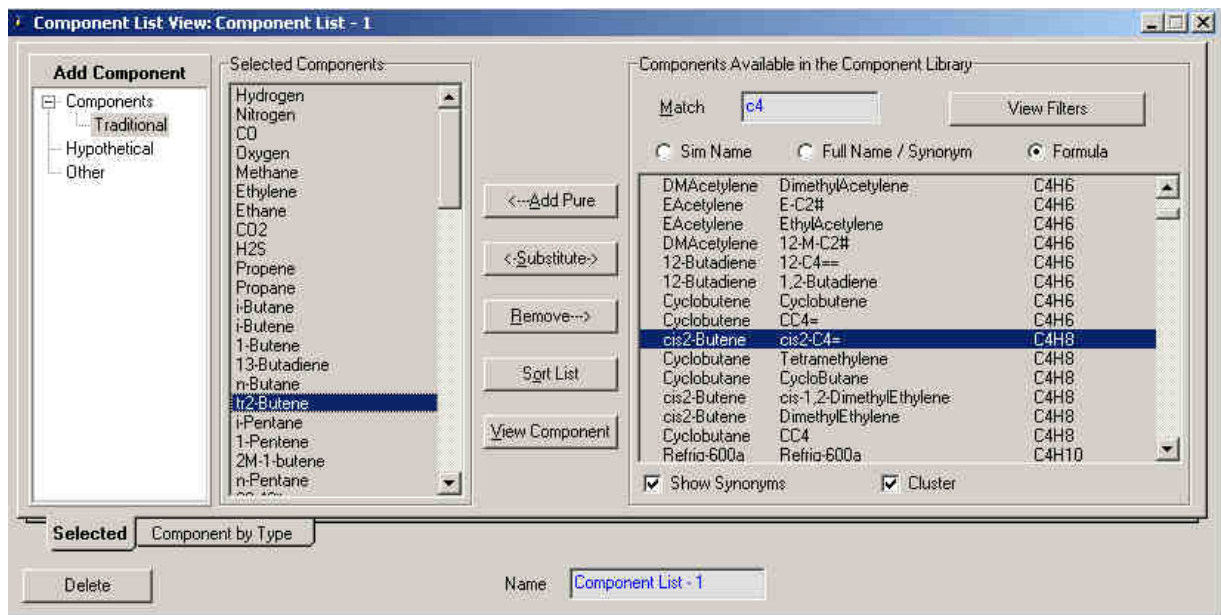


Figure 4.8: Adding additional components to petroleum component list

Once we import a component list, HYSYS will create a new component list called “Component List-1”. We can view the elements of this component lists by selecting “Component List-1” and clicking on “View” in the Simulation Basis Manager (Figure 4.7). We can add additional components or modify the order of the elements in the component list. We note that the standard FCC component list is quite complete and model most refining processes. The rigorous FCC model does not predict components are not part of the “petroleumComp1.cml” list. However, these additional components may be used in production fractionation models of the associated with the FCC model. For the purposes of this simulation we will add cis-2-butene and benzene.

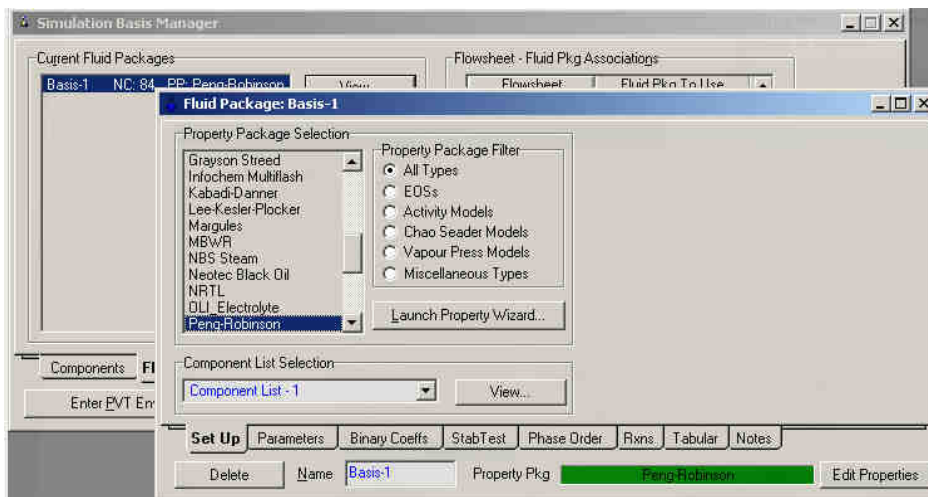


Figure 4.9: Select Thermodynamics for Fluid Package

The next step is the selection of a ‘Fluid Package’ for this model. The ‘Fluid Package’ refers the thermodynamic system associated with the chosen list of components. We move to the ‘Fluid Pkgs’ tab in the Simulation Basis Manager and add click ‘Add’ (Figure 4.9) Aspen HYSYS will automatically choose the component list and present options for a ‘Property Package’ for these components. The FCC system is mostly hypothetical and light hydrocarbons. Consequently the

Peng-Robinson equation of state is sufficient. We discuss the implications of the process thermodynamics in a previous chapter of this text. In the case of the FCC model, equation of state or hydrocarbon correlation methods (Grayson-Streed, etc.) can sufficiently model the processes.

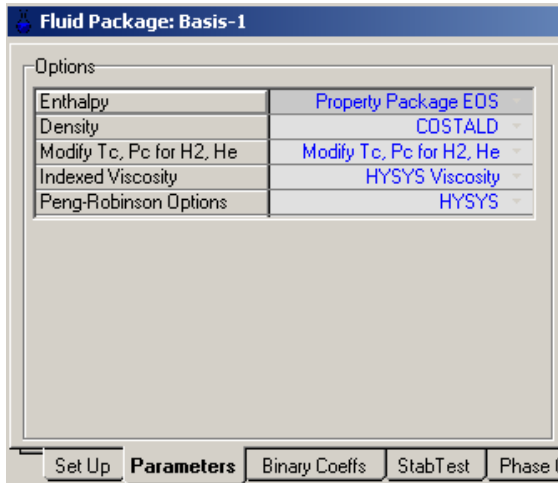


Figure 4.10: Thermodynamic options for Fluid Package

It is important to note that even when we choose an equation-of-state approach, Aspen HYSYS does not calculate all physical properties from the equation of state. For hydrocarbons, equations of state do not generally predict the equilibrium properties of very light components such as hydrogen. In addition, density predictions (especially in the heavy hydrocarbon range) can be quite poor. We almost always modify the equation of state to account for these deficiencies. For the FCC process we choose the COSTALD method to predict the liquid density (Figure 4.10).

	Hydrogen	Methane	Ethane
Hydrogen	---	0.20200	0.22310
Methane	0.20200	---	0.00224
Ethane	0.22310	0.00224	---
Ethylene	0.00740	0.02150	0.01230
Propane	0.21420	0.00683	0.00126
Propene	-0.10360	0.03300	-0.00190
i-Butane	0.20370	0.01311	0.00457
n-Butane	0.19410	0.01230	0.00410

Treatment of Interaction Coefficients Unavailable from the L
 Estimate HC-HC / Set Non HC-HC to 0.0

Set Up Parameters **Binary Coeffs** StabTest PK
 Delete Name Basis-1 Property Pk

Figure 4.11: Binary interaction parameters for Fluid package

The last step before building the FCC flowsheet is to verify the interaction parameters (Figure 4.11). If we had chosen a correlation based approach (Grayson-Streed, etc.) we do not have to examine the interaction parameters. Since we chose an equation of state approach, we must make sure that the binary interaction parameters for the equation of state are meaningful. In Aspen HYSYS, the interaction parameters for defined components (such as methane, ethane, etc.) come from an internal databank based on experimental data. For hypothetical petroleum components, we can either set the interaction parameters to 0 or estimate these values based on correlations. Note that that often little difference in practice whether or not the interactions are set to zero or estimated for lumped components. Especially for the FCC process, both methods yield nearly identical results. Once we have chosen an option the interaction parameters, we can return to the Simulation Basis Manager and click on ‘Enter Simulation Environment’ to begin building the process model.

4.5 Workshop I: Basic FCC model

The initial flowsheet presents a blank interface where we can place different objects from the Object palette shown in Figure 4.12. The initial tool palette only shows typical unit operations and does not show the advanced Aspen HYSYS/Petroleum Refining objects. We will use both toolbars to build out the complete FCC model. We can bring the up the advanced palette by pressing F6.

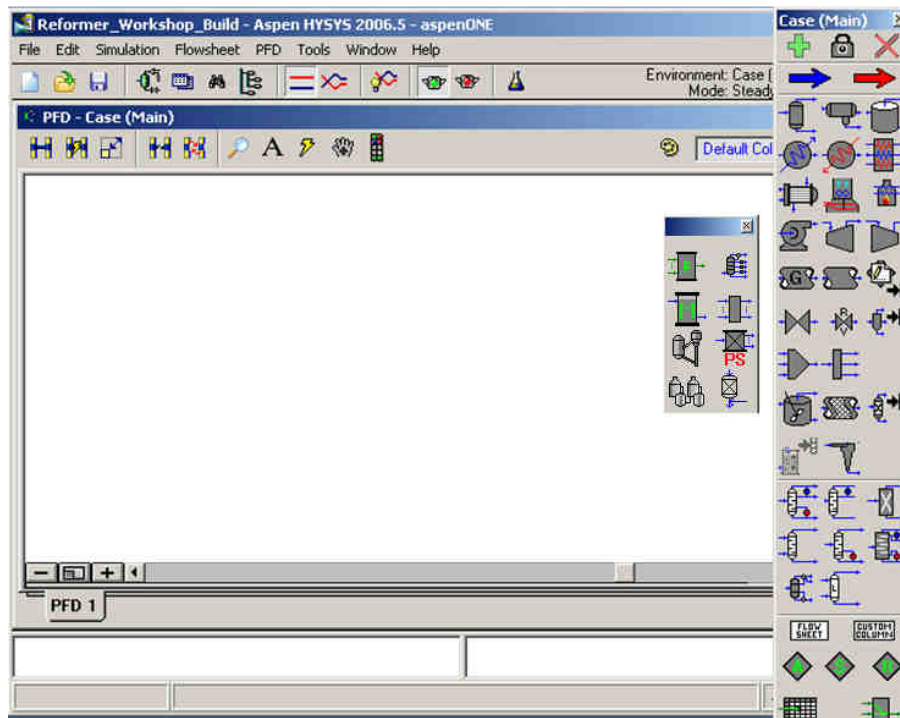


Figure 4.12: Initial Aspen HYSYS Flowsheet

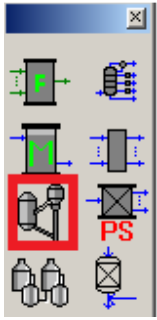


Figure 4.13: Aspen HYSYS/Petroleum Refining unit operation palette

We select the FCC icon from the Refining Reactors palette and click on the FCC icon and place the icon on the flowsheet. Placing the icon invokes the several sub-models that prepare the flowsheet for additional objects and creates a large depiction of the reformer object on the flowsheet.

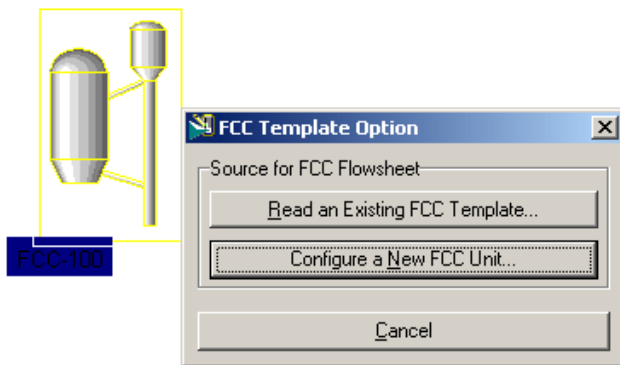


Figure 4.14: Adding initial FCC unit

The first step is to choose whether to use a FCC template or configure a new unit. Aspen HYSYS has several FCC templates that reflect several popular types of industrial FCC configurations. Figure 4.14 shows the initial window when we place a FCC object on the

Flowsheet. If we choose a template, we do not have to assign the reactor dimensions and select catalyst configuration. However, in this workshop, we will build a FCC unit from scratch, so we choose ‘Configure a New FCC Unit’.



Figure 4.15: Selecting FCC configuration

The FCC configuration requires choosing the riser configuration, number and type of regenerators and catalyst configuration. We may also specify additional downstream fractionation in the form of a simplified main fractionator for the FCC effluent. However, we note that a simplified model for fractionation that may not be appropriate for a detailed and integrated process flowsheet. We recommend building a rigorous flowsheet based on standard Aspen HYSYS fractionation objects. In subsequent sections, we will build a complete fractionation section using rigorous stage-by-stage models. In Figure 4.15, we select a FCC unit with one riser, one-stage regenerator and no fractionation model and click “Next>”. We may also use the “Allow Midpoint Injection” to allow for a FCC riser that has multiple injection points.

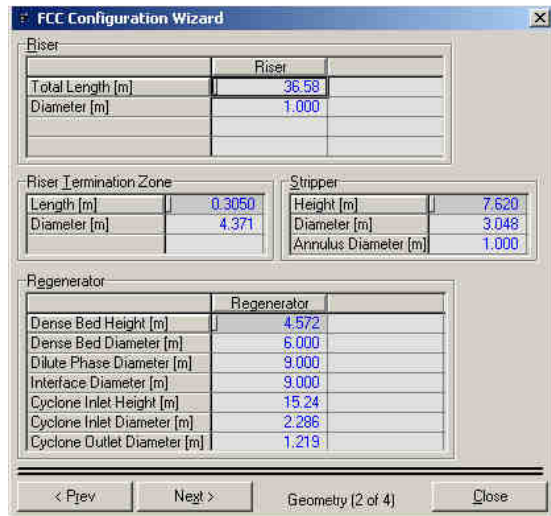


Figure 4.16: Sizing the dimensions of the FCC unit

In the next window, we must specify the key dimensions for the FCC unit. The values in Figure 4.16 reflect typical values for a one-riser, one-regenerator FCC unit. While all measurements are required, the key measurements are the length and diameter of the Riser and the height and diameter of the dense and dilute phase in the regenerator. We can estimate all other values (i.e. use values in Figure 4.16) without significantly affecting model results. We click “Next>” after entering all measurements.



Figure 4.17: Specifying heat loss from different locations of the FCC Unit

Aspen HYSYS now requests to enter to the heat loss for each section of the FCC unit as shown in Figure 4.17. In general, these values are not available and we recommend using the default values of 0 for all heat losses. These heat losses can account for changes to due to external cooling or heating surrounding the unit. Generally, these values are not significant and may be safely ignored. We click “Next>” to complete the initial unit configuration.

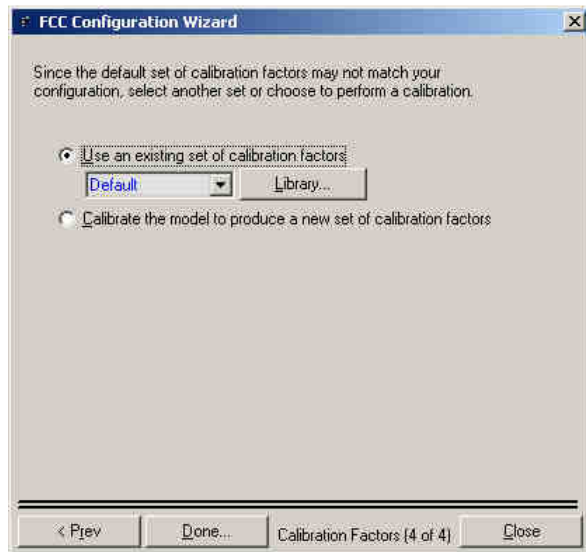


Figure 4.18: Select default calibration parameters

The last step is the calibration factors for this particular unit (Figure 4.18). The calibration factors refer to tuning factors for a specific unit. These tuning factors allow us to match model results with current plant performance. Since we will be adjusting or calibrating these tuning factors in this chapter, we choose the “Default” factors. It is possible to have several different sets of tuning factors or calibrations corresponding to a variety of process, feedstock and catalyst configurations. However, we recommend that each file should not have more than one set of calibration or tuning factors in addition to the “Default” calibration factors.

4.6 FCC Feed configuration

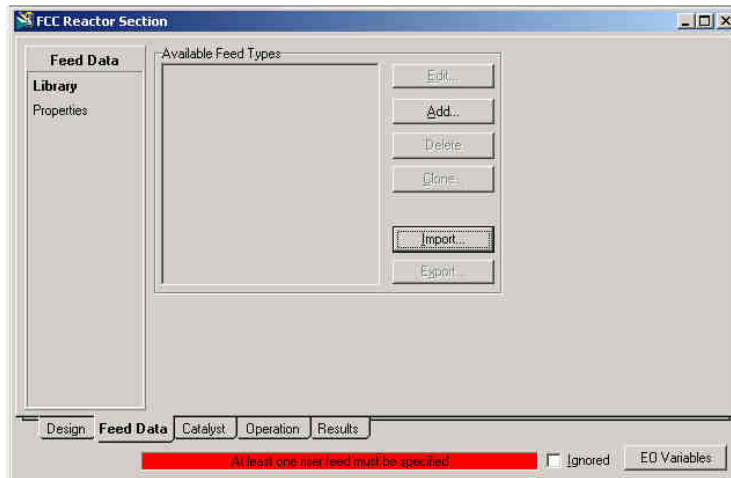


Figure 4.19: Assign feed types to feed data

After we complete the basic FCC configuration, we must specify the feed details. We double-click on the FCC icon on the flowsheet to bring up the FCC configuration window shown in Figure 4.19. We select the “Feed Data” to assign a Feed type for this model. A feed type refers to how Aspen HYSYS will translate the bulk property information into kinetic lumps. Aspen HYSYS supplies a variety of feed type templates for FCC feeds from a variety sources such as Vacuum Gas Oil (VGO), Hydrotreated Vacuum Gas Oil (HTVGO), etc. We click “Import” to import feed types from the feed library. The location of the feed library appears in Figure 4.20.

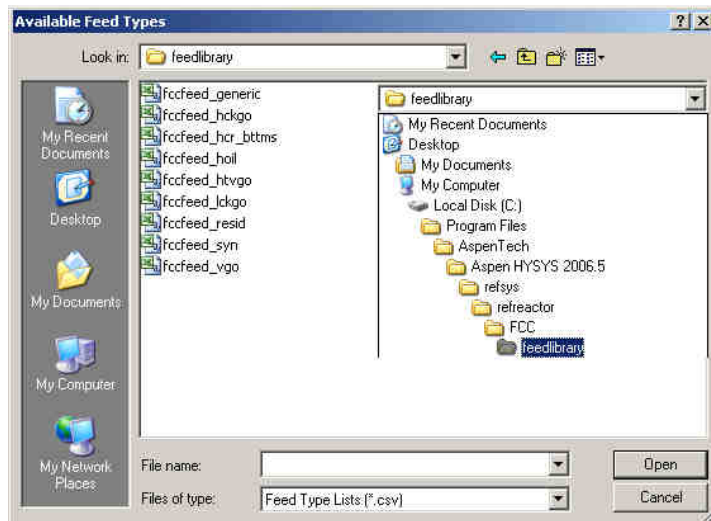


Figure 4.20: FCC feed type library

For this model, we will only choose “fccfeed_vgo.csv”. We note that it is possible to include multiple feed types in the same model. In most cases, the VGO feed type is appropriate for most FCC configurations. Even if the FCC feed is a mixture of gas oil from various sources, we recommend using the VGO feed type. If the FCC feed is largely residue type feed, then we recommend using the “fccfeed_resid.csv” feed type.

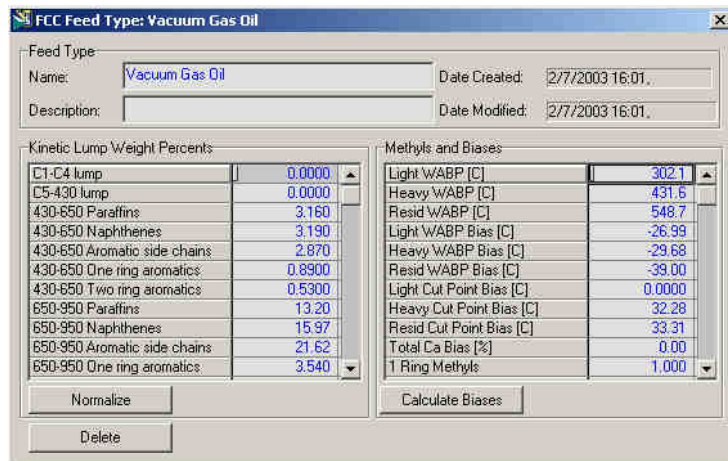


Figure 4.21: Feed type template

When we import the feed type, Aspen HYSYS shows the details of the feed type as shown in Figure 4.21. The “Kinetic Lump Weight Percents” indicate the starting composition of the kinetic lumps and the “Methyls and Biases” indicate how various bulk properties affect the final lump composition. Aspen HYSYS uses the biases to calculate actual kinetic lumps with the bias vectors. The bias vectors essentially correct the kinetic lump composition for the measured bulk properties (which we will enter) from the reference bulk properties in the feed type. We will not modify any information in this window and simply close it to continue the feed configuration process.

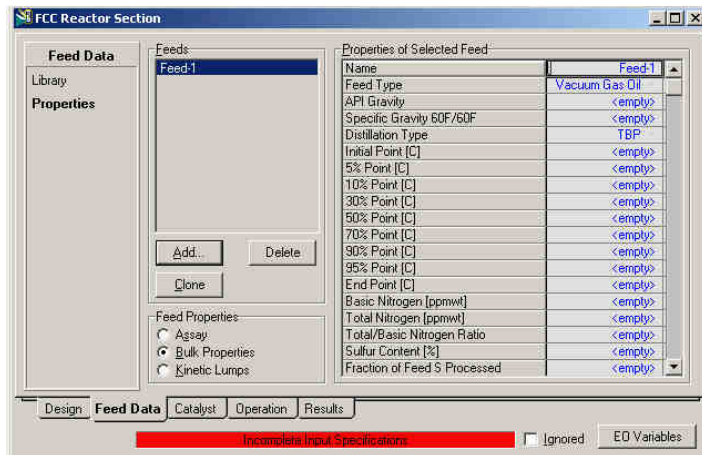


Figure 4.22: Feed bulk property information window

We will return to the “Feed Data” tab and select the “Properties” section to begin entering the bulk properties of the feed (Figure 4.22). We select the “Bulk Properties” option for the Feed properties. The minimum required data are the distillation curve of the feed, specific gravity, basis or total nitrogen, sulfur content, Conradson Carbon Residue (Concarbon) and metals content (Vanadium, Nickel, Sodium, Iron and Copper) of the feed. We expect that these properties are part of the routine analysis of the feed to the FCC unit.

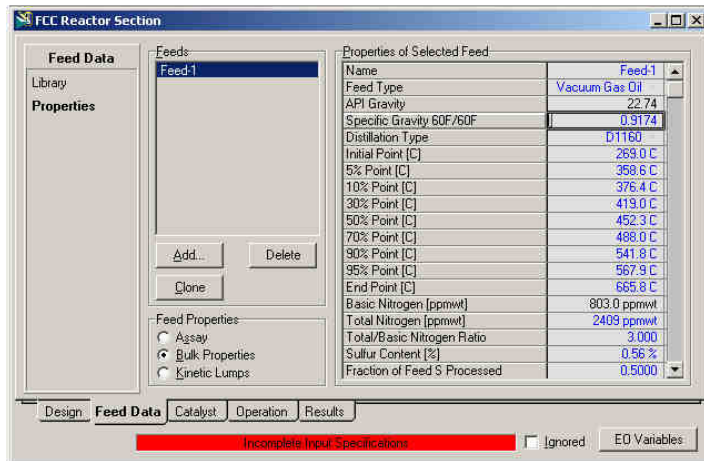


Figure 4.23: Completed feed bulk property information window

Figure 4.23 shows the completed feed properties table using the feed information given in Table 4.1. If both total and basic nitrogen are not available, we typically use a value of 3.0 for the Total to basic nitrogen ratio. In addition, we typically use 0.5-0.6 the fraction of feed sulfur processed. Residue-type feeds typically have lower amounts of the fraction of feed sulfur processed. While these values are not exact, they will suffice for initial model. We also provide some guidelines for related feed information estimates in Table 4.5. However, it is important to provide reasonably accurate and update to date values for the metals content of the feed. The metals content significantly contributes to the coke production in the unit. Since the riser and regenerator are heat-integrated in the FCC unit, this can affect the overall yield prediction from the unit.

Table 4.5: Typical range of properties for FCC feed

Bulk property	Typical range or guideline
Specific Gravity	0.8 – 1.2

Concarbon (wt. %)	1 – 3
Basic Nitrogen (ppmwt)	500 – 1000
Total/Basic Nitrogen Ratio	3.0
Sulfur content (ppmwt)	< 2
Fraction of feed sulfur processed	0.5 - 0.6
Total Aromatic content (wt. %)	20 – 30 (for straight run VGO)
Nickel and Iron content (ppmwt)	10x – 100x (Vanadium + Sodium + Copper)

Table 4.5 gives typical values for straight-run VGO and can serve a reality check for data collected during analysis. The nitrogen and sulfur content can increase the rate of catalyst deactivation significantly, while the high metals content can promote excessive production of hydrogen and light gas. We must be aware of these factors when developing the FCC model.

This completes the feed configuration of the FCC unit. We may add additional feeds to the unit at this point (with the same feed type). For this simulation, we will only use one feed.

4.7 FCC Catalyst configuration

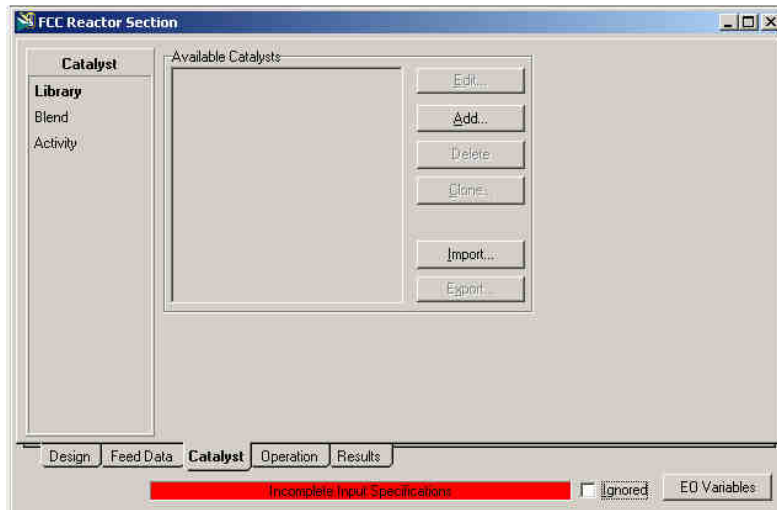


Figure 4.24: Initial catalyst library window

The next step in building in the model is selecting the catalyst blend in the unit. We select the “Catalyst” Tab in the FCC Reactor Section Window as shown in Figure 4.24. The process for importing a catalyst blend is similar to the process for importing feed types. We click on the “Import...” button to bring up the import window for the catalysts.

Figure 4.25 shows the location of the catalyst library and also lists the available catalyst types. A catalyst type essentially contains tuning or calibration factors responsible for light gas distribution, small adjustments to product bulk properties (RON, MON, etc.) and distribution of coke produced by the metal function of the catalyst. The catalyst library contains catalyst from a variety of manufacturers and sources. If the exact catalyst is not available, we recommend using a similar match. It is possible to tune away variations in the tuning factors due to catalyst type, but this may produce an overcalibrated model with unrealistic yield predictions. For this model, we will use the “af-3.csv” catalyst.

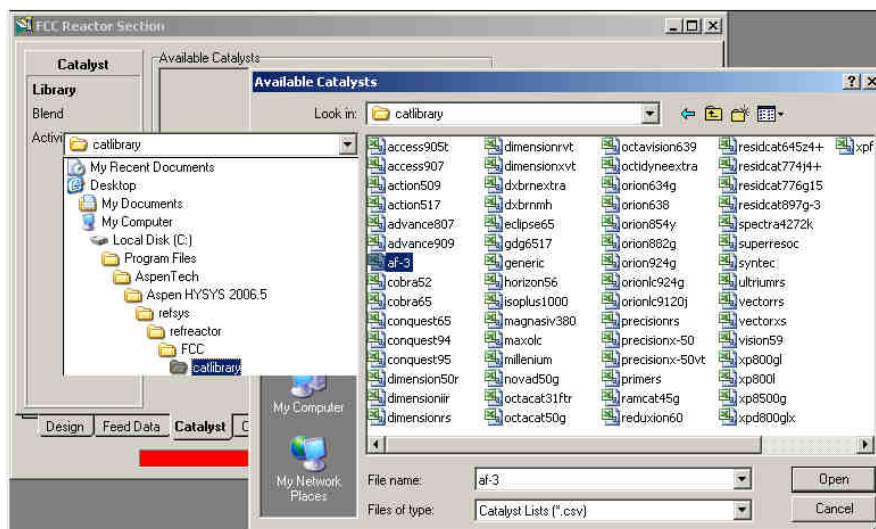


Figure 4.25: Catalyst library

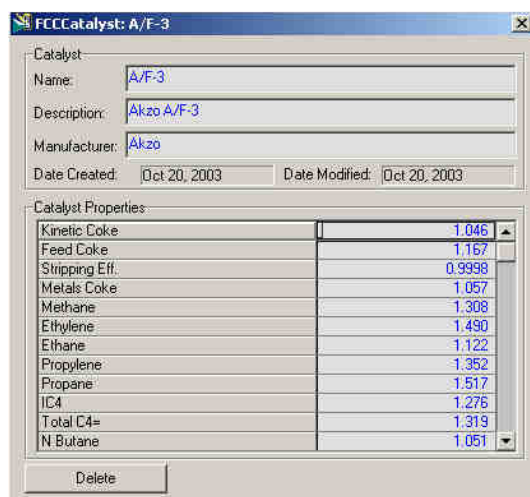


Figure 4.26: Catalyst parameters

Once we choose a catalyst, Aspen HYSYS will display a summary of the key features of the catalyst (See Figure 4.26). We can use this list to compare with the true product specifications from the catalyst manufacturer. If the catalyst is not acceptable, we can click 'Delete' to remove the catalyst and try another entry from the catalyst library. As we mentioned in the previous

paragraph, it is not critical to find an exact match. Once we have added all catalysts we require, we can close the catalyst information window and return the “FCC Reactor Section”

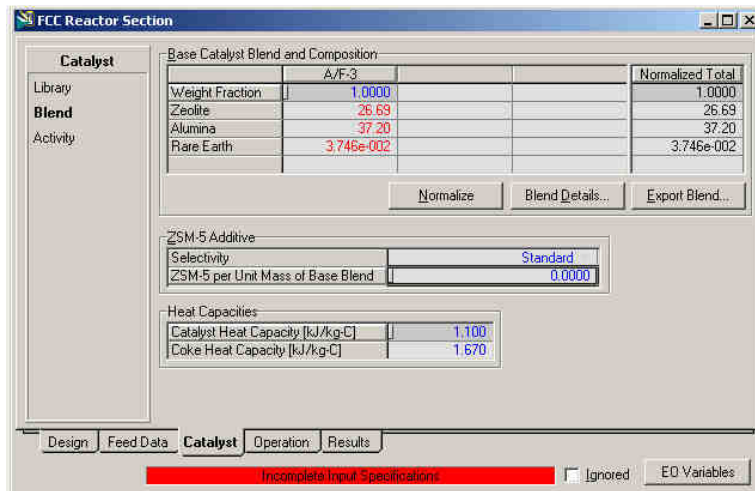


Figure 4.27: Catalyst parameters

Next we must specify the catalyst blend. The catalyst blend refers two or more different kinds of catalysts from the catalyst library. We can assign individual weight fractions for each of the catalysts in the blend. In our model, we are using only one type of catalyst, so we set the weight fraction to 1.0 in Figure 4.27. We use the default values for the heat capacities of the catalyst and coke. These values are generally not measured; however, we expect only small deviations from the default value in the actual FCC unit.

We must also specify if any ZSM-5 additive is present in the catalyst. The “ZSM-5 per Unit Mass” variable acts as another tuning factor to adjust model yields of the unit. We may use an average value or set the ZSM-5 content to 0 if the information is not available. Since we will tune the unit to an actual product distribution, it is not essential that this value is exactly the same as the actual unit.

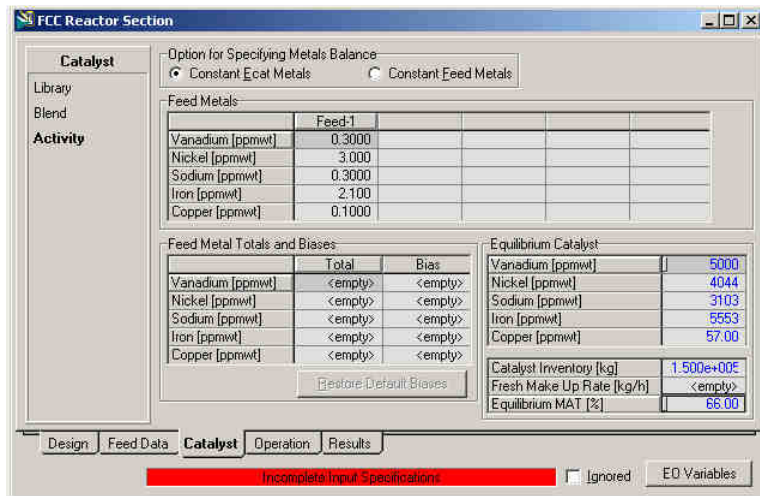


Figure 4.28: Catalyst activity factor and equilibrium metals content

The last step in catalyst configuration is to specify the “Activity” section of the “Catalyst” Tab in the FCC Reaction Section Window as shown in Figure 4.28. The Activity of the catalyst essentially refers to the effect of metals on catalyst deactivation. We can either maintain a constant level of metals on the catalyst or keep adjust the feed metals content to match makeup rates and equilibrium activity. We recommend the using “Constant Ecat Metals” option since the information required is available from routine equilibrium catalyst analysis of the FCC catalyst.

We will specify the metals content of the equilibrium catalyst and equilibrium microactivity test (MAT) value. When we use this option, Aspen HYSYS will automatically calculate the makeup of catalyst required to maintain the equilibrium MAT and keep the metals content on the catalyst fixed. The total catalyst inventory refers to the total amount of catalyst available to the FCC unit. We can now specify the operating variables for the FCC unit model.

4.8 FCC Operating variables configuration



Figure 4.29: Main application menu bar (hold solver)

Before we specify the operating variables of the FCC unit, we will use the main application toolbar (see Figure 4.29) to hold the solver. Holding the solver ensures that the solver will not immediately solve once we specify all variables for the FCC unit. It is generally a good idea to hold the solver before changing many operating variables as we do in the following sections. We hold the solver clicking on the red stop sign in the main application tool bar. We can release the solver by clicking on the green go sign in the toolbar.

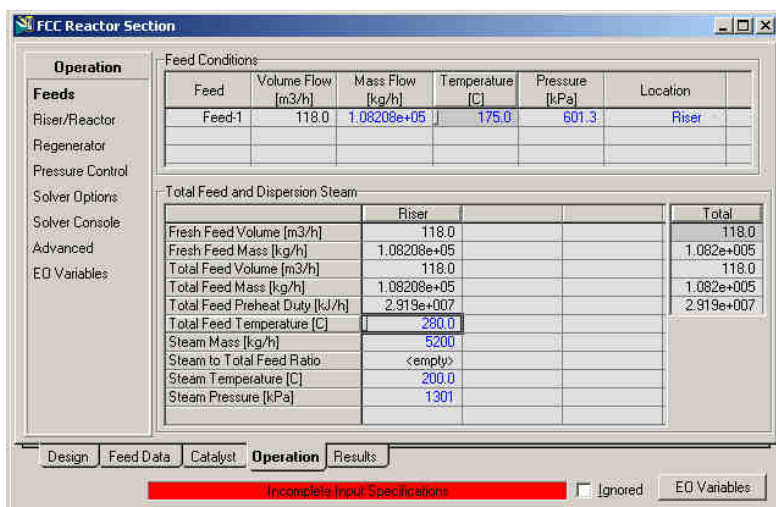


Figure 4.30: Specify feed conditions

We specify the feed rate, temperature and pressure into the preheater before the feed enters the riser in Figure 4.30. If we have multiple injection points, we can specify the feed into the injection points as well. To specify the actual temperature of the feed entering the riser, we must

either set the preheat duty or a preheat temperature. Since we have a single feed, we set the preheat outlet temperature to plant value. We must also specify the steam flow and conditions associated with the feed into the riser inlet. Typical values for dispersion steam are 1-5 wt% of the fresh feed rate.

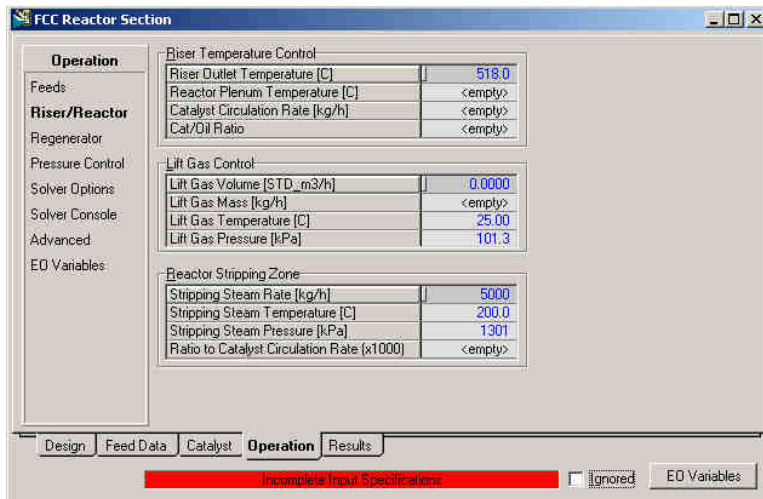


Figure 4.31: Riser conditions and steam input

The next step is to specify the operating variables for the riser and reactor as show in Figure 4.31. In most FCC units, control strategies generally fix the riser outlet temperature (ROT) as a setpoint, so the ROT is a natural specification for the riser. It is also possible to specify the Cat/Oil ratio or circulation rate but these specifications make the model quite difficult to converge. We recommend using the ROT as an initial specification and then shifting to other possible specifications.

We also specify the flowrate and conditions of the Lift Gas and Reactor Stripping Zone in Figure 4.31. The lift gas is typically an inert in the cracking process and the steam for the reactor stripping zone minimizes thermal cracking due to high temperatures. We must at least supply the

stripping steam rate to ensure that the model converges to a reasonable solution. The stripping steam rate is roughly on the order of 1-5 wt% of the fresh feed. The next step is to specify the regenerator operating variables.

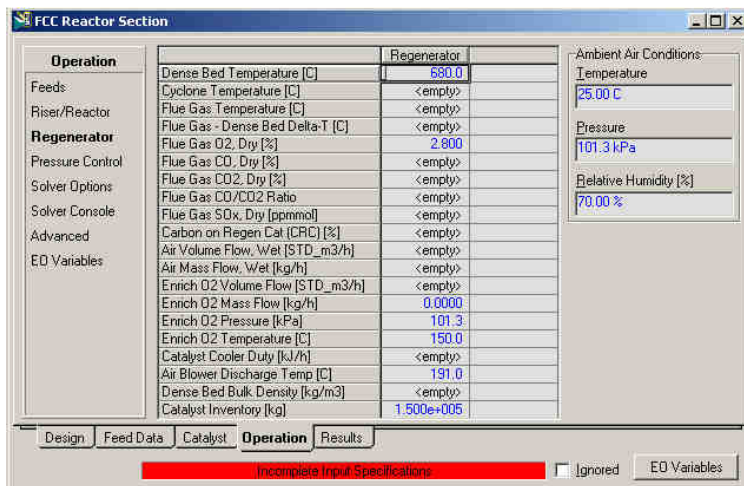


Figure 4.32: Regenerator operating parameters

In Figure 4.32, we specify regenerator operating variables. The key variables are the dense bed temperature, flue gas oxygen (O₂) composition and catalyst inventory. The flue gas composition and dense bed temperature fixes the air flow rate and coke combustion rate for the regenerator. Some FCC units include side coolers and enriched oxygen streams to completely combust the coke on the catalyst. We may specify these as well; however, they are not common with mostly straight run VGO type feeds. We enter nominal values for the ambient air conditions, and blower discharge temperature. In the typical range for these variables, there is little effect on process performance.

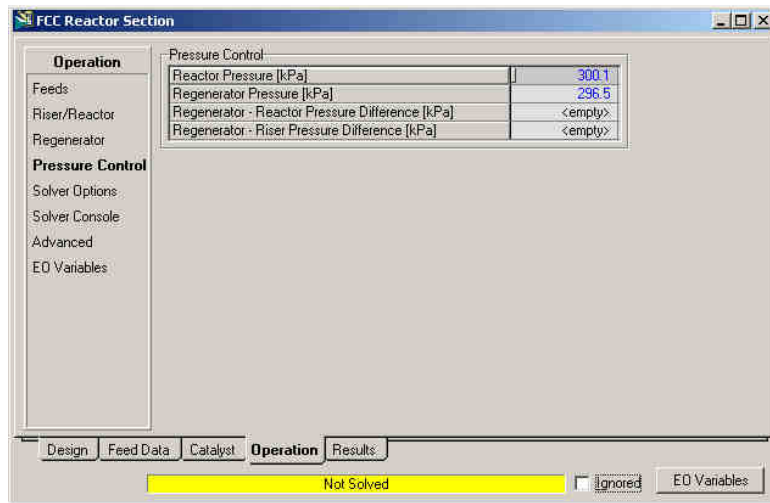


Figure 4.33: Pressure control (Reactor Pressure should be greater than regenerator pressure)

We show the last step in configuring operating variables in Figure 4.33. All refiners continuously measure the reactor and regenerator pressure to ensure that catalyst is flowing through the unit. Accurate values here will aid in better predictions of catalyst circulation rate through the riser and the Catalyst to Oil ratio. We also note that once we enter the pressure measurements in Figure 4.33, Aspen HYSYS will indicate that we are ready to solve the model.

4.9 Initial model solution

Before solving the model, we must ensure that the solvers parameters will lead to robust convergence. We bring up the Solver options by selecting the “Solver Options” section in “Operation” Tab. Figure 4.34 shows the recommend values for the solver options. We have chosen these values based on our experience with running with model.

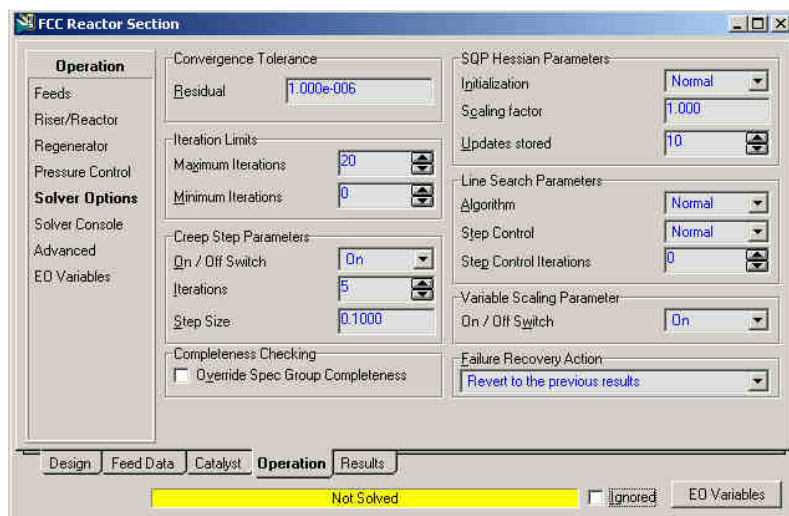


Figure 4.34: Solver convergence options

In general, we do not recommend modifying the constraints for the Residual, Hessian Parameters and Line search parameters. When running the model for the first time, we increase the number creep iterations and Maximum Iterations. Creep iterations refer to initial small changes in the process variables when the starting guesses are very poor (the Jacobian cannot indicate a direction that will decrease the residual). The maximum iterations refer to how times the solver will iterate though the model before exiting. Depending on process parameters, the initial solution may take up to 30-40 iterations.



Figure 4.35: Main application menu bar (activate solver)

We activate the solver by clicking on the green go button in the main application bar as shown in Figure 4.35. The solver output appears in the lower right hand corner of the PFD window.

We show the solver output for the configured model in Table 4.6. Column 1 of the table indicates the number of iterations performed since starting the solver. The residual convergence function indicates how far we are from satisfying the process model equations. When we run the model for the first time, residuals on the order of $1e7$ are expected. As we approach the solution, the residual drops to closer and closer to zero. Column 3 and Column 4 refer to the residual of the objective function. We use the objective function only during calibration, therefore it is zero for this model run. The solver used by Aspen HYSYS converges very quickly to solution once the changes in the process equations starting appearing to be linear. This is the case when we are in the vicinity of the solution. The solver indicates the vicinity of the solution through columns 5 and 6. The Worst model column indicates which part of the reformer model is furthest from the solution. This is useful for tracking down issues when the model fails to converge. The last lines of the output show several running statistics for the solver.

Table 4.6: Initial solver output

Iteration	Residual Convergence Function	Objective Convergence Function	Objective Function Value	Overall Nonlinearity Ratio	Model Nonlinearity Ratio	Worst Model
0	5.632D+07	0.000D+00	0.000D+00	9.952D-01	9.904D-01	RISER
	<Line Search Creep Mode ACTIVE> ==> Step taken 1.00D-01					
1	3.111D+07	0.000D+00	0.000D+00	7.542D-01	-7.747D+00	RXOUT
	<Line Search Creep Mode ACTIVE> ==> Step taken 1.00D-01					
2	1.360D+07	0.000D+00	0.000D+00	8.177D-01	-3.284D+00	RXOUT
	<Line Search Creep Mode ACTIVE> ==> Step taken 1.00D-01					
3	4.579D+06	0.000D+00	0.000D+00	3.163D-02	-3.811D+00	REGEN
	<Line Search Creep Mode ACTIVE> ==> Step taken 1.00D-01					
	<Line Search ACTIVE> ==> Step taken 5.16D-02					
4	1.774D+06	0.000D+00	0.000D+00	7.363D-01	-1.524D+00	RXOUT
	<Line Search Creep Mode ACTIVE> ==> Step taken 1.00D-01					
5	2.297D+06	0.000D+00	0.000D+00	-1.210D+00	-6.959D+01	RXADJ
	<Line Search ACTIVE> ==> Step taken 2.26D-01					
6	1.350D+07	0.000D+00	0.000D+00	-1.086D+02	-3.164D+02	REACTOR
	<Line Search ACTIVE> ==> Step taken 1.00D-01					
	<Line Search ACTIVE> ==> Step taken 1.00D-02					
7	3.563D+07	0.000D+00	0.000D+00	-4.966D+01	-1.844D+02	PRTCALC

```

      <Line Search ACTIVE> ==> Step taken 1.00D-01
      <Line Search ACTIVE> ==> Step taken 1.06D-02
      8      5.573D+06  0.000D+00  0.000D+00  -9.780D-01  -1.812D+02  PRTCALC
      <Line Search ACTIVE> ==> Step taken 2.53D-01
      9      4.781D+06  0.000D+00  0.000D+00   1.468D-01  -1.049D+01  PRTCALC
     10     2.857D+05  0.000D+00  0.000D+00   9.716D-01   9.429D-01  REGEN
     11     1.135D+03  0.000D+00  0.000D+00   9.895D-01   9.641D-01  REACTOR
     12     5.599D-03  0.000D+00  0.000D+00   9.999D-01   9.985D-01  RREXP
     13     1.990D-07  0.000D+00  0.000D+00

```

Successful solution.

Optimization Timing Statistics	Time	Percent
=====	=====	=====
MODEL computations	2.60 secs	46.85 %
DMO computations	2.45 secs	44.14 %
Miscellaneous	0.50 secs	9.01 %
-----	-----	-----
Total Optimization Time	5.55 secs	100.00 %

Problem converged

In general, the FCC model should converge with 20 seconds on recent computer hardware. If solution requires more than 20 seconds, it is likely that one or more specifications conflict.

4.10 Viewing model results

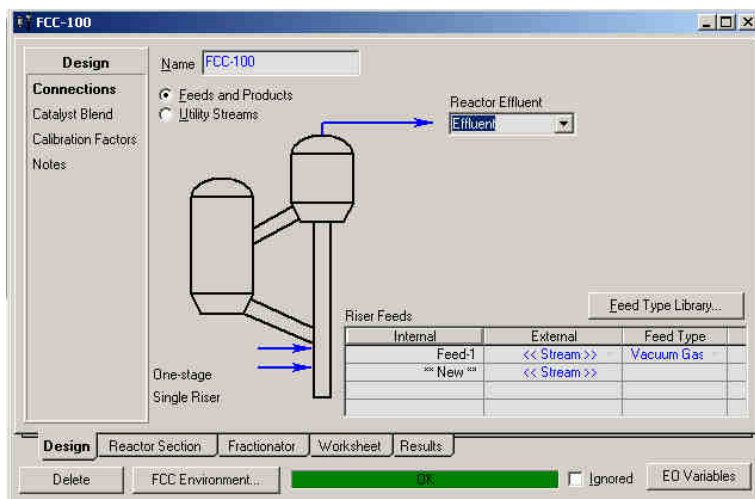


Figure 4.36: Add effluent stream to PFD

Figure 4.36 shows the converged FCC unit operation window after Aspen HYSYS has successfully solved the model. We connect an effluent stream by bringing up the “Connections” section of the Design Tab and typing in “Effluent” for the Reactor Effluent stream. A stream titled “Effluent” will appear on the PFD and we can use this stream to build further downstream fractionation units.

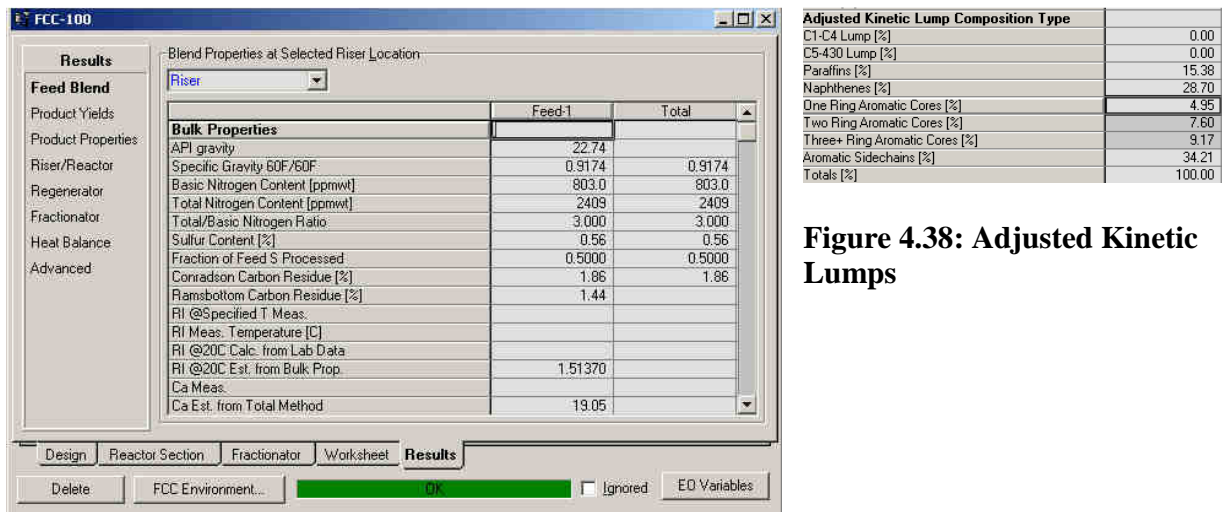


Figure 4.38: Adjusted Kinetic Lumps

Figure 4.37: Navigate FCC results

The “Results” Tab in Figure 4.37 summarizes various model results in different categories. The Feed Blend tab in Figure 4.37 shows the bulk property information and kinetic lumping for each feed entering the riser. An important check is the sum of the adjusted aromatic core compositions. In Figure 4.38, the sum of the adjusted aromatic cores is 21.7 wt%. This value should be close to the “Ca. Est. from Total Method” and measure the aromatic content of feed. If these values differ significantly (> 10 wt. %), especially the sum of the aromatic cores and measure aromatic content, we may have chosen a feed type that does not represent the actual feed to the unit accurately.

	Volume Flow [m3/h]	Mass Flow [kg/h]	Volume % [%]	Weight % [%]
H2S		324.9373		0.3003
Fuel Gas	5.8113	4888.5961	4.9167	4.5178
Propane	5.7620	2927.1075	4.8750	2.7051
Propylene	10.8288	5619.0847	9.1618	5.1928
nButane	3.1519	1841.3901	2.6666	1.7017
iButane	6.8962	3890.0056	5.8346	3.5949
Butenes	12.0926	7364.5025	10.2311	6.8059
Naphtha C5-430F	56.5722	43093.3405	47.8634	39.8244
LCD 430-650F	19.5841	17261.9092	16.5693	15.9525
Bottoms 650F+	13.7989	14837.5098	11.6747	13.7120
Coke Yield		6159.9498		5.6927
Total	128.6867	108208.3333	108.8764	100.0000
Conversion			71.7561	70.3355

Figure 4.39: Square cut product yields

We can view the overall product yields in “Product Yields” section. The yields shown in Figure 4.39 are square cut yields. Square cut yields refer to the fixed end points for each cut. For example, the Naphtha cut ranges from C5 to 430 F. This is often quite different from the plant cut. The end point of the plant naphtha cut is generally lower, therefore the square cut yield is often much higher than the plant yield. We will produce a true plant cut using rigorous fractionation in a subsequent workshop.

The screenshot shows the 'Results' window of the FCC-100 software. The window title is 'FCC-100'. On the left, there is a sidebar with categories: 'Results', 'Feed Blend', 'Product Yields', 'Product Properties', 'Riser/Reactor', 'Regenerator', 'Fractionator', 'Heat Balance', and 'Advanced'. The 'Product Properties' section is active, displaying a table with the following data:

	CS-265F	265-430F	430-650F	650F+
API Gravity	63.60	39.91	30.24	0.9185
Specific Gravity	0.7253	0.8255	0.8749	1.069
Sulfur [%]	0.04	0.12	0.57	0.92
RON	93.86	91.02		
MON	84.08	79.17		
(R+M)/2	88.97	85.10		
Paraffins [%]	33.93	19.95	9.49	4.40
Olefins [%]	49.86	17.01	0.00	0.00
Naphthenes [%]	9.47	6.96	11.50	4.80
Aromatics [%]	6.74	56.08	79.01	90.80
Cloud Point [C]			-18.79	
Concarbon [%]	0.01	0.05	0.10	0.35
Basic Nitrogen [ppmw]	3.816	14.62	107.8	212.8

At the bottom of the window, there are tabs for 'Design', 'Reactor Section', 'Fractionator', 'Worksheet', and 'Results'. Below the tabs are buttons for 'Delete', 'FCC Environment...', 'OK', 'Ignored', and 'EO Variables'.

Figure 4.40: Properties of square cut products

Figure 4.40 shows the “Product Properties” of each square cut from the model. Since the square cut yields not directly reflect plant yields, model results for each property may not exactly match plant values. We need rigorous fractionation to compare model results with plant measurements. In addition, we will likely improve the agreement of product properties when we calibrate the model in the next workshop.

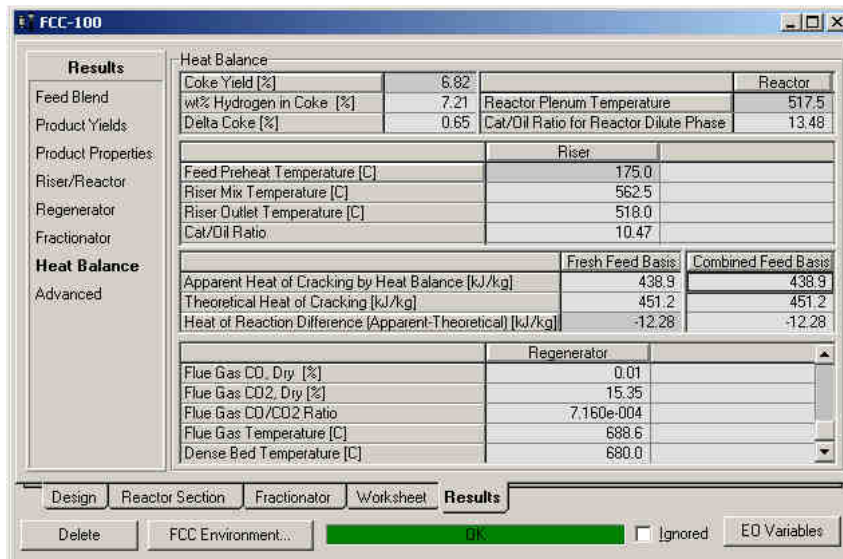


Figure 4.41: Overall heat balance between riser and regenerator

The last set of significant results is the “Heat Balance” section in Figure 4.41. The Heat balance shows the overall coke yield and delta coke for the process. In addition, the model also calculates the catalyst-to-oil ratio (Cat/Oil) and catalyst circulation rate. Aspen HYSYS uses the delta coke, catalyst circulation rate and kinetic lumps to calculate an Apparent Heat of Cracking. This value represents the combined heat release from all the cracking reactions. In addition, we can also calculate a theoretical heat of cracking with overall mass and heat balance constraints alone. In most cases, the apparent and theoretical heats of cracking should be quite similar (< 15% relative error). In Figure 4.41, the relative error is less than 3%. Agreement between the theoretical and apparent heats of cracking indicates that kinetic model does not violate thermodynamic constraints.

Once we verify that the model is making reasonable initial predictions, we can proceed to the calibration phase. In the calibration phase, we will adjust the tuning factors that come from the choice of feed and catalyst types.

4.11 Workshop II: Calibrating basic FCC model

In section, we will calibrate the model based on known product yield and reactor performance.

Calibration involves four distinct steps:

1. Pulling data from current simulation
2. Enter measured process yields and performance based on that current simulation
3. Update the activity factors to match this plant yield and performance
4. Push calibration data back to the simulation

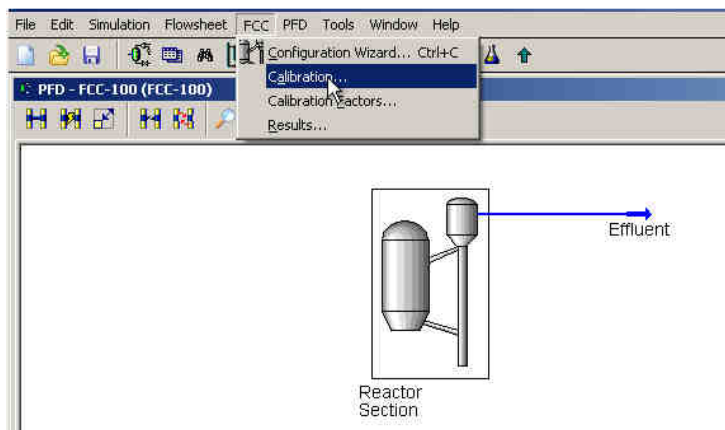


Figure 4.42: Entering FCC calibration environment

We begin the first step of model calibration procedure using a converged initial model. The converged initial model will provide initial guesses for the activity factors which greatly

simplifies the model calibration procedure. We enter the model calibration environment by first entering the FCC sub-flowsheet and then selecting the “FCC > Calibration” menu option from the application menu bar (as shown in Figure 4.42). Figure 4.43 shows the FCC calibration environment.

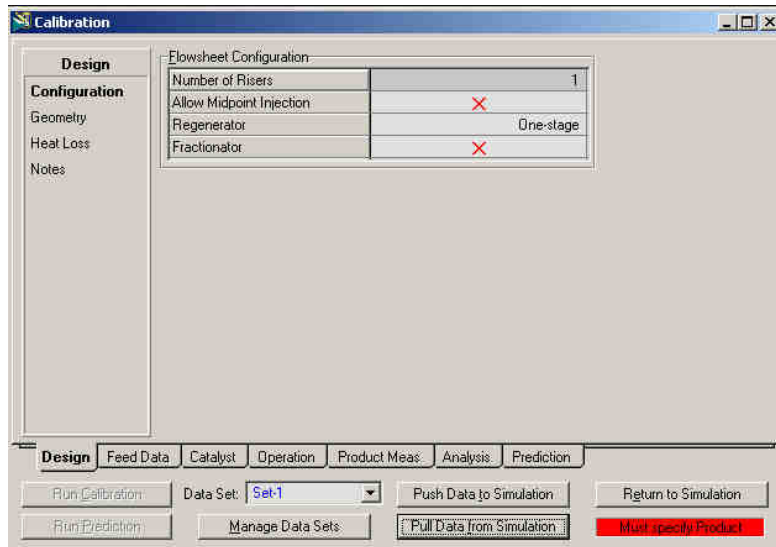


Figure 4.43: FCC calibration window

The first step is to “Pull data” from the simulation. When Aspen HYSYS pulls data, current operating conditions, feed stock information and process parameters enter the FCC environment. A Calibration refers to the set of the activity factors that produce a given product yield and reactor performance (which we provide to the calibration environment) based on current model state. We pull data by click on the “Pull Data from Simulation” button (Figure 4.44).

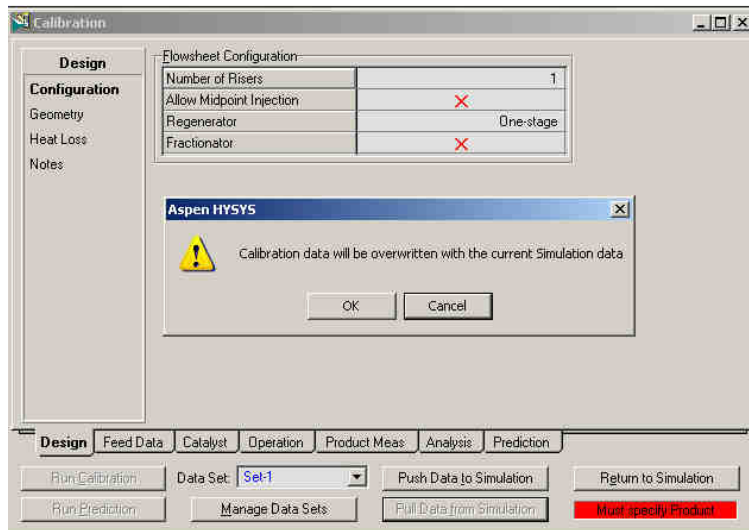


Figure 4.44: Pull current simulation data into calibration environment

When we pull data from the simulation, Aspen HYSYS will warn us that current calibration data will be overwritten by the current model results as shown in Figure 4.44. We can use the “Manage Data Sets” feature to allow multiple calibration data-sets. This may be useful if the industrial FCC unit runs under very different operating scenarios. However, for the purposes of this workshop, we will use only one calibration data-set.

Aspen HYSYS will pull all the feedstock information and process operating after we confirm the calibration data overwrite. The status bar now indicates that we must specify product measurements to begin the calibration process. If necessary, we can modify the operating variables (such as Riser Outlet temperature, etc.) of the FCC unit in addition to the measured values. However, we recommend creating a new model file if the operating scenarios are very different.

The second step in model calibration is specifying the measured yields and process performance. Click on the “Prod Meas.” Tab to bring up the Cuts interface (see Figure 4.45). In the Cuts interface, we can specify how many plant cuts of light gases, LPG, naphtha, light cycle oil (LCO) or diesel and bottoms this particular FCC unit has. FCC units typically have two light gas cuts: the dry gas (C1-C2) and the output from the desulfurization unit (H2S). The LPG (C3 – C4) stream typically leaves from the gasoline stabilizer. The remaining liquid cuts leave from the main fractionator unit. Depending on the type of the FCC unit, there may be two naphtha cuts (Light and Heavy) and two cycle oil cuts (LCO and HCO).

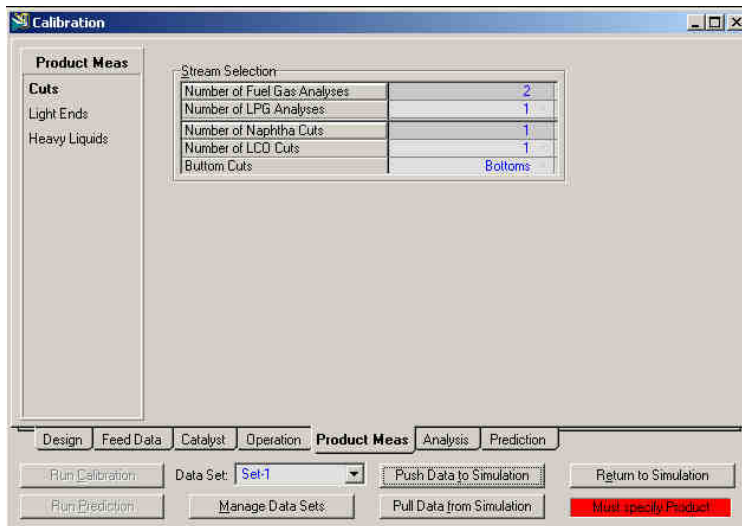


Figure 4.45: Specify cuts for plant measurement data

Once we select the number of cuts, we must enter the data from the light ends and the heavy liquids as shown in Figure 4.45. If the plant draws multiple light gas streams, we recommend using the same number of streams. Aspen HYSYS will automatically combine to light ends analysis to reconstruct the reactor effluent. We enter the data for Fuel Gas 1 (Dry Gas), Fuel Gas 2 (Sour Gas, H2S) and LPG 1 (Gasoline Stabilizer Overhead). Many times, the light ends

analysis for the Naphtha cuts may be missing. We recommend either using the nominal values given in Figure 4.46 or use correlations mentioned in Chapter 2 to estimate the butane content using the measured Reid Vapor Pressure (RVP) of the naphtha. In addition, we can also try to use a simple material balance around the gasoline stabilizer to estimate the C4 composition of the naphtha cut. However, we note that if we use any estimation method for the C4 content during calibration, the model will likely produce poor predictions for Gasoline RVP and overhead temperatures for the gasoline stabilizer column.

Light Ends	Fuel Gas 1	Fuel Gas 2	LPG 1	Naphtha
Gas Rate [STD_m3/h]	5781.75	425.915	<empty>	<empty>
Liquid Rate [m3/h]	<empty>	<empty>	35.6917	<empty>
Mass Rate [kg/h]	4833.00	667.000	19542.0	<empty>
Composition	Mole %	Mole %	Volume %	Volume %
N2 [%]	22.4600	0.600000	0.000000	0.000000
O2 [%]	0.000000	0.000000	0.000000	0.000000
CO [%]	1.73500	0.000000	0.000000	0.000000
CO2 [%]	1.78500	30.5000	0.000000	0.000000
H2S [%]	0.000000	68.5000	0.000000	0.000000
H2 [%]	25.5050	0.000000	0.000000	0.000000
C1 [%]	23.3300	0.200000	0.000000	0.000000
C2 [%]	11.2250	0.200000	1.00000e-002	0.000000
C2= [%]	11.2600	0.000000	0.000000	0.000000
C3 [%]	0.250000	0.000000	13.5450	0.000000
C3= [%]	1.01000	0.000000	-41.5100	0.000000
nC4 [%]	0.235000	0.000000	4.67500	-0.140000
iC4 [%]	0.440000	0.000000	18.0250	0.350000
iC4= [%]	0.380000	0.000000	12.4950	4.00000e-002

Figure 4.46: Measured light gas yield and composition

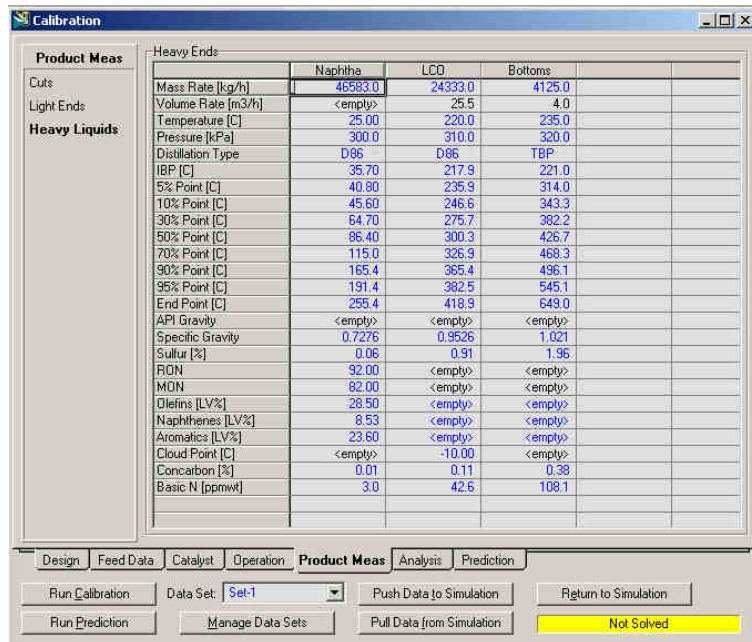


Figure 4.47: Measure liquid product yield and properties

Figure 4.47 shows the entry window for the Heavy Liquid section of the Prod Meas. Tab. The measures required for the Naphtha and LCO cuts are routine measurement data. The distillation curve, density, concarbon, sulfur content and nitrogen content are required for all the heavy liquid cuts. In addition, the Olefins, Naphthenes and Aromatics content are required for at least one of the cuts. In addition, we must also enter Cloud Point for all LCO type cuts. In most cases, we cannot obtain the distillation curve of the bottoms cut (Routinely not measured or only partial measurement available). Kaes¹ provides a simple correlation to estimate the TBP curve of a bottoms cut as a function of density only. In general, we do not require accurate values for the TBP curve of the bottoms since it is typically not a significant product.

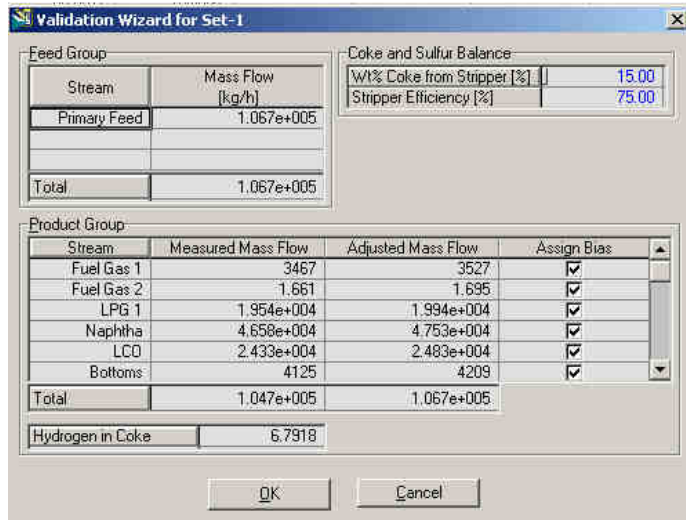


Figure 4.48: Mass balance validation wizard

Once we finish entering the heavy liquids product measurements in Figure 4.47, the status button of the calibration will turn yellow and indicate that the model is “Not Solved”. At this point, we begin step 3 of the calibration process.

We click “Run Calibration” to bring up the Validation Wizard as shown in Figure 4.48. The Validation Wizard allows us to assign biases to each measured flow rate since the sum of the all flow measurements typically does not match completely the feed flow rate. The bias allows us to slightly adjust the measured flow rates to ensure an overall material balance. If the adjustments due to the biases are small, we do not recommend removing biases from any product measurements. However, if the adjustments are significant, we should go back and check if all product flow rates and measurements are accurate. Lastly, we also note that mass flow rates for the Fuel Gas cuts are much smaller than the values we entered in Light Ends section. This is because inorganic compounds (H₂, N₂, O₂, CO₂, H₂S, etc.) are not included in the overall

material balance. We begin calibration by clicking “OK” in the Validation Wizards. Table 4.7 shows the progress of the solver during the calibration run.

Table 4.7: Solver output during calibration run

Iteration	Residual Convergence Function	Objective Convergence Function	Objective Function Value	Overall Nonlinearity Ratio	Model Nonlinearity Ratio	Worst Model
0	5.429D+03	0.000D+00	0.000D+00	4.353D-01	-1.360D+01	REACTOR
	<Line Search Creep Mode ACTIVE> ==> Step taken 1.00D-01					
1	4.399D+03	0.000D+00	0.000D+00	9.921D-01	-7.499D+00	RXMIX
	<Line Search Creep Mode ACTIVE> ==> Step taken 1.00D-01					
2	3.565D+03	0.000D+00	0.000D+00	9.930D-01	-3.092D+00	RXMIX
	<Line Search Creep Mode ACTIVE> ==> Step taken 1.00D-01					
3	2.889D+03	0.000D+00	0.000D+00	9.936D-01	-1.615D+00	RXMIX
	<Line Search Creep Mode ACTIVE> ==> Step taken 1.00D-01					
4	2.341D+03	0.000D+00	0.000D+00	9.940D-01	-8.735D-01	RXMIX
	<Line Search Creep Mode ACTIVE> ==> Step taken 1.00D-01					
5	1.897D+03	0.000D+00	0.000D+00	9.222D-01	-3.700D+03	RXMIX
6	6.096D+01	0.000D+00	0.000D+00	9.665D-01	4.983D-01	RXMIX
7	1.628D-02	0.000D+00	0.000D+00	9.934D-01	6.650D-01	REGEN
8	4.462D-06	0.000D+00	0.000D+00	9.999D-01	9.999D-01	REACTOR
9	3.776D-10	0.000D+00	0.000D+00			

Successful solution.

Optimization Timing Statistics	Time	Percent
=====	=====	=====
MODEL computations	2.23 secs	41.14 %
DMO computations	2.77 secs	51.11 %
Miscellaneous	0.42 secs	7.75 %
-----	-----	-----
Total Optimization Time	5.42 secs	100.00 %

Problem converged

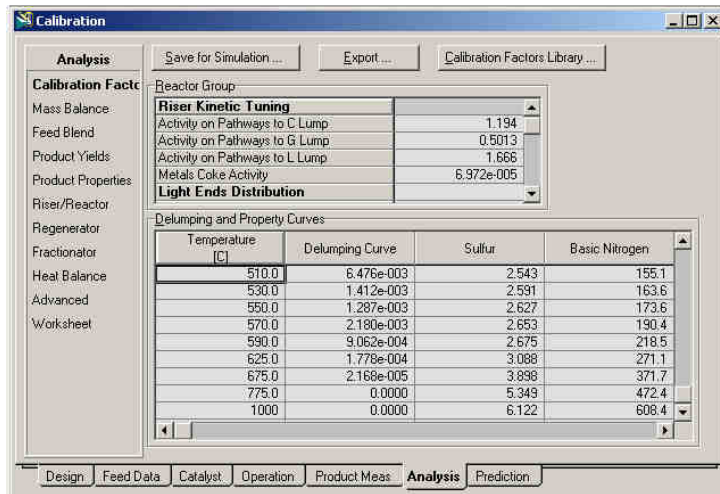


Figure 4.49: Calibrated activity factors

The calibration process for the FCC is “square”. This implies that there are no user adjustable tuning factors unlike the Aspen HYSYS Reformer or Hydrocracking models. In the other words, the number of tuning parameters equals the number of available measurements and the calibration is much simpler root-finding exercise. In general, the calibration process is quick and converges within 20 iterations. If there is difficulty during calibration, it is mostly likely due to inconsistent product measurements.

Figure 4.49 shows the key results of the calibration procedure. The Reactor group tuning parameters control the activity of each group of kinetic pathways and the light ends distribution. The delumping curves convert the kinetic lumps into fractionation lumps appropriate for a petroleum refining component slate. An important check of the calibration appears in Figure 4.50. The theoretical and apparent heat of cracking should not be significantly different (< 5 % relative error). If we meet this error threshold, we conclude that the calibration procedure is successful.

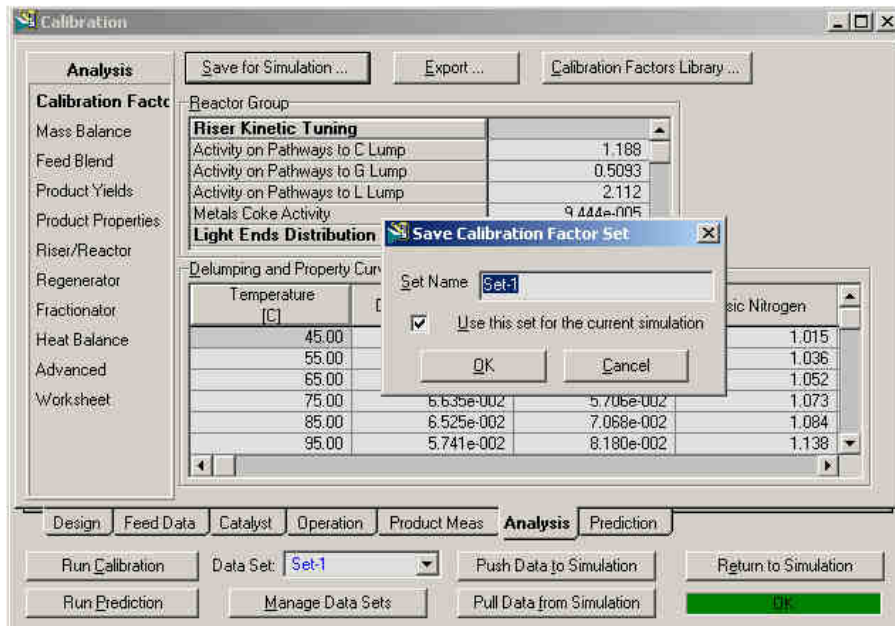


Figure 4.51: Save calibration factors for current calibration

To return back the FCC unit PFD environment, we click on “Push Data to Simulation” to return the calibration factors back to the main environment as shown in Figure 4.52. Aspen HYSYS may prompt to hold solver when returning to the main environment. Since the FCC unit solves very quickly, we can choose “No” and force the solver to run when we return the main environment.

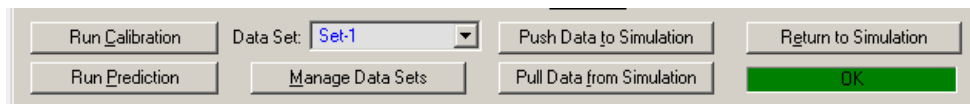


Figure 4.52: Return calibration factors to main FCC environment

This completes the calibration workshop for the FCC unit. At this point we can perform case studies and build additional downstream fractionation units. In the next workshop, we will

briefly go through some of the issues involved in building a complete downstream fractionation process for this FCC Unit.

4.12 Workshop III: Build main fractionator and gas plant system

The effluent from the FCC unit is a broad mixture of light gases and liquid products that will be recovered as LPG, Gasoline and Diesel (Light and Heavy Cycle Oil). The downstream fractionation units separate the reactor effluent into the product cut through a series of distillation and absorption columns. The main components of the downstream fractionation are:

- Main Fractionator Column – Recovers most naphtha, cycle oil and bottoms product
- Overhead wet gas system – Recompresses main fractionator overhead gas product to recover additional naphtha
- Primary Absorber Column – Returns light naphtha to the gasoline stream
- Primary Stripper Column – Removes heavy components from naphtha and returns these components to the diesel or LCO section of the main fractionator
- Sponge Oil Absorber Column – Uses an LCO draw to remove very light components (<C₂) from the primary absorber overhead vapor
- Debutanizer/Gasoline Stabilization Column – Separates LPG (C₃-C₄) from product gasoline stream.

For this workshop, we will describe the main fractionator. The remainder of fractionation section is quite similar to other units in the refinery and may be simulated quite easily using standard Aspen HYSYS unit operations. Although we only describe the main fractionation in this section, a complete fractionation model (including the gas plant) is available in the examples that accompany this text.

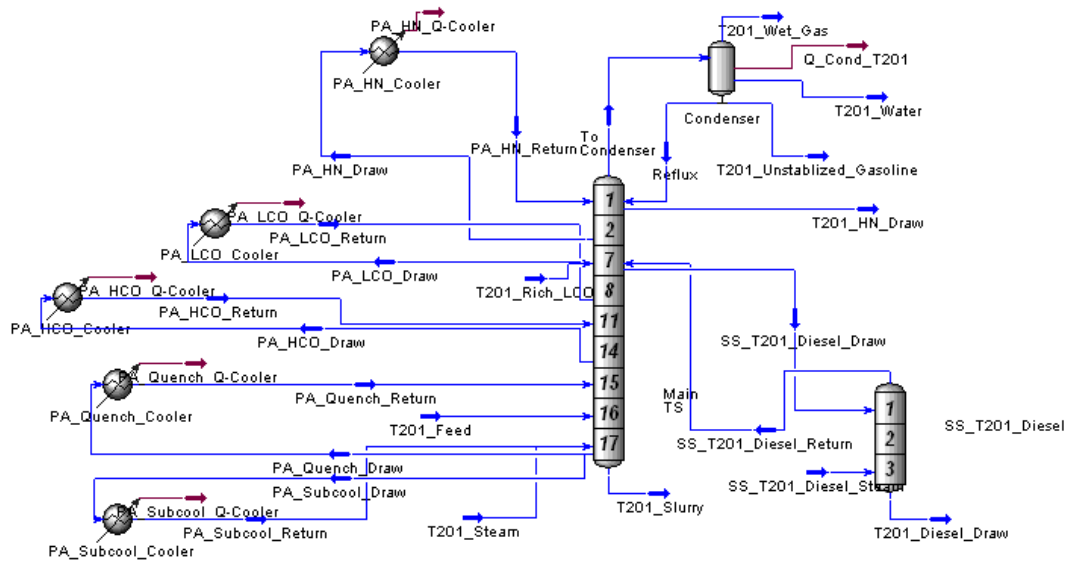


Figure 4.53: Aspen HYSYS configuration for the main fractionator

Figure 4.53 shows the unit and stream configuration for the main fractionator in Aspen HYSYS.

To build the main fractionator, we follow the same procedure as a crude distillation tower described in an earlier chapter:

1. Create a refluxed absorber using the standard Aspen HYSYS unit operation palette and specify the overhead vapor-liquid (hydrocarbon and water decant) draws and bottoms residue stream. We show the number of stages and draw and feed locations in Figure 4.53.
2. Specify the pressure profile and initial temperature estimates (Figure 4.54)
3. Connect the FCC effluent (T201_Feed) and primary steam feed to the unit (T201_Steam)
4. Solve the column to obtain an initial temperature profile.
5. Create a side draw for the heavy naphtha stream (T201_HN_Draw) and specify its draw rate.

6. Run the column to update the temperature profile.
7. Add the diesel side stripper (SS_T201_Diesel) along with the side stripper steam flow (SS_T201_Diesel_Steam) and specify the draw rate of T201_Diesel_Draw.
8. Solve the column to update the temperature profile.
9. Create a new stream T201_Rich_LCO to represent return from sponge or LCO oil absorber. Set this new stream to same composition as the diesel draw and fix the mass flow rate at 5% of the diesel draw. Connect this steam to the return stage of the diesel side stripper.
10. Solve the column to update the temperature profile.
11. Add each pumparound cooler sequentially with specifications of pumparound flow rate and temperature change. Solve the column after adding each pumparound. Figure 4.55 shows the results of a converged model.

Once we solve the column using the following procedure, we use alternative specifications to allow more flexibility in the column model. This is especially the case when the flowrate to the column changes significantly. Table 4.8 lists possible replacements for the original specifications.

Table 4.8: Valid specifications for main fractionator

Original specification	Flexible specification
Overhead liquid draw rate	Condenser Temperature
Heavy Naphtha draw rate	Heavy Naphtha 95% D86 Cut Point
Pumparound temperature change	Pumparound duty (loose specification) Pumparound return temperature (tight specification)

Diesel draw rate	Diesel 95% D86 Cut Point
Bottoms draw rate	Top stage temperature or flash stage temperature

The standard Inside-Out algorithm can solve the main fractionator with ease when we follow the procedure mentioned above. However, flat distillation cuts or very tight specifications may not allow the standard method to converge robustly. We suggest the following changes to improve convergence behavior in Aspen HYSYS:

1. Use the modified Inside-Out method with adaptive damping (see Figure 4.56). The modified method deals much better with tight product specifications.
2. Decrease the tolerance for Heat/Spec error. This method can significantly improve convergence when reconciling the recycle loops in the overall fraction model.

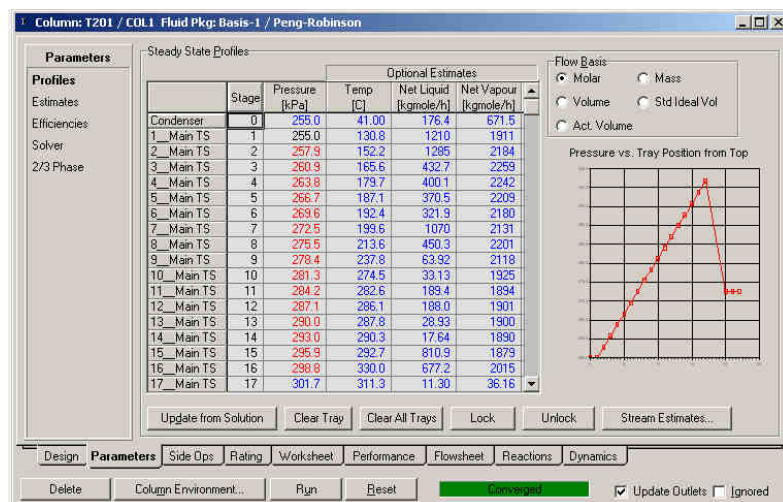


Figure 4.54: Pressure profile and temperature estimates

yield-related case studies. An important consideration during FCC operation is to improve the yield of a particular key component. Since the FCC unit is a large producer of a gasoline, we generally want to maximize the throughput and conversion of feed to gasoline. In the previous chapter regarding FCC modeling and kinetics, we extensively discussed how changes in feed rate and operating temperatures can affect the yield of the unit. We will perform two case studies using Aspen HYSYS that illustrate the effects of feed and riser temperature in practice.

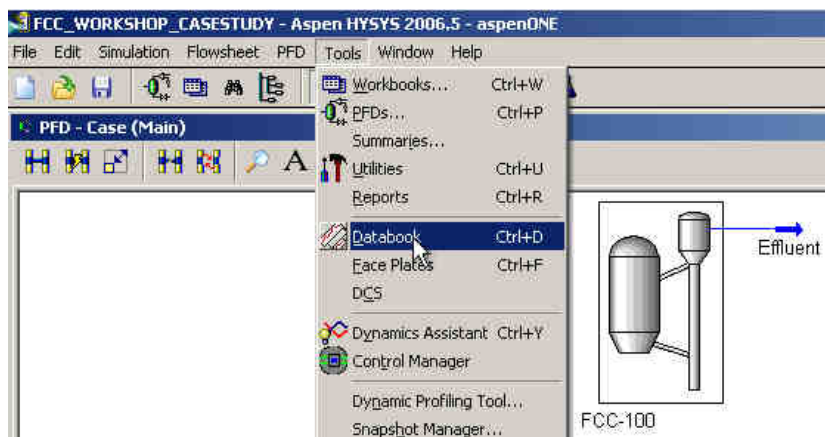


Figure 4.57: Initialize Databook from Aspen HYSYS menu

We begin by creating the case study using the Databook feature of Aspen HYSYS. Figure 4.57 show the menu option from main flowsheet interface. The Databook interface is organized Variables, Process Charts and Case studies. We must first add the variables we to observe or change into the Variables Tab. To add a variable, click 'Insert' to bring up the Variable Navigator. The Variable Navigator appears as shown in Figure 4.58.

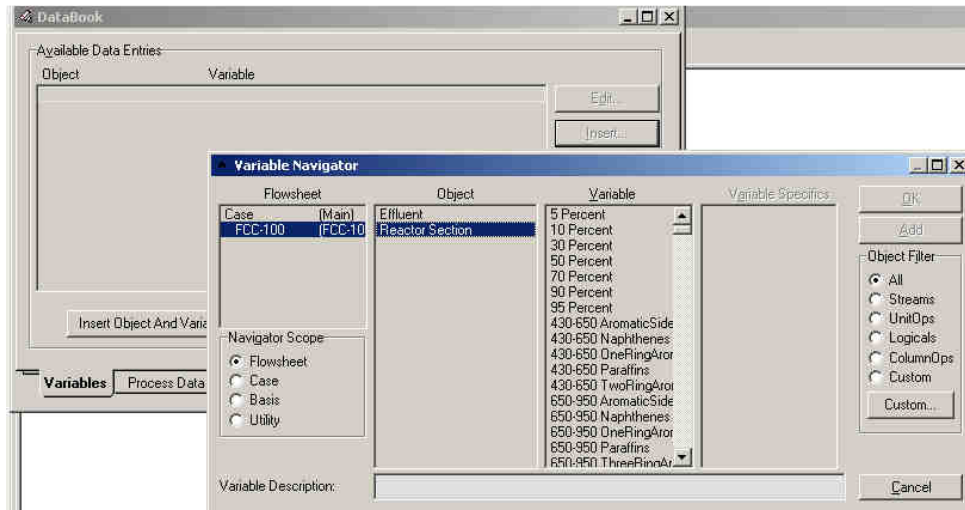


Figure 4.58: Aspen HYSYS Variable Navigator

The Variable Navigator allows us to add variables and parameters from a given unit operation for observation during the case study. In this case study, we want to study the effect of feed rate and riser outlet temperature (ROT) on the overall conversion and yield distribution of products from the FCC. Since, we are only focused on the yield, we use the square cuts from the model directly. It is possible to perform the same case study on the basis of plant cuts. In that case, we would add a simple component splitter to separate the reactor effluent on the basis of initial and end points of the cuts. However, for this example we will use square cuts exclusively.

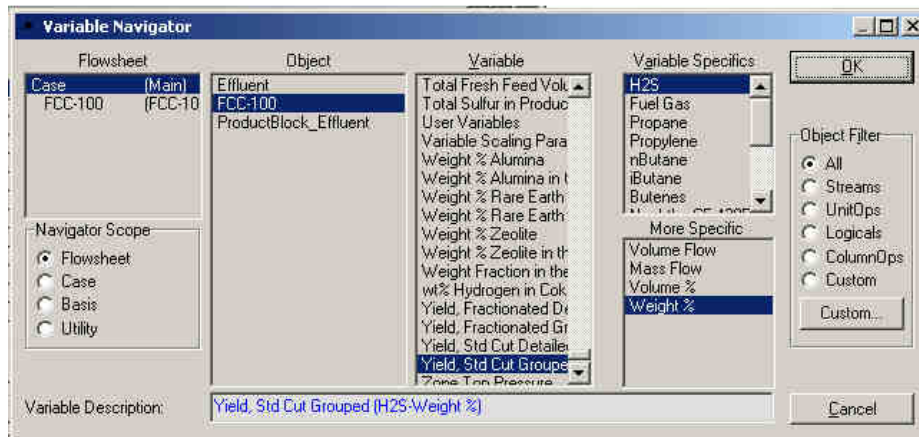


Figure 4.59: Variable navigator for FCC unit parameters and conditions

Figure 4.59 shows how we can access the variables and operating parameters for the FCC unit operation. Using the Variable Specifics list, we add all square yields and the total conversion. Once we select a variable in the Variables Specifics list, we click “OK” to insert the variable into the case study. We repeat this process until we add all variables. Figure 4.60 shows list of all variables involved in the case study. The next step is to create a case study using the “Case Studies” tab.

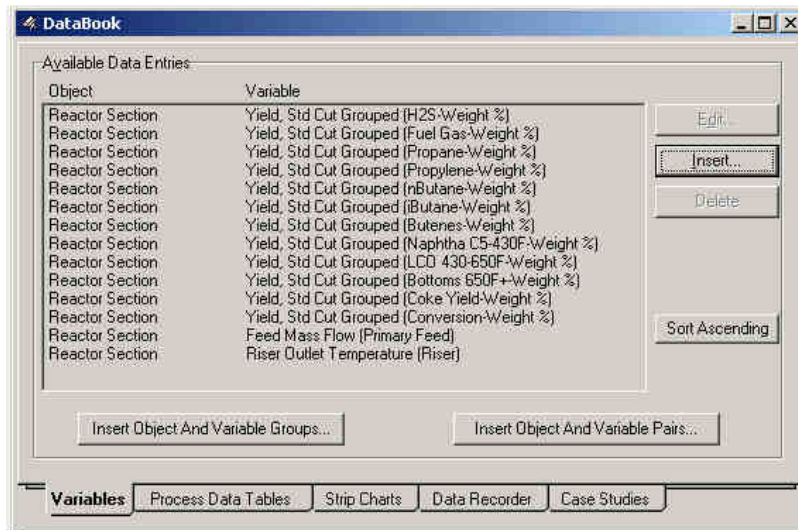


Figure 4.60: Add variables to databook

We click “Add” in the Case Studies Tab to create new case study “Case Study 1” as shown in Figure 4.61. Once we create the case study, we must select the variables that we will change in the course of the case study (Independent variables) and variables we want to observe (Dependent variables). In general, it is not possible to set product yields as independent variables. Aspen HYSYS issues an error if we cannot set a particular variable’s type as independent. For the first case study, the only independent variable is the Feed Flow rate.

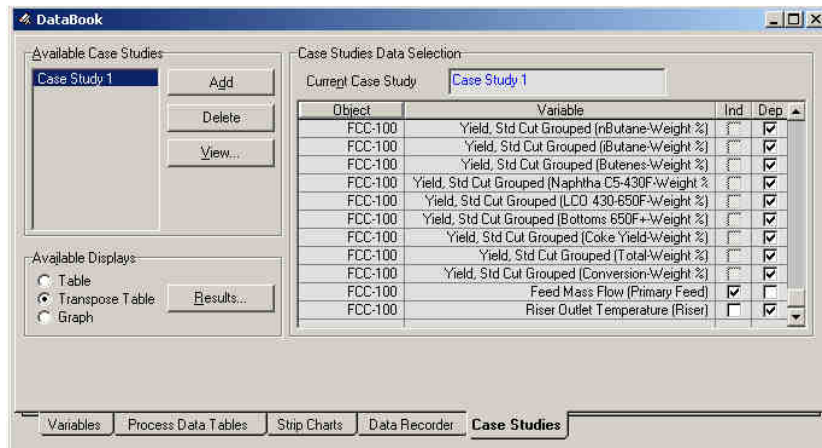


Figure 4.61: Select dependent and independent variables for case studies

After we create the case study, we must specify the upper and lower bounds for the manipulated (independent) variables. We will vary with the feed flow rate from 90 tons/hr. to 115 tons/hr. with a 2.0 tons/hr step size as show in Figure 4.62. We also select the ‘Step Downward’ option. This option means that the case study will start at the High or Upper bound and go towards the Low Bound. We have chosen this method because the FCC model converges very quickly at higher flowrates. However, the results will be the same as even if we do not choose the “Step Downward” option.

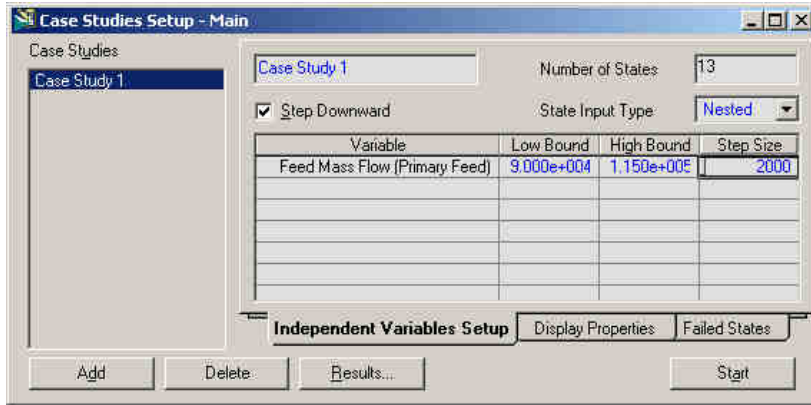


Figure 4.62: Case study setup for feed rate change

We run the case study by clicking “Start”. At this point, the lower right corner window of the PFD will indicate that the solver runs multiple times. If the solver fails for an intermediate step in the case study, we recommend increasing the number of creep and total iterations in the Solver Options Window. Once the case study is complete, we can click on the “Results” button to view the results of the case study.

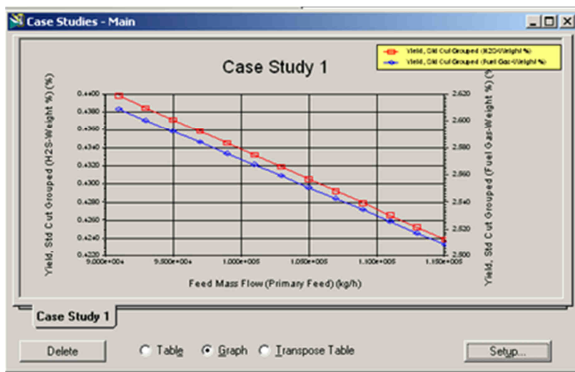


Figure 4.63: Graphical results from case study

State	Mass Flow (Primary Feed) (g/h)	H2S Cut Grouped (%)	Fuel Gas Cut Grouped (%)	Propane Cut Grouped (%)
State 1	1.150e+005	0.42	2.51	2.35
State 2	1.130e+005	0.43	2.52	2.36
State 3	1.110e+005	0.43	2.53	2.36
State 4	1.090e+005	0.43	2.53	2.37
State 5	1.070e+005	0.43	2.54	2.38
State 6	1.050e+005	0.43	2.55	2.39
State 7	1.030e+005	0.43	2.56	2.40
State 8	1.010e+005	0.43	2.57	2.40
State 9	9.900e+004	0.43	2.58	2.41
State 10	9.700e+004	0.44	2.58	2.42
State 11	9.500e+004	0.44	2.59	2.43
State 12	9.300e+004	0.44	2.60	2.43
State 13	9.100e+004	0.44	2.61	2.44

Figure 4.64: Tabular results from case study

The results of the case study initially appear as a graph (see Figure 4.63). The lines represent the values of the first two dependent variables as a function of the feed mass flow rate. We can alternatively view in the results in a tabular form by selecting ‘Transpose Table’ option as show in Figure 4.64.

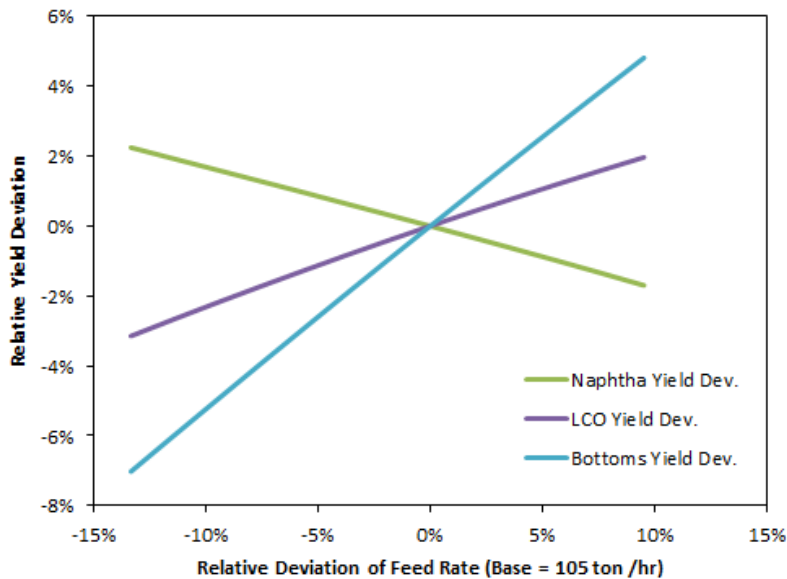


Figure 4.65: Effect of feed rate change on product yield change

We summarize the results of the case study (at a riser outlet temperature of 510 °C) in Figure 4.65. As the feed rate increases to the unit, we note that there is a significant loss in the naphtha square cut yield. In addition, both the LCO and Bottoms yield increase significantly. We discuss the reason for loss of naphtha yield extensively in the previous chapter. The loss is essentially a result of low residence time in the riser which prevents catalytic cracking of the feed. In fact, most of the bottoms product can likely be recovered as LCO at a lower feed rate. So, if we are trying to increase the throughput of the unit, we must also increase the cracking temperature to

account for the lowered residence time. We will study an increase in cracking temperature in the next case study.

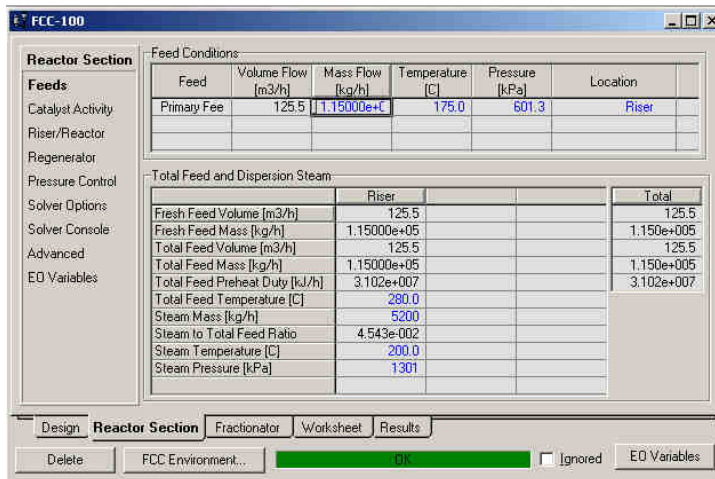


Figure 4.66: Increase feed flow rate for riser outlet temperature case study

To study the effect of riser temperature at higher unit throughput, we must create a case where will vary the riser outlet temperature. First, we increase the feed flow rate to the unit Reactor Section of the FCC unit operation window. For this example, we set the feed flow rate to 115 tons/hr as shown in Figure 4.66 and solve the model. If the model does not converge, we can increase the number of creep and total iterations in the Solve Options Section.

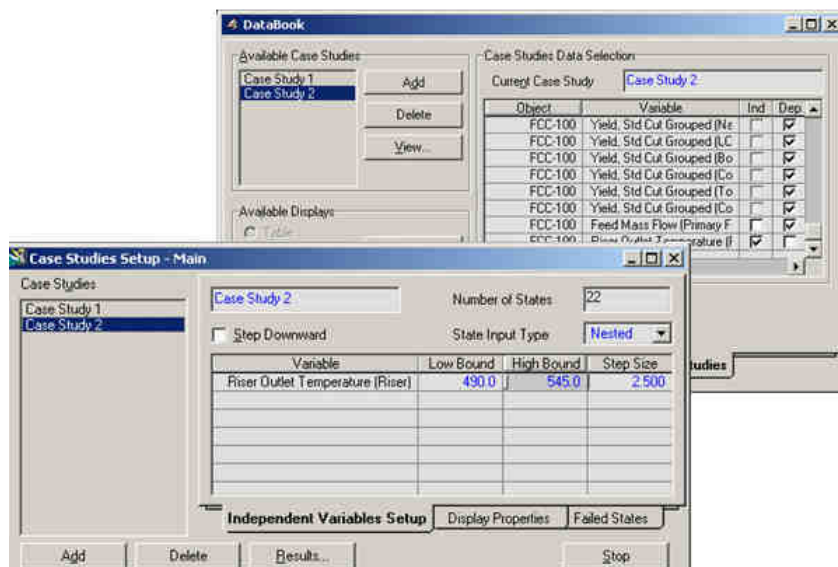


Figure 4.67: Case study setup for riser outlet temperature

We return to the DataBook through the main application menu and bring up the Case Studies Tab again. We add another case study ‘Case Study 2’ using the same procedure as earlier. This time we set the feed mass flow rate as a dependent variable and set the Riser outlet temperature (ROT) as the independent variable. We specify the range for the ROT as 480 °C – 545 °C with a step size of 2.5 °C. The model tends to have difficulty converging at higher temperatures so we start from the Low bound and move to High bound. Consequently, we do not select the Step Downward option in Figure 4.67. The results of the case study appear in Figure 4.68 and Figure 4.69. We summarize the results of the case study in Figure 4.70.

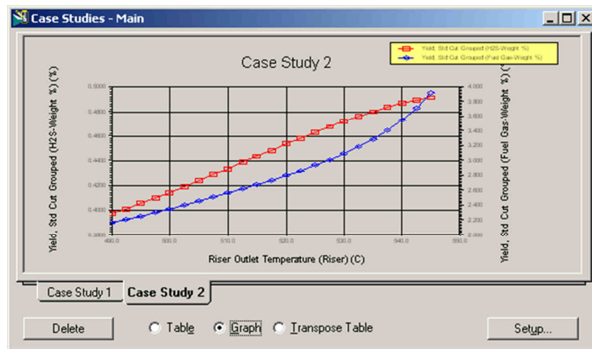


Figure 4.68: Graphical results from case study

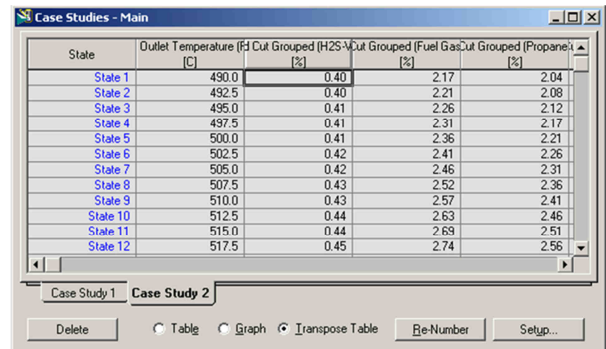


Figure 4.69: Tabular results from case study

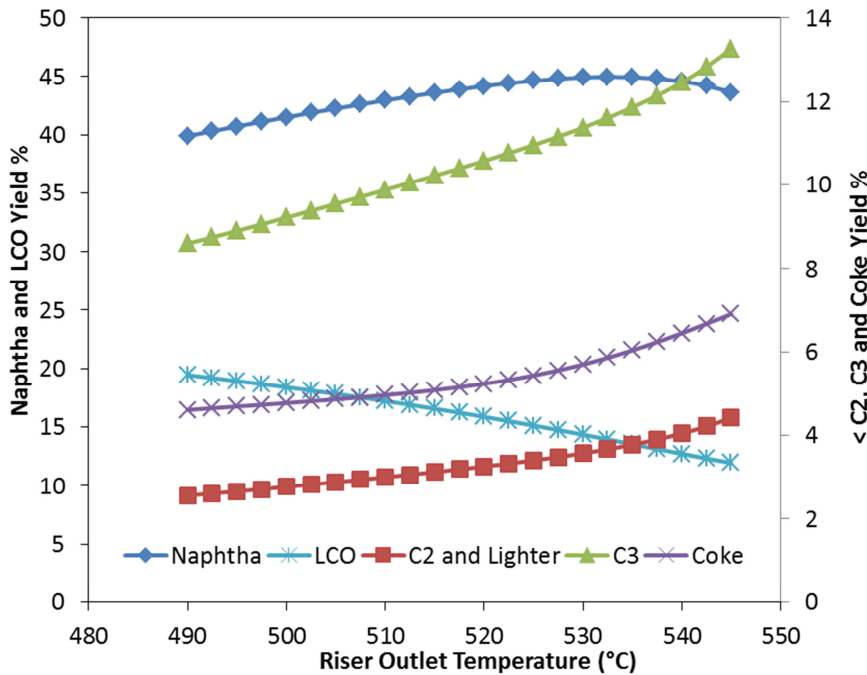


Figure 4.70: Product yield as a function of riser outlet temperature

Figure 4.70 shows as we increase the riser outlet temperature, the yield of naphtha also increases until we reach about 532 °C. At this point the naphtha yield drops and we have a dramatic increase in the production of light gases and coke. In addition, there is also a significant decrease in the LCO yield. All of these trends are a result of the naphtha “overcracking” curve. We

discussed this phenomenon extensively in the preceding chapter. Gasoline “overcracking” is a result of excessive thermal cracking and catalyst activation. Thermal cracking tends to produce many light compounds (C1 – C4). This explains the increase in C2, C3 yields. In addition, Coke yield increases because of increased coke deposits in the riser and subsequent catalyst deactivation. The lack of catalytic cracking activity explains the loss in LCO yield (since most of the feed that could have been cracked to LCO is now cracked directly in light gases). Figure 4.70 in conjunction with case study can help identify operating scenarios (flowrate and temperatures) to increase yield or shift product distribution slate from the FCC Unit.

4.14 Workshop V: Generate DELTA-BASE vectors for linear programming (LP) based planning

An important application of the calibrated model is the generation of LP DELTA-BASE vectors for refinery planning. The DELTA-BASE vectors essentially represent a linearized model of FCC unit as a function of a several key variables. We have extensively discussed linear models in a previous chapter. In this workshop, we will demonstrate how to generate LP DELTA-BASE vectors for the calibrated FCC for use with a specific planning software, Aspen PIMS.

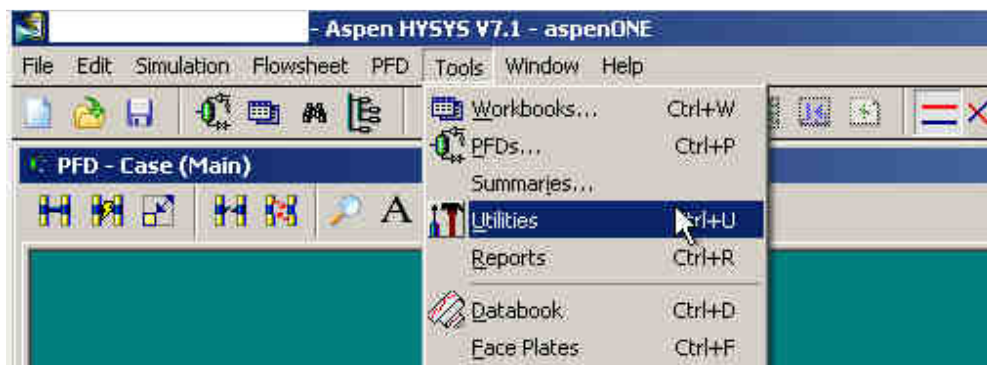


Figure 4.71: Creating the DELTA-BASE utility from main application menu bar

We can attempt to linearize the model by identifying key operating parameters and manually running the model for each chosen operating parameter. However, Aspen HYSYS provides a utility to automate this process. We can access the utility by going to the Tools > Utilities in main application menu as shown in Figure 4.71.

Once we select the Utilities menu entry, Aspen HYSYS shows a list of available utilities. There are many types of utilities available to modify different aspects of the model. To generate DELTA-BASE vectors, we must choose the appropriate utility. In recent versions of Aspen HYSYS, this utility is called the “Common Model Utility” as shown in Figure 4.72. Figure 4.73 shows “Delta Base Utility” used in older versions. Both versions are equivalent for the purposes of this workshop. We select either utility and click Add Utility.

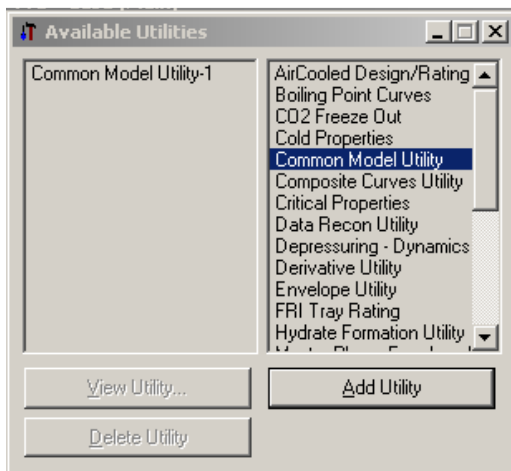


Figure 4.72: Common Model Utility

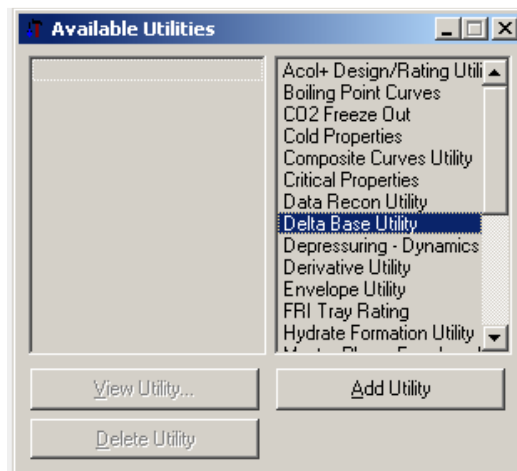


Figure 4.73: Delta Base Utility

Figure 4.74 shows the Delta Base Utility configuration window. We must first identify the scope of the Delta-Base Utility. The scope refers to flowsheet objects we will modify during the course of the study. We choose the entire FCC unit as the scope of the utility as shown in Figure 4.75.

To use the Delta Base utility, we must first choose independent and dependent variables. The independent variables refer to model drivers or key operating parameters that control the yield of the unit. In the case of the FCC unit, the key operations parameters are feed specific gravity, concarbon and sulfur content.

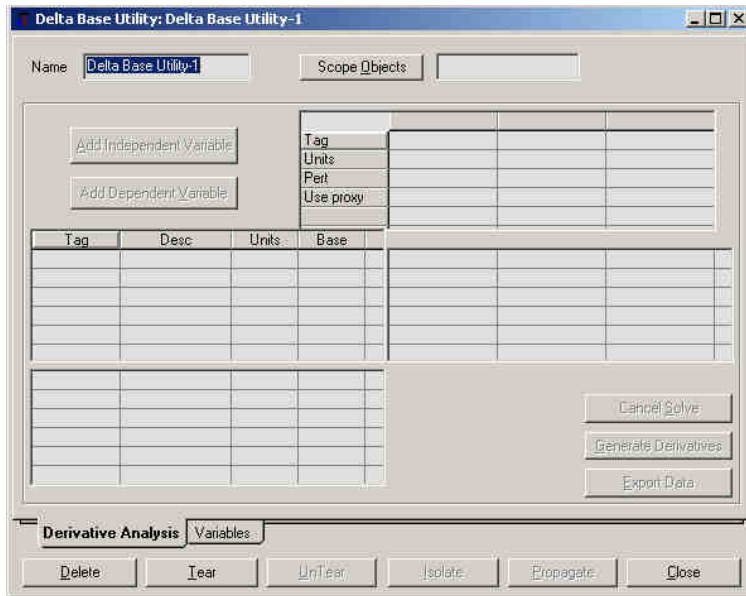


Figure 4.74: Delta-Base Utility Configuration window

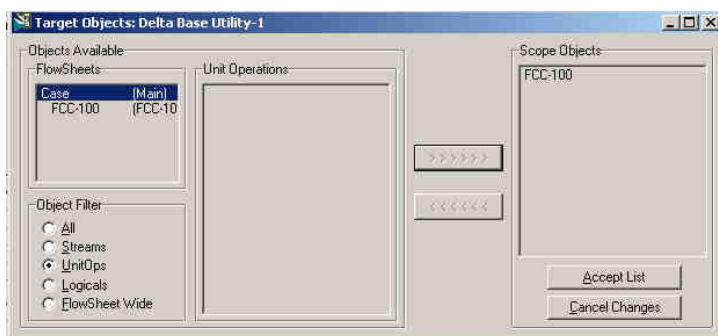


Figure 4.75: Scope of Delta-Base utility

We add independent variables by clicking on the “Add Independent variables” button on the configuration window. The Variable Navigator (used in earlier workshops) appears and we select the following variables:

- FCC – 100 > Reactor Section > Feed Specific Gravity > Feed – 1
- FCC – 100 > Reactor Section > Feed Conradson Carbon > Feed – 1
- FCC – 100 > Reactor Section > Feed Sulfur Content > Feed – 1

Figure 4.76 shows how we can add the specific gravity to the independent variables. We repeat this process for the other independent variables. A description of each variable added appears in the “Desc.” section.

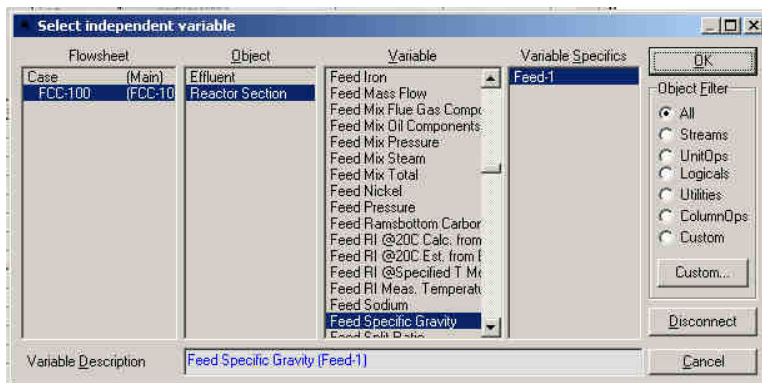


Figure 4.76: Adding specific gravity as an independent variable

After adding all the independent variables (Figure 4.77), we must add the dependent variables. The dependent variables in the case of refinery planning almost always refer to the yields of the key products from the FCC unit. In this workshop we use the square cut yields of the products. However, if we wish to use plant cut yields, we can use a simple component splitter to remap the product effluent from the FCC unit plant cuts based on a TBP cut points.

- Case > FCC-100 > Yield, Std. Cut. Grouped > H2S
- Case > FCC-100 > Yield, Std. Cut. Grouped > Fuel Gas
- Case > FCC-100 > Yield, Std. Cut. Grouped > Propane
- Case > FCC-100 > Yield, Std. Cut. Grouped > Propylene
- Case > FCC-100 > Yield, Std. Cut. Grouped > nButane
- Case > FCC-100 > Yield, Std. Cut. Grouped > iButane
- Case > FCC-100 > Yield, Std. Cut. Grouped > Butenes
- Case > FCC-100 > Yield, Std. Cut. Grouped > Naphtha C5-430F
- Case > FCC-100 > Yield, Std. Cut. Grouped > LCO 430F – 650 F
- Case > FCC-100 > Yield, Std. Cut. Grouped > Bottoms 650+ F
- Case > FCC-100 > Yield, Std. Cut. Grouped > Coke

Once we have added all the variables the Delta-Base utility window appears as shown in Figure 4.78.

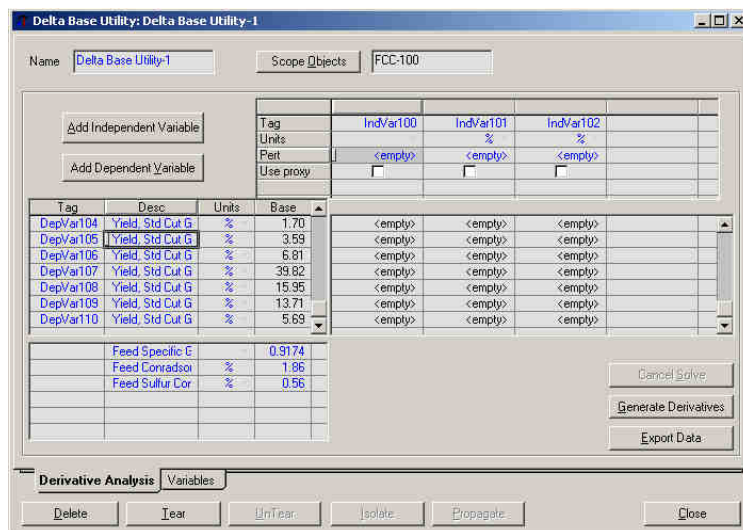


Figure 4.79: All dependent variables added to Delta-Base Utility

The next step is to choose a perturbation amount for each variable. Since the Delta Base Utility generates a linearized model of the FCC unit, we must choose the range over which we want linearize the model. We have discussed this issue significantly in Chapter 2. For this workshop, we will perturb each independent variable by 10% of its original base value as show in Figure 4.80. We can click “Generate Derivatives” to begin running the model.

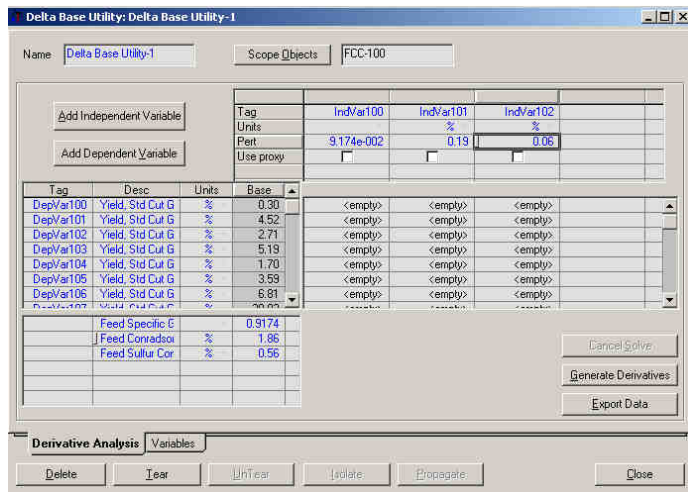


Figure 4.80: Perturb independent variables

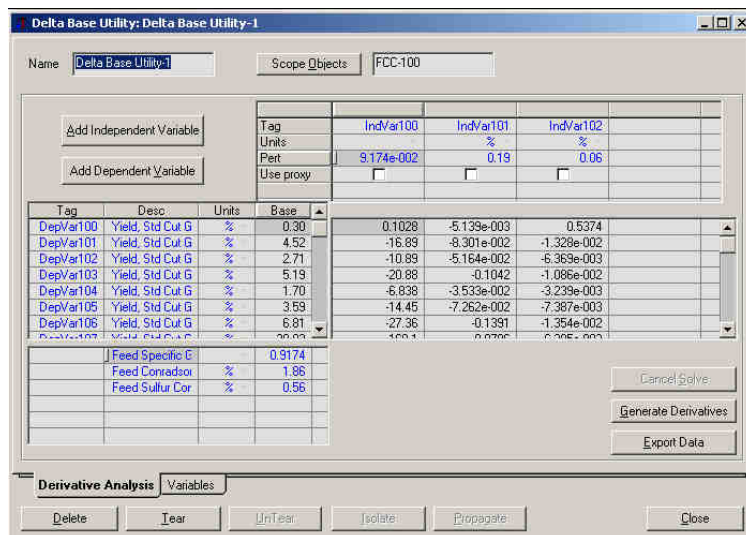


Figure 4.81: Results from Delta Base utility

Once we click the “Generate Derivatives” button, the model runs several times at the base and perturbed values of the independent variables. The DELTA BASE values appear in the table shown in Figure 4.81. These values may be directed copied into an Excel spreadsheet for Aspen PIMS or exported for further study. We can export the table to a PIMS style interface by clicking the “Export Data”. The exported data appears as shown in Figure 4.82.

	A	B	C	D	E	F	G
1		TEXT	BAS	IndVar100	IndVar101	IndVar102	***
2	*				%	%	
3	DepVar100	Yield, Std Cut Grouped (H2S-Weight %) %	0.300289	0.102767	-0.00514	0.537381	
4	DepVar101	Yield, Std Cut Grouped (Fuel Gas-Weight %) %	4.517763	-16.889	-0.08301	-0.01328	
5	DepVar102	Yield, Std Cut Grouped (Propane-Weight %) %	2.705067	-10.8879	-0.05164	-0.00637	
6	DepVar103	Yield, Std Cut Grouped (Propylene-Weight %) %	5.192839	-20.8811	-0.10417	-0.01086	
7	DepVar104	Yield, Std Cut Grouped (nButane-Weight %) %	1.701708	-6.83804	-0.03533	-0.00324	
8	DepVar105	Yield, Std Cut Grouped (iButane-Weight %) %	3.594922	-14.4537	-0.07262	-0.00739	
9	DepVar106	Yield, Std Cut Grouped (Butenes-Weight %) %	6.805855	-27.3569	-0.13912	-0.01354	
10	DepVar107	Yield, Std Cut Grouped (Naphtha C5-430F-Weight %) %	39.82442	-160.133	-0.87061	-0.06305	
11	DepVar108	Yield, Std Cut Grouped (LCO 430-650F-Weight %) %	15.95248	54.15585	0.294465	-0.15798	
12	DepVar109	Yield, Std Cut Grouped (Bottoms 650F+-Weight %) %	13.71198	191.188	0.631644	-0.21528	
13	DepVar110	Yield, Std Cut Grouped (Coke Yield-Weight %) %	5.692676	11.99323	0.435531	-0.04639	
14	*						
15		Feed Specific Gravity (Feed-1)	0.9174	1			
16		Feed Conradson Carbon Residue (Feed-1)	1.86		1		
17		Feed Sulfur Content (Feed-1)	0.561			1	
18							

Figure 4.82: PIMS style output for DELTA-BASE vectors

If necessary we can also rename all the variables to be consistent with PIMS DELTA-BASE vectors. To rename variables, we enter news names for each entry in the corresponding “Tag” box as show in Figure 4.83. When we re-export the delta-base table, all variables will be replaced with the new tags as shown in Figure 4.84.

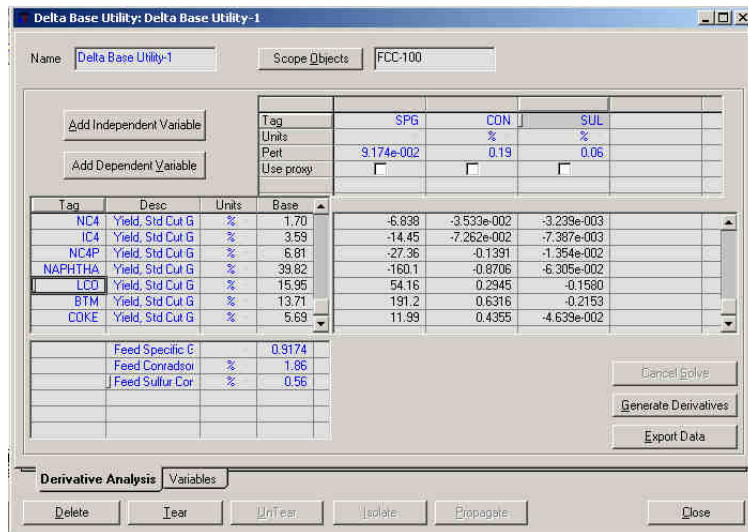


Figure 4.83: Renaming variables in Delta Base Utility

	A	B	C	D	E	F	G
1		TEXT	BAS	SPG	CON	SUL	***
2	*				%	%	
3	SOURGAS	Yield, Std	0.30029	0.102753	-0.00515	0.537358	
4	DRYGAS	Yield, Std	4.517763	-16.889	-0.08301	-0.01328	
5	C3	Yield, Std	2.705067	-10.8879	-0.05164	-0.00637	
6	C3P	Yield, Std	5.192839	-20.8811	-0.10417	-0.01087	
7	NC4	Yield, Std	1.701708	-6.83804	-0.03533	-0.00324	
8	IC4	Yield, Std	3.594923	-14.4537	-0.07262	-0.00739	
9	NC4P	Yield, Std	6.805855	-27.3569	-0.13912	-0.01355	
10	NAPHTHA	Yield, Std	39.82442	-160.133	-0.87062	-0.06308	
11	LCO	Yield, Std	15.95248	54.15586	0.294472	-0.15796	
12	BTM	Yield, Std	13.71198	191.1881	0.631652	-0.21525	
13	COKE	Yield, Std	5.692675	11.99324	0.435534	-0.04638	
14	*						
15		Feed Spec	0.9174	1			
16		Feed Conr	1.86		1		
17		Feed Sulfu	0.561			1	

Figure 4.84: Renamed variables and tags in PIMS interface

4.15 References

1. Kaes, G. L. *Refinery Process Modeling A Practical Guide to Steady State Modeling of Petroleum Processes*; The Athens Printing Company: Athens, GA, 2000.

5. Guide for modeling CCR units in Aspen HYSYS/Petroleum Refining

5.1 Introduction

In this chapter, we go through an example of how to organize data, build and calibrate a model for a catalytic reformer using Aspen HYSYS/Petroleum Refining. We discuss some key issues in model development and how to estimate missing data required by Aspen HYSYS/Petroleum refining. We divide this task into four workshops:

- a. Workshop I: Building a basic Catalytic Reformer Model
- b. Workshop II: Calibrating the basic Catalytic Reformer Model
- c. Workshop III: Building a downstream fractionation system
- d. Workshop IV: Performing case study to identify different RON scenarios

5.2 Process Overview and Relevant Data

Figure 5.1 shows typical continuous catalyst regeneration (CCR) that we will use to build the model in question. We extensively discussed the features and operating issues associated with this type unit in an earlier chapter of this text. In the context of this chapter, we also build models for the remixing and hydrogen recontactor section of this flowsheet. Table 5.1 through Table 5.5 show some typical operating data for this unit.

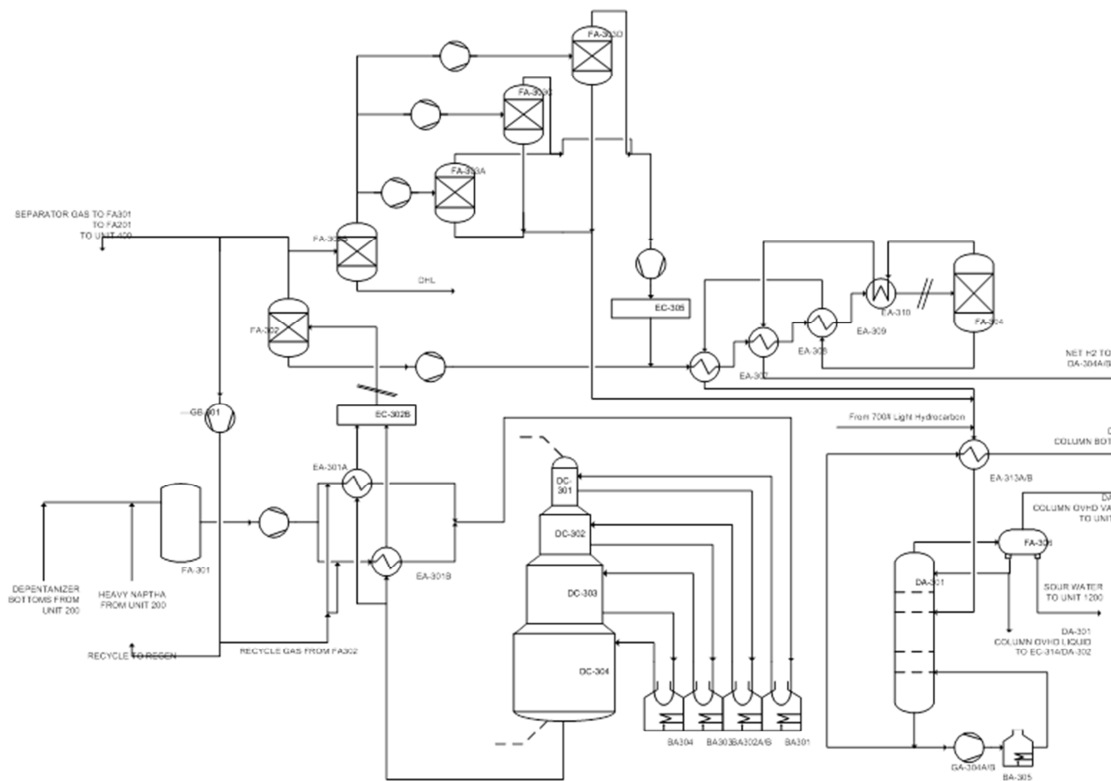


Figure 5.1: Typical CCR Reforming Unit

Table 5.1: Feed Properties

ASTM D-		(Wt. %)	P	N	A
86					
IBP	78	C2	-	-	-
5%	90	C3	-	-	-
10%	96	C4	0	-	-
30%	108	C5	0.78	0.18	-

50%	119	C6	5.4	5.01	0.91
70%	133	C7	10.72	12.05	2.56
90%	152	C8	9.62	13.68	0.93/0.67/1.74/0.71
95%	160	C9	8.13	11.14	2.61
EBP	170	C10+	6.42	6.74	-
S. G.	0.745	Sum	41.07	48.8	10.13

Table 5.2: Product Composition Profile

Comp. (vol%)	Recycle		DA301 Top	DA301 Top
	H2	Rich H2	Vapor	Liquid
H2	86.72	94.06	36.89	0.66
CH4	2.61	2.40	5.64	0.44
C2H6	2.86	1.78	18.50	8.29
C3H8	3.33	1.10	22.04	28.32
C3H6	0.01	0.00	0.00	0.12
iC4H10	1.56	0.31	7.82	20.32
nC4H10	1.24	0.19	5.53	18.02

iC5H12	1.08	0.11	2.56	15.95
nC5H12	0.59	0.05	0.95	7.62
C4=			0.07	0.26

Table 5.3: DA301 Liquid Product Composition

ASTM D-86		(Wt. %)	P	N	A
IBP	74	C2		-	-
5%	85	C3		-	-
10%	94	C4	0	-	-
30%	112	C5	0	0.27	-
50%	128	C6	0.2	0.53	7.925
70%	145	C7	7.22	0.65	20.72
90%	165	C8	5.87	0.54	3.4/5.11/11.1/6.3
95%	173	C9	1.17	-	20.62
EBP	208	C10+	-	-	8.75
S. G.	0.83	Sum	14.46	1.99	83.55

Table 5.4: Overall Product Flowrate and yield

Stream	Rate (tons/hr)
--------	----------------

Feed	175.9
Net Rich H2	12.4
DA301 Ovhd. Vapor	3.3
DA301 Ovhd. Liquid	21.7
DA301 Bttms. Liquid	138.5

Table 5.5: Reactor Configuration

Reactor Bed	Length (m)	Loading (kg)	Inlet Temp. (°C)	ΔT (°C)
#1	0.54	1.275e4	516.0	110.4
#2	0.69	1.913e4	513.6	64.2
#3	0.96	3.188e4	513.1	36.4
#4	1.41	6.375e4	515.0	23.1

5.3 Aspen HYSYS and initial component and thermodynamics setup

We start by opening Aspen HYSYS. The typical path to Aspen HYSYS is to enter the Start > Programs > AspenTech > Aspen Engineering Suite > Aspen HYSYS. Early versions may include a menu entry titled Aspen RefSYS. The correct program to start is Aspen HYSYS (Shown in Figure 5.2). We dismiss the “Tip” dialog and select File > New > Case. We wish to include fractionation, so we do not choose “Reformer” alone.

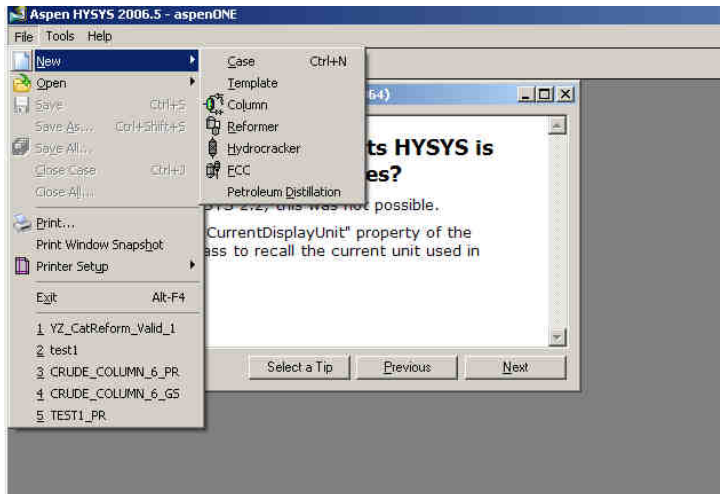


Figure 5.2: Initial Startup of Aspen HYSYS

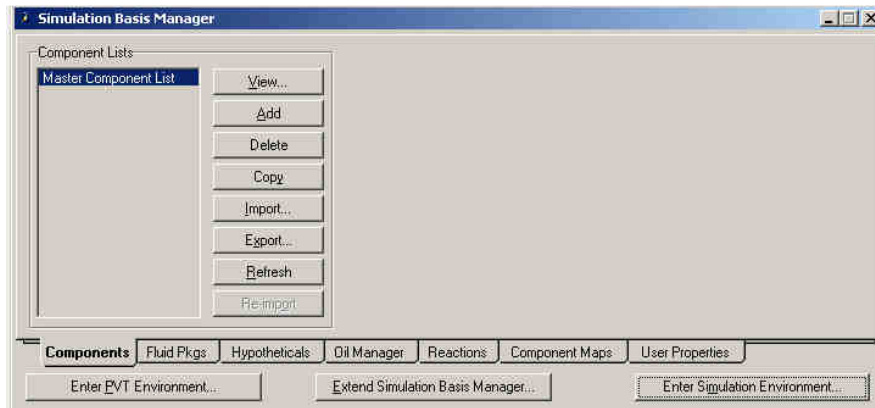


Figure 5.3: Adding a component List

The first in creating the model is the selection of a standard set of components and a thermodynamic basis to model the physical properties of these components. When we create a new simulation, we must choose the components and thermodynamics appropriate for the process using the Simulation Basis Manager. The Simulation Basis Manager allows us to define components and associated thermodynamics in Aspen HYSYS. Components may be added manually through the Add button shown in Figure 5.3. However, we have a predetermined set of the components for the reformer model.

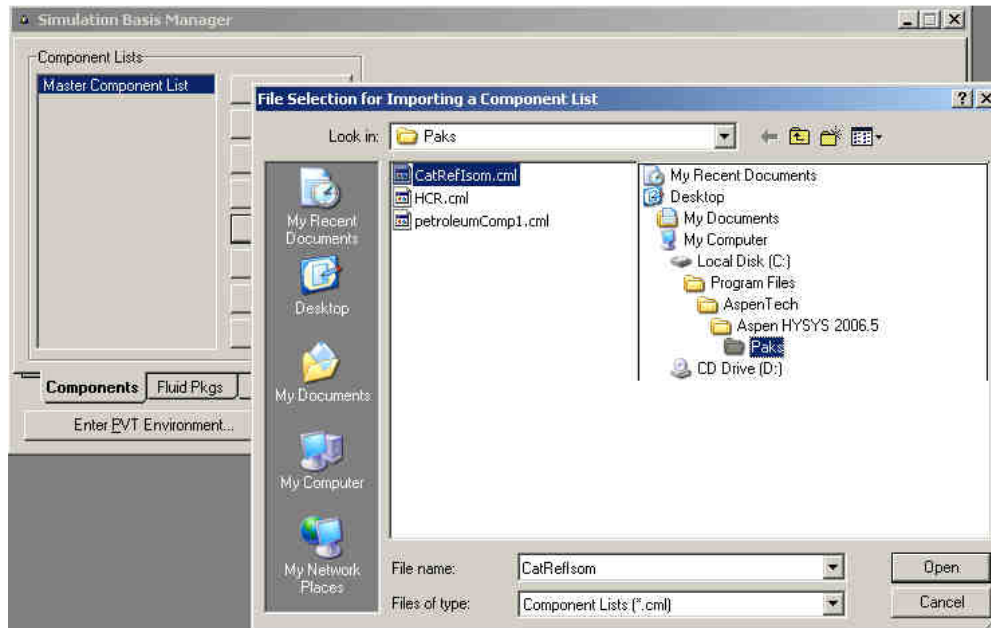


Figure 5.4: Importing Reformer Component List

To import these components, we click ‘Import’ and navigate to the directory location, “C:\Program Files\AspenTech\Aspen HYSYS 2006.5” and select the “CatReform.cml” as the component list (Figure 5.4). The path shown in reflects a standard installation of Aspen HYSYS/Petroleum Refining software.

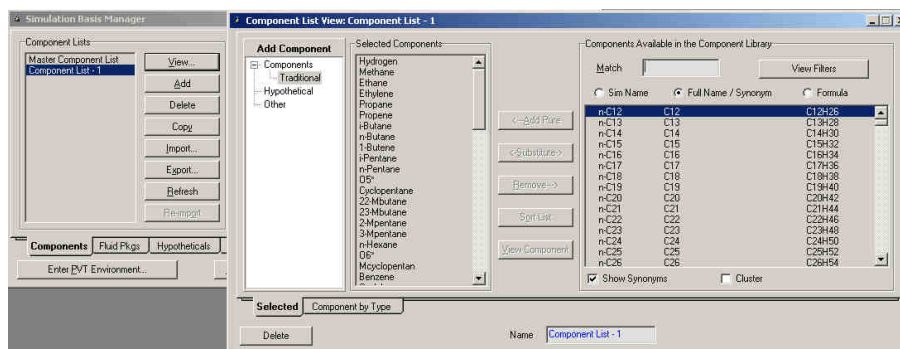


Figure 5.5: Initial Component list for reforming process

Once we import a component list, HYSYS will create a new component list called “Component List-1”. We can view the elements of this component lists by selecting “Component List-1” and clicking on “View” in the Simulation Basis Manager (Figure 5.5). We can add more components or modify the order of the elements in the component list. We note that the standard reforming component list is quite complete and model most refining processes. The rigorous reforming model does not predict components are not part of the “CatReform.cml” list. However, these additional components may be used in production fractionation models of the associated with the reformer model.

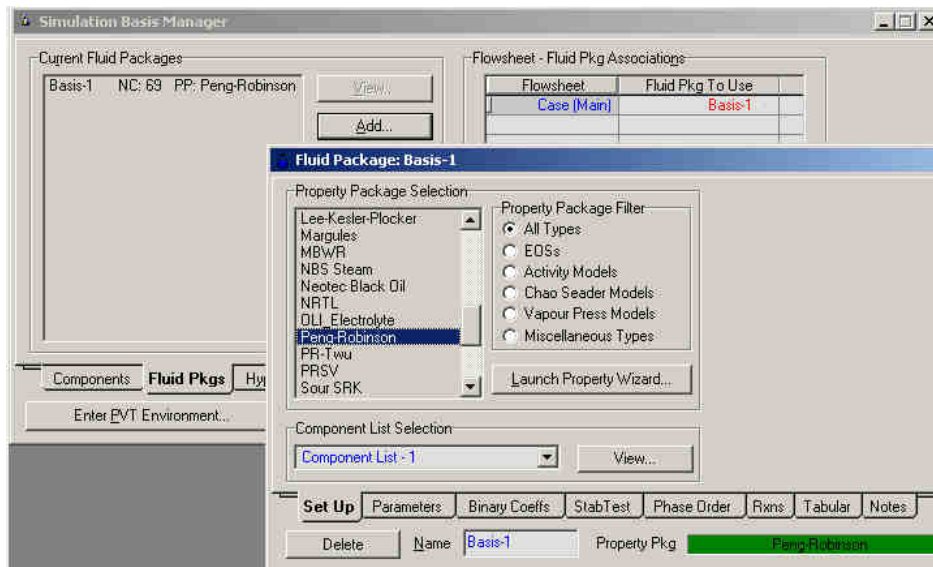


Figure 5.6: Select Thermodynamics for Fluid Package

The next step is the selection of a ‘Fluid Package’ for this model. The ‘Fluid Package’ refers the thermodynamic system associated with the chosen list of components. We move to the ‘Fluid Pkgs’ tab in the Simulation Basis Manager and add click ‘Add’ (Figure 5.6). Apsen HYSYS will automatically choose the component list and present options for a ‘Property Package’ for these components. The reformer system is mostly hydrocarbons and consequently the Peng-Robinson

equation of state is sufficient. We discuss the implications of the process thermodynamics in a previous chapter of this text. In the case of the reformer model, equation of state or hydrocarbon correlation methods (Grayson-Streed, etc.) can sufficiently model the process.

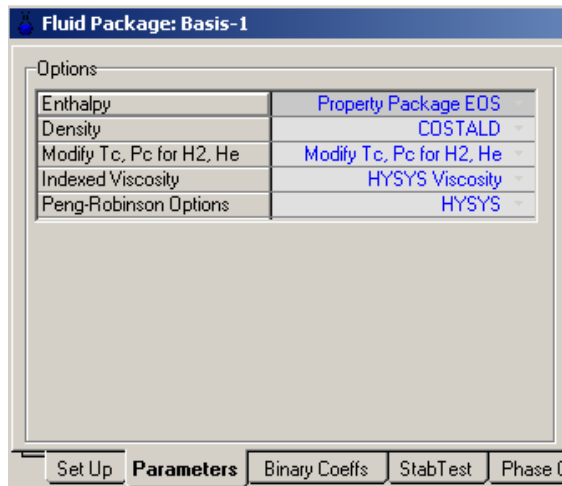


Figure 5.7: Thermodynamic options for Fluid Package

It is important to note that even when we choose an equation-of-state approach, Aspen HYSYS does not calculate all physical properties from the equation of state. For hydrocarbons, equations of state do not generally predict the equilibrium properties of very light components such as hydrogen. In addition, density predictions (especially in the heavy hydrocarbon range) can be quite poor. We almost always modify the equation of state to account for these deficiencies. For the reforming process we choose the COSTALD method to predict the liquid density (Figure 5.7).

Fluid Package: Basis-1

Equation of State Interaction Parameters

	Hydrogen	Methane	Ethane
Hydrogen	---	0.20200	0.22310
Methane	0.20200	---	0.00224
Ethane	0.22310	0.00224	---
Ethylene	0.00740	0.02150	0.01230
Propane	0.21420	0.00683	0.00126
Propene	-0.10360	0.03300	-0.00190
i-Butane	0.20370	0.01311	0.00457
n-Butane	0.19410	0.01230	0.00410

Treatment of Interaction Coefficients Unavailable from the L
 Estimate HC-HC / Set Non HC-HC to 0.0

Set Up Parameters **Binary Coeffs** StabTest PK

Delete Name Property Pk

Figure 5.8: Binary interaction parameters for Fluid package

The last step before building the reformer flowsheet is to verify the interaction parameters (Figure 5.8). If we had chosen a correlation based approach (Grayson-Streed, etc.) we do not have to examine the interaction parameters. Since we chose an equation of state approach, we must make sure that the binary interaction parameters for the equation-of-state are meaningful. In Aspen HYSYS, the interaction parameters for defined components (such as methane, ethane, etc.) come from an internal databank based on experimental data. For lumped components, such as (A8, A9, etc.), we can either set the interaction parameters to 0 or estimate these values based on correlations. Note that that often little difference in practice whether or not the interactions are set to zero or estimated for lumped components. Especially for the reformer process, both methods yield nearly identical results. Once we have chosen an option the interaction parameters, we can return to the Simulation Basis Manager and click on ‘Enter Simulation Environment’ to begin building the process model.

5.4 Workshop I: Basic reformer configuration

The initial flowsheet presents a blank interface where we can place different objects from the Object palette shown in Figure 5.9. The initial tool palette only shows typical unit operations and does not show the advanced Aspen HYSYS/Petroleum Refining objects. We will use both toolbars to build out the complete reformer model. We can bring the up the advanced palette by pressing F6.

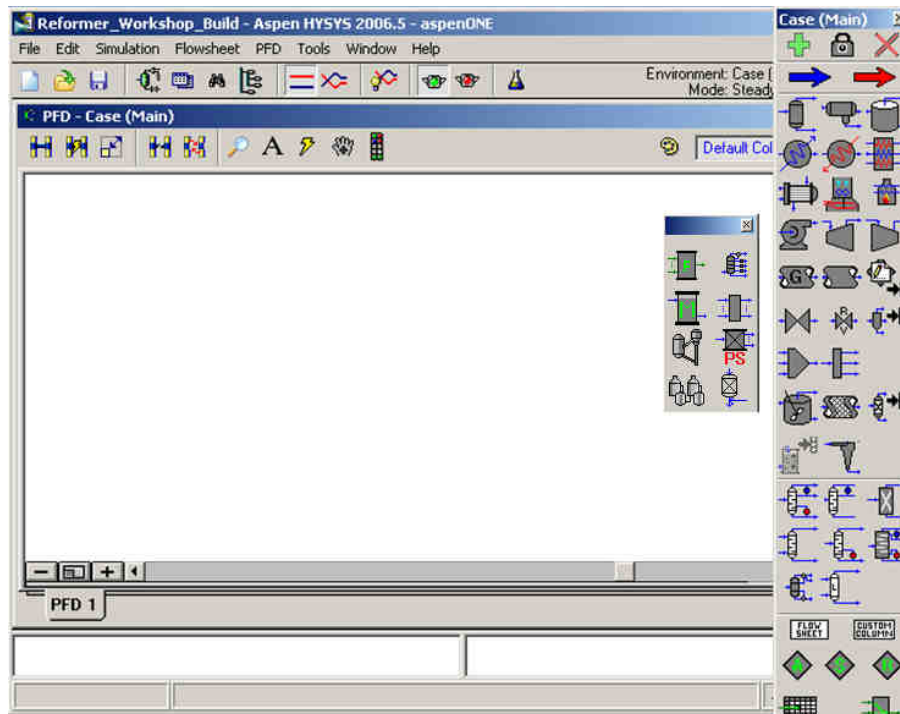


Figure 5.9: Refining Reactor Palette

We select the Reformer icon from the Refining Reactors palette and click on the Refomer icon and place the icon the flowsheet. Placing the icon invokes the several sub-models that prepare the flowsheet for additional objects and creates a large depiction of the reformer object on the flowsheet.

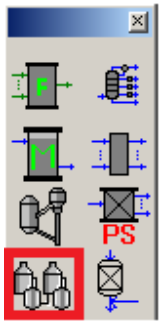


Figure 5.10: Reformer Icon in Refining Reactors Palette

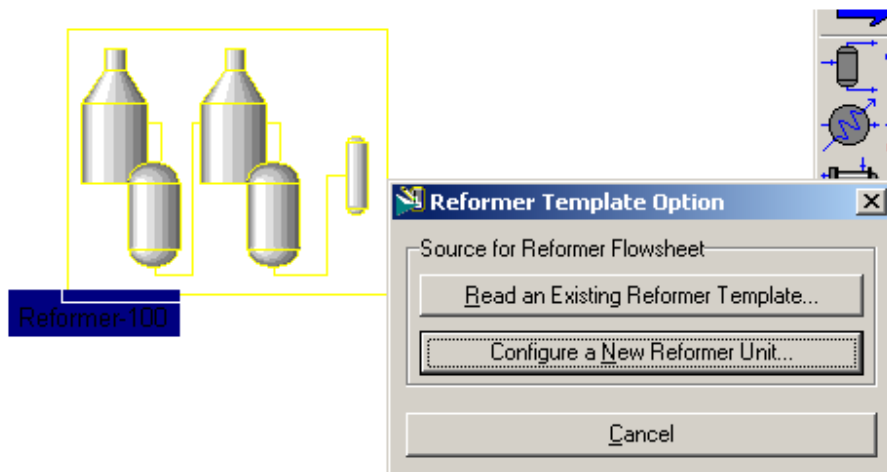


Figure 5.11: Initial Reformer Window

The first step is to choose whether to use a reformer temperature or configure a new unit. Aspen HYSYS has several reformer templates that reflect several popular types of industrial reformer configurations. Figure 5.11 shows the initial window when place a Reformer object on the Flowsheet. If we choose a template, we do not have to assign the reactor dimensions and catalyst loadings. However, in this workshop, we will build a reformer from scratch, so we choose ‘Configure a New Reformer Unit’.

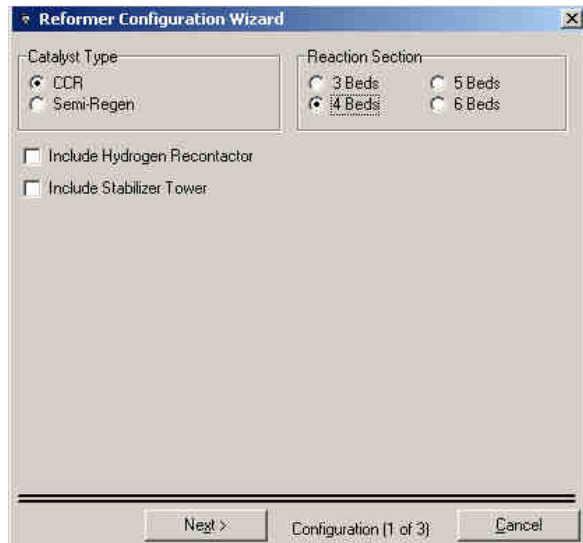


Figure 5.12: Basic Reformer Configuration

The reformer configuration requires choosing the type of reformer, number of reactors and their dimensions and catalyst loadings for each reactor. Additionally, we may also specify additional downstream fractionation equipment such as hydrogen recontactor and stabilizer tower.

However, we note that the selecting options produce a simplified model for fractionation that may not be appropriate for a detailed and integrated process flowsheet. We recommend building a rigorous flowsheet based on standard Aspen HYSYS fractionation objects. In Figure 5.12, we select a CCR reformer with 4 reactor beds and click “Next>”.



Figure 5.13: Reactor dimensions and Catalyst loadings

The primary catalyst configuration is the dimension of the catalyst bed and associated catalyst loading. Here the catalyst loading refers to the amount of catalyst exposed to feed in each reactor bed. The Length refers to the distance the feed travels radially through the catalyst bed. The most important parameters are the catalyst loadings and it is important to obtain accurate values from industrial data. We use the data given earlier in the chapter. The values shown in Figure 5.13 may not be applicable to all CCR reformer plants but provide a good starting point. The void fraction and catalyst density are not that significant for product predictions but they effect predictions of pressure drop across the reactor beds. The default values given are acceptable for many types of reformers.

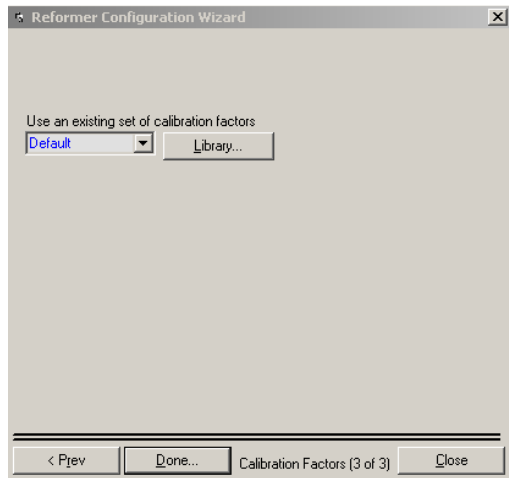


Figure 5.14: Choose Calibration Factors

The last step in reformer configuration is to choose calibration factors for the model as shown in Figure 5.14. The calibration factors refer to the various reaction and process parameters that we will calibrate to match plant performance and predict new operating scenarios. The Default values are based on calibration from a variety of different sources. In general, these factors also provide an initial guess that we refine through the calibration process. For the initial model run, we choose the default and click “Close.”

5.5 Input feedstock and process variables

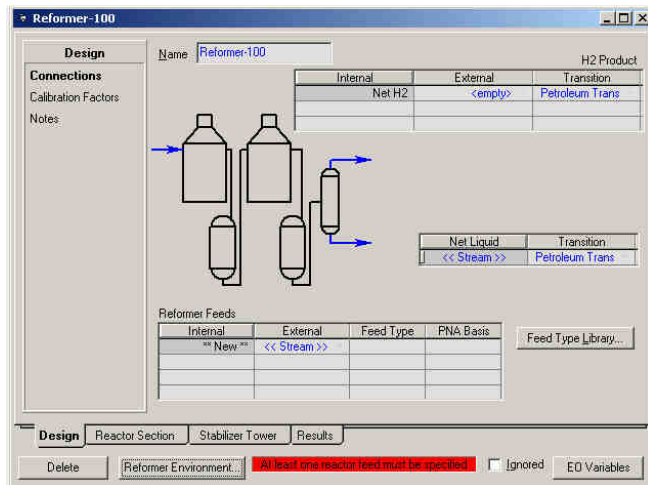


Figure 5.15: Primary Control Window for Reformer

Figure 5.15 shows the primary control window for the Reformer model. Through this window, we can enter feed and process information and view model results. To manipulate the feedstock information, we must drill down to the Reformer sub-model. We enter the Reformer sub-model by clicking on “Reformer” Environment.

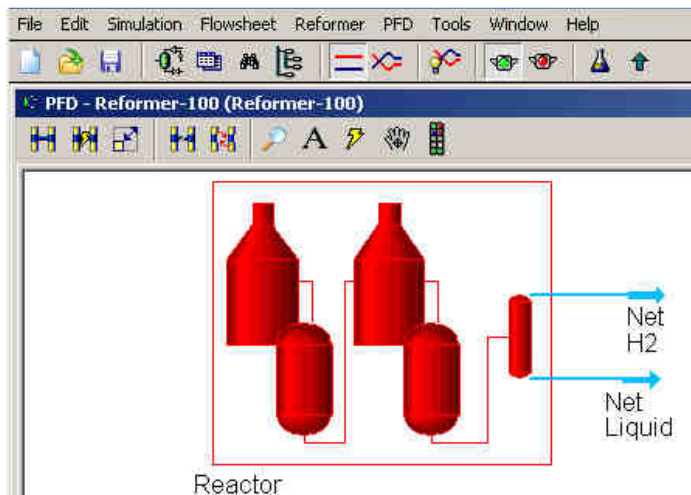


Figure 5.16: Reformer Sub-Model Flowsheet

Figure 5.16 shows the Reformer sub-model. We note the Net Hydrogen and Net Liquids streams are already attached to the reformer model. The Reformer model depiction appears red because there is not enough information to solve the model. When enough information is available, the depiction turn yellow and we can proceed to solve. We manipulate the feedstock information by double-clicking on the Reactor sub-model icon to bring up the Reactor sub-model window.

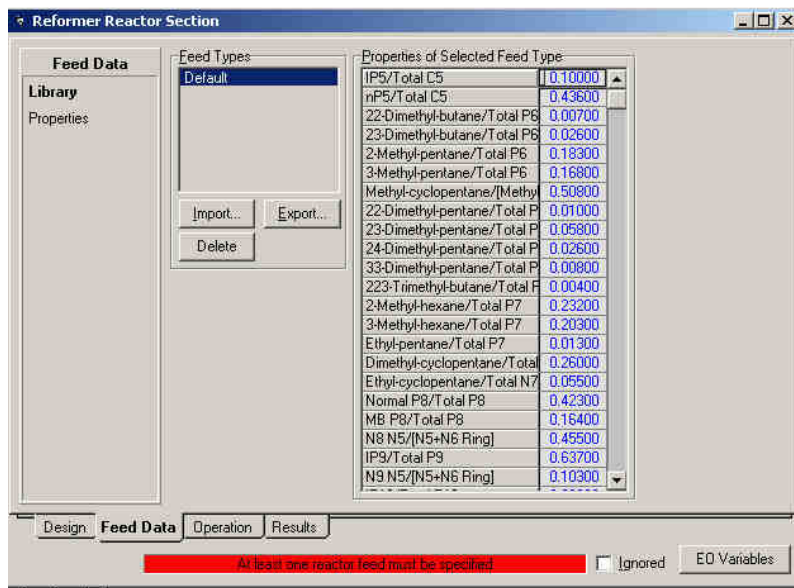


Figure 5.17: Feed Data Tab

Figure 5.17 shows the Feed Data tab from the Reformer sub-model. The Feed Type is a basic set of relationships and initial values for the all kinetic lumps in the reactor model. Aspen HYSYS uses bulk property information such as density, distillation curves and total PNA content in conjunction with the feed type to predict the composition of feed lumps to the model. The 'Default' type is sufficient for light-to-heavy naphtha. However, there is no guarantee that a particular feed type represents represent the actual feed accurately. Aspen HYSYS will attempt to manipulate the feed composition to satisfy bulk property measures given. In general, we

advise users to develop a few sets of compositional analysis to verify the kinetics lumps calculated by Aspen HYSYS. We discuss a process to verify these lumps later.

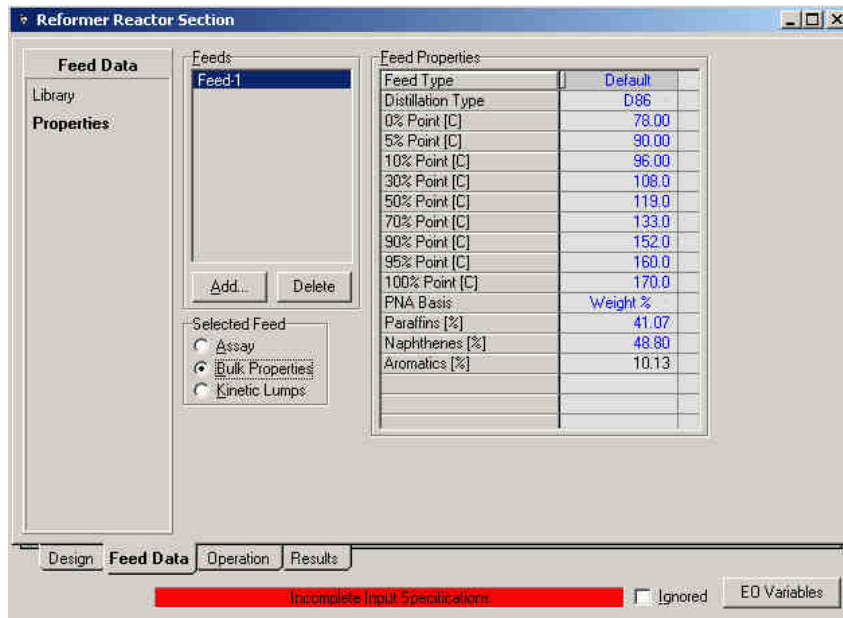


Figure 5.18: Bulk Property Information

We enter the measured bulk property information in the “Properties” section of the Feed Data Tab as shown in Figure 5.18. These data come from sample process data given earlier in this chapter. Once we enter the bulk feed information, it is important to “Hold” the solver. By design, Aspen HYSYS will attempt to recalculate the model the instant we make a change. This can be inconvenient and may cause convergence problems when we change many variables. To “Hold” the solver, simply select the Red Stop sign in the top toolbar of the flowsheet window (Figure 5.19).

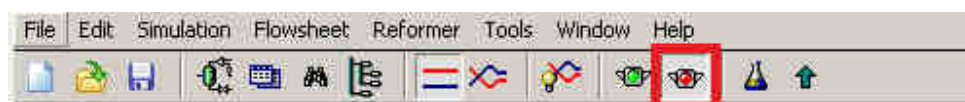


Figure 5.19: Hold Aspen HYSYS Solver

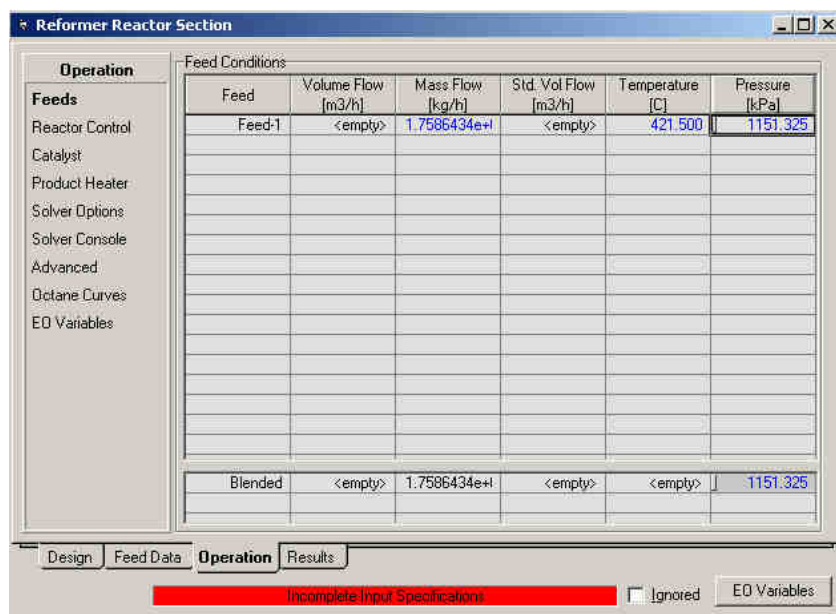


Figure 5.20: Feed Flow Rate Specifications

We now input other operation details by navigating to the “Operation” Tab and “Feeds” section of the Reformer sub-model (see Figure 5.20). The flowrates and process parameters should reflect an operating schedule where actual reformer is running smoothly. It is difficult to use a model based on upset data for future predictions of stable operating scenarios. We discussed some techniques and approaches in a previous to ensure that the data collected for the model reflects stable operation.

After we enter the feedstock information, we must define operating temperatures and associated process variables. We enter the “Reactor Control” section and define the operating temperature of each bed. There are two ways specify reactor inlet temperature. In the first method, we enter the weight averaged inlet temperature (WAIT) for all the reactors and specify a bias for each reactor. In the second method, we enter a reactor reference temperature and specify a bias for each reactor. We use the second method to accurately fix the inlet temperature of each bed. We

recommend this method when running the model for the first time. This ensures that inlet temperatures are accurate for the purposes of calibration. We show how to input the reactors temperatures in Figure 5.21.

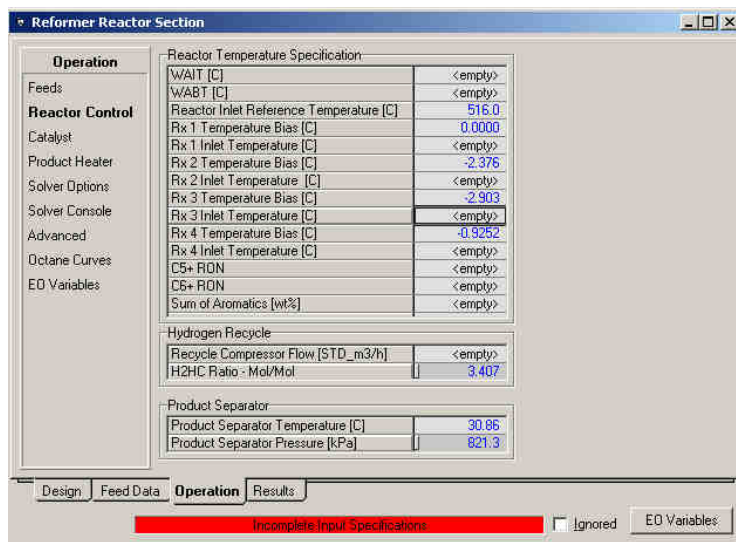


Figure 5.21: Reactor Temperature Specifications

The full equation-oriented (EO) nature of the Reformer model technically allows us to enter the octane number of the product and back-calculate required inlet temperatures to achieve the specified octane number. However, it is very unlikely that an uncalibrated model will converge with those specifications. We recommend entering reactor temperatures directly.

Additionally, we must also enter the Hydrogen-to-Hydrocarbon ratio for the recycle process in the Reformer model. The typical range of this value for CCR reforming units is 3-4. Reforming plants routinely measure this value and we expect to enter accurate values. The product separator refers to the conditions of the first separator after leaving the last reforming reactor. This value should be accurate if we do not plan to build a downstream fractionation model.

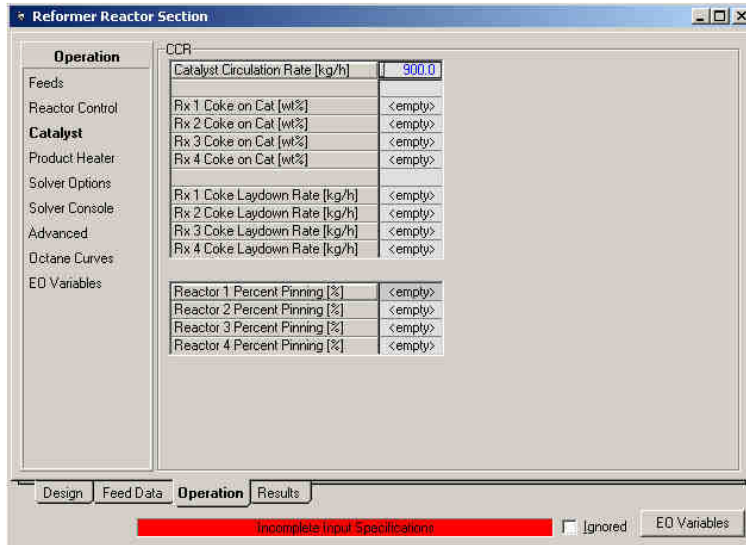


Figure 5.22: Catalyst Specifications

In Figure 5.22, we enter the “Catalyst” section of “Operation” Tab. We must enter an estimate for the catalyst circulate rate since we are modeling a CCR unit. Users will note that it is possible to enter other specifications in the Catalyst Section, however, only the circulation rate ensures robust convergence.

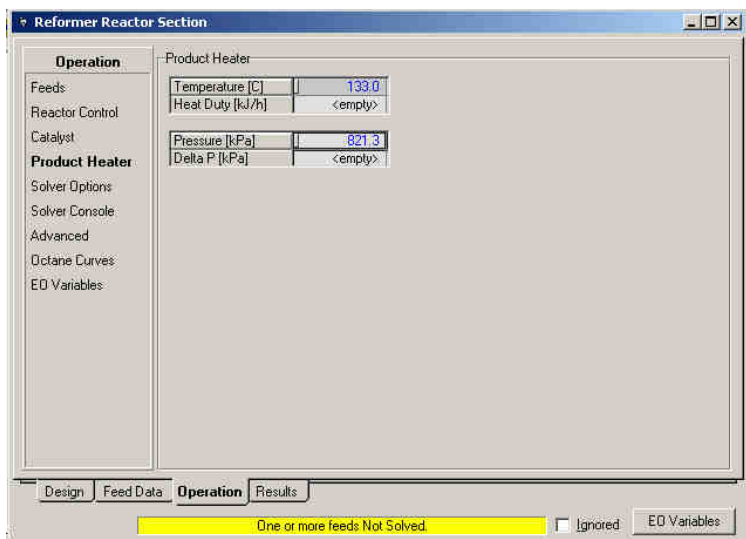


Figure 5.23: Product Heater Specifications

The last process operation parameters are the product heater specifications. Since we are building a rigorous fractionation section in this example, we only enter estimated values. If there is no fractionation model planned, we can enter measured values for the heater immediately preceding the gasoline stabilization tower. In Figure 5.23, once we enter the product heater specifications, we notice a yellow bar indicating that we are ready to solve the model. In the next section, we will discuss how to solve the model and ensure robust convergence.

5.6 Solver parameters and running initial model

Before solving the model, we must ensure that the solvers parameters will lead to robust convergence. We bring up the Solver options by selecting the “Solver Options” section in “Operation” Tab. Figure 5.24 shows the recommend values for the solver options. We have chosen these values based on our experience with running with model.

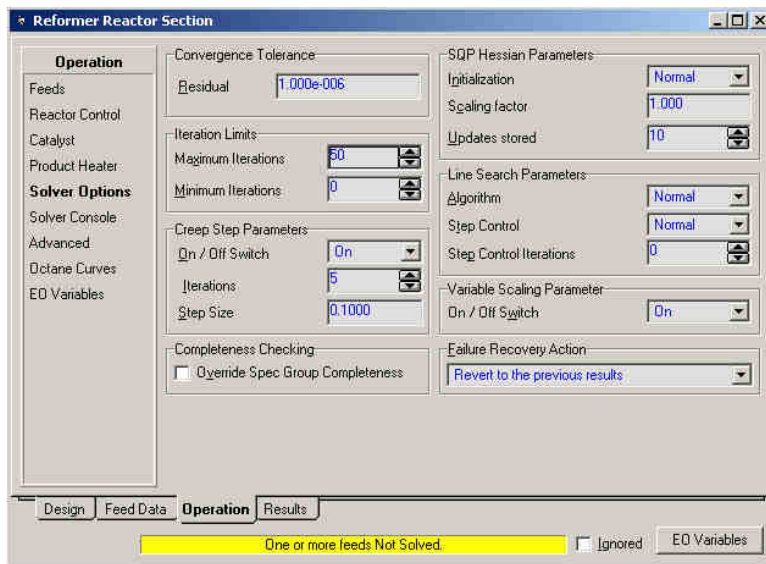


Figure 5.24: Solver Parameters

In general, we do not recommend modifying the constraints for the Residual, Hessian Parameters and Line search parameters. When running the model for the first time, we increase the number creep iterations and total maximum iterations. Creep iterations refer to initial small changes in the process variables when the starting guesses are very poor. The maximum iterations refer to how times the solver will iterate though the model before exiting. Depending on process parameters, the initial solution may take up to 30-40 iterations.



Figure 5.25: Main Application Toolbar

To begin solving the model, we select the green start icon in the flowsheet toolbar as shown in Figure 5.25. Several initializations step will appear in the lower right corner window of the application. The solution process may take several minutes and the software appears momentarily disabled while solver status messages appear in the lower right corner window.

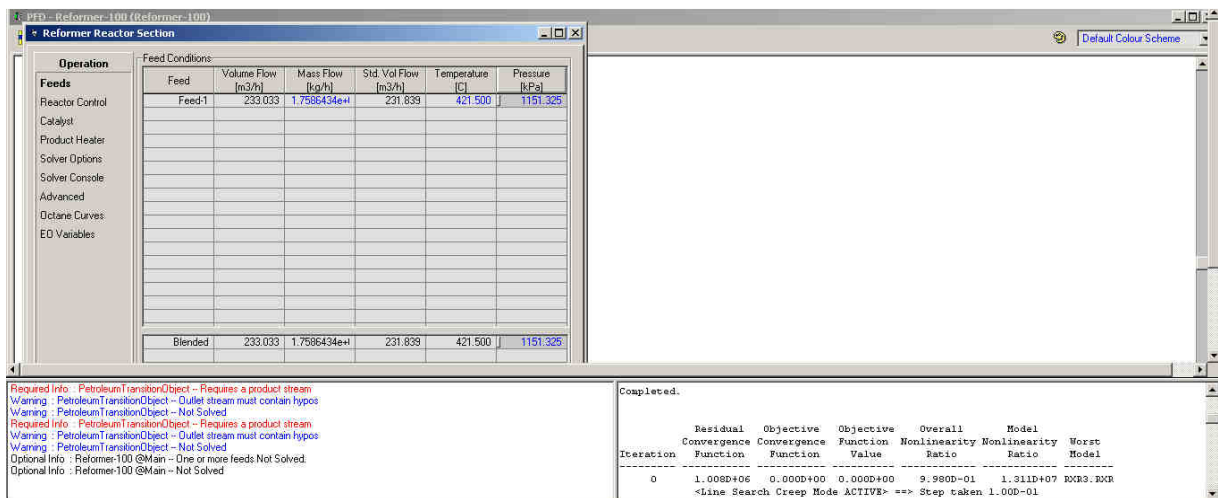


Figure 5.26: Aspen HYSYS Flowsheet interface

We show the solver output for the configured model in Table 5.6. Column 1 indicates the number of iterations performed since starting the solver. The residual convergence function indicates how far we are from satisfying the process model equations. When we run the model for the first time, residuals on the order of 1e9 and 1e10 are expected. As we approach the solution, the residual drops to closer and closer to zero. Column 3 and Column 4 refer to the residual of the objective function. We use the objective function only during calibration, therefore it is zero for this model run. The solver used by Aspen HYSYS converges very quickly to solution once the changes in the process equations starting appearing to be linear. This is the case when we are in the vicinity of the solution. The solver indicates the vicinity of the solution through columns 5 and 6. The Worst model column indicates which part of the reformer model is furthest from the solution. This is useful for tracking down issues when the model fails to converge. The last lines of the output show several running statistics for the solver.

Table 5.6: Initial Solver output

Iteration	Residual Convergence Function	Objective Convergence Function	Objective Function Value	Overall Nonlinearity Ratio	Model Nonlinearity Ratio	Worst Model
0	1.008D+06	0.000D+00	0.000D+00	9.980D-01	1.311D+07	RXR3.RXR
	<Line Search Creep Mode ACTIVE> ==> Step taken 1.00D-01					
1	1.120D+06	0.000D+00	0.000D+00	7.641D-01	-2.433D+01	RXR4.RXACT
	<Line Search Creep Mode ACTIVE> ==> Step taken 1.00D-01					
2	1.244D+06	0.000D+00	0.000D+00	8.444D-01	-1.642D+01	RXR4.RXACT
	<Line Search Creep Mode ACTIVE> ==> Step taken 1.00D-01					
3	1.356D+06	0.000D+00	0.000D+00	-2.501D+01	-5.249D+03	RECSPL
	<Line Search Creep Mode ACTIVE> ==> Step taken 1.00D-01					
	<Line Search ACTIVE> ==> Step taken 1.00D-02					
4	1.368D+06	0.000D+00	0.000D+00	8.900D-01	-1.477D+01	RXR4.RXACT
	<Line Search Creep Mode ACTIVE> ==> Step taken 1.00D-01					
5	1.481D+06	0.000D+00	0.000D+00	-9.084D+00	-8.954D+03	RXR4.RXACT
	<Line Search ACTIVE> ==> Step taken 1.00D-01					
6	1.692D+06	0.000D+00	0.000D+00	-2.203D+01	-5.946D+03	RXR4.RXACT
	<Line Search ACTIVE> ==> Step taken 1.00D-01					
7	2.364D+06	0.000D+00	0.000D+00	-3.671D+01	-3.878D+03	RXR4.RXACT

							<Line Search ACTIVE> ==> Step taken 1.00D-01
8	4.636D+06	0.000D+00	0.000D+00	-3.553D+01	-2.513D+03	RXR4.RXACT	<Line Search ACTIVE> ==> Step taken 1.00D-01
9	1.165D+07	0.000D+00	0.000D+00	-2.449D+01	-1.635D+03	RXR4.RXACT	<Line Search ACTIVE> ==> Step taken 1.00D-01
10	3.102D+07	0.000D+00	0.000D+00	-1.622D+01	-1.077D+03	RXR4.RXACT	<Line Search ACTIVE> ==> Step taken 1.00D-01
11	7.906D+07	0.000D+00	0.000D+00	-1.074D+01	-7.225D+02	RXR4.RXACT	<Line Search ACTIVE> ==> Step taken 1.00D-01
12	1.864D+08	0.000D+00	0.000D+00	-7.159D+00	-4.950D+02	RXR4.RXACT	<Line Search ACTIVE> ==> Step taken 1.00D-01
13	4.040D+08	0.000D+00	0.000D+00	-4.809D+00	-3.470D+02	RXR4.RXACT	<Line Search ACTIVE> ==> Step taken 1.00D-01
14	8.059D+08	0.000D+00	0.000D+00	-3.237D+00	-2.489D+02	RXR4.RXACT	<Line Search ACTIVE> ==> Step taken 1.18D-01
15	1.661D+09	0.000D+00	0.000D+00	-1.996D+00	-1.611D+02	RXR4.RXACT	<Line Search ACTIVE> ==> Step taken 1.67D-01
16	4.001D+09	0.000D+00	0.000D+00	-9.044D-01	-7.821D+01	RXR4.RXACT	<Line Search ACTIVE> ==> Step taken 2.63D-01
17	1.173D+10	0.000D+00	0.000D+00	4.793D-03	-2.409D+01	RXR4.RXACT	<Line Search ACTIVE> ==> Step taken 5.02D-01
18	3.714D+10	0.000D+00	0.000D+00	6.974D-01	-2.005D+00	RXR4.RXACT	
19	6.486D+10	0.000D+00	0.000D+00	9.996D-01	9.919D-01	ISOMP5	
20	3.602D+04	0.000D+00	0.000D+00	1.000D+00	9.999D-01	ISOMP5	
21	1.813D-04	0.000D+00	0.000D+00	1.000D+00	9.998D-01	RXR3.RXR	
22	5.628D-16	0.000D+00	0.000D+00				

5.7 Viewing model results

After we complete the initial model solve, we can view the model results by navigating to 'Results' tab and clicking the 'Summary' section. The Summary sections shows combined yield of the many products relevant to the reforming process. Figure 5.27 shows that the results from the initial model run. We note that the results are mostly close to the plant measurements. This indicates that we will not have to do significant amounts of calibration to match model and plant performance and yields. We can also obtain the detailed yield results for each lump by going to the 'Product Yields' section and select Grouped or Detailed yields as shown in Figure 5.28.

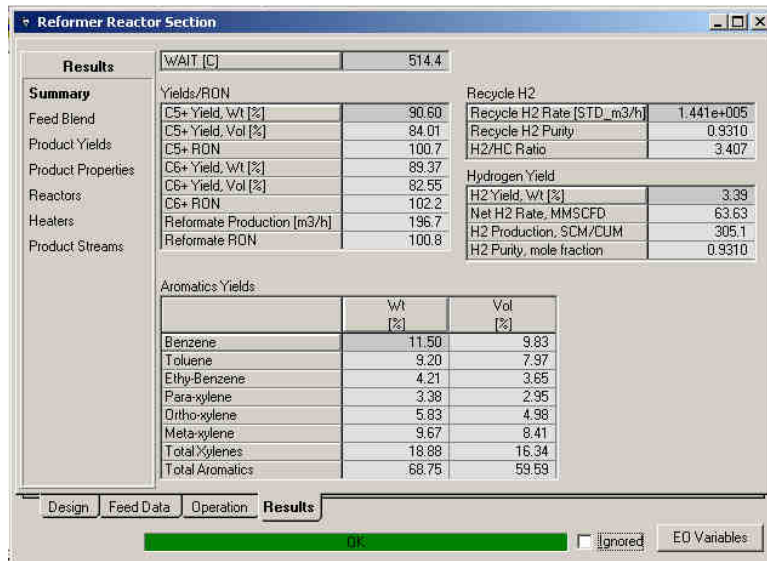


Figure 5.27: Reformer results summary

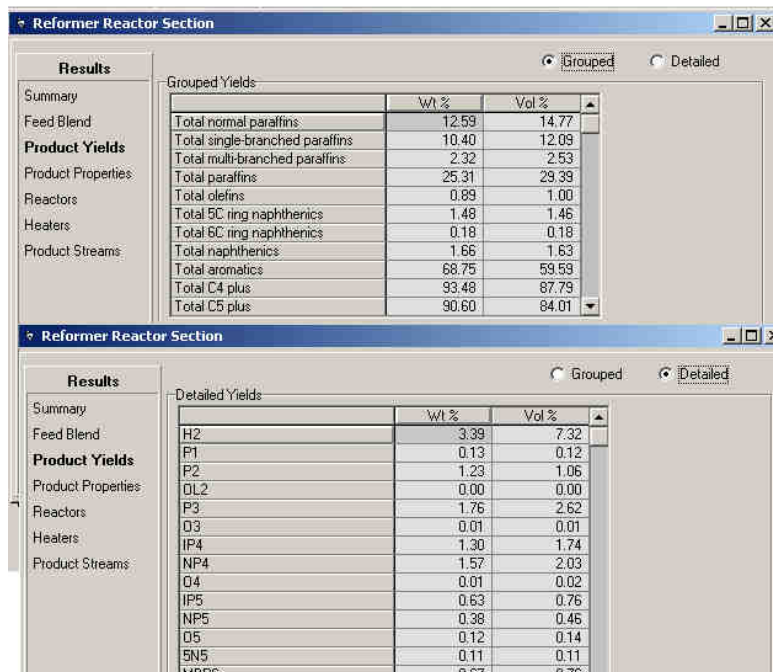


Figure 5.28: Reformer yield results

We can also view the reactor temperature and flow profile by selecting the 'Reactors' section in the Results Tab, as shown in Figure 5.29. Again, we note that the predicted temperature drop for

each reactor bed compares well with the measured temperature drop. Most of the temperature change is due to the naphthene dehydrogenation reactions. Since we made reasonable predictions of the aromatic content, we expect the reactor temperatures to agree as well.

	Reactor 1	Reactor 2	Reactor 3	Reactor 4
Inlet Temperature [C]	516.0	513.6	513.1	515.0
Outlet Temperature [C]	395.1	446.7	472.0	492.2
Delta T [C]	120.8	66.89	41.11	22.90
Inlet Pressure [kPa]	1248	1129	1070	1040
Outlet Pressure [kPa]	1232	1120	1064	1036
Delta P [kPa]	15.85	9.212	5.479	4.223
Inlet Molar Flow [kgmole/h]	7739	9095	9953	1.051e+00
Outlet Molar Flow [kgmole/h]	9094	9953	1.051e+00	1.084e+00
Residence Time [seconds]	000:00:5.0i	000:00:5.7i	000:00:8.3i	000:00:15.:

LHSV	1.024
WHSV	1.379

Figure 5.29: Reactor performance results

This completes in the initial model solution based on bulk property information. We can return to the parent flowsheet by clicking the green up arrow on the flowsheet toolbar (shown in Figure 5.30). Once we return to the main flowsheet we can attach true products streams by entering names for the Net H₂ and Net Liquid Streams (see Figure 5.31) and selecting the Basic Transition (see Figure 5.32).

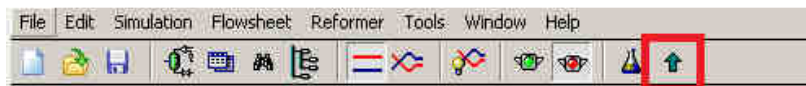


Figure 5.30: Returning to the main flowsheet

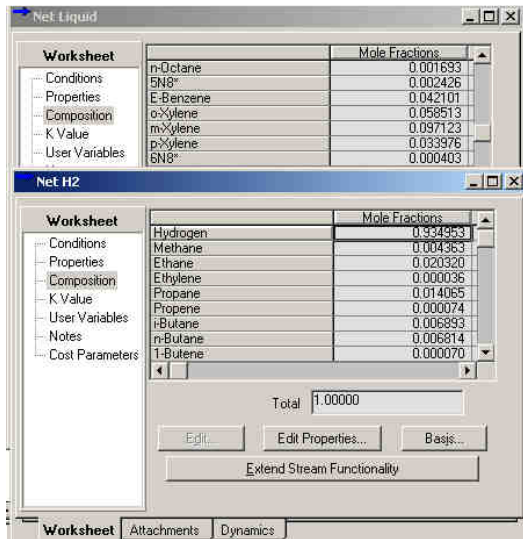


Figure 5.31: Composition of Net H2 and Net Liquid streams

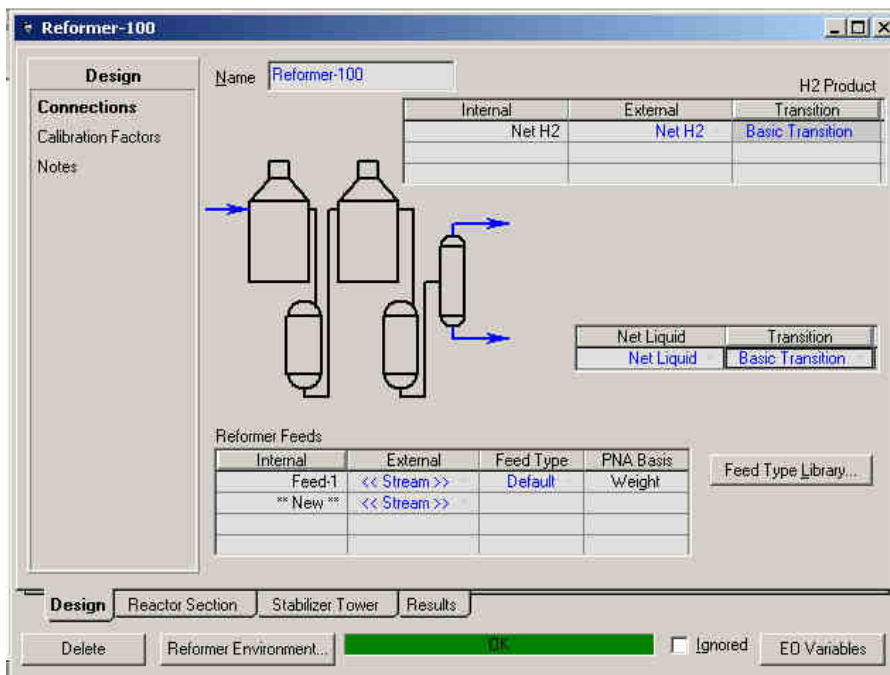
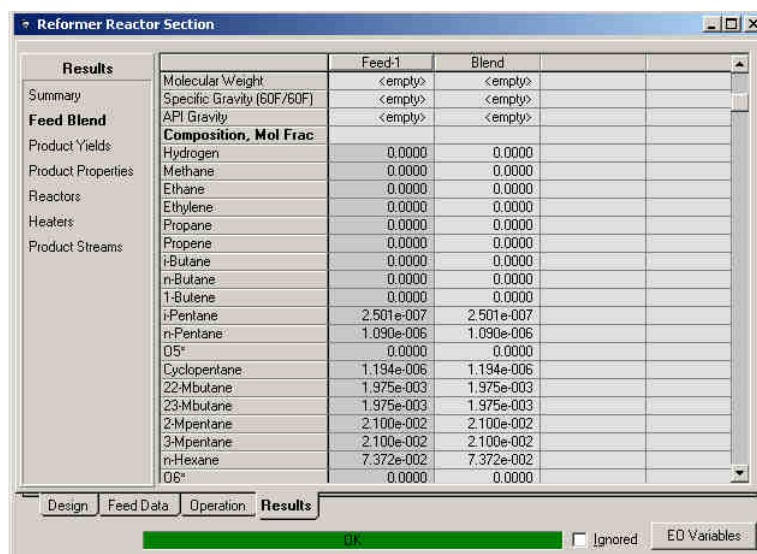


Figure 5.32: Connect External Streams to Reformer flowsheet

5.8 Updating results with molecular composition information

In the previous section, we built and solved the reformer model using bulk property and total PNA information only. This approach works reasonably when the actual feedstock is quite similar to the 'Default' or selected feed type. In actual refinery operation, the feed type may change quickly or may not have been analyzed for feed type information. In this section, we discuss an approach to integrate measured molecular composition analysis with the feed type to improve modeling results. This method has shown significant improvement in model predictions, especially in the petrochemical reformers where accurate predictions of aromatic content are significant.



	Feed-1	Blend
Molecular Weight	<empty>	<empty>
Specific Gravity (60F/60F)	<empty>	<empty>
API Gravity	<empty>	<empty>
Composition, Mol Frac		
Hydrogen	0.0000	0.0000
Methane	0.0000	0.0000
Ethane	0.0000	0.0000
Ethylene	0.0000	0.0000
Propane	0.0000	0.0000
Propene	0.0000	0.0000
i-Butane	0.0000	0.0000
n-Butane	0.0000	0.0000
1-Butene	0.0000	0.0000
i-Pentane	2.501e-007	2.501e-007
n-Pentane	1.090e-006	1.090e-006
Q5*	0.0000	0.0000
Cyclopentane	1.194e-006	1.194e-006
2,2-Mbutane	1.975e-003	1.975e-003
2,3-Mbutane	1.975e-003	1.975e-003
2-Mpentane	2.100e-002	2.100e-002
3-Mpentane	2.100e-002	2.100e-002
n-Hexane	7.372e-002	7.372e-002
Q6*	0.0000	0.0000

Figure 5.33: Feed blending results

Once we solve the model using the bulk property information, we can obtain the feed lump composition from the 'Feed Blend' Section of the 'Results' Tab as shown in Figure 5.33. The composition in mole fraction represents Aspen HYSYS' best estimate of the composition from the bulk information and chosen feed Type. In our example, we also have the detailed

compositional analysis by PNA and carbon number. We show these measured compositions in the Sample Data section of this chapter.

Figure 5.34 shows a spreadsheet in Microsoft Excel that accepts the measured molecular information and Aspen HYSYS's best estimate of the composition. Using both sets of data, we can rescale Aspen HYSYS's estimate to match the measure composition. Essentially, we rescale the estimates to match plant data for each compositional and carbon group number while keeping isomer ratios constant.

	A	B	C	D	E	F	G	H	I	S	T	U
1	Feed transform for Refsys model											
2	(Created by Kiran Pashikanti, Dec 29 2008)											
3												
4	Actual Plant Data											
5	P	C5	0.73%	41.61%					Feed-1	Lump	wt%	wt PERCE
6		C6	5.46%				Hydrogen	0	H		0.00%	0.00
7		C7	11.80%			P01-1	Methane	0	P01-1		0.00%	0.00
8		C8	10.58%			P02-1	Ethane	0	P02-1		0.00%	0.00
9		C9	8.57%			O02-1	Ethylene	0	O02-1		0.00%	0.00
10		C10	4.47%			P03-1	Propane	0	P03-1		0.00%	0.00
11	N	C5	0.15%	50.20%		O03-1	Propene	0	O03-1		0.00%	0.00
12		C6	5.13%			P04-1	i-Butane	0	P04-1		0.00%	0.00
13		C7	13.05%			P04-2	n-Butane	0	P04-2		0.00%	0.00
14		C8	15.28%			O04-1	1-Butene	0	O04-1		0.00%	0.00
15		C9	12.15%			P05-1	i-Pentane	2.50E-07	P05-1		0.14%	0.14
16		C10	4.44%			P05-2	n-Pentane	1.09E-06	P05-2		0.59%	0.59
17	A	C6	0.95%	8.19%		O05-1	O5*	0	O05-1		0.00%	0.00
18		C7	2.14%			N05-1	Cyclopentane	1.19E-06	N05-1		0.15%	0.15
19		C8	2.95%			P06-1	22-Mbutane	1.97E-03	P06-1		0.09%	0.09
20		C9	2.15%			P06-2	23-Mbutane	1.97E-03	P06-2		0.09%	0.09
21		C10	0.00%			P06-3	2-Mpentane	2.10E-02	P06-3		0.96%	0.96
22						P06-4	3-Mpentane	2.10E-02	P06-4		0.96%	0.96
23						P06-5	n-Hexane	7.37E-02	P06-5		3.36%	3.36
24						O06-1	O6*	0	O06-1		0.00%	0.00
25	Distribution calculated by Refsys											
26	P	C5	0.00%	34.32%	High	A06-1	Benzene	1.09E-02	A06-1		0.95%	0.95
27		C6	9.74%		OK	N06-2	Cyclohexane	1.05E-01	N06-2		2.52%	2.52
28		C7	6.26%		Low	P07-1	22-Mpentane	2.07E-03	P07-1		0.37%	0.37

Figure 5.34: Feed re-scaling spreadsheet

We perform this rescaling by copying the results of the 'Feed Blend' (Figure 5.33) from Aspen HYSYS into Column I of the spreadsheet. We also enter the measured compositional information in Column C. The results of the re-scaling appear in Column U. We must now enter

the re-scaled feed information back into the reformer model. We must reenter the Reformer sub model and enter the Feed Data Tab.

Figure 5.35 shows the Feed Data Tab. We select Kinetic Lumps instead of Bulk Properties. Aspen HYSYS will now prompt to indicate that we are discarded the bulk property information. We confirm this change and edit the Kinetic lumps directly. We copy the results from Column U of the spreadsheet into the Edit Lumps dialog as shown in Figure 5.36. We enter the new feed lump composition by weight and normalize to make sure the sum of all the lump compositions is 1. The solver will automatically resolve the model using the new feed lump composition. In general, the initial residual should be on the order of $1e3$ to $1e4$, which indicates that only changes to the model are the feed lump compositions.

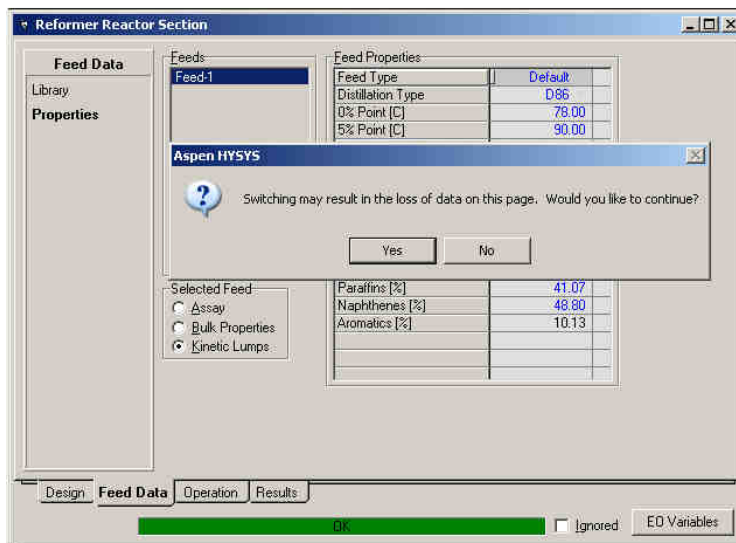


Figure 5.35: Changing from the bulk property data to kinetic lumps

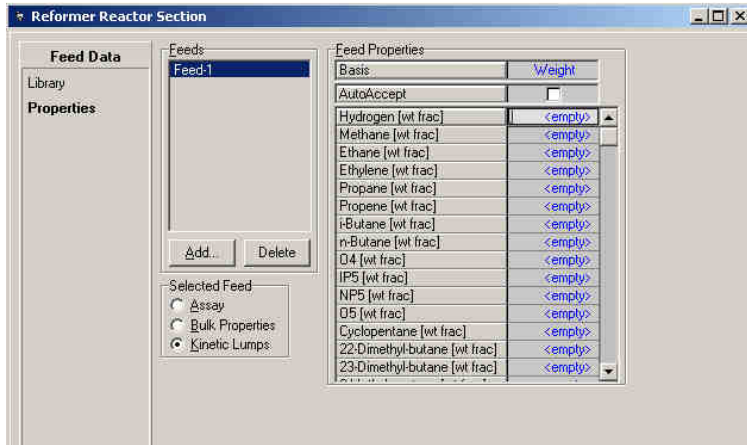


Figure 5.36: Kinetic Lump composition entry window

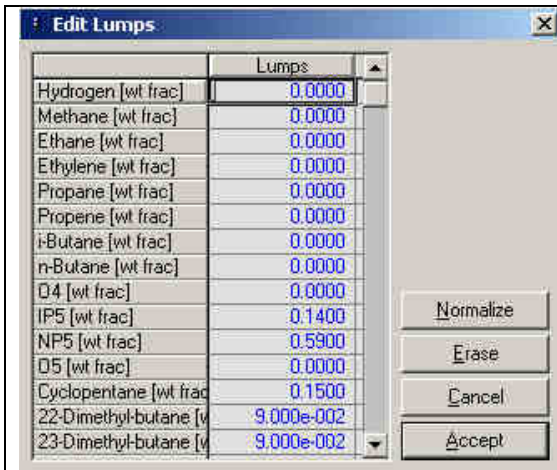


Figure 5.37: Enter Lump Composition

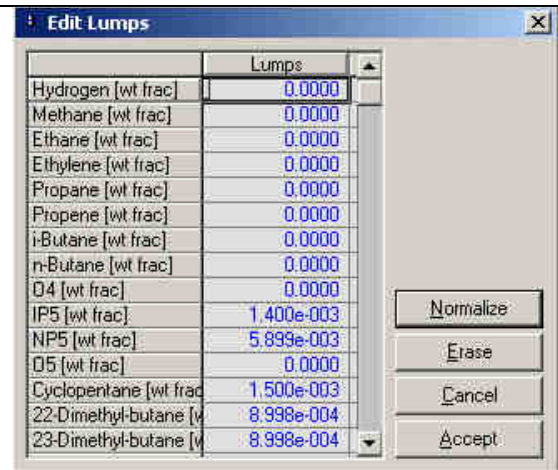


Figure 5.38: Enter Lump Composition
(After Normalization)

5.9 Workshop II: Model calibration

In section, we will calibrate the model based on known product yield and reactor performance.

Calibration involves four distinct steps:

1. Pulling data from current simulation
2. Enter measured process yields and performance based on that current simulation
3. Update the activity factors to match this plant yield and performance
4. Push calibration data back to the simulation

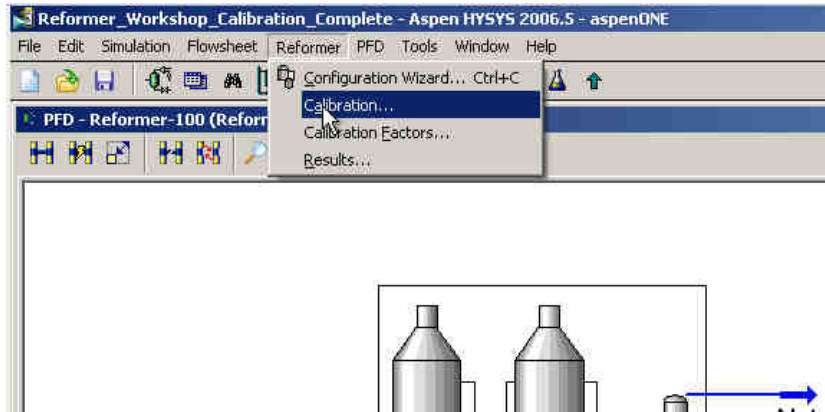


Figure 5.39: Starting the Reformer Calibration Environment

We begin the first step of model calibration procedure using a converged initial model. The converged initial model will provide initial guesses for the activity factors which greatly simplifies the model calibration procedure. We enter the model calibration environment by first entering the reformer sub-flowsheet and then selecting the “Reformer > Calibration” menu option from the application menu bar (as shown in Figure 5.39). Figure 5.40 shows the reformer calibration environment.

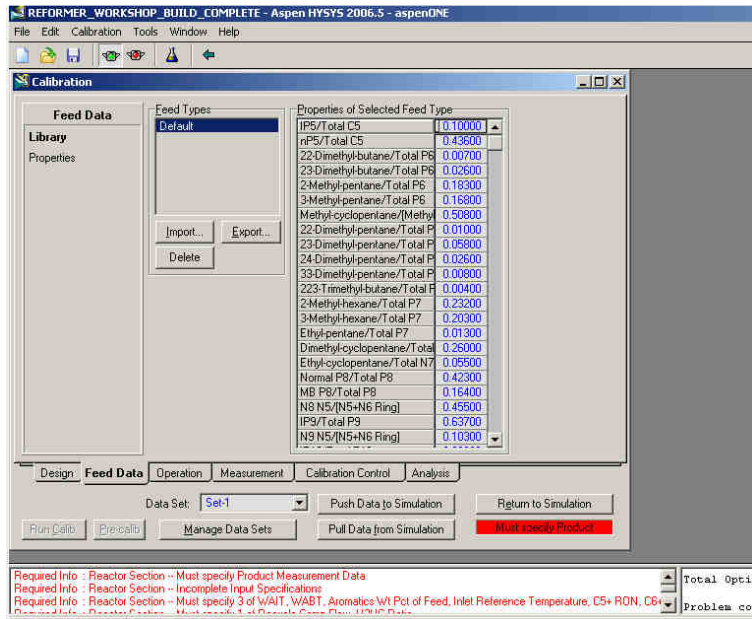


Figure 5.40: Reformer Calibration Environment

The first step is to “Pull data” from the simulation. When Aspen HYSYS pulls data, current operating conditions, feed stock information and process parameters enter the reforming environment. A Calibration refers to the set of the activity factors that produce a given product yield and reactor performance (which we provide to the calibration environment) based on current model state. We pull data by click on the “Pull Data from Simulation” button (Figure 5.41).

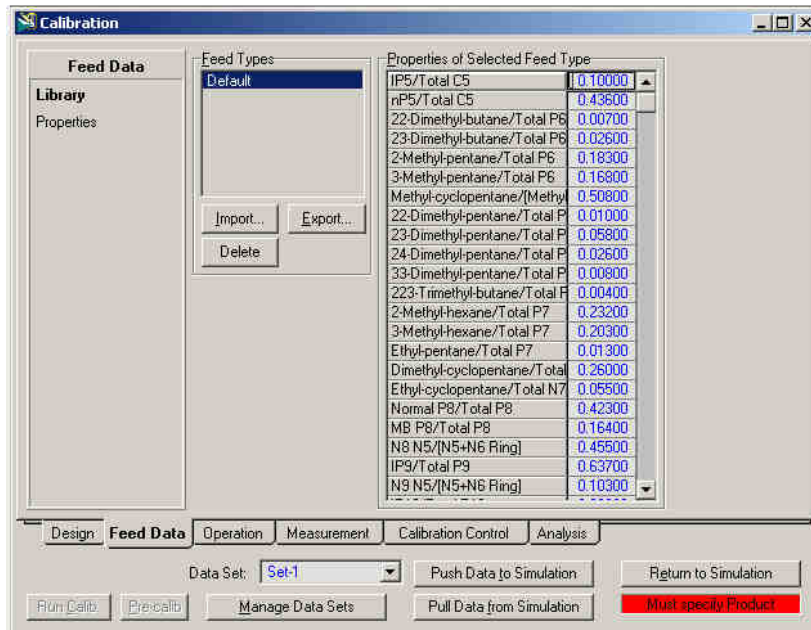


Figure 5.41: Pull Data from model results

When we pull data from the simulation, Aspen HYSYS will warn us that current calibration data will be overwritten by the current model results as shown in Figure 5.42. We can use the Data-Set feature (in Figure 5.43) to allow multiple calibration data-sets. This may be useful if the industrial reformer runs under very different operating scenarios. However, we for the purposes of this workshop, we will use only one calibration data-set.

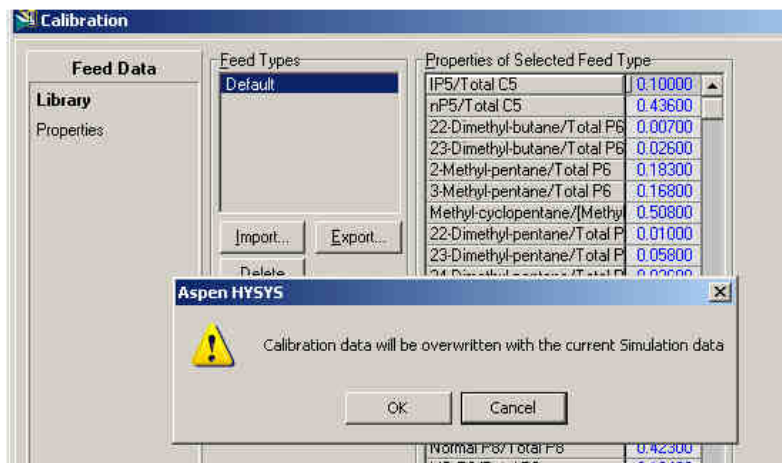


Figure 5.42: Importing initial model solution

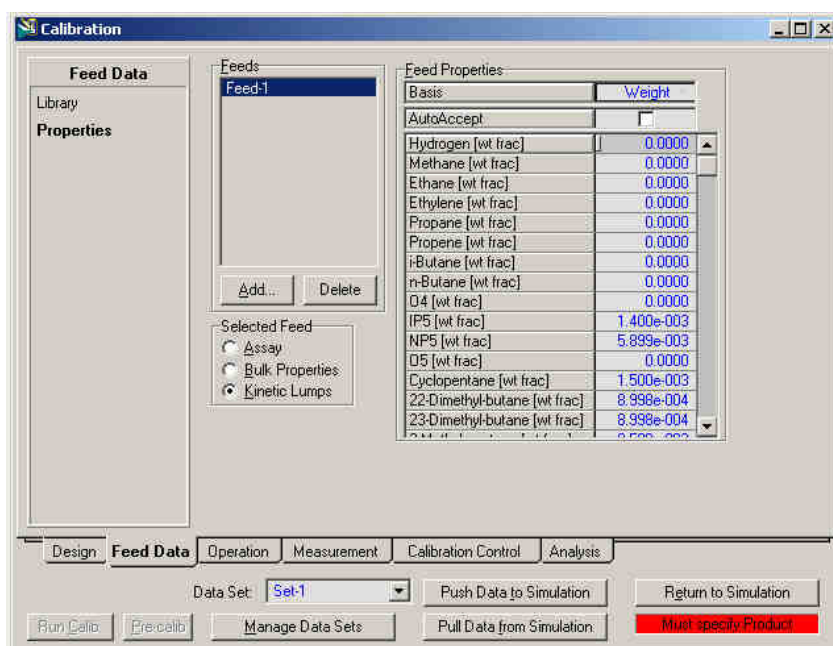


Figure 5.43: Feed composition on weight basis

Aspen HYSYS will pull all the feedstock information and process operating after we confirm the calibration data overwrite. The status bar now indicates that we must specify product

measurements to begin the calibration process. If necessary, we can modify the operating variables (such as WAIT, etc.) of the reformer in addition to the measured values. However, we recommend creating a new model file if the operating scenarios are very different.

The second step in model calibration is specifying the measured yields and process performance. Click on the Measurement Tab to bring up the Operation interface (see Figure 5.44). In the Operation section, we must enter values for reactor temperature drop and recycle hydrogen purity. We can enter in the pressure drops and measure octane values of the product. The default values come from the current model results. Entering new pressures drops allows us to account for unexpected flow behavior in the reforming reactors. Figure 5.45 shows the complete input window for the Operation Section.

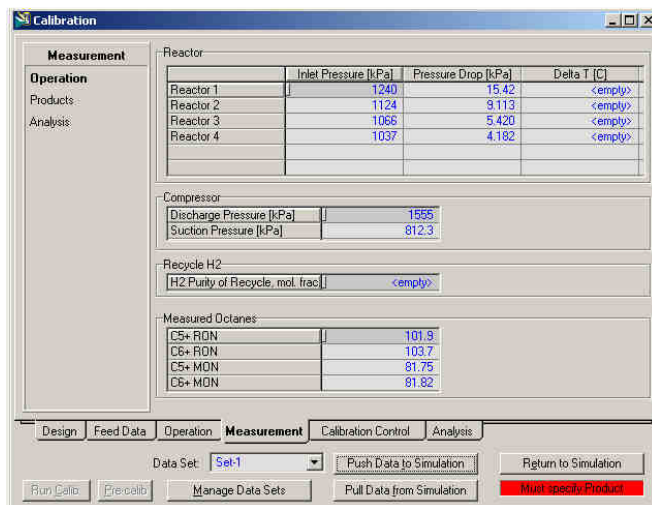


Figure 5.44: Reactor Performance Tab

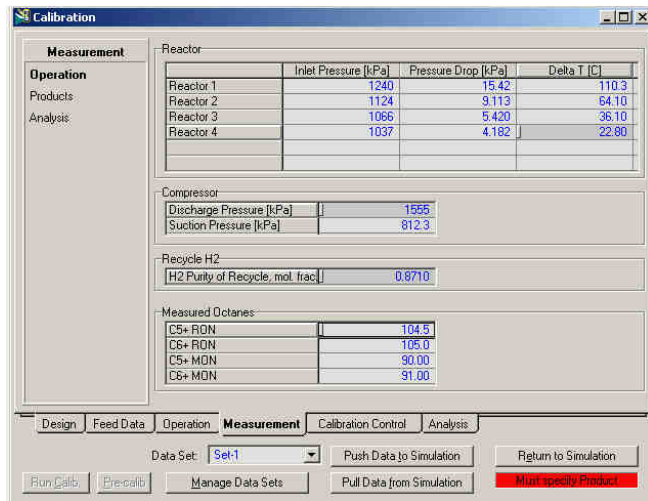


Figure 5.45: Completed Reactor Performance Tab

Next we specify the flow rates, yields and composition of all the key streams from the reformer. A compositional analysis is necessary make sure that we model key reaction paths accurately. We recommend that users enter all compositional information for gas streams in Mol% and all compositional information for liquid streams in Vol. % or Weight%. Given the data available, we can enter the flow rates of each steam on a gas flow or mass flow basis. We note that internally, Aspen HYSYS will convert all measurements into a Mol.% to ensure overall material balance in the model results.

	Net H2	H2 to Fuel	Stab OH Vapor	Stab OH Liquid	Reformat	Total
Gas Rate [STD_m3/h]	7.921e+004	0.0000	3393	9829	3.309e+004	1.255e+005
Liquid Rate [m3/h]	104.3	0.0000	8.639	39.86	171.9	324.7
Mass Rate [kg/h]	1.242e+004	0.0000	3284	2.172e+004	1.436e+005	1.810e+005
RON					105.1	
MON					102.0	
Composition	Mol%	Mol%	Mol%	Vol%	Wt%	Wt%
H2 [%]	94.06	87.10	44.38	0.66	0.00	3.59
P1 [%]	2.40	2.67	6.98	0.44	0.00	0.83
P2 [%]	1.78	2.87	18.29	8.29	0.00	2.08
OL2 [%]	0.00	0.00	0.00	0.00	0.00	0.00
P3 [%]	1.10	3.22	18.46	28.32	0.00	4.71
O3 [%]	0.00	0.01	0.00	0.12	0.00	0.01
IP4 [%]	0.31	1.42	5.82	20.32	0.00	3.12
NP4 [%]	0.19	1.12	3.79	18.02	0.00	2.70
O4 [%]	0.00	0.00	0.00	0.26	0.00	0.03
IP5 [%]	0.11	1.02	1.64	15.95	0.00	2.43
NP5 [%]	0.05	0.57	0.59	7.62	0.00	1.16
O5 [%]	0.00	0.00	0.05	0.00	0.00	0.00
SN5 [%]	0.00	0.00	0.00	0.00	0.25	0.19
MBP6 [%]	0.00	0.00	0.00	0.00	2.36	1.88
SBP6 [%]	0.00	0.00	0.00	0.00	2.36	1.88
NP6 [%]	0.00	0.00	0.00	0.00	2.36	1.88
IP6 [%]	0.00	0.00	0.00	0.00	0.00	0.00

Figure 5.46: Product measurement tab

We suggest a few guidelines when entering compositional data:

- If analysis for H2 to Fuel stream is not available, we can enter 85-87 mol% H2 as the composition for the stream
- Measurements for the Stabilizer overhead liquid can often be confused. Often there is little difference in the model results if we choose Mol. % or Vol. % for the original data. The molar volumes of these light components are roughly similar, so errors due to mistaken Mol. % or Vol% are often quite small.
- If we do not have of all isomer of a given kinetic lump (such as P8, SBP8, MBP8, etc.) then it is possible to distribute the total measured lump over the three components. However, we must make sure not to include isomer ratio as a calibration activity factor. This comment does not apply to xylenes. We must have the isomer ratio of xylenes to proceed with the calibration.

- We can group the aromatics higher than 9 into a single lump as A10. This is acceptable since we will not calibrate on aromatics higher than A9 and allow the model to calculate aromatic composition higher than A9 freely.

Once we enter the composition information correctly, the status bar will turn yellow (see Figure 5.46), indicating that we are ready to begin varying activity factors.

In Step 3 of the calibration, we will use Aspen HYSYS to vary several activity factors in order to minimize the objective function. We define the objective function as the weighting sum of the absolute deviations from the model prediction and measure data. We can select terms in the objective function by going to the “Objective” section of the Calibration Control Tab. We show this interface in Figure 5.47.

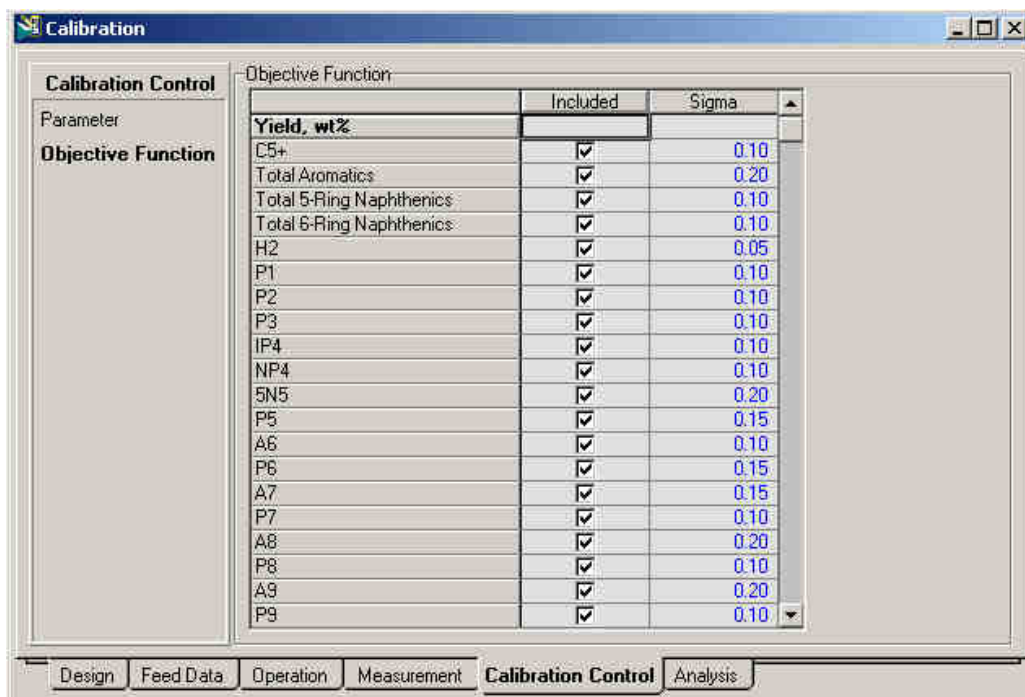


Figure 5.47: Initial objective function

The initial objective function is quite strict and requires significantly detailed analysis use for calibration purposes. We suggest an alternative objective function that works well when the compositional analysis is limited. In addition, less strict objective function helps make sure that the model does not become fixed or overcalibrated to a single data set.

Table 5.7: Weighting factors for less strict objective function

Model prediction	Weight
C5+ Yield	0.10
Total Aromatic Yield	0.20
H2 Yield	0.05
P1 Yield	0.10
P2 Yield	0.10
P3 Yield	0.10
IP4 Yield	0.10
NP4 Yield	0.10
5N5 Yield	0.20
P5 Yield	0.15
A6 Yield	0.10
P6 Yield	0.15
A7 Yield	0.15
P7 Yield	0.10
A8 Yield	0.20
P8 Yield	0.10

A9 Yield	0.20
A10 Yield	0.20
P10 Yield	0.10
Recycle Gas Purity	0.01
Reactor 1 ΔT	0.75
Reactor 2 ΔT	0.75
Reactor 3 ΔT	0.75
Reactor 4 ΔT	0.75

Terms that do not appear in Table 5.7 are not part of the initial calibration. Low weightings indicate that agreement with a given term is more significant than other terms. We generally do not include isomer ratios as part of the initial calibration. Once we have completed an initial calibration, we use another data set to further calibrate the model using the original strict objective function. For the purposes of this workshop, we will perform the calibration only once.

Once we select the objective function, it is good practice to run a model pre-calibration. The model pre-calibration ensures that we are starting the model the in a feasible location and indicates if the calibration process will succeed. We run the pre-calibration by clicking the “Pre-Calib” button in the calibration environment (Figure 5.48).



Figure 5.48: Pre-Calibration in the Reformer Calibration

When we run the Pre-Calibration of the model, Aspen HYSYS presents the Validation Wizard for this data set. The key results in this wizard are Mass and Hydrogen closure of this dataset. Figure 5.49 shows initial state of the wizard. We note that there is a significant Mass and Hydrogen imbalance. We can attempt to correct error by changing the bias for each stream. The biases refer to how the stream flow will be adjusted to ensure that Mass and Hydrogen balance is closed. Figure 5.50 shows that we can improve the imbalance by unselecting the bias for the reformat.

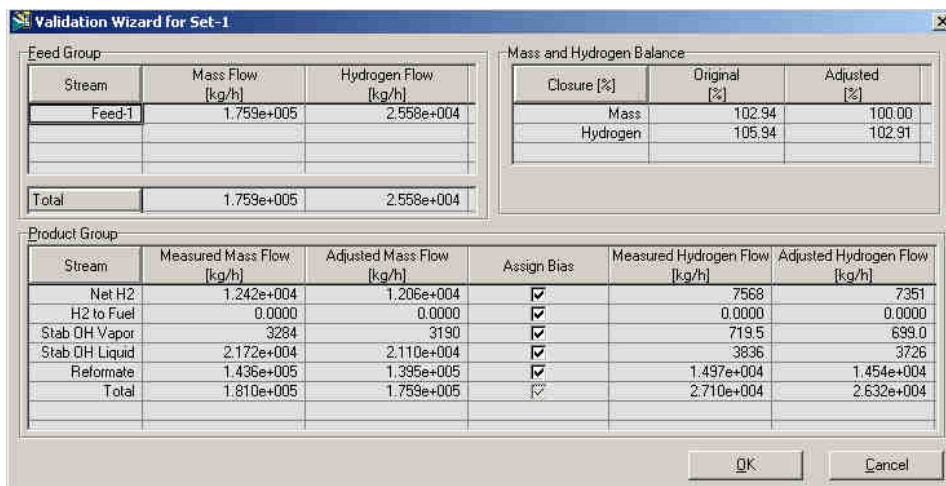


Figure 5.49: Assign Bias

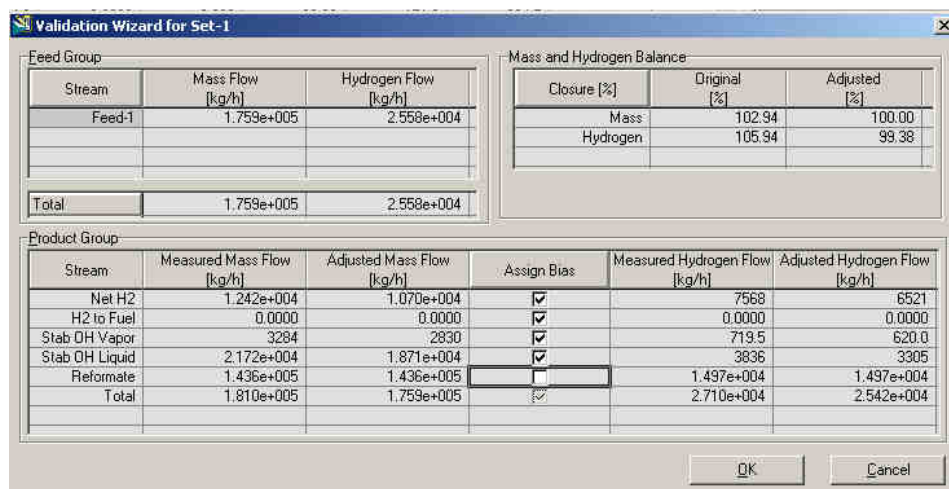


Figure 5.50: Assign Bias – Select Reformate

Changing the Assign Bias does not mean that calibration will improved. Significant mass and hydrogen imbalance indicates that the dataset may be inconsistent. The first resort to verify the measurement data and obtain updated measurements if necessary. If we cannot close the mass balance, we can proceed with calibration. However, we must realize that a close calibration may not be possible and we must view model prediction with extra caution.

The next step is to choose model activity factors to vary during the calibration run. We select activity factors by navigating the to the Parameter section of the Calibration Control Tab (Shown in Figure 5.51). To include a factor in the calibration, we must check the “Included box” for that factor and specify an upper and lower bound for that factor as shown in Figure 5.52. The bounds for the upper and lower factor must reasonable to avoid overcalibrating the model. We discuss upper and lower bounds for kinetic factors in a previous chapter. Table 5.8 also presents some reasonable upper and lower bounds for the most common activity factors.

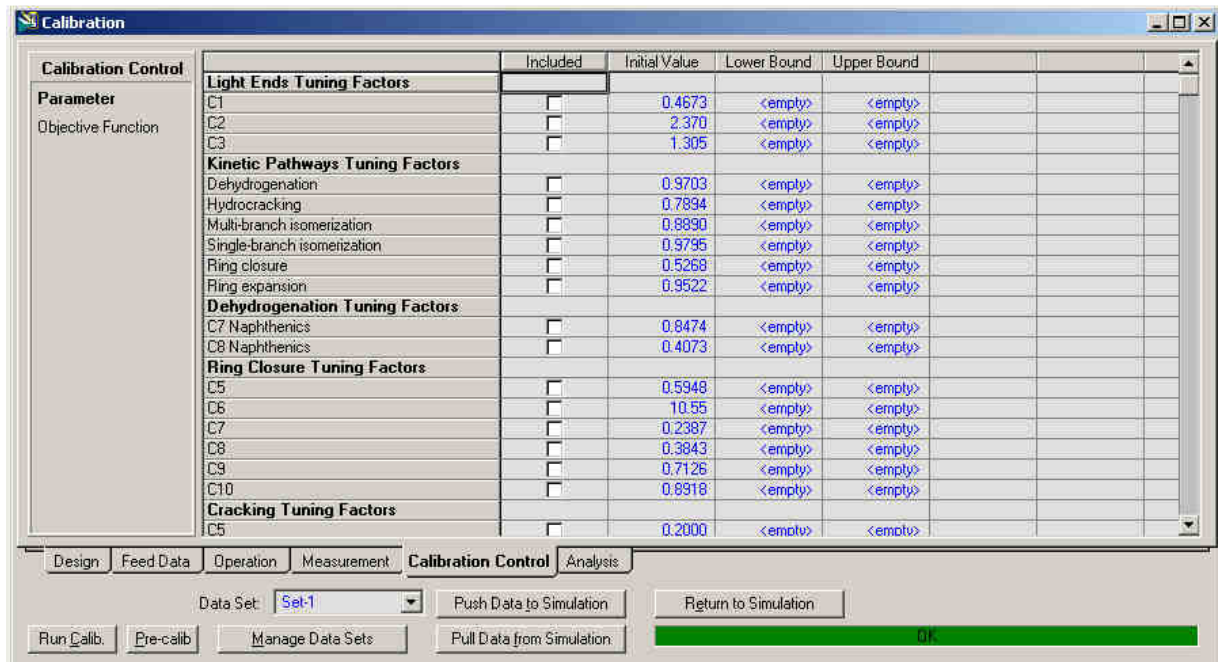


Figure 5.51: Calibration-Parameters

Global Activity Tuning Factors				
Reactor 1	<input checked="" type="checkbox"/>	4.063	0.1000	10.00
Reactor 2	<input checked="" type="checkbox"/>	1.140	0.1000	10.00
Reactor 3	<input checked="" type="checkbox"/>	0.6065	0.1000	10.00
Reactor 4	<input checked="" type="checkbox"/>	0.3051	0.1000	10.00

Figure 5.52: Set upper and lower bounds for global activity tuning factors

We calibrate the model by selecting each group of factors in Table 5.8 one at a time and subsequently run the for each group selection. For example, when we calibrate the model for the first time, we should select the Global Activity Tuning Factors and enter the appropriate bounds from Table 5.8 (Figure 5.52). Then we will click on Run Calib. to start the optimization process.

We will run the process at least 5 times, selecting a different group to calibrate each time.

The output from the solver appears in

Table 5.9. Our goal is to reduce the value final of column 4, “Objective Function Value” to some small value. For an accurate calibration, the objective function should be lower than 250-300 using the weightings given in Table 5.7.

Table 5.8: Suggested activity factors for calibration

Group #	Terms	Range
1	Global Activity Tuning Factors	1-200
2	Dehydrogenation and Hydrocracking Tuning Factors	0.1-1
3	Isomerization, Ring Closure and Expansion Tuning Factors	0.1-1
4	Individual Tuning Factors for C7, C8	0.1-1
5	Light gas yield (C1 and C2 only)	0.1 – 10

Table 5.9: Solver output during calibration

Iteration	Residual Convergence Function	Objective Convergence Function	Objective Function Value	Overall Nonlinearity Ratio	Model Nonlinearity Ratio	Worst Model
0	2.604D-09	5.887D-01	7.186D+03	8.662D-01	3.174D-01	PSEP
	<Line Search Creep Mode ACTIVE> ==> Step taken 3.00D-01					
1	1.298D-03	1.168D+00	6.087D+03	4.749D-01	-1.653D+01	RECV
	<Line Search Creep Mode ACTIVE> ==> Step taken 3.00D-01					
2	9.571D-03	2.573D+00	4.624D+03	-1.015D+00	-5.052D+01	PRODHTR
	<Line Search Creep Mode ACTIVE> ==> Step taken 3.00D-01					
	<Line Search ACTIVE> ==> Step taken 7.44D-02					
3	7.210D-03	2.068D-01	3.981D+03	9.750D-01	7.025D-01	RXR4.RXHTR
	<Line Search Creep Mode ACTIVE> ==> Step taken 3.00D-01					
4	4.288D-03	1.795D-01	3.761D+03	9.610D-01	7.275D-01	RXR4.RXHTR
	<Line Search Creep Mode ACTIVE> ==> Step taken 3.00D-01					
5	3.513D-03	9.406D-02	3.589D+03	8.233D-01	3.467D-01	PRODHTR

6	3.792D-03	6.084D-02	3.361D+03	6.239D-01	-1.330D+00	RXR4.RXHTR
7	1.027D-03	1.863D-03	3.239D+03	9.845D-01	1.421D+00	
8	4.122D-05	3.809D-04	3.247D+03	9.691D-01	7.403D-01	
9	2.321D-06	6.648D-05	3.246D+03	9.129D-01	4.952D-01	
10	9.317D-07	3.307D-06	3.246D+03			

Successful solution.

Optimization Timing Statistics	Time	Percent
=====	=====	=====
MODEL computations	5.64 secs	8.19 %
DMO computations	61.99 secs	90.01 %
Miscellaneous	1.24 secs	1.80 %
-----	-----	-----
Total Optimization Time	68.87 secs	100.00 %

Problem converged

Each time we successfully run a calibration, we can verify how far model predictions are measured input values given to Aspen HYSYS. We go the Calibration Factors section (see Figure 5.53) in the Analysis Tab of the Calibration Environment. The "Delta" column indicates the difference between the measured and model value for a given term of the objective function. Contribution indicates the given term's contribution to the objective function (Delta/Weighting). Using the steps in Table 5.8, we can reduce the objective function value to 180. This is below our 250-300 criteria for a reasonable model.

Once we finish calibrating the model to some small residual (<250-300) we should export the results back to the main reformer flowsheet. This is step 4, the last step, of the model calibration.

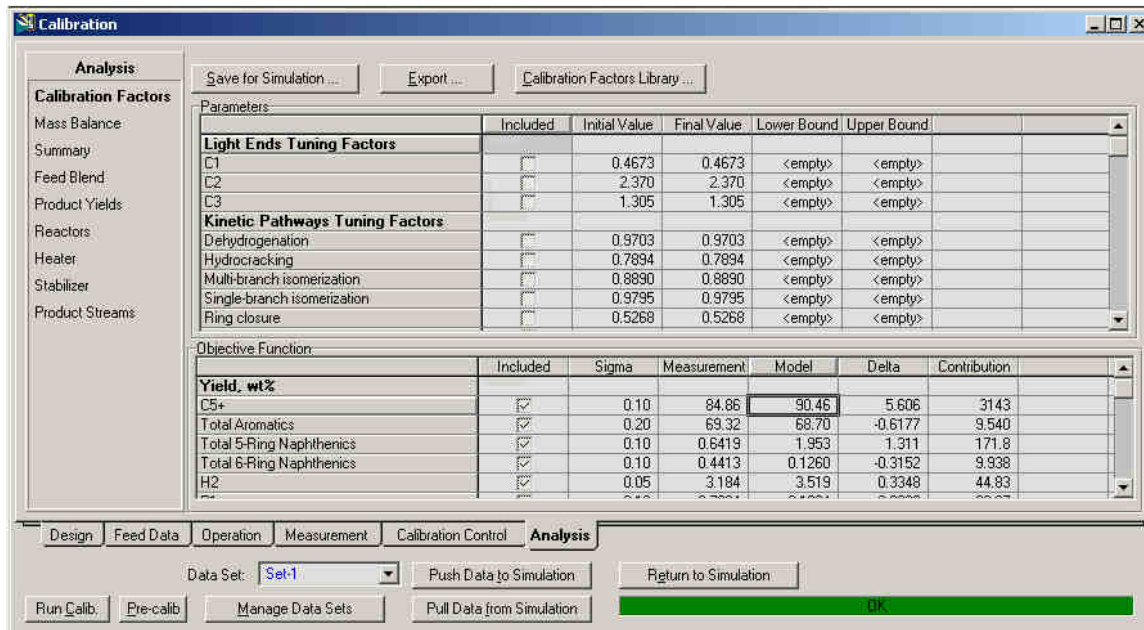


Figure 5.53: Calibration Factors-Analysis

We save the model calibration by clicking ‘Save for Simulation...’ in the Analysis tab of the Refomer Calibration Environment. Aspen HYSYS will prompt us (see Figure 5.54) to save this calibration as ‘Set-1’. We can have multiple calibrations for the same reformer and use different calibrations sets for different operating scenarios. We recommend only having only calibration set per reformer model file.

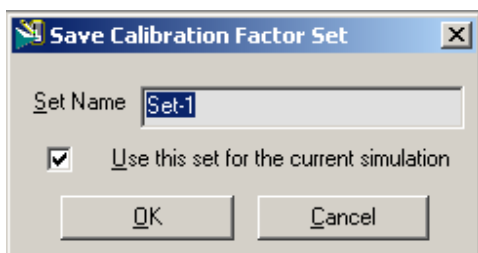


Figure 5.54: Save Calibration Factor Set

After saving the Calibration, we should put the solver in holding mode to make sure that Aspen HYSYS exported the calibration factors properly. We will return the Reformer Sub Flowsheet environment. We recommend that users go through each one of the tabs in Reformer Sub Flowsheet environment to make sure the input data has not changed. It is also important to make sure that basis for the Kinetic lumps is same as what was chosen initially (In this work, we always use Wt.%, see Figure 5.56). We can release the solver to allow Aspen HYSYS to solve the model as shown in Figure 5.55.

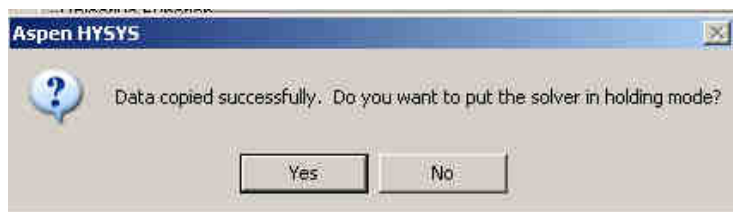


Figure 5.55: Prompt to hold Aspen HYSYS solver

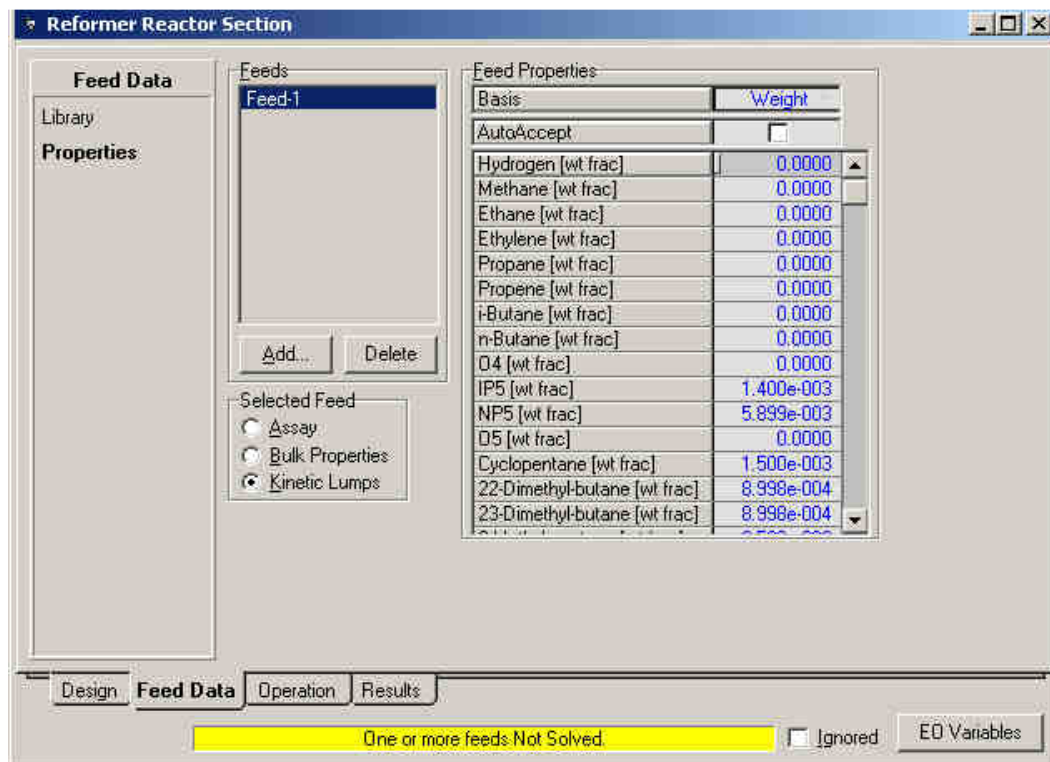


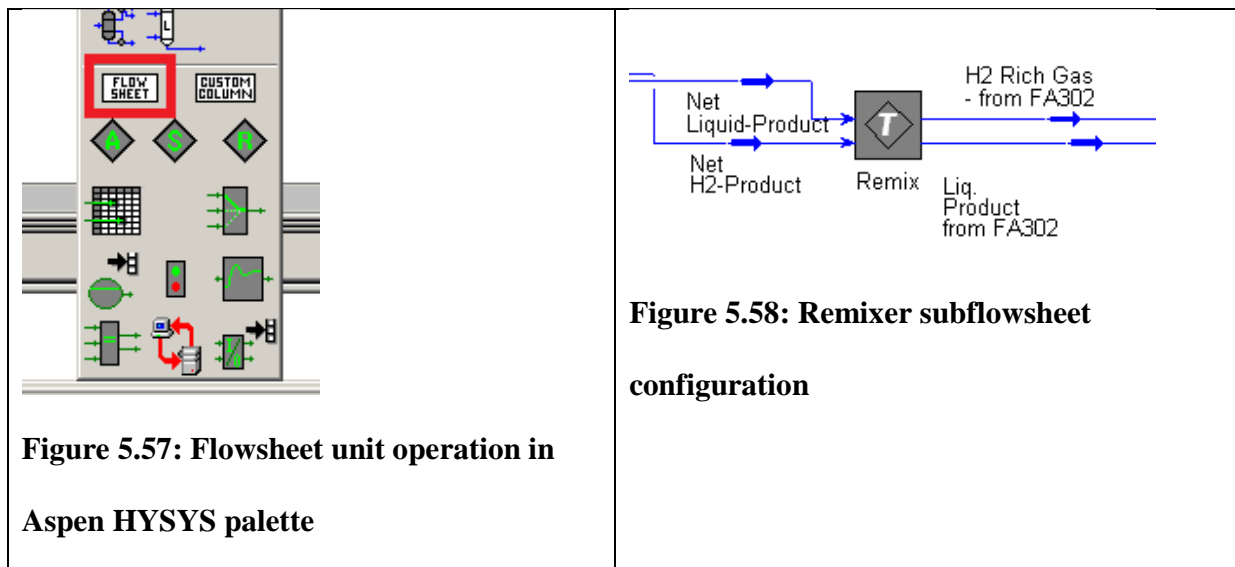
Figure 5.56: Verify feed basis for Feed Data

We return to the main flowsheet to complete the calibration process for the Reformer Model.

5.10 Workshop III: Build a downstream fractionation

The next step is to build downstream fractionation system. The downstream fraction for this CCR reformer has three distinct steps:

1. Product remixer
2. Hydrogen recontactor
3. Primary Gasoline/LPG Stabilizer and Aromatics recovery



We build a sub flowsheet environment for the product remixer by returning to the main flowsheet and creating a sub flowsheet. We create a sub flowsheet using the “FLOWSHEET” icon in the Aspen HYSYS toolbar palette shown in Figure 5.57. The new subflowsheet appears in on the main flowsheet as large icon with “T” marker. We can double click the icon to bring up the subflowsheet connections window.

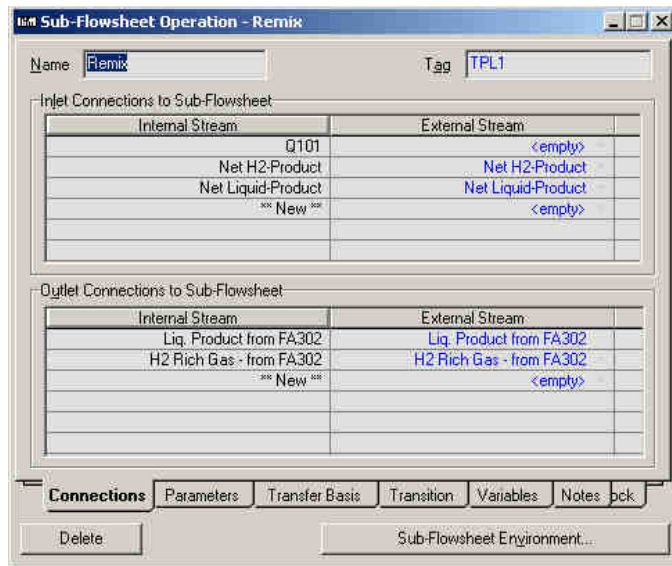


Figure 5.59: Inlet-Outlet connections for Remixer subflowsheet

We attach the inlet connections to the sub-flowsheet and begin building the internal structure of the sub-flowsheet. We will attach the outlet connections once we have completed building the flowsheet.

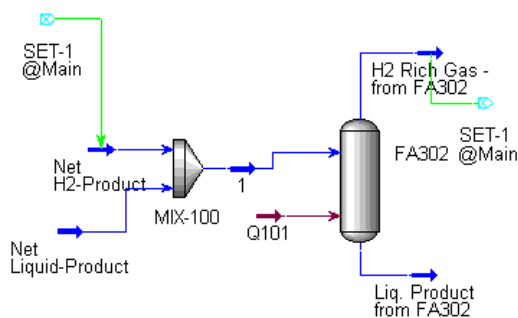


Figure 5.60: Subflowsheet for Remixer

Using the standard Aspen HYSYS objects, we build a simple mixer and separator to remix the product streams and flash the mixed product at the temperature and pressure of the primary product separator. The outlet gas from FA302 represents the initial release of net gas. We use a

Set object to ensure the temperature of the flash is the same as the Net H2 product from the reformer model. Once we finish building this sub-flowsheet, we can connect outlet feeds as shown in Figure 5.61.

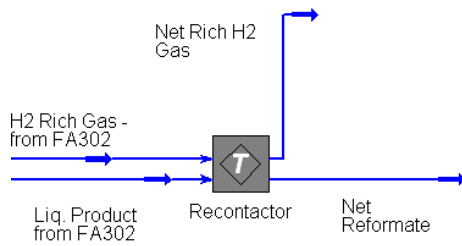


Figure 5.61: Subflowsheet for Recontactor

We now proceed to building the hydrogen recontacting section of the fractionation system. Using the same procedure as before, we create a subflowsheet for the Recontactor. The goal of the recontacting section is improve separation of the light ends from the net gas stream and recover aromatics lost in the initial net gas stream. Figure 5.62 shows the relevant inlet and outlet stream names and variables for the subflowsheet.

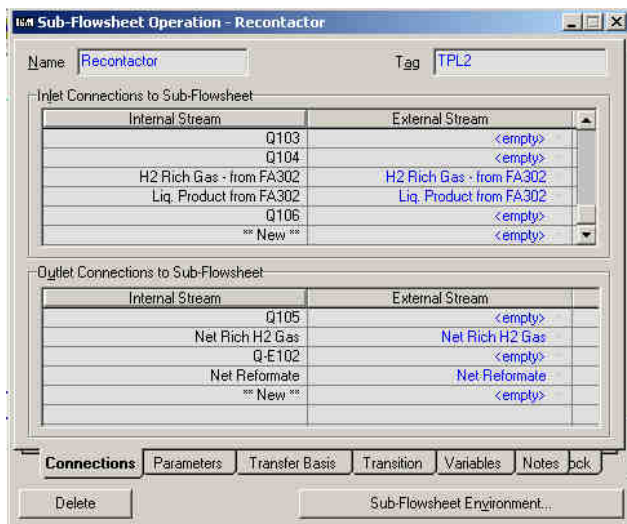


Figure 5.62: Subflowsheet for Recontactor

6	10.11	-
13	30.00	-
Net Rich H2 Gas	-	5681

Before the Net Liquid enters the gasoline stabilizer, we must heat the product to a temperature suitable for fractionation. In the actual refinery process, the product heater is often integrated with the bottoms outlet of the gasoline splitter or other columns. However, for the purposes of this simulation we use a simple heat exchanger instead. For more detailed simulations, we advise the use of cross exchangers to accurately model the model the duty required for the fractionation.

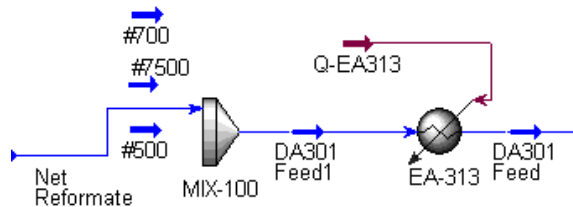


Figure 5.64: DA301 Preheater

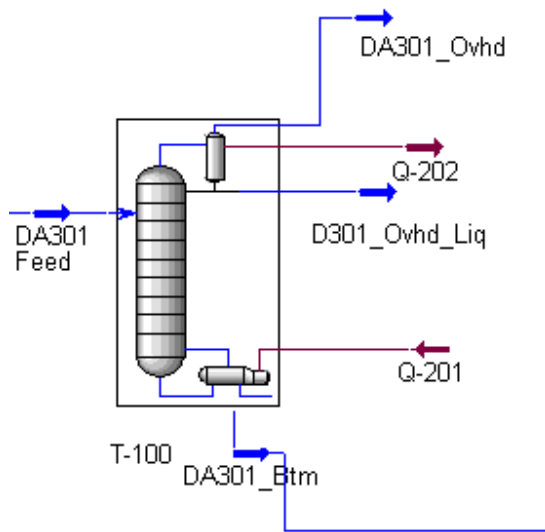


Figure 5.65: DA301 Flowsheet

Figure 5.65 shows the stream configuration for the primary gasoline stabilizer. The overhead gas contains mostly light C1-C2 components that did not leave the Net H2 stream. The overhead liquid draw is mostly C3-C4 components which form an LPG like stream. The bottoms stream represents the stabilized gasoline or aromatic enriched liquid product from the reformer.

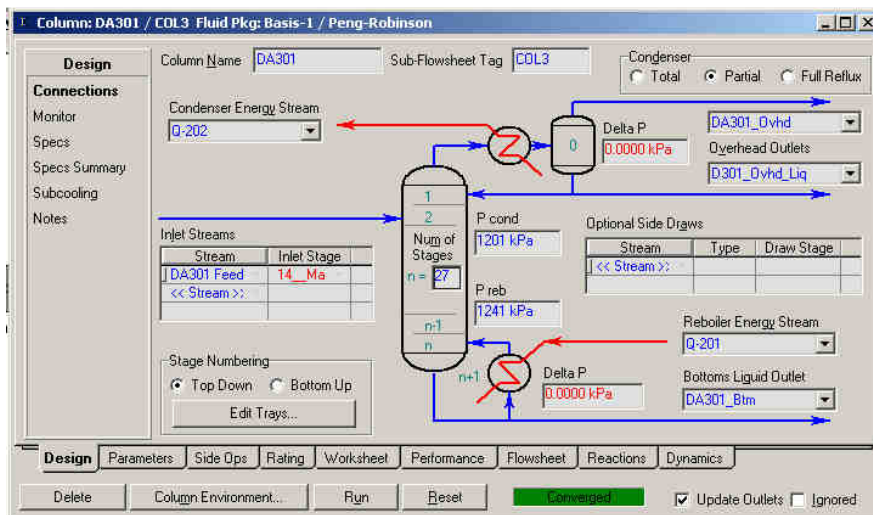


Figure 5.66: DA301 Configuration

We show the pressure profile and number of stages required for the gasoline splitter in Figure 5.66. We note that use a fewer number of stages than the industrial process. We use this approach to approximate the column's overall efficiency at 50-60%. We discussed the advantages of overall column efficiency over stage-by-stage efficiencies in Chapter 2. In general, using the overall column efficiency approach leads to more robust and predictable column model operation.

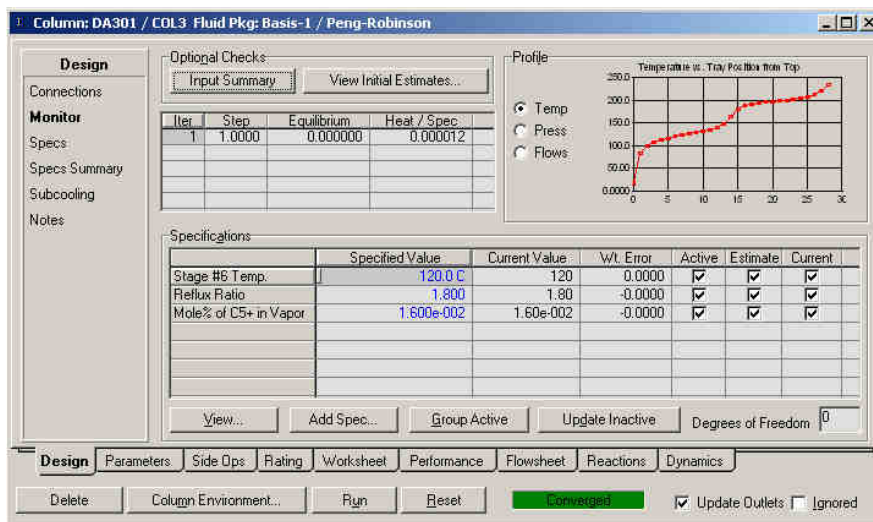


Figure 5.67: DA301 Specifications

Since we have three draw streams on DA301 we will require 3 independent specifications for the column to converge robustly as shown in Figure 5.67. Typically, we will use the reflux ratio, temperature of a particular stage and mole purity (either C4 or C5 in the overhead liquid or vapor) as specifications for the column. If the column is operating as a gasoline splitter, we may want to use the Reid Vapor Pressure (RVP) of the bottoms as a performance specification. If the column does not converge, we can use the alternate specifications of overhead draw rate, reflux ratio and bottoms draw to ensure that the column converges to a solution. Once we have a solution, it is quite easy to converge on a performance specification.

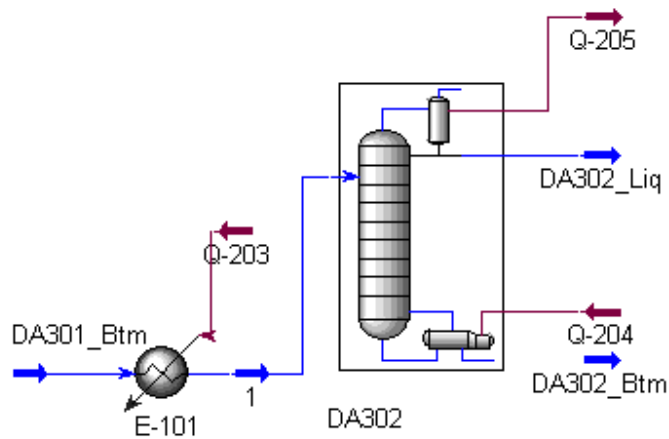


Figure 5.68: DA302 Flowsheet

Since this reformer is part of a petrochemical complex, the product from the gasoline splitter enters an aromatics fractionation column. Column DA302 (see Figure 5.68) separates toluene and lighter components from xylenes and heavier components. The bottoms product of DA301 enters a heat exchanger to bring down the temperature of the gasoline product to a suitable fractionation temperature.

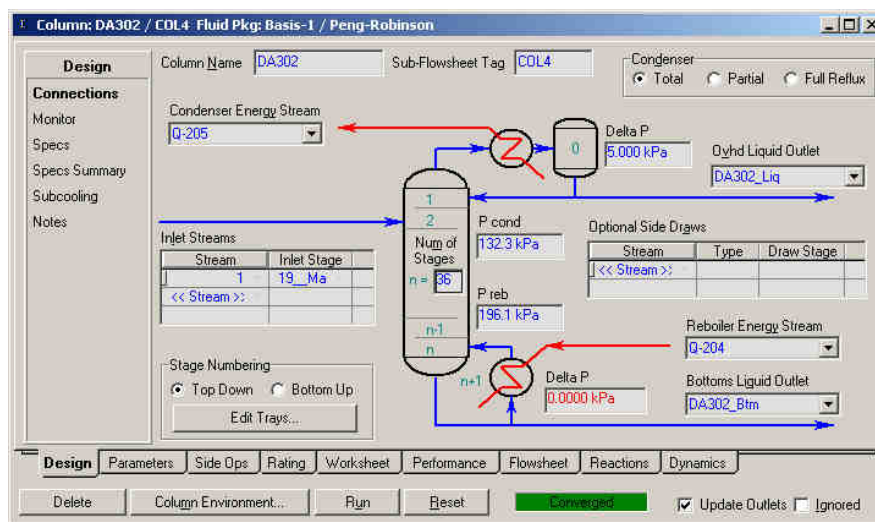


Figure 5.69: DA302 Column configuration

Figure 5.69 shows the pressure profile and number of stages required for the aromatics column. Again, we use the same principle of overall column efficiency (60-70%) to calculate the number of ideal stages required for the column model. We note that the industrial columns may include a small vent stream in the condenser for this column. However, depending on the thermodynamic model chosen, the feed to DA302 may not contain any light components. If we create a vent stream, it is likely that the column will have difficulty converging since we expect the vent stream to be a very small.

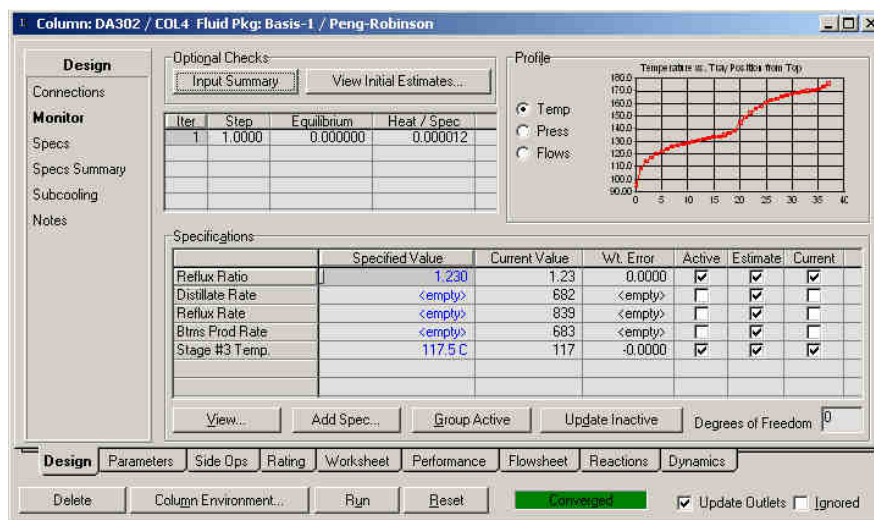


Figure 5.70: DA302 specifications for aromatic splitter

Since DA302 has two draws in the column, we will require two specifications. We typically run the column with the overhead draw rate and reflux ratio as the initial set of specifications (see Figure 5.70). Once we have a converged solution, we can use stage temperature as a performance specification to match plant operation.

5.11 Workshop IV: Case study to vary RON and product distribution profile

In this section, we will use the calibrated model to perform a case study to determine operating conditions to produce a desired product yield. The composition of the feed to the reformer may change quickly, and the composition of lighter naphthenes (N5, N6) can change dramatically with the changes to the IBP of the feed. In the earlier chapter, we discussed several situations that change the product yield with changes in operating conditions and feedstock composition. The most basic, yet useful, case study is to vary the reactor temperature and H₂/C ratio and the effect on product RON and aromatic yields.

We developed the initial model using Reactor Inlet Temperature and associated temperature biases for each reactor. This is useful for a specific reformer plant; however this method can mask the effect of reactor temperature on the process. We will instead use the WAIT to control to the reactor temperature.

We change the reactor to the WAIT basis by first holding the solver and prevent it from running while we change the reactor temperature. We note the calculated WAIT from the current solution and copy the value. We paste the value back into the WAIT textbox and release the solver. The solution process should be quite quick with the initial residual on the order of 1e-3 or lower.

Higher residuals may indicate the model was overcalibrated or the model is very sensitive the operation conditions. In both cases, we will likely have to recalibrate the model with more recent data.

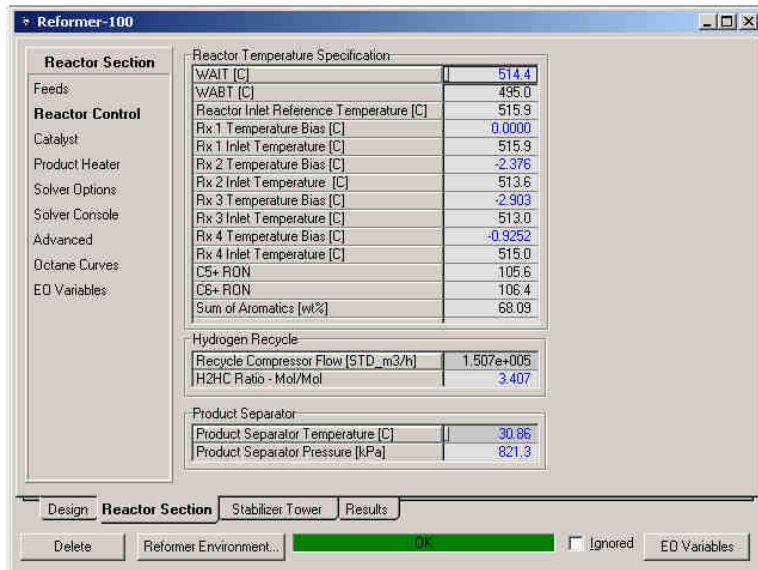


Figure 5.71: Change reactor temperature to WAIT basis

Our goal is to observe product yields as functions of the WAIT and H2HC ratio. It is possible to manually change each WAIT and H2HC ratio and re-run the model each time. However, given the typical run time for the Reformer solver, this quickly becomes a tedious process. It is better to use the Case Study features of Aspen HYSYS to automate this process. In addition, since the Case Study feature will run the model at a variety of conditions and if we successfully solved a model, we can make sure that the model is not overcalibrated.

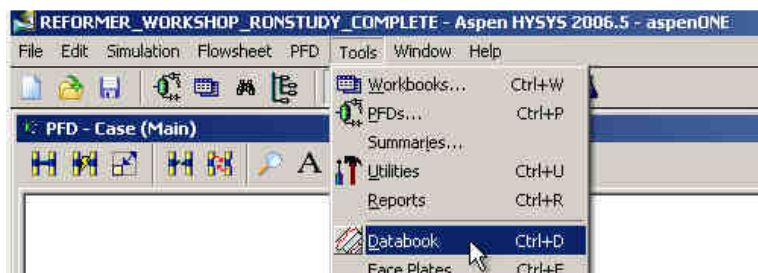


Figure 5.72: Menu to create case study through Databook interface

We create the case study using the Databook feature of Aspen HYSYS. Figure 5.72 shows the menu option from main flowsheet interface. The Databook interface is organized by Variables, Process Charts and Case studies. We must first add the variables we to observe or change into the Variables Tab. To add a variable, click 'Insert' to bring up the Variable Navigator. The Variable Navigator appears as shown in Figure 5.73.

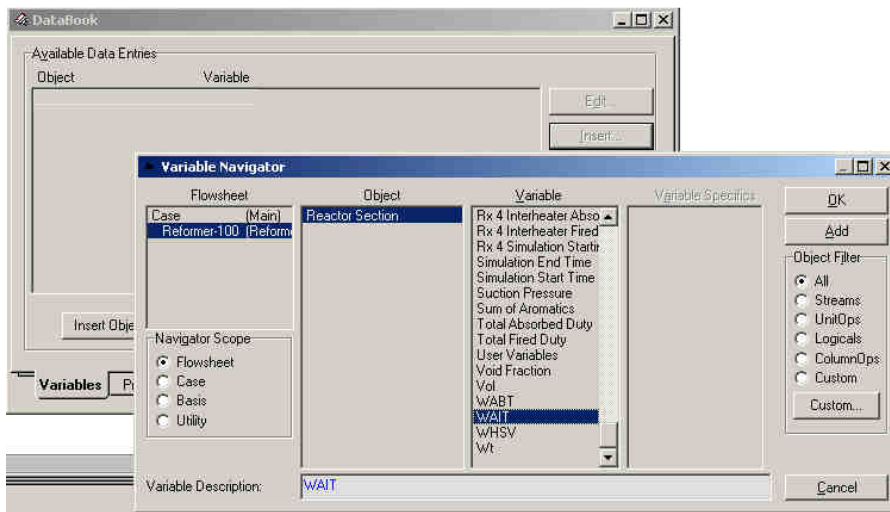


Figure 5.73: Variable Navigator for Reformer object

We add variables from the Reformer object, we select the Reformer object in the FlowSheet List. The Variable List will show all variables that belong to the Reformer object. We can scroll through this list and click 'Add' to add a particular variable to the Databook. When we have finished selecting all the variables we can click Cancel to return to the main Databook interface. Table 5.11 shows the variables we will need for this case study. Figure 5.74 shows the Databook after we add all key case study variables.

Table 5.11: Variables for RON case study

Variable	Type
----------	------

WAIT	Independent
C5+ RON and C6+ RON	Dependent
H2HC Ratio	Independent
Detailed Yields (Total Aromatics, Total C8 Aromatics)	Dependent
Detailed Yields (A6, A7)	Dependent
Detailed Yields (H2, P1, P2, P3)	Dependent

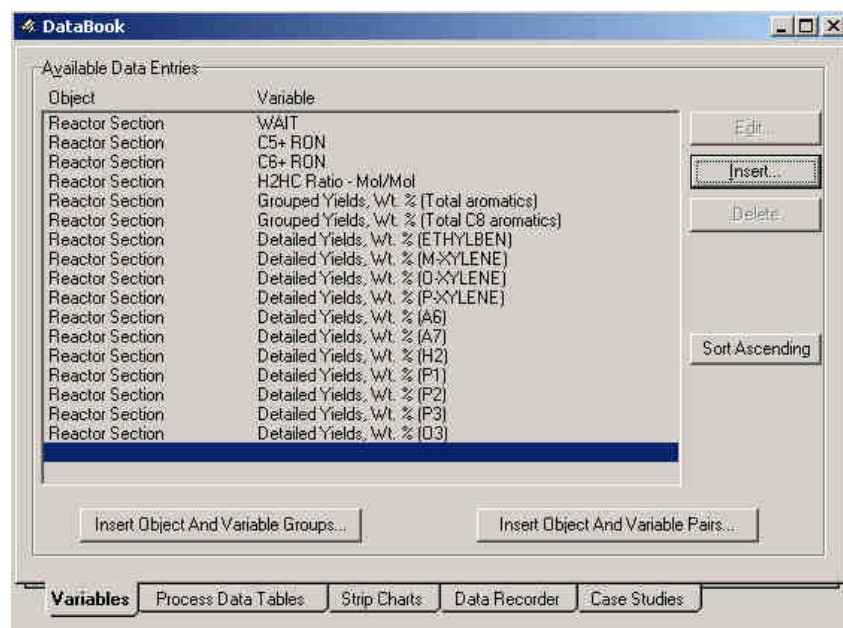


Figure 5.74: Databook after adding variables

We begin the case study by going to the Case Studies tab of the Databook. We can create and run multiple case studies with the Case Studies interface. To create a case study, we click 'Add' and Aspen HYSYS creates a new case study with the title 'Case Study 1'. We change this title by entering a new name in the textbox following the label 'Current Case Study'.

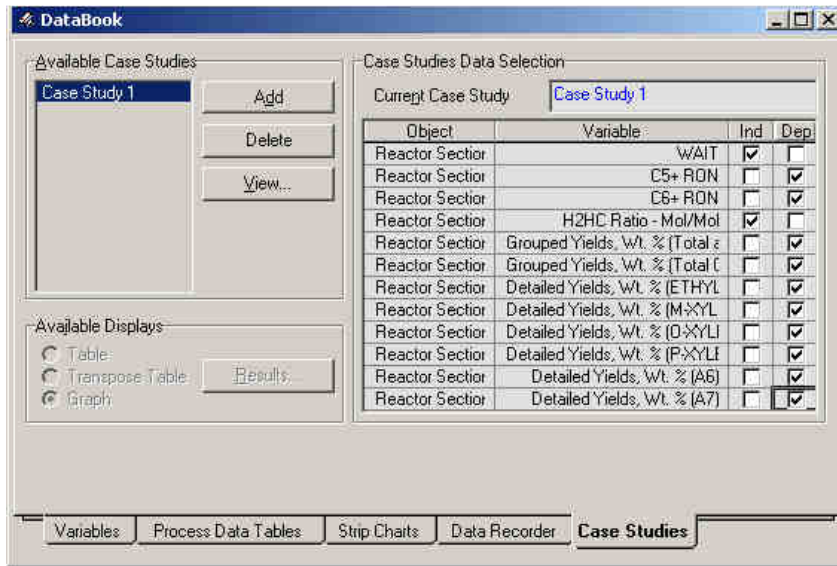


Figure 5.75: Selecting variable types for case study

Once we create the case study, we must select the variables that we will change in the course of the case study (Independent variables) and variables we want to observe (Dependent variables). Table 5.11 shows the type of each variable in this case study. In general, it is not possible to set product yields as independent variables. Aspen HYSYS issues an error if we cannot set a particular variable's type as independent.

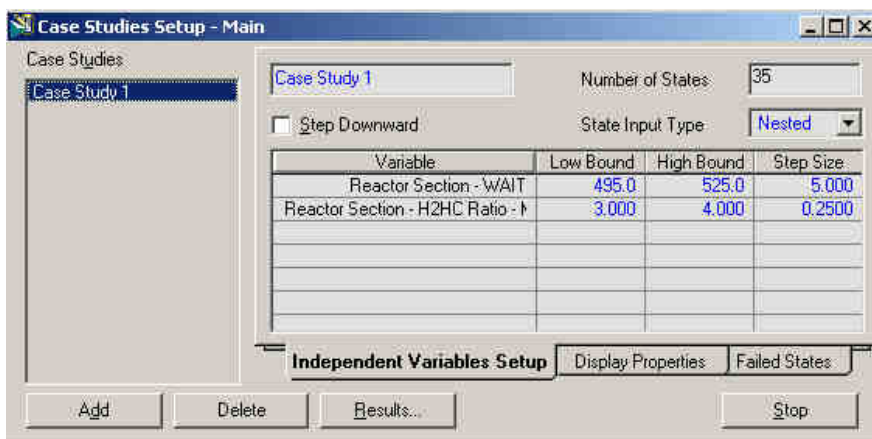


Figure 5.76: Case study setup

We click View to set the upper and lower bounds for the case study. We change the WAIT from 495 °C to 525 °C inclusively in 5 °C increments. We also change the H2HC ratio from 3.0 to 4.0 with an increment of 0.25. The number of states indicates how many times the Refomer model will run with various input. We generally advise against running more than 40-50 states at a time since the total run time for more than 50 states can be quite significant. In most cases, the reformer operating temperatures does not more than 10 °C or so during normal operation. We click on Start to begin running the case studies. We will observe the solver running in the lower right corner of the flowsheet.

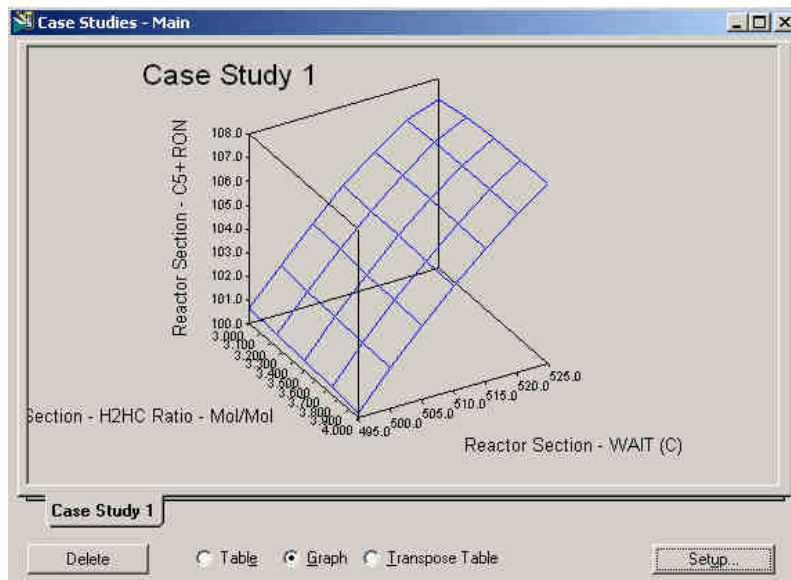


Figure 5.77: Graphical results of case study

Figure 5.77 shows the results of the case study. We can view this graph by clicking the ‘Results...’ button. The default is to show the Graph with the results of the case study. In general, we can see the general trend at the high reactor temperatures and low H2HC ratios increase the RON of the product. We can view the numerical results of the case study by selecting the ‘Transpose Table’ option. The results appear in the order of increasing WAIT and

H2HC ratio. Figure 5.78 shows the results table for this case study. We copy these results into Microsoft Excel and create the graphs in Figure 5.79 to Figure 5.82.

State	Reactor Section - WAH [C]	Reactor Section - H2HC Ratio	Reactor Section - C5+ R	Reactor Section - C6+ R	Yields, Wt. % (Total aro [%])
State 1	495.0	3.000	100.7	101.1	64.39
State 2	495.0	3.250	100.6	101.0	64.22
State 3	495.0	3.500	100.5	100.9	64.05
State 4	495.0	3.750	100.4	100.8	63.88
State 5	495.0	4.000	100.2	100.7	63.72
State 6	500.0	3.000	102.1	102.7	65.60
State 7	500.0	3.250	102.0	102.6	65.44
State 8	500.0	3.500	101.9	102.5	65.28
State 9	500.0	3.750	101.8	102.4	65.11
State 10	500.0	4.000	101.7	102.3	64.95
State 11	505.0	3.000	103.5	104.1	66.68
State 12	505.0	3.250	103.4	104.0	66.53
State 13	505.0	3.500	103.3	103.9	66.37
State 14	505.0	3.750	103.2	103.9	66.21
State 15	505.0	4.000	103.1	103.8	66.05

Figure 5.78: Numerical results for case study

When we graph the results using Microsoft Excel, we find several interesting trends in the data that not are readily apparent from the initial results graph and numerical results. The case study shows that as temperature increases, the RON and yield of aromatic products increases as well (Figure 5.79 and Figure 5.80). However, at around 520 °C for a H2HC ratio of 3.0, we find that the yield begins to drop. This is due to the increased deactivation of the catalyst at high temperature and low H2HC ratio. We observe that we can alleviate this situation by increasing the H2HC ratio.

An interesting side-effect of increasing the H2HC ratio is that around 520 °C, we will start to see marked increases in the production of light gases and hydrogen yield (Figure 5.81 and Figure 5.82). While initially, these increases appear small, they can have a significant effect on downstream fractionation. Excessive amounts of light gas can overload recycle compressors and increase the condensing duty requirements for stabilizing columns.

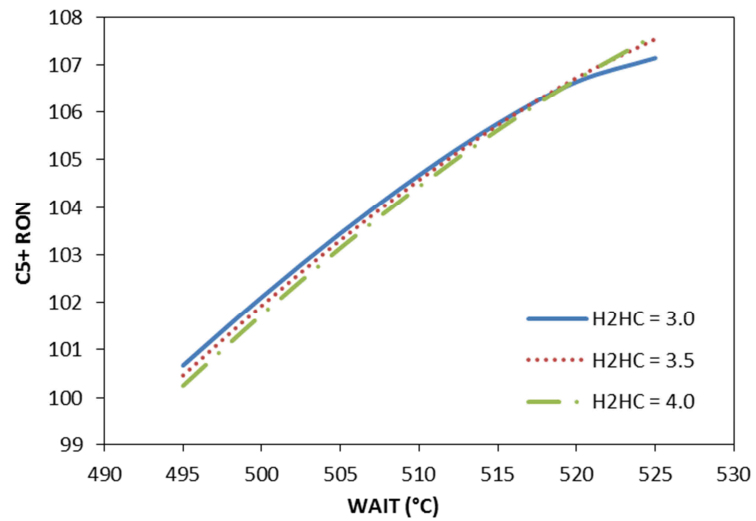


Figure 5.79: RON as a function of WAIT and H2HC ratio

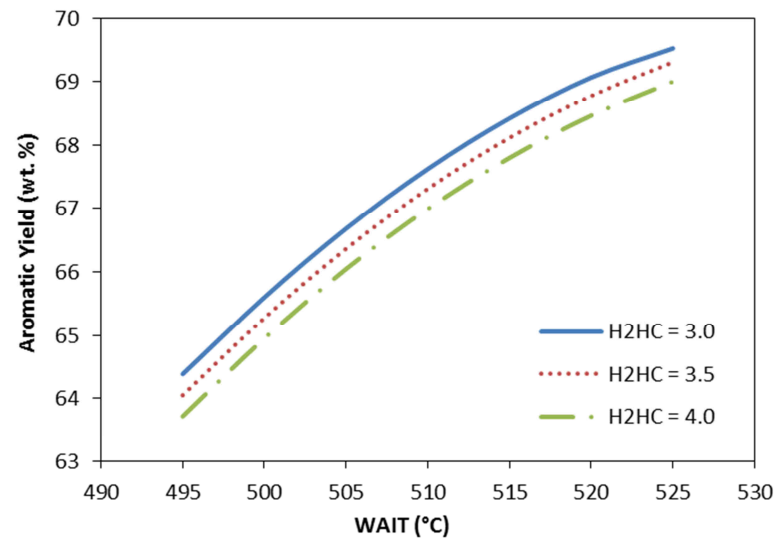


Figure 5.80: Aromatic Yield as a function of WAIT and H2HC ratio

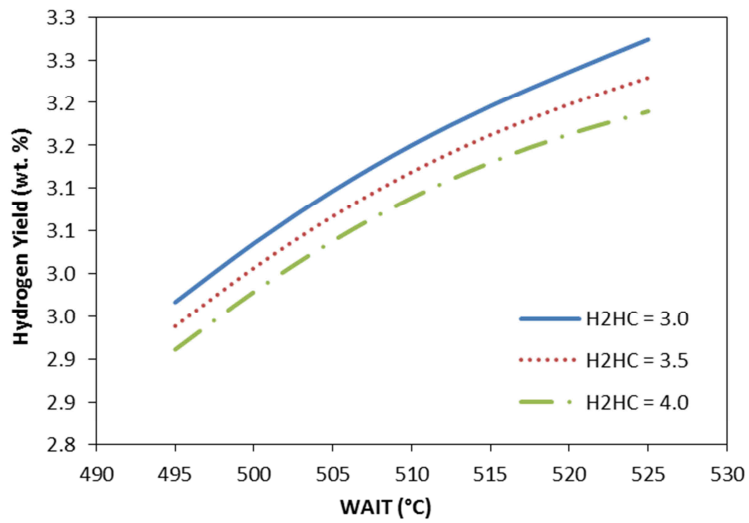


Figure 5.81: Hydrogen Yield as a function of WAIT and H₂HC ratio

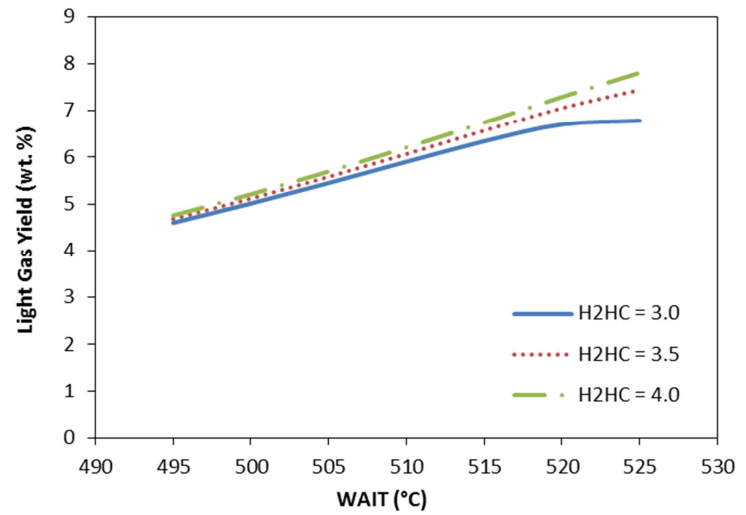


Figure 5.82: Light Gas Yield as a function of WAIT and H₂HC ratio

6. Conclusions

6.1 Summary

This work presents a rational methodology for rating and optimizing refinery reaction and fractionation systems. This rational process involves identifying relevant process data, validating this process data, calibrating kinetic and fractionation models while remaining faithful to experimentally observed reaction kinetics and process thermodynamics; and finally, providing useful applications of these calibrated models in the context of industrial refinery operation.

We present this methodology through two detailed accounts involving the modeling of Fluid Catalytic Cracking (FCC) and Continuous Catalyst Regeneration (CCR) Catalytic units. The key highlights of these accounts are:

1. Review of process details and existing literature for modeling a typical FCC unit
2. Description of the Aspen HYSYS FCC model and 21-Lump kinetics
3. Technique to fill out partial distillation curves using statistical functions
4. Regression of parameters for a new PNA correlation for petroleum fractions
5. Technique to infer molecular composition of FCC feedstock from routine analysis
6. Application of the FCC model to a large-scale refinery process showing less than 2.0% AAD for key product yields and satisfactory predictions of product composition and product quality (composition/distillation data, density and flash point)
7. Case studies that use the FCC model to investigate industrially useful changes in operation
8. Strategy to transfer results from this FCC model into LP-based refinery planning tool

9. Review of process details and existing literature for modeling a typical CCR reforming unit
10. Discussion of kinetic and reactor model in Aspen HYSYS/Petroleum Refining
11. Guidelines for dealing with the physical properties of the reforming kinetic lumps in the context of the radial flow reactors and process fractionators
12. Detailed process to infer molecular composition of reformer feed when plant data is limited
13. Identification of key issues relevant to calibration and how to prevent over-calibration of reforming reactor model
14. Application of model to industrial plant data that shows good agreement with plant measurements in yield and composition of key products
15. Investigation of various phenomena in reforming reactors and their effects on product yield and composition in the form of industrially useful case studies
16. Transition of the results from rigorous reforming non-linear model to an existing LP model for refinery planning

6.2 Future Directions

There are several areas of focus for future work in this area: improving capabilities of fractionation and kinetic lumping models, increasing fidelity of unit models and finally improved overall workflows to further encourage the use of refining models in industry.

Several key issues in kinetic and fractionation lumping remain poorly defined and studied. A few glaring issues that hinder the capabilities of kinetic and fractionation lumps are:

- The ability to carry compositional information (assay data) from crude distillation models to downstream unit operations. One potential approach is to define a global component list that can carry very detailed information about the feed. This is the approach taken by structure-oriented lumping method described in earlier sections. However, this method relies on very extensive data analysis that often not available routinely in the refinery
- There is no public database of petroleum fraction composition available for developing correlations to convert bulk property information into chemical composition information. Development of such a database can greatly reduce the uncertainty in existing correlations and help identify new bulk property descriptors for new correlations.

Another set issues concerns the fidelity unit-level models used for kinetic modeling. Most work (including the present work) uses an idealized reactor model with corrections to account for various hydrodynamic phenomena. Key areas for improvement are:

- Development of generalized correlations that predict pressure drop and slip factor in various types of catalytic reactors. These correlations would be particularly useful in the context of the complex hydrodynamics of FCC risers. These correlations will likely be functions of reaction geometry and detailed phenomena that cannot be published in open literature. Hence, collaboration between academic researchers and industrial professionals is critical in this area.
- The ability to transition results from detailed computational fluid dynamics (CFD) models to simpler models to correct for non-ideal reactor behavior.

The final area of improvement is the development of workflows to encourage use of refining models in industry. Improvements in this area will come mostly from industrial experts in conjunction with academic researchers. Some key issues in this area are:

- Details of the refining process that discuss the interplay between planning, scheduling and operation. An understanding of the true constraints facing refiners, especially in the areas of crude selection and unit flexibility is largely incomplete. This level of detail will help guide academic researchers in developing more useful refining models and associated workflows.
- Sample datasets (crude feedstock selection, product constraints, etc.) from refiners will help researchers identify workflows that can support more detailed kinetic models.